

**Structural and functional characterisation of the mitochondrial
membrane protein human voltage-dependent anion channel
(HVDAC) and the membrane protein-targeting Conotoxin
Conkunitzin-S1 by solution NMR**

Dissertation

zur Erlangung des Doktorgrades

der Mathematisch-Naturwissenschaftlichen Fakultäten

der Georg-August-Universität zu Göttingen

vorgelegt von

Monika Bayrhuber

aus Kiel

Göttingen 2007

D7

Referent: Prof. Dr. Christian Griesinger

Korreferent: Prof. Dr. Ulf Diederichsen

Tag der mündlichen Prüfung:

Summary

This thesis sheds light on the mode of action of membrane proteins and their ligands. Two model systems were chosen: the membrane protein was the human voltage dependent anion channel (HVDAC) and the membrane protein targeting toxin was Conkunitzin-S1.

HVDAC is located in the outer mitochondrial membrane. It is primarily responsible for metabolite flux of the mitochondria. The structure of HVDAC was determined conjointly by NMR-spectroscopy and X-ray crystallography. This is the first time that these methods were united to solve a de novo protein structure. It is the first structure of a human, mitochondrial ion channel. HVDAC adopts a β -barrel fold composed of 18 β -strands and it has an N-terminal α -helix. The N-terminal part, which is known to contain the voltage-sensing domain, shows in solution an increased flexibility. The C-terminal part is mainly responsible for binding of interaction partners. The pro-apoptotic protein Bid and the anti-apoptotic protein Bcl-x_L as well as the lanthanide Gadolinium compete for this site. The antidepressant fluoxetine interacts mainly with the C-terminal loop, while interaction sites of nucleotides are distributed over the whole sequence.

Conkunitzin-S1 (Conk-S1) is a 60-residue neurotoxin from the venom of the cone snail *Conus striatus* that interacts with voltage-gated potassium channels. Conk-S1 shares sequence homology with Kunitz type proteins but contains only two out of the three highly conserved cysteine bridges, which are typically found in these small, basic protein modules. In this study the three-dimensional structure of Conk-S1 has been solved by multidimensional NMR spectroscopy. The solution structure of recombinant Conk-S1 shows that a Kunitz fold is present, even though one of the highly conserved disulfide crosslinks is missing. Introduction of a third, homologous disulfide bond into Conk-S1 results in a functional toxin with similar affinity for *Shaker* K⁺ channels. Scanning mutagenesis revealed, that Conk-S1 adopts a different mode of binding than the structurally homologous dendrotoxins from snake venom. The affinity of Conk-S1 can be enhanced by a pore mutation within the *Shaker* channel pore indicating an interaction of Conk-S1 with the vestibule of K⁺ channels.

Zusammenfassung

Diese Doktorarbeit gibt Aufschluss über die Wechselwirkungen von Membranproteinen und ihren Liganden. Hierfür wurden zwei Modell-Systeme gewählt: als Membran Protein wurde der menschliche spannungsabhängige Anionen Kanal (HVDAC) gewählt, als Membran Protein Ligand das Toxin Konkunitzin-S1.

HVDAC sitzt in der äußeren mitochondrialen Membran. Er ist hauptsächlich für den Metabolitenaustausch der Mitochondrien verantwortlich. Die Struktur des HVDAC wurde gemeinschaftlich mittels der NMR-Spektroskopie und der Röntgenstrukturanalyse aufgeklärt. Dies ist das erste mal, das beide Methoden vereint wurden um eine de novo Protein Struktur zu lösen. Es ist die erste Struktur eines menschlichen, mitochondrialen Ionenkanals. HVDAC liegt als β -Fass vor, das aus 18 β -Strängen aufgebaut ist. Außerdem hat es eine N-terminale α -Helix. Der N-terminale Teil, der bekannterweise für die Spannungsabhängigkeit verantwortlich ist, zeigt in Lösung eine gesteigerte Flexibilität. Der C-terminale Teil ist hauptsächlich für die Bindung von Interaktionspartnern verantwortlich. Das pro-apoptische Protein Bid und das anti-apoptische Protein Bcl-x_L wie auch das Lanthanid Gadolinium konkurrieren um diese Bindungsstelle. Das Antidepressivum Fluoxetin interagiert hauptsächlich mit der C-terminalen Schleife, während Interaktionsstellen von Nukleotiden über die ganze Sequenz verteilt sind.

Konkunitzin-S1 (Conk-S1) ist ein 60-Reste großes Neurotoxin aus dem Gift der Kegelschnecke *Conus striatus*, das mit spannungsabhängigen Kaliumionen Kanälen interagiert. Conk-S1 hat Sequenzhomologien zu Kunitz-artigen Proteinen, besitzt aber nur zwei von den drei hochgradig konservierten Cysteinbrücken, die typischerweise in diesen kleinen, basischen Proteinen gefunden werden. In dieser Studie wurde die drei-dimensionale Struktur des Conk-S1 mit multidimensionaler NMR-Spektroskopie gelöst. Rekombinantes Conk-S1 zeigt eine Kunitz-Faltung, obwohl eine der drei hochkonservierten Disulfid-Quervernetzungen fehlt. Die Einführung der dritten, homologen Disulfidbrücke ergibt ein funktionales Toxin, mit gleicher Affinität zu dem *Shaker* K⁺ Kanal. Mutagenesestudien ergaben, dass Conk-S1 auf unterschiedlich Weise an Kaliumkanäle bindet als die strukturell homologen Dendrotoxine aus Schlangengiften. Die Affinität von Conk-S1 kann mit einer Mutation innerhalb der *Shaker* Kanalpore gesteigert werden. Dies zeigt die Interaktion des Conk-S1 mit dem Vestibulum des Kaliumkanals an.

Acknowledgements

I am deeply grateful to the head of the department Prof. Christian Griesinger for the opportunity to do my Ph.D. in his department, which provided an excellent scientific environment with an outstanding equipment and exceptional scientist, and of course for his interest, encouragement and useful remarks.

I would like to express my deep and sincere gratitude to my direct supervisors Dr. Markus Zweckstetter, who supervised the NMR part, and Dr. Stefan Becker, who supervised the molecular biology part of this thesis, for all their constant help, stimulating suggestions, support and advice.

I am sincerely grateful to Prof. Heinrich Terlau from the Max Planck Institute for Experimental Medicine in Göttingen for the supervision of the electrophysiology part of this work and to Michael Ferber for training me in recording voltage clamp experiments.

I owe my most sincere gratitude to Thomas Meins from the Max Planck Institute for Biochemistry in München, his supervisors Dr. Kornelius Zeth and Prof. Dieter Oesterhelt and the technical assistance Christl Weyrauch for the most productive collaboration on the HVDAC project, for the provision of a huge amount of various samples and for the whole crystallographic work on the HVDAC, which crucially benefited from the help of Clemens Vornrhein from Global Phasing Ltd. Cambridge, UK.

I owe gratitude to Prof. Olivera from the University of Utah for providing the clone of Conk-S1.

I thank Prof. Ulf Diederichsen for accepting me as an external Ph.D. student in the Chemistry Faculty of the Georg-August University, Göttingen.

My deep and warm thanks go to many other people without whom this work would have been impossible:

to Vinesh Vijayan for getting me started at the spectrometers and for his continuous support during my thesis,

to Dr. Jochen Junker for his help with structure calculations,

to my office mates Sigrun Rumpel, Daniela Fischer and Julien Orts for their cordiality, helpfulness and the very useful discussions,

to Petra Widawka, Karin Giller, Kamila Budzyn, Annett Sporning and Mona Honemann for expert technical help,

to Kerstin Overkamp for training me in using the HPLC and the MS, and of course also for the HPLC runs and mass spectra done by her,

to Roland Graf, who established the expression conditions of Conk-S1,

to Young-Sang Jung and Jegannath Korukottu for help with different computational aspects,

and to the rest of my department for a delightful working atmosphere.

I want to thank my friends for distracting my mind, for cheering me up or for joining my joy at the respective occasions, especially Nils who was always there for me.

Finally I want to thank my family for their constant, loving care and support, which gave me the strength to finish this thesis.

Publication list:

The following papers have been published ahead of this thesis:

M. Bayrhuber, V. Vijayan, M. Ferber, R. Graf, J. Korukottu, J. Imperial, J. E. Garrett, B. M. Olivera, H. Terlau, M. Zweckstetter, S.Becker. Conkunitzin-S1 is the first member of a new Kunitz-type neurotoxin family. Structural and functional characterization. *Journal of Biological Chemistry*, **2005**, 25, 23766-70

M. Bayrhuber, R. Graf, M. Ferber, M. Zweckstetter, J. Imperial, J. E. Garrett, B. M. Olivera, H. Terlau, S.Becker. Production of recombinant Conkunitzin-S1 in *Escherichia coli*. *Protein Expression & Purification*, **2006**, 47, 640-4

J. Korukottu, M. Bayrhuber, P. Montaville, V. Vijayan, Y. S. Jung, S. Becker, M.Zweckstetter. Fast high-resolution protein structure determination by using unassigned NMR data. *Angewandte Chemie International Edition English*, **2007**, 46, 1176-9

Table of contents

Abbreviations	13
1 Introduction	17
1.1 Structure determination of Membrane proteins	17
1.2 Membrane proteins as drug targets	18
1.3 Cone Snails and Conotoxins	19
1.4 Rationale and Outline	20
2 Materials and Methods	21
2.1 General Materials	21
2.1.1 Chemicals and enzymes	21
2.1.2 Bacterial strains	22
2.1.3 Oligonucleotide primers for mutagenesis of Conk-S1	22
2.1.4 Equipment	23
2.2 General Methods	25
2.2.1 Molecular biology methods	25
2.2.1.1 Agarose gel electrophoresis	25
2.2.1.2 Isolation of DNA	25
2.2.1.3 Site-directed mutagenesis	26
2.2.1.4 DNA sequencing	27
2.2.1.5 Determination of DNA concentration and purity	27
2.2.1.6 Transformation of <i>E. coli</i>	27
2.2.2 Methods for protein expression	27
2.2.2.1 Cultivation of <i>E. coli</i>	29
2.2.2.2 Storage of <i>E. coli</i>	30
2.2.2.3 Cell lysis	30
2.2.3 Protein purification and investigation	30

2.2.3.1 Protein refolding	32
2.2.3.2 CBD-Ssp DnaB intein tag cleavage	32
2.2.3.3 Cation exchange chromatography	33
2.2.3.4 Reversed phase - high performance liquid chromatography (RP-HPLC)	33
2.2.3.5 Sodium dodecyl sulphate – polyacrylamide gel electrophoresis (SDS-PAGE)	33
2.2.3.6 Determination of protein concentration	34
2.2.3.7 Electrospray Quadrupole Mass spectrometry	34
2.2.3.8 Site-directed spin-labeling (SDSL)	34
2.2.4 Electrophysiological methods	35
2.2.4.1 <i>Xenopus</i> oocyte handling	36
2.2.4.2 Electrophysiological measurements	37
2.2.5 NMR spectroscopy	38
2.2.5.1 Secondary Structure determination	38
2.2.5.2 Mapping of interaction sites	39
2.2.5.3 Solvent exchange experiments	40
2.2.5.4. Residual dipolar couplings (RDCs)	40
2.2.5.4.1 Alignment media	40
2.2.5.4.2 RDC measurements	41
2.2.5.4.3 Evaluation of the residual dipolar couplings with PALES	41
2.2.5.5 Estimation of the molecular weight from $T_{1\rho}$	42
2.2.5.6 Steady state heteronuclear $^{15}\text{N}\{^1\text{H}\}$ -nuclear Overhauser effects (NOEs)	43

2.2.5.7 Paramagnetic relaxation enhancement	43
3 Structural and functional investigation of HVDAC	46
– the first structure of a human, mitochondrial ion channel	
3.1 Introduction	46
3.2 Materials and methods	49
3.2.1 Production of HVDAC1 for NMR analysis	49
3.2.1.1 Cloning of HVDAC1-His ₆	50
3.2.1.2 Site directed mutagenesis of HVDAC1-His ₆	51
3.2.1.3 Expression of HVDAC1-His ₆	52
3.2.1.3.1 Expression of ² H, ¹⁵ N and ¹³ C labelled HVDAC1-His ₆	52
3.2.1.3.2 Expression of selective labelled HVDAC1-His ₆	53
3.2.1.4 Purification and refolding of HVDAC1-His ₆	56
3.2.1.4.1 Purification of HVDAC1-His ₆ inclusion bodies	56
3.2.1.4.2 Refolding of denatured HVDAC1-His ₆	56
3.2.1.4.3 Purification of refolded HVDAC1-His ₆	57
3.2.1.5 Preparation of HVDAC1-His ₆ NMR samples	57
3.2.2 NMR samples	57
3.2.3 NMR Spectroscopy	58
3.2.4 Structure determination by NMR Spectroscopy and X-ray crystallography	59
3.3 Results	60
3.3.1 NMR Resonance Assignment Strategy	60

3.3.2 Resonance Assignment and Secondary Structure	64
3.3.3 Solvent Accessibility And Dynamics	67
3.3.4 Topology model	71
3.3.4.1 Mutations that probe the position of the N-terminal helix	72
3.3.5 Structure Determination of human VDAC by NMR and X-ray crystallography	74
3.3.6 Functional investigation of HVDAC	76
3.3.6.1 ADP-Titration	77
3.3.6.2 Fluoxetine-Titration	77
3.3.6.3 Interaction of HVDAC with anti-apoptotic Bcl-x _L	79
3.3.6.4 Interaction of HVDAC with pro-apoptotic Bid	80
3.3.6.5 Calcium (II) chloride and Gadolinium (III) chloride-Titration	82
3.4 Discussion	84
3.4.1 The combination of NMR and X-ray crystallography for structure determination of membrane proteins	84
3.4.2 NMR and X-ray Structure of HVDAC	86
3.4.3 Comparison of the human VDAC structure with existing models	88
3.4.4 Support for the presented structure from “in silico” analysis	94
3.4.5 Biological relevance of enhanced flexibility in the N-terminus	97
3.4.6 Functional investigation of HVDAC	99
3.4.6.1 ADP-Titration	99
3.4.6.2 Fluoxetine-Titration	99
3.4.6.3 Interactions with pro- and anti-apoptotic proteins	101

3.4.6.4 Calcium (II) chloride and Gadolinium (III) chloride-Titration	105
3.5 Conclusions	106
4 Structural and functional investigation of Conk-S1	108
4.1 Introduction	108
4.2 Materials and methods	110
4.2.1 Expression, refolding and purification of Conk-S1	110
4.2.2 NMR Sample Preparation	112
4.2.3 NMR Resonance Assignment and Structure Calculation	112
4.2.4 Electrophysiological Measurements	114
4.3 Results	114
4.3.1 Refolding and Purification of Conk-S1	114
4.3.2 Resonance Assignment and Tertiary Structure	116
4.3.3 Functional characterization with voltage clamp experiments	120
4.4 Discussion	124
4.4.1 Comparison of Conk-S1 with the structures of BPTI and dendrotoxins	125
4.4.2 Comparison of the NMR and crystal structure of Conk-S1	126
4.4.3 Functional investigation of Conk-S1	127
4.5 Conclusions	132
References	133
Appendix	139
A Chemical shift assignment of HVDAC	139
B Chemical shift assignments of Conk-S1	140
C NMR restraints of Conk-S1	144
C.1 Residual dipolar couplings	144
C.2 Dihedral angles	146

C.3 Coupling constants	148
C.4 Distance constraints	149
D Pulse-programs and parameters used for HVDAC	154
D.1.1 TROSY-HSQC pulse-program	154
D.1.2 TROSY-HSQC parameters	156
D.2.1 HetNOE pulse-program	159
D.2.2 HetNOE parameters	162
D.3.1 T1rho pulse-program	165
D.3.2 T1rho parameters	167
D.4.1 NOESY-TROSY-HSQC pulse-program	170
D.4.2 NOESY-TROSY-HSQC parameters	173
D.5.1 HMQC-NOESY pulse-program	176
D.5.2 HMQC-NOESY parameters	178
D.6.1 TROSY-HNCA pulse-program	181
D.6.2 TROSY-HNCA parameters	185
D.7.1 TROSY-MQ-HNCOCA pulse-program	187
D.7.2 TROSY-MQ-HNCOCA parameters	192

Abbreviations:

A

A_λ	absorption at wavelength λ
ADP	adenosine di phosphate
AIF	apoptosis inducing factor
ATP	adenosine tri phosphate

B

BMRB	biological magnetic resonance bank
BPTI	Bovine Pancreatic Trypsin Inhibitor

C

Conk-S1	Conkunitzin-S1
Conk-S1^{CC}	Conkunitzin-S1 G16C Q40C
cRNA	complementary ribonucleic acid
CSL	combinatorial selective labelling scheme

D

DNA	desoxyribonucleic acid
dNTP	desoxyribonucleotide triphosphate

E

<i>E.coli</i>	<i>Escherichia coli</i>
EDTA	ethylene diamine tetraacetic acid
EM	electron microscopy
ESI	electrospray ionization

F

FPLC	fast protein liquid chromatography
-------------	------------------------------------

G

γ nuclear magnetogyric ratio

GPCRs G-protein-coupled receptors

H

h Planck's constant

HEPES 2-[4-(2-hydroxyethyl)1-piperazinyl] ethansulfonic acid

HPLC high performance liquid chromatography

HSQC heteronuclear single quantum correlation

HVDAC1 human voltage dependent anion channel 1

I

IMP integral membrane protein

INEPT insensitive nuclei enhancement by polarisation transfer

IPTG isopropyl- β -D-thiogalactopyranoside

K

kDa kilo-Dalton ($=10^3$ g/mol)

L

LB Luria Bertani

LDAO Lauryldimethylamine-oxide

M

MOM mitochondrial outer membrane

mq multiple quantum

MS mass spectrometry

MTSL 1-oxy-2,2,5,5-tetramethyl-3-pyrroline-3-methyl)-methanethio-sulfonate

MW molecular weight

MWCO molecular weight cutoff

μ_0	magnetic permeability of vacuum
N	
NFR	normal frog Ringers
NMR	nuclear magnetic resonance
NOE	nuclear Overhauser effect
NOESY	nuclear Overhauser effect spectroscopy
O	
OD	optical density
P	
PAGE	polyacrylamide gel electrophoresis
PCR	polymerase chain reaction
PDB	protein data bank
PMSF	phenylmethylsulphonyl fluoride
PRE	paramagnetic relaxation enhancement
PTP	permeability transition pore
R	
R1	longitudinal or spin-lattice relaxation rate
R2	transversal or spin-spin relaxation rate
RDC	residual dipolar coupling
rmsd	root mean square deviation
RNA	ribonucleic acid
RP-HPLC	reversed phase-high performance liquid chromatography
S	
SAIL	stereo-array isotope labelling
SDS	sodium dodecylsulfate
SDSL	site-directed spin-labelling
<i>Shaker</i>-$\Delta 6-46$	<i>Shaker</i> K ⁺ channel with removed N-terminal inactivation

	Domain
SVD	singular value decomposition
T	
T₁	longitudinal or spin-lattice relaxation time
T₂	transversal or spin-spin relaxation time
TEMED	N,N,N',N'-tetramethylethylenediamine
TFA	trifluoroacetic acid
TOCSY	total correlation spectroscopy
TOM	translocase of the outer membrane
Tris	tris(hydroxymethyl)-amino-methan
TROSY	tranverse relaxation optimised spectroscopy
τ	correlation time for the electron-nuclear interaction
τ_c	global or rotational correlation time
V	
VDAC	voltage dependent anion channel
Y	
YT	yeast/tryptone

1

Introduction

1.1 Structure determination of Membrane proteins

Membrane proteins can be either integral or peripheral to the membrane. Peripheral membrane proteins are to some degree water-soluble and tether to the membrane by an anchoring group. Integral membrane proteins (IMPs) contain several transmembrane segments and are therefore insoluble in water. IMPs are essential for cellular transport processes and intercellular signalling. They constitute roughly 20-30% of the eukaryotic genomes^[1]. Despite their wide abundance and physiological importance, out of the over 35.000 protein structures deposited in the Protein Data Bank (pdb), there are only 250^[2] (state 27.03.07) coordinate files of membrane proteins. This under-representation of membrane proteins in the pdb has two major reasons. First it stems from their complex expression behaviour^[3]. Secondly it results from the difficulty to obtain high-quality crystals suitable for X-ray diffraction. This is due to the fact, that IMP's are highly hydrophobic. Thus they have to be solubilised for example in detergent micelles, which are inherently resistant to forming ordered crystal lattices^[4]. Therefore solution nuclear magnetic resonance (NMR) spectroscopy could be a viable alternative to X-ray diffraction. However, out of the 250 deposited coordinate files, only 5 were investigated by NMR spectroscopy. The major problem for solution NMR is the size limit. As molecular masses increase, NMR spectra become increasingly difficult to interpret because of spectral crowding and line broadening due to fast transverse relaxation^[5]. Since the IMPs form a complex with the detergent micelles the overall molecular weight of the

studied particle is significantly increased. Membrane proteins with masses in the same order as those of the micelles will determine the size of the complex. Therefore the complex size cannot be minimized simply by choosing a detergent known to form small micelles^[6].

Nevertheless, several recent developments make structure determination of IMP's by solution NMR feasible^[7]. Transverse relaxation-optimised spectroscopy (TROSY) -based methods^[8] provide a substantial improvement of ¹⁵N-nuclei relaxation behaviour, especially at high field strengths (900 MHz)^[7]. Full deuteration of side chains further improves the relaxation behaviour^[9], while partial protonation yields additional distance constraints^[10]. Especially cell free expression systems provide the opportunity for advanced labelling schemes. The stereo-array isotope labelling (SAIL)^[5] optimises the samples with respect to spectral quality and information content. Another approach, the combinatorial selective labelling scheme (CSL)^[11], is able to speed up the assignment process dramatically. Long range distance constraints can be obtained from residual dipolar couplings (RDCs)^[12] and from strategically placed paramagnetic spin labels^[13].

1.2 Membrane proteins as drug targets

Due to their physiological relevance membrane proteins constitute 60% of all drug targets^[14]. Out of these are at least 40% integral membrane proteins, of which 66% are rhodopsin like G-protein-coupled receptors (GPCRs), 20% are ligand-gated and 14% voltage-gated ion channels. Under the top 20 prescription drugs based on total sales 16 act against IMPs (Med Ad News, May 2005, drug target location from DrugBank^[15]). This clearly points out the immense potential of membrane protein

targeting compounds. One combinatorial library of compounds interacting with IMPs is provided by nature. These are the conotoxins that form the venome of cone snails.

1.3 Cone Snails and Conotoxins

Cone snails are a genus of toxic, carnivorous gastropodes, which consists of approximately 500 species^[16]. They thrive in tropical, marine habitats. Each *Conus* species has evolved its own large molecular repertoire of venom components, different from that of every other *Conus* species. A general rationale for this can be found in the complete web of biological interactions present in marine communities^[17]. All these species use a similar strategy for hunting. They carry a hollow, harpoon-shaped tooth, with which they inject a highly potent venom into their prey^[18] (see Fig. 1).



Fig. 1^[18] *Conus purpurascens* rapidly catching a clown fish.

Each *Conus* species developed probably over 100 different venom components. This leads to an estimate of over 50.000 different pharmacologically active components^[19]. These components, the conotoxins, are small, peptidic toxins. The majority binds with high affinity and specificity to various ligand- or voltage-gated ion channels but also some conotoxins are known, that interact with GPCRs (reviewed in ^[20]). Since only a minuscule fraction of the total conotoxin diversity has so far been characterised in detail^[20] and since conotoxins interact with essential drug targets (see 1.2) there is a

high interest from the pharmacological point of view to continue investigating this combinatorial library provided by nature.

1.4 Rationale and Outline

The aim of this thesis is to shed light on the mode of action of membrane proteins and their ligands. Two model systems were chosen: a membrane protein and a membrane protein targeting conotoxin. The membrane protein is the human voltage dependent anion channel (HVDAC) from the mitochondrial outer membrane. The conotoxin is Conkunitzin-S1 (Conk-S1), a Kunitz-type protein from *Conus striatus*. Both proteins shall structurally and functionally be analysed. NMR-spectroscopy is chosen as a major tool for these investigations. This is done because only NMR-spectroscopy is able to investigate proteins in solution, ergo in their physiological relevant form. Additionally it allows for the determination of dynamics, which are prerequisite for protein/protein interactions. The HVDAC will also be investigated by X-ray crystallography in the framework of the thesis of Thomas Meins. The aim is to solve the structure conjointly by NMR-spectroscopy and X-ray crystallography, because the complex behaviour of HVDAC pushes both methods at their limits.

Functional investigations for the HVDAC will solely be done by NMR-spectroscopy; Conk-S1 will functionally be investigated by electrophysiology.

The following work is divided in 3 chapters. Chapter 2 describes the materials and the general methods that have been used during this thesis, Chapter 3 and 4 include experimental details, structure elucidation and functional analysis of HVDAC and Conk-S1, respectively.

2

Materials and Methods

2.1 General Materials

2.1.1 Chemicals and enzymes

All chemicals and enzymes used during this work are summarised in Table 1.

Table 1 Chemicals and enzymes

Chemicals/Enzymes	Company
Agar, DNase I, IPTG	AppliChem, Darmstadt, Germany
ammonium chloride (>98 % 15N)	Cambridge Isotope Laboratories, Andover, USA
¹³ C6-D-glucose (>98 % ¹³ C)	Spectra Stable Isotopes, Columbia, USA
BamHI, CIAP, _HindIII, NcoI, NdeI, _X174DNA/BsuRI(HaeIII), T4-DNA ligase	Fermentas, St. Leon-Rot, Germany
ammonium molybdate tetrahydrate, ascorbic acid, Coomassie Brilliant Blue R-250, copper chloride dihydrate, iron (II) sulfate heptahydrate	Fluka, Neu-Ulm, Germany
DTT	Gerbu, Gaiberg, Germany
agarose, kanamycin sulphate	GibcoBRL, Karlsruhe, Germany
Ficoll 400	ICN Biomedicals Inc, Costa Mesa, USA
Bench Mark protein ladder	Invitrogen, Karlsruhe, Germany
acetic acid, α-D(+)-glucose monohydrate, ammonium acetate, ammonium chloride, ammonium hydrocarbonate, boric acid, disodium hydrogen phosphate, ethanol, glycerol, glycine, hydrochloric acid, manganese chloride dihydrate, magnesium sulfate heptahydrate, sodium chloride, sodium dihydrogen phosphate, sodium hydroxide, TFA, thiaminechloride hydrochloride, Tris, urea	Merck, Darmstadt, Germany
BSA	New England Biolabs, Ipswich, USA
Hot Star Taq, Ni-NTA Agarose, QIAGEN Plasmid Midi Kit, QI-Aprep Spin Miniprep Kit,	Qiagen, Hilden, Germany
cobalt chloride hexahydrate	Riedel-de Haën, Seelze, Germany
CompleteT M protease inhibitors, CompleteT M protease inhibitors EDTA-free, elastase, protease K, trypsin	Roche Diagnostics, Mannheim, Germany
acetonitrile, ampicillin sodium salt, APS, dipotassium hydrogen phosphate, ethidium bromide, EDTA, HEPES, imidazole, magnesium chloride hexahydrate, MES, MOPS, potassium dihydrogen phosphate, Rotiphorese Gel 30, sodium acetate, TEMED, tryptone, yeast extract	Roth, Karlsruhe, Germany
SDS	Serva, Heidelberg, Germany
Turbo Pfu DNA polymerase, dNTP	Stratagene, La Jolla, USA
MTSL	Toronto Research Chemicals, Toronto, Canada

2.1.2 Bacterial strains

Bacterial strains used in this work are summarized in Table 2

Table 2 Bacterial strains

Strain	Genotype	References
BL21(DE3)	F ⁻ , <i>ompT</i> , <i>hsdS_B</i> (<i>r_B</i> ⁻ , <i>m_B</i> ⁻), <i>dcm</i> , <i>gal</i> , λ (DE3)	[21]
XL1-Blue	<i>recA1 endA1 gyrA96 thi-1 hsdR17 supE44 relA1 lac</i> [F' <i>proAB lacI^qZ</i> ΔM15Tn10 (Tet ^r)]	Stratagene
XL2-Blue	<i>recA1 endA1 gyrA96 thi-1 hsdR17 supE44 relA1 lac</i> [F' <i>proAB lacI^qZ</i> ΔM15Tn10 (Tet ^r) Amy Cam ^r]	Stratagene
XL10-Gold [®]	Tet ^R Δ(<i>mcrA</i>)183 Δ(<i>mcrCB-hsdSMR-mrr</i>)173 <i>endA1 supE44 thi-1 recA1 gyrA96 relA1 lac Hte</i> [F' <i>proAB lacI^qZ</i> ΔM15 Tn10 (Tet ^R) Amy Cam ^R]	Stratagene

Plasmids containing the desired gene were transformed into the *Escherichia coli* (*E. coli*) expression strain BL21(DE3). Plasmids modified with the QuikChange[®] site-directed mutagenesis kit (Stratagene) were transformed into either *E. coli* XL1-Blue, XL2-Blue or XL10-Gold.

2.1.3 Oligonucleotide primers for mutagenesis of Conk-S1

All primers used for the mutagenesis of Conk-S1 were ordered from Invitrogen (Karlsruhe, Germany). They are summarised in Table 3. Bases that differ from the wild type sequence are shown in bold.

Table 3 Oligonucleotide primers for the mutagenesis of Conk-S1

Name	Sequence 5' - 3'	Mutation
ConS6	GAGAATTTACTACAATAGCGCT GC AAAACAGTGTTTAAGGTTTCGAT	R29A (5'-3')
ConS7	ATCGAACCTTAAACACTGTTTT GC AGCGCTATTGTAGTAAATTCTC	R29A (3'-5')
ConS8	GAATTTACTACAATAGCGCTAGAG GC ACAGTGTTTAAGGTTTCGATTAC	K30A (5'-3')
ConS9	GTAATCGAACCTTAAACACTGT GC TCTAGCGCTATTGTAGTAAATTC	K30A (3'-5')
ConS10	GTGGGTCGGGCACAG CG GGCTGAGAAGAGAAT	K18A (5'-3')
ConS11	ATTCTCTTCTCAGCC GC TGTGCCCGACCCAC	K18A (3'-5')
ConS12	GTGTTTAAGGTTTCGAT GC CACAGGACAAGGAGGCAAC	Y37A (5'-3')

Name	Sequence 5' - 3'	Mutation
ConS13	GTTGCCCTCCTTGTCCCTGTGG C ATCGAACCTTAAACAC	Y37A (3'-5')
ConS14	GACAGTGGGT C GTGCACAAAGGCTGAG	G16C (5'-3')
ConS15	GGTT C GATTACACAGGAT TG CGGAGGCAACGAAAAC	Q40C (5'-3')
ConS16	GAGAATTTACTACAATAGCGCTAA AA AGACAGTGT T TAAGGTT C GATTACAC	R29KK30R (5'-3')
ConS17	GTGTAATCGAACCTTAAACACTGT C TTT T AGCGCTATTGTAGTAAATT C TC	R29KK30R (3'-5')
ConS18	CAAAGGCTGAGAAGAGAAT TG CCTACAATAGCGCTAGAAAAC	Y24A (5'-3')
ConS19	GTTTTCTAGCGCTATTGTAG GC AATTCTCTCTCAGCCTTTG	Y24A (3'-5')
ConS20	TAGAAAACAGTGT T TAAGG GC CGATTACACAGGACAAGGAG	F35A (5'-3')
ConS21	CTCCTTGTCCCTGTGTAATCG GC CCCTTAAACACTGTTTTCTA	F35A (3'-5')
ConS22	CGGGCACAAAGGCTGAG GC GAGAATTTACTACAATAGC	K21A (5'-3')
ConS23	GCTATTGTAGTAAATTCT CG CCTCAGCCTTTGTGCCCCG	K21A (3'-5')
ConS24	GGGCACAAAGGCTGAGAAG GC CAATTTACTACAATAGCGC	R22A (5'-3')
ConS25	GCGCTATTGTAGTAAATT GC CTTCTCAGCCTTTGTGCC	R22A (3'-5')
ConS26	ATTCCTCGAGGAAGGAT GC ACCGAGTCTATGCGATCT	R3A (5'-3')
ConS27	AGATCGCATAGACTCGGT GC ATCCTTCC T CGAGGAAT	R3A (3'-5')
ConS28	CGCTAGAAAACAGTGT T TAG CG TTTCGATTACACAGGACAAG	R34A (5'-3')
ConS29	CTTGTCCCTGTGTAATCGAAC GC TAAACACTGTTTTCTAGCG	R34A (3'-5')
ConS30	GGCAACGAAAACAATTT TG CCCGTACTTACGATTGCCAAC	R48A (5'-3')
ConS31	GTTGGCAATCGTAAGTACGG GC AAAATTGTTTTCGTTGCC	R48A (3'-5')
ConS32	GCAACGAAAACAATTT TG CG GC TACTTACGATTGCCAACG	R49A (5'-3')
ConS33	CGTTGGCAATCGTAAGT AG CGCGAAAATTGTTTTCGTTGC	R49A (3'-5')
ConS34	AACAATTTTCGCCGTACT GC CGATTGCCAACGAACGTG	Y51A (5'-3')
ConS35	CACGTT C GTGGCAATCG GC AGTACGGCGAAAATTGTT	Y51A (3'-5')
ConS36	GCCG T ACTTACGATTGCCAA GC AACGTGCTGTATACATG	R55A (5'-3')
ConS37	CATGTATACAGACACGTT GC TTGGCAATCGTAAGTACGGC	R55A (3'-5')

2.1.4 Equipment

Laboratory instruments and consumables are summarised in Table 4.

Table 4 Instruments and consumables

Common Name	Identifier/Company
Balances	Sartorius B 3100 S, Sartorius, Göttingen, Germany Sartorius AC 210 S, Sartorius, Göttingen, Germany
Centrifuges	Beckmann-Coulter Avanti J-20 and J-301, rotors: JLA 8.100, JLA 9.100, JLA 16.250, JA 25.50 Ti, JA 30.50 Ti, Krefeld, Germany Eppendorf Centrifuge 5415D, Wesseling-Berzdorf, Germany Eppendorf Centrifuge 5804, Wesseling-Berzdorf, Germany Heraeus Biofuge primo, Kendro, Hanau, Germany
Concentrators	Microcon, YM-3 and YM-10, Amicon, Bedford, USA Centricon, YM-3 and YM-10, Amicon, Bedford, USA Centriplus, YM-3 and YM-10, Amicon, Bedford, USA Vivaspin 2 ml MWCO 10.000 PES, Vivascience, Hannover, Germany
Desalting	NAPT M -10, Amersham Pharmacia Biotech, Freiburg, Germany PDT M -10, Amersham Pharmacia Biotech, Freiburg, Germany
Dialysis	Slide-A-Lyzer Dialysis Cassettes, MWCO 3500, 0.1-0.5 ml Capacity, Pierce Biotechnology, Inc., Rockford, IL, USA Slide-A-Lyzer Dialysis Cassettes, MWCO 10000, 0.1-0.5 ml Capacity, Pierce Biotechnology, Inc., Rockford, IL, USA Spectra Por membranes, MWCO 10000, Roth, Karlsruhe, Germany Spectra Por membranes, MWCO 3500, Roth, Karlsruhe, Germany
Electrophoresis	Kodak Electrophoresis documentation and analysis system 120, Eastman Kodak Co., New York, NY, USA Power Pac 300, BioRad, München, Germany Polyacrylamide gel electrophoresis: Mini-PROTEAN 3 Cell, BioRad, München, Germany Agarose gel electrophoresis: Mini-Sub Cell GT, BioRad, München, Germany
-80 °C freezer	MDF-U71V Ultra-low temperature freezer, SANYO Electric Co., Ltd, Osaka, Japan
Filtering	sterile filter 0,20 µm, Sartorius, Göttingen, Germany
FPLC	Äkta prime, Amersham Pharmacia Biotech, Freiburg, Germany Äkta basic, Amersham Pharmacia Biotech, Freiburg, Germany HiTrap™ SP XL, Amersham Pharmacia Biotech, Freiburg, Germany
HPLC	system 1: UV-975, PU-980, LG-980-02, DG-980-50, AS-2055Plus, CO-200, JASCO International, Groß-Umstadt, Germany system 2: MD-910, PU-980, LG-1580-04, DG-1580-54, AS-950-10, CO-200, JASCO International, Groß-Umstadt, Germany system 3: MD-2010Plus, PU-2080Plus, LG-2080-04, DG-2080-54, AS-2055Plus, CO-200, JASCO International, Groß-Umstadt, Germany Vydac C18 10x250 mm, Hesperia, CA, USA Vydac C18 4.6x250 mm, Hesperia, CA, USA
Incubator	Infors Multitron HT, Einsbach, Germany Certomat R, B. Braun Biotech International, Melsungen, Germany
Lyophilisation	Christ Alpha 2-4, B. Braun Biotech International, Melsungen, Germany
NMR	AVANCE 400, Bruker, Karlsruhe, Germany AVANCE 600, Bruker, Karlsruhe, Germany DRX 600, Bruker, Karlsruhe, Germany AVANCE 700, Bruker, Karlsruhe, Germany DRX 800, Bruker, Karlsruhe, Germany AVANCE 900, Bruker, Karlsruhe, Germany Quality NMR Sample Tubes 5 mm, Norell, Inc., Landisville, NJ, USA Shigemi NMR tube 5 mm, Shigemi Corp., Tokyo, Japan

2.2 General Methods

2.2.1 Molecular biology methods

2.2.1.1 Agarose gel electrophoresis

All solutions used for Agarose gel electrophoresis are summarized in Table 5. DNA fragments were separated on horizontal agarose gels. These gels were prepared by melting 1 % (w/v) agarose in 1 x TBE buffer and adding 25 µl ethidium bromide/l 1 % agarose. Each DNA sample was mixed with 1/5 volumes of 5 x DNA-loading buffer. Gels were run at a constant voltage of 100 V, imaged under UV-light and digitized for documentation.

Table 5 Solutions for Agarose gel electrophoresis

Application	Solution name	Substance	Amount	
Agarose gel	5 x DNA loading buffer	Ficoll 400	12.5 g	
		EDTA pH 8	2.5 ml, 0.5M	
		SDS	0.5 g	
		bromphenol blue	25 mg	
		xylene cyanol FF	25 mg	
		H ₂ O	up to 50 ml	
		Tris	108 g	
		10 x TBE buffer	boric acid	55 g
			EDTA pH	40 ml, 0.5M

2.2.1.2 Isolation of DNA

10 ml E. coli XL2-blue overnight cultures were used for purification of up to 20 µg plasmid DNA with the help of the QIAprep Spin Miniprep Kit. Plasmid DNA was isolated from the cell pellets according to the producer's instructions. For removal of enzymes, salts and buffers, columns with a silica gel membrane

(QIAquick spin columns) were used according to the producer's instructions.

2.2.1.3 Site-directed mutagenesis

Single site amino acid changes were generated using the QuikChange[®] site-directed mutagenesis kit (Stratagene). Primers used for mutagenesis were designed according to the instruction manual and are included in Table 3. The 50 µl PCR reaction mixtures contained 125 ng of each primer, 10 ng plasmid DNA template, 6.25 µmol dNTPs and 2.5 units Turbo Pfu DNA polymerase in Cloned Pfu buffer. The cycling after an initial step at 95 °C for 30 s was performed as follows: 1.) denaturing for 30 s at 95 °C, 2.) annealing for 1 min at 55 °C and 3.) elongation for 1 min per kb of plasmid length at 68 °C. For creating single nucleotide changes and for creating double or triple nucleotide changes the number of cycles was 12 and 16, respectively.

Multiple site amino acid changes were generated using the QuikChange[®] multi-site-directed mutagenesis kit. The 25 µl PCR reaction mixtures contained 100 ng of each primer, 100 ng plasmid DNA template, 6.25 µmol dNTPs and 1 µl QuikChange[®] Multi enzyme blend. The cycling after an initial step at 95 °C for 1 min was performed as follows: 1.) denaturing for 1 min at 95 °C, 2.) annealing for 1 min at 55 °C and 3.) elongation for 2 min per kb of plasmid length at 65 °C.

Following temperature cycling, 10 units of Dpn I restriction enzyme were directly added to each PCR reaction mixture and incubated for 1 h at 37 °C. 1 µl of the reaction mix was transformed into *E. coli* XL1-blue or *E. coli* XL2-blue for single site-, and into *E. coli* XL10-gold for multiple site directed mutagenesis (see 2.1.2). The plasmid DNA was isolated (see 2.2.1.2) and the desired mutation was confirmed by DNA sequencing (see 2.2.1.4).

2.2.1.4 DNA sequencing

Sequencing of purified plasmid DNA was performed via the extended Hot Shot DNA sequencing service of Seqlab (Göttingen, Germany). 200 µl PCR tubes with a flat lid were loaded with a total volume of 7 µl containing 20 pmol of primer and 0.6-0.7 µg plasmid DNA in water.

2.2.1.5 Determination of DNA concentration and purity

The absorption at 260 nm (A_{260}) was measured to determine the DNA concentration. An A_{260} of 1 equals 50 µg/ml dsDNA^[22]. The ratio of A_{260}/A_{280} was calculated. A ratio between 1.8 and 2 indicates reasonably pure DNA, suitable for DNA sequencing.

2.2.1.6 Transformation of *E. coli*

1 µl plasmid DNA was added to 50 µl competent cells and incubated for 30 min on ice. Cells were subjected to a heat shock of 42 °C for 45 s and subsequently cooled for 2 min on ice. Afterwards the cells were supplemented with 0.5 ml of 2 x YT medium and incubated for 1 h at 37 °C. Finally the cells were plated onto LB-agar plates containing ampicillin.

2.2.2 Methods for protein expression

All solutions used for cultivation, storage and lysis of *E. coli* cells are summarised in Table 5. The culture media utilised in the expression of Conk-S1 (Table 6) were sterilised by autoclaving. Prior to usage 100µg/l ampicillin was added to each medium. Agar plates were prepared by adding 15g agar to 1 l of medium. The ampicillin- and IPTG-stock solutions were sterile filtrated and stored at -20°C.

Table 6 Culture media for expression of Conk-S1

Application	Solution name	Substance	Amount
Culture medium for bacteria	2 x YT	tryptone	16 g
		yeast extract	10g
		NaCl	10g
		H ₂ O	up to 1 l
	LB	tryptone	10 g
		yeast extract	5 g
		NaCl	10 g
		H ₂ O	up to 1 l
	M9 minimal medium	Na ₂ HPO ₄	6.8 g
		KH ₂ PO ₄	3.0 g
		NaCl	0.5 g
		NH ₄ Cl or ¹⁵ NH ₄ Cl	1.0 g
		glucose or ¹³ C ₆ -glucose	4.0 g
		MgSO ₄	2ml, 1M
		CaCl ₂	50µl, 2M
		thiaminechloride•HCl	0.03 g
		trace elements	10 ml
		H ₂ O	Up to 1 l
		Trace elements for M9 minimal medium	trace elements stock solution
MnCl ₂ •2 H ₂ O	0.094 g		
CoCl ₂ •6 H ₂ O	0.08 g		
ZnSO ₄ •7 H ₂ O	0.07 g		
CuCl ₂ •2H ₂ O	0.03 g		
H ₃ BO ₃	0.002 g		
(NH ₄) ₆ Mo ₇ O ₂₄ •4H ₂ O	0.025 g		
H ₂ O	up to 100 ml, stir 10 min		
Antibiotic	ampicillin stock solution	ampicillin sodium salt	100 mg/ml
		EDTA	0.5 g, stir over night
Inductor for transcription	IPTG stock solution	IPTG	1M

Application	Solution name	Substance	Amount
		Tris/HCl pH 8.5	20 mM
Cell lysis	lysis buffer	NaCl	500 mM
		PMSF	0.5 mM
		EDTA	1 mM

2.2.2.1 Cultivation of *E. coli*

Conk-S1 and its mutants were expressed in the *E. coli* strain BL21(DE3). All cells were grown at 37° C in media containing the antibiotic ampicillin (100 µg/l). The pre- and expression-culture were shaken vigorously. In order to start the cultivation from a single colony cells were grown overnight on an agar plate made of LB medium. From this plate a single colony was picked to inoculate a 2 ml 2 x YT overday preculture. Of this preculture 30µl were added to a 30 ml LB overnight preculture. The expression culture for protein expression was prepared by inoculating 1 l LB medium with 20 ml of the overnight preculture. For the preparation of ¹⁵N and ¹³C isotopic labelled samples the 2 x YT medium and the LB medium were replaced by LB and M9 minimal medium, respectively. The M9 minimal medium utilises NH₄Cl and glucose as sole nitrogen and carbon sources, which can be used ¹⁵N and ¹³C labelled, as required. The optical density of the expression culture was measured regularly at 600 nm (OD₆₀₀), in order to follow the cell growth. Protein expression was induced at an OD₆₀₀ of 0.6-0.7 by addition of IPTG, to a final concentration of 1 mM. The cells were harvested at an OD₆₀₀ of 1.7-1.9 by centrifugation at 10153 x g and 4°C for 17 min.

2.2.2.2 Storage of *E. coli*

Cell pellets were stored at -80°C. For long term storage of the *E. coli* strains a part of the LB preculture was mixed with sterile 50 % glycerol at a ratio of 2.33:1 (v/v). This mixture was also stored at -80°C.

2.2.2.3 Cell lysis

Cell pellets from 1 l culture were resuspended on ice in maximal 70 ml lysis buffer. The cells were lysed by ultrasonication for 5 x 20 s. In between each stroke the suspension was cooled on ice for 2-5 min. Inclusion bodies were pelleted by centrifugation at 75000 x g at 4°C for 40 min.

2.2.3 Protein purification and investigation

All solutions used for refolding and purification of Conk-S1 are summarised in Table 7.

Table 7 Purification and refolding of Conk-S1

Application	Solution name	Substance	Amount
Protein refolding	denaturing buffer	guanidine/HCl	6 M
		β -mercaptoethanol	50 mM
		Tris/HCl pH 8.0	50 mM
	refolding buffer 1	guanidine/HCl	3 M
		reduced glutathione	2 mM
		oxidised glutathione	0.2 mM
		EDTA	2 mM
		Tris/HCl pH 8.0	50 mM
	refolding buffer 2	reduced glutathione	2 mM
		oxidised glutathione	0.2 mM
		EDTA	2 mM

Application	Solution name	Substance	Amount
Protein purification	intein cleavage buffer	Tris/HCl pH 6.5	20 mM
		NaCl	0.5 M
		EDTA	1 mM
		PMSF	0.5 mM
	cation exchange buffer A	Hepes pH 7	50 mM
	cation exchange buffer B	Hepes pH 7	50 mM
		NaCl	1 M
	HPLC buffer A	H ₂ O	99.9 %
		TFA	0.1 %
	HPLC buffer B	acetonitrile	99 %
		TFA	0.1 %
	SDS-PAGE	APS stock solution	H ₂ O
APS			10 % (w/v)
destaining solution		H ₂ O	90 %
		acetic acid	10 %
4 x protein loading buffer		SDS	1.7 g
		Tris/HCl pH 6.8	7.5 ml, 1M
		glycerol	23 ml
		bromphenol blue	50 mg
		β-mercaptoethanol	0.5 ml
		H ₂ O	up to 50 ml
running buffer		SDS	1 g
		Tris	3.03 g
	glycine	14.4 g	
	H ₂ O	up to 1 l	
	staining solution	Comassie Brilliant blue G250	2.2 g
		acetic acid	100 ml
isopropanol		250 ml	
H ₂ O		650 ml	

Application	Solution name	Substance	Amount
SDS-PAGE	stacking gel (3 %)	Rotiphorese Gel 30	250µl
		Tris/HCl	2M, 313µl
		10% SDS	25 µl
		10% APS	25 µl
		TEMED	2 µl
		H ₂ O	1.88 µl
	seperating gel (12.5 %)	Rotiphorese Gel 30	250µl
		Tris/HCl	2M, 313µl
		10 % SDS	25 µl
		10 % APS	25 µl
		TEMED	2 µl
		H ₂ O	1.88 µl

2.2.3.1 Protein refolding

The inclusion body pellet was dissolved in 20 ml denaturing buffer (Table 7). Insoluble debris was removed by centrifugation at 75000 x g at 4°C for 1 h. The supernatant was successively dialysed against 1 l of refolding buffer 1 and 2 for each 16 h at 4 °C. Precipitant was removed by centrifugation at 75000 x g at 4° C for 20 min.

2.2.3.2 CBD-Ssp DnaB intein tag cleavage^[23]

The cleavage of the CBD-Ssp DnaB intein tag from the peptide was induced by a pH jump from pH 8 to pH 6.5 (see 4.3.1). This was performed by dialysis of the protein solution against the intein cleavage buffer (Table 7) for 5h at 4 °C, followed by 16 h of dialysis at room temperature.

2.2.3.3 Cation exchange chromatography

Cation exchange chromatography was conducted on an Äkta prime low pressure liquid chromatography system on a 1 ml HiTrapTM SP XL column. The column was successively equilibrated with 10 bed volumes of cation exchange buffer A (Table 7), 10 bed volumes of cation exchange buffer B (Table 7) and again 10 bed volumes of cation exchange buffer A. The flow rate for equilibration was 1 ml/min. The sample was loaded at a flow rate of 1 ml/min. After sample loading the column was washed with 10 to 20 bed volumes of buffer A, to remove unbound impurities. The peptide was eluted with a 30 ml linear gradient to buffer B at a flow rate of 0.5 ml/min. Fractions of 0.5 ml size were collected.

2.2.3.4 Reversed phase - high performance liquid chromatography (RP-HPLC)

RP-HPLC was conducted on JASCO systems on an analytical or a semi-preparative VYDAC C18 reversed phase column. The column was pre-equilibrated with RP-HPLC buffer A (Table 7). The elution was performed at a flow rate of 1 ml/min for the analytical column and 3 ml/min for the semi-preparative column. A linear gradient of 0-60 % RP-HPLC buffer B in 30 min was applied.

2.2.3.5 Sodium dodecyl sulphate – polyacrylamide gel electrophoresis (SDS-PAGE)^[24]

The discontinuous Tris-glycine buffer system as described by Laemmli^[24] was used to separate proteins by molecular weight. All gels had a stacking gel with an acrylamide concentration of 3 % and a separating gel with 12.5 % acrylamide. The solutions for the stacking and separating gel are given in Table 7. Since Conk-S1 has a molecular weight smaller than 10 kDa, 2 M Tris/HCl pH 8.8 was used as the

stacking/separation gel buffer instead of the usually utilised 1 M buffer^[25]. Protein samples were mixed with 4 x protein loading buffer and were denatured at 100 °C for 5 min before loading. The gels were run at 25 mA. Staining of the gels was done with Coomassie blue R-250 by heating the gel in staining solution for 90 s in the microwave. Afterwards staining solution was removed, the gels were washed with water and incubated in destaining solution in the microwave for 2 times 90 s. Finally, the SDS-gels were imaged and digitized for documentation.

2.2.3.6 Determination of protein concentration

The concentration of proteins in solution was determined, according to the Lambert-Beer law, by measuring the absorption at 280 nm (A_{280}).

$$A_{\lambda} = \epsilon_{\lambda} \cdot c \cdot d \quad (1)$$

A_{λ} : absorption at wavelength λ

ϵ_{λ} : molar extinction coefficient at wavelength λ in $M^{-1}cm^{-1}$

c: protein concentration (M)

d: thickness of the cuvette (cm)

2.2.3.7 Elecspray Quadrupole Mass spectrometry

For Elecspray Quadrupole Mass spectrometry the source capillary was set to 2.94 kV. Scans were acquired in positive-ion mode at m/z 500-2500. It was performed after RP-HPLC (see 2.2.3.4).

2.2.3.8 Site-directed spin-labeling (SDSL)

SDSL is a technique to introduce a paramagnetic spin label into a protein. It is based on a specific reaction between the spin label and an amino acid. In the most

common procedure, a unique sulfhydryl group of a cysteine is selectively modified with a paramagnetic nitroxide reagent^[26]. Single cysteine mutants of HVDAC for the attachment of a spin label were prepared by Thomas Meins. They were modified with the thiol-specific nitroxide spin label reagent (1-oxy-2,2,5,5-tetramethyl-3-pyrroline-3-methyl)-methanethiosulfonate (MTSL). 100 µg/µl MTSL in cold acetone was added to the protein solution at a 3 to 5-fold molar excess and incubated for at least 1.5 h at room temperature. Excess spin label was removed by dialysis. Complete labeling with MTSL was verified by ESI-MS (see 2.2.3.7).

2.2.4 Electrophysiological methods

All solutions used for the electrophysiological investigation of Conk-S1 are summarised in Table 8.

Table 8 Electrophysiological investigation of Conk-S1

Application	Solution name	Substance	Amount	
Digestion of follicular layer	collagenase solution	collagenase type 2	200 mg	
		Ca ²⁺ -free Barth medium	200 ml	
	Ca ²⁺ -free Barth medium	NaCl	84 mM	
		KCl	10 mM	
		NaHCO ₃	2.5 mM	
		Tris/HCl pH 7.4	7.5 mM	
Washing and incubation of oocytes	Barth medium	NaCl	84 mM	
		KCl	10 mM	
		NaHCO ₃	2.5 mM	
			Ca(NO ₃) ₂	6.5 mM
			CaCl ₂	0.6 mM
			Tris/HCl pH 7.4	7.5 mM
			antibiotic solution	2 % (v/v)
	antibiotic solution	cefuroxime / zinnacel 750	4 mg/l	
		penicillin / streptomycin	100U/ml	

		K-aspartate	200 mM
Hypertonic incubation solution	skinning solution	KCl	20 mM
		MgCl ₂	1 mM
		EGTA	10 mM
		HEPES pH 7.4	10 mM
Measuring solution	normal frog Ringer	NaCl	115 mM
		KCl	2.5 mM
		CaCl ₂	1.8 mM
		HEPES pH 7.2	10 mM
Anesthetic for <i>Xenopus laevis</i>	anaesthetic solution	tricaine	2.5 g
		H ₂ O	1 l

2.2.4.1 *Xenopus* oocyte handling

Female *Xenopus laevis* (Fig. 2a) were incubated in anaesthetic solution at 0° C for 30 min. Afterwards the ovarian tissue containing oocytes at different stages of maturation was surgically removed.

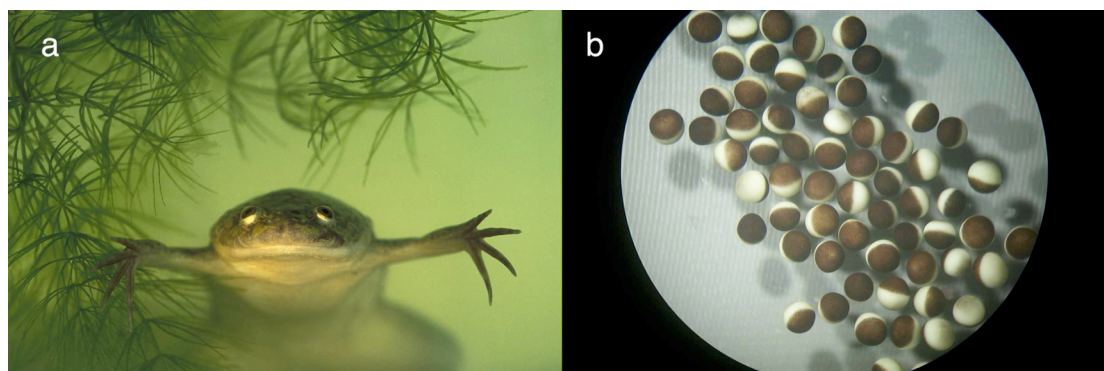


Fig. 2 a) *Xenopus laevis*^[27] b) *Xenopus laevis* oocytes^[28]

This tissue was incubated for 2-3 hours in collagenase solution at 17°C in order to remove the follicular cell layer partially by digestion. The surgery and the following digestion was done by technicians of the molecular and cellular neuropharmacology

group of Heinrich Terlau at the Max-Planck-Institute for experimental medicine in Göttingen. The enzymatic reaction was stopped by washing the oocytes extensively in Barth medium. For further investigation oocytes between stage IV and VI (Fig. 2b) were selected and stored in Barth medium at 17°C. Into each of these oocytes approx. 50 nl of a 0.25 µg/µl cRNA solution of the corresponding Shaker K⁺ channel were injected. Afterwards they were incubated in Barth medium at 17°C for 1-3 days in order to allow the expression of the ion channels. Then the oocytes were incubated in the hypertonic skinning solution for approx. 3 min at room temperature, which induces a shrinking of the oocytes. The outer vitelline membrane of the oocytes was then removed mechanically with fine tweezers. For the electrophysiological measurements the oocytes were washed once with normal frog Ringers (NFR). Finally each of them was placed in a measuring chamber containing NFR.

2.2.4.2 Electrophysiological measurements

Whole-cell currents were recorded under two-electrode voltage-clamp control using a Turbo-Tec amplifier (npi electronic, Tamm, Germany). The intracellular electrodes were filled with 2 M KCl and had a resistance between 0.4 and 1 MΩ. Current records were low-pass filtered at 1 KHz (-3 db) and sampled at 4 kHz. The bath solution was NFR containing 115 mM NaCl, 2.5 mM KCl, 1.8 mM CaCl₂ and 10 mM Hepes (pH 7.2) (NaOH). All electrophysiological experiments were performed at room temperature (19-22 °C). Toxin-containing solutions were applied continuously during the whole experiment from a reservoir through a silicon tube directly into the bath chamber. Whole-cell currents at a test potential of 0 mV were measured every 15 s during toxin application.

The IC₅₀ values of Conk-S1 and its mutants were calculated from the reduction of whole-cell currents at a test potential of 0 mV obtained from oocytes expressing *Shaker* K according to the relationship $IC_{50} = fc/(1-fc)[Tx]$, where *fc* is the fractional current and [Tx] is the toxin concentration. Data are given as means ± the standard deviation (rmsd).

The *k*_{on} and *k*_{off} values were obtained by an exponential fit [$y = y_0 + A \cdot \exp(-k \cdot x)$] to the experimental data during decrease and increase of the current, obtained during the wash-in and wash-out of the peptide. This is possible because the “on” reaction is pseudo first order, due to the constant toxin concentration, and the “off” reaction is first order.

2.2.5 NMR spectroscopy

NMR sample preparation for HVDAC is described in the doctoral thesis of Thomas Meins^[29] and is repeated here in chapter 3.2.1.5 The sample preparation of Conk-S1 is described in chapter 4.2. The chemical shift assignment strategy for the 32 kDa membrane protein HVDAC is given in chapter 3.3.1, for the 7 kDa soluble protein Conk-S1 in chapter 4.2.3. For the HVDAC, all spectra were measured in a TROSY version, with exception of the NOESY-HMQC.

2.2.5.1 Secondary Structure determination

Relative to random coil chemical shifts CA and C' resonances tend to shift upfield in β-strands and extended sheets and downfield in helices. The opposite trend holds for CB resonances^[30]. Therefore secondary structure elements can be identified by subtracting the random coil (δC_{coil}) from the experimental chemical shift (δC_{exp}). Tabulated random coil values were used. The secondary chemical shift ($\Delta\delta C$) is

defined as the difference between δC_{exp} and δC_{coil} . To derive secondary structure information, the secondary chemical shifts were combined using the following formula:

$$\Delta\delta(\text{CA CB C}') = \Delta\delta\text{CA} - \Delta\delta\text{CB} + \Delta\delta\text{C}' \quad (2).$$

If CB chemical shifts were not available $\Delta\delta\text{CA}$ and $\Delta\delta\text{C}'$ were added. In this notation negative secondary chemical shifts indicate β -strands and positive values indicate α -helices.

2.2.5.2 Mapping of interaction sites

Chemical shifts depend on the local electronical environment of a nucleus. If effectors bind to a protein, this environment changes at the interaction site. This causes perturbations of the chemical shifts. These perturbations can be followed in every NMR-spectrum. ^{15}N - ^1H -HSQC or ^{15}N - ^1H -TROSY-HSQC spectra have a high sensitivity. Therefore chemical shift values can be easily followed in the ^{15}N - ^1H -HSQC spectrum during a titration. The titration was done by a stepwise addition of the effector to the desired protein NMR-sample and subsequent recording of a ^{15}N - ^1H -HSQC spectrum. During the titration the pH of the NMR-sample was held constant. The chemical shift perturbations upon receptor addition are commonly combined with the following equation^[31]:

$$\Delta\delta_{\text{HN}} = \sqrt{\frac{(\Delta\delta_{\text{N}} / 5)^2 + (\Delta\delta_{\text{H}})^2}{2}} \quad (3)$$

$\Delta\delta_{\text{HN}}$: average amide chemical shift perturbation

$\Delta\delta_{\text{N}}$: amide nitrogen chemical shift changes

$\Delta\delta_{\text{H}}$: amide proton chemical shift changes

Residues with the largest ^{15}N and ^1H chemical shift changes upon the NMR titration define the binding interface.

2.2.5.3 Solvent exchange experiments

To investigate the solvent accessibility D_2O exchange experiments were carried out. Amide protons, which are involved in tight hydrogen bonds or which are buried in the hydrophobic core of a protein, will exchange much slower with the D_2O than protons, which are exposed to the solvent. Therefore the peak intensity for solvent exposed residues will be reduced in D_2O . For the D_2O exchange the desired NMR-sample was lyophilised and subsequently redissolved in D_2O . Afterwards consecutive TROSY-HSQC spectra were recorded. The first spectrum was recorded 1 h after dissolving the sample in D_2O and ran for 3 h and 13 min. Residues, which did show a peak in this spectrum, were considered to be in secondary structure elements. Residues, which did not show a peak in this spectrum, were considered to be in loops or flexible secondary structure elements.

2.2.5.4. Residual dipolar couplings (RDCs)

2.2.5.4.1 Alignment media

Under isotropic solution condition dipolar couplings average exactly to zero as a result of Brownian rotational diffusion, which is many orders of magnitude faster than the recording of a NMR-signal^[32]. Therefore anisotropic alignment media^[12, 33, 34], which induce a slightly preferred orientation of the molecule, are needed to observe RDCs. Conk-S1 was partially aligned in a non-ionic liquid crystalline medium based on a mixture of *n*-alkyl-poly(ethylene glycol) and *n*-alkyl alcohol^[35] (see 4.2.2). For the alignment of HVDAC charged copolymer gels were tested, which

were especially optimised for integral membrane proteins^[36]. The composition of the charged gels was varied extensively, but in most gels no NMR signal of the ^{15}N , ^2H -HVDAC was observed. This is due to the restriction of rotational diffusion of the protein in the gel^[36]. Signal was observed in a positively charged 5% gel composed of acrylamide and (3-acrylamidopropyl)-trimethylammonium chloride in a 1:1 ratio, both containing N.N'-methylenebisacrylamide in a 37.5:1 ratio. However, the signal to noise ratio was too low to record a 2D TROSY-HSQC.

2.2.5.4.2 RDC measurements

$^1\text{D}_{\text{N-H}}$, $^1\text{D}_{\text{CA-HA}}$, $^1\text{D}_{\text{N-C}}$ and $^1\text{D}_{\text{C-CA}}$ were measured in the quantitative J correlation manner as described in chapter 4.2.3.

2.2.5.4.3 Evaluation of the residual dipolar couplings with PALES^[37]

The magnitude (normalized to $^1\text{D}_{\text{N-H}}$) and rhombicity of the alignment tensor were determined from the histogram of dipolar couplings by the program PALES^[37].

In order to determine the agreement between experimentally observed RDCs and crystal- or NMR-structures the RDCs were back calculated based on the respective structures. This was done using singular value decomposition (SVD) as implemented in PALES. The correlation coefficient of the back calculated and experimental RDCs were used to describe the consistency between the structure and the observed RDCs.

2.2.5.5 Estimation of the molecular weight from $T_{1\rho}$

The rotational correlation time (τ_c) is proportional to the effective hydrodynamic radius (r_H) of a molecule. For approximately spherical globular proteins τ_c can be calculated from Stokes' law^[38]:

$$\tau_c = \frac{4\pi\eta_w r_H^3}{3kT} \quad (4)$$

in which η_w is the viscosity of the solvent, k is the Boltzmann constant and T is the temperature. The hydrodynamic radius can be very roughly estimated from the molecular weight (MW) of a protein by assuming that the specific volume of a protein is $\bar{V} = 0.73 \text{ cm}^3/\text{g}$ and that a hydration layer of $r_w = 1.6$ to 3.2 \AA (corresponding to one-half to one hydration shell) surrounds the protein^[38]:

$$r_H = \left[\frac{3\bar{V}MW}{4\pi N_A} \right]^{\frac{1}{3}} + r_w \quad (5)$$

For 20°C in water solution the combination of equation (3) and (4) gives roughly:

$$\tau_c [\text{ns}] \sim 0.5MW [\text{kDa}] \quad (6)$$

τ_c is proportional to transverse relaxation time $T_{1\rho}$. In the heteronuclear case this gives^[38]:

$$\tau_c [s] = \frac{5r_{AB}^6 64\pi^4}{\gamma_A^2 \gamma_B^2 h^2 \mu_0^2 T_{1\rho}} \quad (7)$$

where r_{AB} is the distance between atom A and B, $\gamma_{A/B}$ is the magnetogyric ratio of atom A or B, h is the Planck constant and μ_0 is the magnetic permeability of the vacuum. For the $T_{1\rho}$ time of the amide nitrogen this results in:

$$\tau_c [\text{ns}] = \frac{1}{1.1T_{1\rho} [s]} \quad (8)$$

The $T_{1\rho}$ time of the amide nitrogen was measured with a spin-lock power of 2.5 kHz. Two 1D experiments with different spin-lock pulse durations were recorded (pulse-sequence is given in Appendix D). The first had a 2 ms (Δ_A) spin-lock pulse, the second a spin lock pulse which length (Δ_B) corresponds to approx. 1.3 times the theoretical relaxation time, estimated from the hypothetical MW. The two spectra were overlaid with X-WINNMR 3.5 and their intensity ratio (I_B/I_A) was determined. The average amide nitrogen $T_{1\rho}$ time is:

$$T_{1\rho} = \frac{\Delta_A - \Delta_B}{\ln(I_B / I_A)} \quad (9).$$

2.2.5.6 Steady state heteronuclear $^{15}\text{N}\{^1\text{H}\}$ -nuclear Overhauser effects (NOEs)

Steady state heteronuclear $^{15}\text{N}\{^1\text{H}\}$ -NOEs were obtained from two spectra, which were recorded in an interleaved manner (pulse-sequence is given in Appendix D). One spectrum was with, the other without proton presaturation during the 5 s relaxation delay. The $^{15}\text{N}\{^1\text{H}\}$ -NOEs for each residue were calculated from the intensity ration of similar $^{15}\text{N}/^1\text{H}$ crosspeaks from both spectra.

2.2.5.7 Paramagnetic relaxation enhancement (PRE)

Enhanced relaxation of the nuclear spins surrounding a paramagnetic centre constituted of one or several unpaired electrons presents one of the most obvious manifestations of paramagnetism^[39]. The relaxation enhancement strongly depends on the distance between the nuclear and the electron spin. Since this effect is visible for significantly longer distances than internuclear interactions long range information can be gained for a molecule with a paramagnetic centre^[40].

For the PRE measurement two TROSY-HSQC spectra were recorded, one with and one without the paramagnetic MTSL-tag (see 2.2.3.8). The peak intensities ratio (I_{para}/I_{dia}) of corresponding $^{15}\text{N}/^1\text{H}$ crosspeaks can be converted in the paramagnetic transverse relaxation rate enhancement (R_2^{para})^[13] by estimating the additional relaxation needed to reduce the peak intensity in the diamagnetic case to the intensity observed in the paramagnetic case. Paramagnetic induced R1 relaxation during t_1 is neglected because it is typically insignificant compared to R2 effects^[41]. Additionally R1 and R2 relaxation effects of the spinlabel on ^{15}N nuclei were considered to be negligible compared to ^1H , because of the lower magnetogyric ratio of ^{15}N (see eq 12)^[13]. R_2^{para} can be calculated from the intensity ratio of a particular amide proton by the following equation^[13]:

$$\frac{I_{para}}{I_{dia}} = \frac{R_2 e^{-R_2^{para} t_{inept}}}{R_2 + R_2^{para}} \quad (10)$$

where R_2 is the intrinsic transverse relaxation rate and t_{inept} is the total inept evolution time (~ 10.5 ms). R_2^{para} is inversely proportional to the distance between the electron and the nuclear spins r ^[13]:

$$r = \left[\frac{K}{R_2^{para}} \left(4\tau + \frac{3\tau_c}{1 + \omega_H^2 \tau_c^2} \right) \right]^{1/6} \quad (11)$$

where τ_c is the correlation time for this electron-nuclear interaction, ω_H is the Lamor frequency of the nuclear spin (proton). K is composed of the physical constants:

$$K = \frac{1}{15} S(S+1) \gamma^2 g^2 \beta^2 \quad (12)$$

in which γ is the nuclear magnetogyric ratio, g is the electronic g factor and β is the Bohr magneton. Overall K is $1.23 \times 10^{-32} \text{cm}^6 \text{s}^{-2}$ ^[42]. For distance calculations τ_c is assumed to be equal to the global correlation time of the protein. Because of low

spectral quality no exact distances were calculated. The residues were rather grouped in two classes. Broadening effects of the MTSL can be observed up to 20-25 Å^[13]. Therefore one group contained peaks, which in the paramagnetic case were broadened beyond detection, indicating that the amide proton was closer than 25 Å to the unpaired electron. The second group contained peaks, which in the paramagnetic case were still detectable, indicating that the amide proton was further than 25 Å away from the unpaired electron.

3

Structural and functional investigation of HVDAC – the first structure of a human, mitochondrial ion channel

3.1 Introduction

The voltage dependent anion channel (VDAC) is a 283 residue protein located in the mitochondrial outer membrane (MOM). It is an aqueous pore and known to be primarily responsible for metabolite flux across the MOM^[43]. In its open state, at low potentials, it is permeable for anions like ATP and ADP. Upon channel closure, at high potentials, it undergoes a selectivity change and small cations like Ca^{2+} can pass^[44]. Therefore it has a regulatory role in the energy metabolism of the mitochondria and is involved in Ca-signalling. Additionally there is substantial evidence that VDAC plays an essential role in apoptosis, because it interacts with different pro- and anti-apoptotic proteins, like tBid^[45] or Bcl-x_L^[46-48].

Mitochondria-dependent apoptosis involves the permeabilisation of both mitochondrial membranes. This leads to release of proapoptotic effectors, like cytochrome c, apoptosis inducing factor (AIF) and endonuclease G^[49]. VDAC has a size exclusion limit of approx. 5 kDa and is therefore not permeable to cytochrome c^[50]. Nevertheless there are strong indications that VDAC is involved in the process of mitochondrial membrane permeabilisation. This has been demonstrated by preventing the Ca^{2+} -induced permeabilisation of the mitochondrial membrane with two polyclonal, specific anti-VDAC antibodies^[51]. These antibodies recognise different VDAC epitopes and inhibit their activity in liposomes. Therefore there are

several models, which try to explain the role of VDAC in apoptosis. Several studies propose a Ca^{2+} -induced formation of a permeability transition pore (PTP), which is big enough to release cytochrome c ^[48, 52, 53]. It is thought, that VDAC is a key component of the PTP^[48, 53-55]. Another model proposes, that the OMM becomes impermeable to small metabolites in early stages of apoptosis^[56]. This would lead to accumulation of metabolites in the inter-membrane space of the mitochondrion resulting in osmotic swelling and disruption of the outer membrane. This hypothesis is based on the fact that VDAC closes upon binding to the proapoptotic protein tBid^[45]. Additionally, Bcl-x_L, an antiapoptotic protein, stabilises the open conformation of VDAC^[46]. Nevertheless, this model disagrees with the fact, that upon VDAC inhibition mitochondrial membrane permeabilisation is inhibited^[51]. If osmotic swelling would induce apoptosis, VDAC inhibition should then rather lead to membrane permeabilisation. A third model proposes, that apoptosis is mediated by large pores formed by Bax alone^[57]. However, Bax-induced apoptosis could be inhibited by selective anti-VDAC antibodies^[51]. This indicates, that Bax induced apoptosis is also dependent on VDAC. However, the involvement of VDAC in apoptosis is a matter of a strong controversy. Recently Baines et al.^[58] demonstrated that by eliminating one or more VDAC isoforms either by genetic knockout or with knock-down using small interfering RNAs, mitochondria were still able to undergo mitochondrial permeability transition in vitro. Yet the authors admit, that cell death in the absence of all three VDAC isoforms may also reflect a defect in the metabolic function of mitochondria, as the VDACS are the most abundant proteins in the mitochondrial outer membrane and maintain homeostasis in ions and other small metabolites.

Due to this diversity of functional models structural information of the VDAC channel and subsequent determination of its binding sites to different effectors could shed light on several aspects of mitochondrial and cellular physiology^[59]. A number of structural models are proposed in the literature. They are based on sequence alignment^[44, 60-62] or biochemical data^[63-66], like accessibility to either proteases or antibodies^[64, 66], or electrophysiological investigations of VDAC-mutants^[63, 65]. All models are consistent in one point. They propose a β -barrel. Nevertheless the models disagree in the number of transmembrane β -strands, which vary from 12 to 19. Additionally they differ in the position of the predicted^[59, 67] N-terminal amphiphilic α -helix. Two models predict the helix to be a part of the barrel wall^[63, 65]. Other models place the helix outside of it^[60, 62, 64].

Further structural information of fungal VDAC could be obtained from 2D crystals by electron microscopy (EM)^[59]. This study provides the molecular envelope with approx. 20 Å resolution. It is consistent with a β -barrel-shape. In general, the barrel wall has several irregular features. It has regions where the walls are shorter than the average, grooves, a flap or a concave bulge. Furthermore the authors propose, that the N-terminal helix is not part of the barrel wall, but extends laterally away from the lumen. Additionally membrane crystals could be obtained from the human VDAC, but diffraction spots extended only up to 8.2 Å^[68]. Similar to the fungal VDAC the authors reported, that the barrel wall has a nonuniform height and that the protein mass is asymmetrically distributed around the diffusion channel.

Since a variety of different structural models has been proposed and structures are only present at very low resolution there is still a strong need for detailed structural information of the VDAC. As described above, membrane proteins are challenging objects to study, both for NMR-spectroscopy and X-ray crystallography.

This is also demonstrated by the fact, that first structural information of the VDAC was present in 1984^[69] and until the year 2007 there was no high resolution structure of the VDAC available. Since until now common methods for high resolution structure determination for the VDAC failed, unconventional methods are required. In collaboration with Thomas Meins, Max-Planck-Institute for Biochemistry, Munich, we determined the high-resolution structure of the biggest part of human VDAC conjointly by NMR-spectroscopy and X-ray crystallography. Only the combination of local information from NMR-spectroscopy and global information from X-ray crystallography is powerful enough to allow a structure determination of this “badly behaved” protein on a reasonable timescale. The human VDAC has indeed a β -barrel fold. It is composed of 18 transmembrane β -strands and an amphiphilic α -helix at the N-terminus, which points inside the barrel in the direction of the C-terminus. It is the first reported structure of a human, mitochondrial integral membrane protein. Furthermore I investigated binding sites for different effectors. It was demonstrated, that the pro-apoptotic protein Bid and the anti-apoptotic Bcl-x_L compete for the same binding site. This site is close to the region, where the N- and the C-terminus close the β -barrel. In contrast to that, interaction sites for nucleotides are distributed over the whole protein.

3.2 Materials and methods

3.2.1 Production of HVDAC1 for NMR analysis

HVDAC1 and its mutants were prepared by Thomas Meins and Christl Weyrauch at the Max-Planck-Institute for Biochemistry in Munich. Later samples were also prepared by Stefan Becker and Karin Giller at the Max-Planck-Institute for

Biophysical Chemistry in Göttingen. This chapter (3.2.1) is taken from the doctoral thesis of Thomas Meins^[29].

3.2.1.1 Cloning of HVDAC1-His₆

The His₆ tagged version of *hVDAC1* was achieved by cloning a *vdac1* containing PCR construct into the pDS56/RBSII-6xHis expression vector yielding pDS56/RBSII-VDAC1His6 (Fig. 3) as described in^[70]

Fig. 3 pDS56/RBSII-VDACHis6-Sequence

```

1  ctcgagaaat cataaaaaat ttattttgctt tgtgagcggg taacaattat aatagattca
61  attgtgagcg gataacaatt tcacacagaa ttcattaaag aggagaaatt aactatgaga
121 ggatccgctg tgccacccac gtatgccgat cttggcaaat ctgccagga tgtcttcacc
181 aagggtatg gattttggctt aataaagctt gatttgaaaa caaatctga gaatggattg
241 gaatttaca gctcaggctc agccaacact gagaccacca aagtgacggg cagtctggaa
301 accaagtaca gatggactga gtacggcctg acgtttacag agaaatggaa taccgacaat
361 aactaggca ccgagattac tgtggaagat cagcttgcac gtggactgaa gctgacctc
421 gattcatcct tctcacctaa cactgggaaa aaaaatgcta aatcaagac aggtacaag
481 cgggagcaca ttaacctggg ctgcgacatg gatttcgaca ttgctggcc tccatccgg
541 ggtgctctgg tgctaggtta cgagggtggt ctggccggct accagatgaa tttgagact
601 gcaaaatccc gagtgaccca gagcaacttt gcagttggct acaagactga tgaattccag
661 cttcacacta atgtgaatga cgggacagag tttggcggct ccattacca gaaagtgaac
721 aagaagttgg agaccgctgt caatcttgcc tggacagcag gaaacagtaa cacgcgctc
781 ggaatagcag ccaagtatca gattgaccct gacgcctgct tctcggctaa agtgaacaac
841 tccagcctga taggtttagg atacactcag actctaaagc caggtattaa actgacactg
901 tcagctcttc tggatggcaa gaacgtcaat gctggtggcc acaagcttgg tctaggactg
961 gaatttcaag caagatctca tcaccatcac catcactaag cttaattagc tgagcttggg
1021 ctctgttga tagatccagt aatgacctca gaactccatc tggatttgtt cagaacgctc
1081 ggttgccgcg gggcgttttt tattggtgag aatccaagct agcttggcga gatttccag
1141 agctaaggaa gctaaaatgg agaaaaaaat cactggatat accaccgttg atatatccca
1201 atggcatcgt aaagaacatt ttgaggcatt tcagtcagtt gctcaatgta cctataacca
1261 gaccgttcag ctggatatta cggccttttt aaagaccgta aagaaaaata agcacaagtt
1321 ttatccggcc tttattcaca ttcttgcccg cctgatgaat gctcatccgg aatttcgtat
1381 ggcaatgaaa gacggtgagc tggatgatag ggatagtgtt cacccttgtt acaccgtttt
1441 ccatgagcaa actgaaacgt tttcatcgct ctggagtgaa taccacgacg atttccggca
1501 gtttctacac atatattcgc aagatgtggc gtgttacggt gaaaacctgg cctatttccc
1561 taaagggttt attgagaata tgtttttcgt ctcagccaat ccctgggtga gtttaccag
1621 ttttgattta aacgtggcca atatggacaa cttcttcgcc cccgttttca ccatgggcaa
1681 atattatacg caaggcgaca aggtgctgat gccgctggcg attcaggttc atcatgccgt
1741 ctgtgatggc ttccatgtcg gcagaatgat taatgaatta caacagtae gcgatgagtg
1801 gcagggcggg gcgtaatttt ttaaggcag ttattggtgc cttaaaacgc ctgggtaat
1861 gactctctag cttgaggcat caataaaac gaaaggctca gtcgaaagac tggcctttc
1921 gttttatctg ttgtttgcg gtgaacgctc tcctgagtag gacaaatccg ccgctctaga
1981 gctgcctcgc gcgtttcggg gatgacggtg aaaacctctg acacatgcat ctcccggaga
2041 cggtcacagc ttgtctgtaa gcggatgccg ggagcagaca agcccgtcag ggcgcgtcag
2101 cgggtgttgg cgggtgtcgg ggcgcagcca tgaccagtc acgtagcgtt agcggagtgt
2161 aacttgctt aactatgcgg catcagagca gattgtactg agagtgcacc atatgcggtg
2221 taaaataccg cacagatgcg taaggagaaa ataccgcatc aggcgctctt ccgcttctc
2281 gctcactgac tcgctgcgct cggctctgct gctgcggcga gcggtatcag ctcactcaa
2341 ggcggttaata cggttatcca cagaatcagg ggataacgca ggaagaaca tgtgagcaa
2401 aggccagcaa aagccagga accgtaaaaa gcccgcgttg ctggcgtttt tccataggt

```

2461 cgcgccccct gacgagcatc acaaaaatcg acgctcaagt cagaggtggc gaaacccgac
2521 aggactataa agataccagg cgtttcccc tggaaagctcc ctctgtgcgt ctctgtttcc
2581 gaccctgccc cttaccggat acctgtccgc ctttctccct tcgggaagcg tggcgctttc
2641 tcaatgctca cgctgtaggt atctcagttc ggtgtaggtc gttcgctcca agctgggctg
2701 tgtgcacgaa cccccggtc agcccgaccg ctgcgcctta tccggtaact atcgtcttga
2761 gtccaacccg gtaagacacg acttatcgcc actggcagca gccactggta acaggattag
2821 cagagcgagg tatgtaggag gtgctacaga gttcttgaag tggtaggcta actacggcta
2881 cactagaagg acagtatttg gtatctgcgc tctgctgaag ccagttacct tcggaaaaag
2941 agttggtagc tcttgatccg gcaaaaaaac caccgctggt agcggtaggt tttttggtt
3001 caagcagcag attacgcgca gaaaaaaaag atctcaagaa gatccttga tcttttctac
3061 ggggtctgac gctcagtgga acgaaaaactc acgttaaggg attttgggtca tgagattatc
3121 aaaaaggatc ttcacctaga tcctttttaa ttaaaaaatga agtttttaaat caatctaaag
3181 tatatatgag taaacttggg ctgacagtta ccaatgctta atcagtgagg cacctatctc
3241 agcgatctgt ctatttcggt catccatagc tgcctgactc cccgtcgtgt agataactac
3301 gatacgggag ggcttaccat ctggccccag tgctgcaatg ataccgcgag acccagcctc
3361 accggctcca gatttatcag caataaacca gccagccgga agggccgagc gcagaagtgg
3421 tcctgcaact ttatccgcct ccatccagtc tattaattgt tgccgggaag ctagagtaag
3481 tagttcgcca gttaatatgt tgcgcaacgt tgttgccatt gctacaggca tcgtggtgct
3541 acgctcgtcg tttggtagtg cttcattcag ctccggttcc caacgatcaa ggcgagttac
3601 atgatcccc atggtgtgca aaaaagcggg tagctccttc ggtcctccga tcggtgtcag
3661 aagtaagttg gccgcagtggt tatcactcat ggttatggca gcactgcata attctctac
3721 tgtcatgcca tccgtaagat gcttttctgt gactggtgag tactcaacca agtcattctg
3781 agaatagtgt atgcggcgac cgagttgctc ttgcccggcg tcaatacggg ataataccgc
3841 gccacatagc agaactttaa aagtgtcat cattggaaaa cgttcttcgg ggcgaaaact
3901 ctcaaggatc ttaccgctgt tgagatccag ttcgatgtaa cccactcgtg cacccaactg
3961 atcttcagca tcttttactt tcaccagcgt ttctgggtga gcaaaaacag gaaggcaaaa
4021 tgccgcaaaa aaggaataa gggcgacacg gaaatgttga atactcatac tcttcctttt
4081 tcaatattat tgaagcattt atcaggggta ttgtctcatg agcggatata tatttgaatg
4141 tatttagaaa aataaacaaa taggggttcc gcgcacattt cccgaaaag tgccacctga
4201 cgtctaagaa accattatta tcatgacatt aacctataaa aataggcgta tcacgagggc
4261 ctttcgtctt cac

3.2.1.2 Site directed mutagenesis of HVDAC1-His₆

Point mutations were introduced into the pDS56/RBS2-His6 cloned HVDAC1 gene with the QuickChange[®] site-directed mutagenesis kit (Stratagene, La Jolla, USA), which used essentially as recommended by Stratagene[™]. The primers for introduction of the indicated point mutations are summarised in Table 9. Double and multi mutants were achieved one after another by introduction of a further point mutation in already mutated plasmids. Successful mutagenesis was verified by DNA sequence analysis.

Table 9 Oligonucleotide primer for the mutagenesis of HVDAC1-His₆

pDS56/RBS2- HVDAC1His6/[mutant]	pDS56/RBS2- HVDAC1His6/[host]	primer
C130S	nativ	5'-gagcacattaacctgggctccgacatggatttcgacattg-3' 5'-caatgtcgaaatccatgtcggagcccagggttaatgtgctc-3'

pDS56/RBS2- HVDAC1His6/[mutant]	pDS56/RBS2- HVDAC1His6/[host]	primer
C235S	nativ	5'-gattgaccctgacgcctccttctcggttaaagtg-3' 5'-cactttagccgagaaggaggcgtcagggccaatc-3'
C130S / C235S	C130S	5'-gattgaccctgacgcctccttctcggttaaagtg-3' 5'-cactttagccgagaaggaggcgtcagggccaatc-3'
S49C / C130S / C235S	C130S / C235S	5'-gaatttacaagctcaggctgcgccaacactgagaccacc-3' 5'-ggtggctcagtggtggcgcagcctgagctttaaattc-3'
S263C / C130S / C235S	C130S / C235S	5'-gtattaaactgacactgtgcgctcttctggatggcaag-3' 5'-cttgccatccagaagagcgcacagtgtcagtttaatac-3'
V20C / C235S	C235S	5'-caaattctgccagggatgcttcaccaagggctatg-3' 5'-catagcccttggtgaagcaatccctggcagatttg-3'

3.2.1.3 Expression of HVDAC1-His₆

All solutions, buffers and media were sterilised by filtration. Applied laboratory ware for bacterial cultivation was heat sterilized at 180 °C for 3 h prior to utilization. All antibiotics were dissolved in 70% ethanol and stored at -20 °C until use. Antibiotics containing media were supplemented with 100 µg/ml ampicillin and if indicated additionally with 25 µg/ml kanamycin shortly before use. Antibiotics containing media are labelled in the following by the indices [media]^{Amp} or [media]^{Amp/Kan}. If not indicated otherwise all cultures were grown in 100% deuterium oxide (D₂O; OntarioPower, Pickering, Canada).

3.2.1.3.1 Expression of ²H, ¹⁵N and ¹³C labelled HVDAC1-His₆

²H, ¹⁵N and ¹³C labelled HVDAC1-His₆ was expressed in the *Escherichia coli* strain M15 [prep4] (Quiagen, Hilden; phenotype: *E. coli* K12 NaI^S Str^S Rif^S Thi⁻ Lac⁻ Ara⁺ Gal⁺ Mtl⁻ F⁻ RecA⁺ Uvr⁺ Lon⁺; carries prep4 (*lacI* encoding repressor plasmid)). Cells were grown in M9 minimal medium (see Table 6). According to labelling requirements, ammonium chloride and glucose have been replaced by ¹⁵N-Ammonium Chloride (¹⁵N, 99%; Larodan Fine chemicals, Malmö, Sweden) and ¹³C-D-Glucose (¹³C6, 99%; D7, 97-98%; Larodan Fine chemicals, Malmö, Sweden) in the expression cultures. Labelled compounds containing media are in the following indicated as ¹⁵N-[media] and ¹⁵N ¹³C-[media], respectively.

Pre-cultures of PDS/RBSII-VDAC1His6 transformed *E. coli* DM15 (prep4) cells were initially grown on non-deuterated M9^{Amp/Kan} at 37°C and 200 rpm overnight. In order to adapt the culture to D₂O based media the cells were consecutively inoculated to ²H-M9^{Amp/Kan} with a D₂O content of 70, 80 and at last 100%. Each culture was thereby incubated for 24 h at 37°C and 200 rpm. After adaption, 1.5 l expression cultures of [²H, ¹⁵N]-M9^{Amp/Kan} or [²H, ¹⁵N, ¹³C]-M9^{Amp/Kan} were inoculated to an OD₆₀₀ of 0.1 AU and incubated in 5 l baffled Erlenmeyer flasks at 37 °C and 200 rpm. Adding IPTG to a final concentration of 1 mM at an OD₆₀₀ of 0.8 AU induced HVDAC I-His₆ inclusion body formation. Cells were harvested 8 h after induction by centrifugation at 5000 g for 30 min, shock frozen in liquid N₂ and stored at -70 °C..

3.2.1.3.2 Expression of selective labelled HVDAC1-His₆

Selective labelled HVDAC1-His₆ was expressed in the amino transferase negative *Escherichia coli* strain DL39 [prep4]. *E. coli* DL39 [prep4] was constructed by transformation of *E. coli* DL39 CGSC#:6913 (CGSC, Yale, USA; phenotype: *F araD139 D(argF-lac)Ui69 rpsL150 relA1 thiA zei-724: :Tn10 glpR gyrA D(glpT-glpA)593*) with the prep4 plasmid via electroporation. The prep4 plasmid was purified from *E. coli* M15 [prep4] (Quiagen, Hilden) overnight cultures using the Qiaprep[®] Miniprep protocol as recommended by Quiagen[™].

E. coli DL39 was grown in algal extract supplemented (AES) media^[71] (Table 10, 11, 12). Selective labelling was achieved by adding the respective labelled amino (Table 13) acids 15 min prior to induction in a tenfold excess compared to the algal extract source to the expression culture.

Table 10 Algal extract supplemented media (AES media)^[71]

substance	amount
M9 Salt deuterated (10x) v.s.	100 ml
Glucose (10% w/v)	10 ml
MgSO ₄ (0.1 M)	20 ml
L-leucine [§]	0.25 g
Vitamin mix	5 ml
Trace element solution	1 ml
Deuterated algal lysate amino acid mixture (10% w/v)*	10 (30) ml [#]
D ₂ O	Ad up to 1000 ml

*) The deuterated algal lysate amino acid mixture was produced and characterised at the MPI of Biochemistry; Dept. of Membrane Biochemistry as described in^[72]. #) Preparatory cultures and overproduction cultures contained 30 ml and 10 ml of the algal extract, respectively. §) The overproduction culture for selective leucine labelling contained no unlabeled leucine.

Table 11 Vitamin mix

substance	amount
Thiamine (B ₁)	100 mg
d-biotin (H)	20 mg
Choline bromide	20 mg
Folic acid (B ₉)	20 mg
Niacin amide (B ₃)	20 mg
d-panthothenic acid (B ₅)	20 mg
Pyridoxal (B ₆)	20 mg
Riboflavin (B ₂)	20 mg
Tris-base (saturated)	0.2 ml
D ₂ O	Ad up to 100 ml

Table 12 Trace element solution

substance	amount
HCl (5M)	16 ml
FeCl ₂ × 4H ₂ O	10 g
CaCl ₂ × 2H ₂ O	370 mg
H ₃ BO ₃	130 mg
CoCl ₂ × 6H ₂ O	36 mg
CuCl ₂ × 2H ₂ O	8 mg
ZnCl ₂	680 mg

substance	amount
Na ₂ MoO ₄ × 2H ₂ O	1.21 g
MnCl ₂ × 4H ₂ O	80 mg
D ₂ O	Ad up to 1000 ml

Table 13 Labeled amino acids

Amino Acid (AA)	Amount AA per 500 ml expression culture
L-Methionine (15N, 95-99%)*	90 mg
L-Leucine (U-13C6, 98%; 15N)*	80 mg
L-Isoleucine (U-13C6,98%; 15N, 98%)*	50 mg
L-Phenylalanine (15N, 98%)*	150 mg
L-Valine (U-13C5,98%; 15N)*	70 mg
DL-Lysine 2HCl (15N2, 98%) [#]	250 mg
L-Tyrosine (15N, 98%) [#]	80 mg
L-Arginin HCl (15N4, 98%) [#]	100 mg
DL-Alanine (15N, 98%) ^S	250 mg

Amino acids were purchased from *) Euriso-top, Saint-Aubin Cedex, France. [#]) OMNI Life Science, Bremen. ^S) Sigma-Aldrich, St. Louis, USA.

Pre-cultures of PDS56/RBSII-VDAC1His6 transformed *E. coli* DDL39 (prep4) cells were initially grown overnight in partially deuterated AES^{Amp/Kan} at 37°C and 200 rpm. In order to adapt the culture to D₂O based media the cells were consecutively inoculated to AES^{Amp/Kan} with a D₂O content of 70, 80 and at last 100%. Each culture was thereby incubated for 24 h at 37°C and 200 rpm. After adaption, 2.0 l pre-cultures of AES^{Amp/Kan} were inoculated to an OD₆₀₀ of 0.1 AU and incubated in 5 l baffled Erlenmeyer flasks at 37 °C and 200 rpm. At an OD₆₀₀ of 0.5 AU, cells were harvested by centrifugation at 5000 g for 30 min and resuspended in 500 ml ²H-M9. The cells were harvested again at 5000 g for 30 min and resuspended in 500 ml AES^{Amp/Kan} for overproduction. The expression culture was further incubated in 2.5 l baffled Erlenmeyer flasks at 37 °C and 200 rpm. After 45 min of incubation the culture was supplemented with the labelled amino acid and

further 15 min later with IPTG to a final concentration of 1 mM. Cells were harvested 12 h after induction by centrifugation at 5000 g for 30 min, shock frozen in liquid N₂ and stored at -70 °C until further use.

3.2.1.4 Purification and refolding of HVDAC1-His₆

3.2.1.4.1 Purification of HVDAC1-His₆ inclusion bodies

Cells were resuspended in buffer 1 (100 mM Tris/HCl pH 7,5; 1 mM EDTA; 5 mM DTT, 100 mM NaCl, 0.2 mM PMSF) and incubated with 0,1 mg/ml Lysozym for 0.5 h. After addition of 1 mM MgCl₂, 0.1 mM MnCl₂ and 0.05 mg/ml DNase I the cells were finally lysed by two French press passes. Inclusion bodies were harvested by centrifugation at 5000 x g for 30 min at 4 °C. The pellet was resuspended in buffer 1 containing 3% w/v OPOE, stirred for 2 h at room temperature and pelleted by centrifugation at 5000 x g for 30 min at 4 °C followed. Finally the pellet was washed with buffer 1 to remove detergent contaminations. Inclusion bodies were then solubilized in buffer 2 (100 mM Tris/HCl pH 7,5; 1 mM EDTA; 5 mM DTT, 6 M guanidinium chloride) and insoluble material was removed by centrifugation at 100 000 x g for 45 min. The denatured HVDAC I-His₆ protein containing supernatant was adjusted with buffer 2 to 15 mg/ml and stored at -70°C.

3.2.1.4.2 Refolding of denatured HVDAC1-His₆

HVDAC I-His₆ refolding was performed at 4 °C by dropwise dilution of solubilized protein in buffer 3 (100 mM Tris/HCl pH 8,0; 1 mM EDTA; 5 mM DTT, 1% w/v LDAO) until a final concentration of 0.6 M guanidinium chloride was reached. The resulting protein solution was stirred over night at 4 °C, centrifuged at 100 000 x g for 45 min and finally 5-fold diluted with buffer 4 (100 mM phosphate buffer pH 7.5).

3.2.1.4.3 Purification of refolded HVDAC1-His₆

The HVDAC I-His₆ protein was bound to a 5 ml Ni²⁺-Sepharose HP column (GE Healthcare), washed with 100 ml buffer 5 (20 mM phosphate buffer pH 7,5; 20 mM imidazole; 0,2% LDAO) and afterwards eluted by 50 ml buffer 6 (20 mM phosphate buffer pH 7,5; 300 mM imidazole; 0,2% LDAO).

3.2.1.5 Preparation of HVDAC1-His₆ NMR samples

HVDAC I-His₆ containing fractions were verified by SDS PAGE and pooled. After determination of the protein concentration at 280 nm wavelength, the HVDAC1-His₆ sample was supplemented with a certain amount of a 15% LDAO solution, depending on the HVDAC1-His₆ concentration. The LDAO volume was adjusted in a way that after concentration of the protein to 0.6 mM the LDAO concentration was 6%. After LDAO addition the sample was dialysed against buffer 7 (25 mM BisTris/HCl pH 6.5, 0.2% LDAO) for 4 h and concentrated with a centrifugal filter device (Amicon Ultra- 30k, Millipore) to a protein content of 0.6 mM HVDAC I-His₆. NMR samples were further supplemented with 0.05% sodium azide and stored at 4 °C until measurement.

3.2.2 NMR samples

NMR spectra of HVDAC were recorded from different samples. They all contained 0.6 mM HVDAC in an aqueous solution of 25 mM BisTris buffer, pH 6.8, and approx. 250 mM Lauryldimethylamine-oxide (LDAO), with 10% D₂O. Assignment spectra were measured on a perdeuterated and ¹⁵N/¹³C-labelled HVDAC sample. ¹⁵N-edited NOESY spectra were measured from a perdeuterated and ¹⁵N/¹³C labelled and an approx. 75% deuterated ¹⁵N-labelled sample. Additionally the 75%

deuterated sample was lyophilised and redissolved in 100% D₂O. TROSY-HSQC spectra were measured from different amino acid specific ¹⁵N and ¹⁵N/¹³C-labelled samples, respectively: ²H-HVDAC-¹⁵N-Met-¹⁵N/¹³C-Leu-¹⁵N/¹³C-Ile, ²H-HVDAC-¹⁵N/¹³C-Val, ²H-HVDAC-¹⁵N-Tyr, ²H-HVDAC-¹⁵N-Ala, ²H-HVDAC-¹⁵N-Phe, ²H-HVDAC-¹⁵N-Lys, ²H-HVDAC-¹⁵N-Arg. Furthermore TROSY-HSQC spectra were measured from different HVDAC mutants: C130S, C235S, C235SV20C, C235SL34C, C235SC130SS49C, C235SC130SS263C. All mutants were approx. 75% deuterated and ¹⁵N-labelled.

3.2.3 NMR Spectroscopy

All spectra were recorded at 37 °C on either Bruker 600, 800 or 900 MHz spectrometers equipped with cryogenic probeheads. Three different TROSY-type triple resonance experiments were recorded: HNCA, HNCOC and multiple quantum (mq) HNCOCA. Additionally ¹⁵N-edited ¹H-¹H NOESY-TROSY^[73] spectra and a mixed-time parallel evolution HMQC-NOESY^[74] spectrum were recorded. The summary of which spectrum was measured on which sample can be found in Table 14. Paramagnetic relaxation enhancement (PRE) data were gained by measuring TROSY-HSQC spectra of MTSL-labelled single cysteine mutants (see 2.2.3.8) of HVDAC and the corresponding reference spectrum without MTSL. Dynamics were studied by measuring steady state heteronuclear ¹⁵N{¹H}-NOEs in a TROSY version^[75] in an interleaved manner. The molecular weight of the protein/micelle complex was estimated by recording a ¹⁵N-edited 1D T1ρ experiment. The NMR data were processed and analyzed using NMRPipe, NMRDraw^[76] and SPARKY (T. D. Goddard and D. G. Kneller, SPARKY 3, University of California, San Francisco, CA).

Table 14 Assignment- and NOESY-spectra

Sample	Experiment	Experimental details	Spectrometer	Remarks
$^2\text{H}(99\%)/^{13}\text{C}/^{15}\text{N}$	TROSY-HNCA	45x25x512 pts, NS 60	900 ^{CRYO}	
$^2\text{H}(99\%)/^{13}\text{C}/^{15}\text{N}$	TROSY-HNCA	47x25x512 pts, NS 56	900 ^{CRYO}	distinguish noise peaks
$^2\text{H}(99\%)/^{13}\text{C}/^{15}\text{N}$	TROSY-HNCA	42x18x512 pts, NS 80	800 ^{CRYO}	optimised to $^2\text{J}_{\text{N-C}\alpha}$
$^2\text{H}(99\%)/^{13}\text{C}/^{15}\text{N}$	TROSY-HNCO	30x30x512 pts, NS 36	600 ^{CRYO}	
$^2\text{H}(99\%)/^{13}\text{C}/^{15}\text{N}$	mq-TROSY-HNCOCA	12x20x512 pts, NS 268	600 ^{CRYO}	
$^2\text{H}(99\%)/^{13}\text{C}/^{15}\text{N}$	15N-NOESY-TROSY	94x20x512 pts, NS 32, 160 ms mixing time	800 ^{CRYO}	high resolution, low sensitivity
$^2\text{H}(75\%)/^{15}\text{N}$	15N-NOESY-TROSY	60x25x512 pts, NS 48, 100 ms mixing time	900 ^{CRYO}	low resolution, high sensitivity
$^2\text{H}(75\%)/^{15}\text{N}$ in 100% D ₂ O	15N-NOESY-TROSY	53x25x512 pts, NS 48, 180 ms mixing time	900 ^{CRYO}	D ₂ O exchange
$^2\text{H}(50\%)/^{15}\text{N}$	15N-NOESY-TROSY	107x19x512 pts, NS 32, 90 ms mixing time	900 ^{CRYO}	
$^2\text{H}(75\%)/^{15}\text{N}$ C235SV20C	15N-NOESY-HMQC	91x25x512 pts, NS 26, 120 ms mixing time	800 ^{CRYO}	

3.2.4 Structure determination by NMR Spectroscopy and X-ray crystallography

The backbone resonance assignment of the NMR-spectra was achieved based on C α chemical shifts and interstrand HN-HN NOEs. Amino acid specific ^{15}N -labelling, chemical shift perturbations due to mutations and PRE data helped with the assignment process. Based on the interstrand HN-HN NOEs a topology model for the backbone with atomic resolution was built.

Parallel to the NMR-investigations HVDAC 1 was crystallised by Thomas Meins for X-ray structure determination. The used SeMet and Pt MAD data sets were collected at the ESRF beamlines ID29 and ID23-1. During the data collection, crystals were maintained at 100 K by a gaseous nitrogen stream. Diffraction data was integrated with MOSFLM^[77], XDS^[78] and d*TREK^[79]. Data scaling and merging was done with SCALA^[80] and prepared by SHELXC for heavy atom substructure determination in SHELXD^[81]. Refinement of Se and Pt sites as well as the phase probability calculations were carried out in SHARP^[82]. Subsequent density modification using different values for solvent content was done with SOLOMON^[83]. Further phase improvement was attempted using inter-crystal averaging of

isomorphous datasets with DMMULTI^[84]. Map interpretation was started by placing poly-alanine fragments of high-resolution beta barrel protein structures (PDB ID 1PRN, 2F1C) in B-factor sharpened^[85] electron density maps with MOLREP^[86]. Subsequent manual placement of further beta-sheets and iterative model building and geometry refinement was performed with O^[87] and COOT^[88], respectively. This resulted in a poly-alanine structural model of HVDAC. The alanines were exchanged manually to the correct amino acid based on the NMR-derived topology model. The starting point for this exchange was the selenium site M132. The rest of the molecule was then oriented and remodelled according to the interstrand HN-HN NOEs, which were translated in hydrogen bonds and the selenium sites, M158 and M230 in COOT. Positioning of the predicted N-terminal helix was done by fitting a model helix into a corresponding portion of the electron density map. Orientation and fitting of the α -helix was verified through the selenium site of M13.

3.3 Results

3.3.1 NMR Resonance Assignment Strategy

Because of strong relaxation, the standard heteronuclear (¹H, ¹³C, ¹⁵N) assignment strategy^[89] was very difficult to use. Out of this standard experiments the HNCA and the HNCO could be recorded. Therefore sequential information was only available for CA chemical shifts. Problematic was the fact, that only 50 % of the expected CA_{i-1} peaks were present in the HNCA spectrum. Therefore, based on the HNCA spectrum, an overall sequential resonance assignment of 50 % could maximally be achieved. To circumvent this, a modified version of the HNCA was recorded. Usually in an HNCA the insensitive nuclei enhancement by polarisation

transfer (INEPT) from N to CA is optimised to the $^1J_{N-CA}$ coupling. This is done by maximising the term, in which the $^1J_{N-CA}$ is modulated by the sinus:

$$2N_yCA_z \text{Sin}[\pi \cdot ^1J_{N-CA} \cdot t] \cdot \text{Cos}[\pi \cdot ^2J_{N-CA} \cdot t] \cdot \text{Exp}[-t/T_2] \quad (13).$$

T_2 is the transverse relaxation time, and t is the INEPT delay. To enhance the CAi-1 peak, the term, in which the $^2J_{N-CA}$ is modulated by the sinus, has to be maximised:

$$2N_yCA_z \text{Sin}[\pi \cdot ^2J_{N-CA} \cdot t] \cdot \text{Cos}[\pi \cdot ^1J_{N-CA} \cdot t] \cdot \text{Exp}[-t/T_2] \quad (14).$$

$^1J_{N-CA}$ was set to 10.9 Hz, $^2J_{N-CA}$ to 8.3 Hz. T_2 was estimated from $T1\rho$ measurements and was set to 25 ms. This led to a maximum at $t = 15.6$ ms. The resulting HNCA spectrum displayed 60 % of the expected CAi-1 peaks. Further improvement in the number of CAi-1 peaks could be obtained by recording a multiple quantum version of a TROSY-HNCOCA, which was kindly provided by Roland Riek (Salk Institute, La Jolla). This finally led to 70 % of the expected CAi-1 peaks, which gives rise to a sequential resonance assignment limit of 70 %, based on the HNCA.

The chemical shift dispersion of CA's is approx. 21 ppm^[38]. Compared to the approx. 55 ppm dispersion of the CB's this is rather small. This leads to the fact that CA chemical shifts appear for the most amino acids in a very similar range. Consequently the amino acid type cannot be unambiguously established from CA chemical shifts alone. This problem was solved by the preparation of different amino acid specific ^{15}N or $^{15}\text{N}/^{13}\text{C}$ -labelled samples. Initially a sample design as proposed by Shi et al.^[90] was planned. They choose two amino acids for $^{15}\text{N}/^{13}\text{C}$ -labelling, which can be readily distinguished by their carbon chemical shifts. Additionally, a third amino acid was ^{15}N -labelled. With such a sample the amino acid type of three residues can be established. Furthermore sequential information can be gained for the two $^{15}\text{N}/^{13}\text{C}$ -labelled residues from e.g. HNCA spectra, if they appear pairwise in the sequence. Based on this scheme a ^{15}N -Met, $^{15}\text{N}/^{13}\text{C}$ -Leu and $^{15}\text{N}/^{13}\text{C}$ -Ile (ILM)

labelled HVDAC sample was prepared. Unfortunately the concentration of ^{15}N and ^{13}C labels was too low to record a HNCA spectrum. Nevertheless, the ^{15}N -TROSY-HSQC spectrum of the ILM labelled sample, which ran for 35 h, exhibited 41 of the 43 expected peaks (95 %). Therefore following selectively labelled samples contained only 1 amino acid, which was ^{15}N -labelled (see 3.2.2). Figure 4 shows the overlay of the TROSY-HSQC spectra for the different selectively labelled samples.

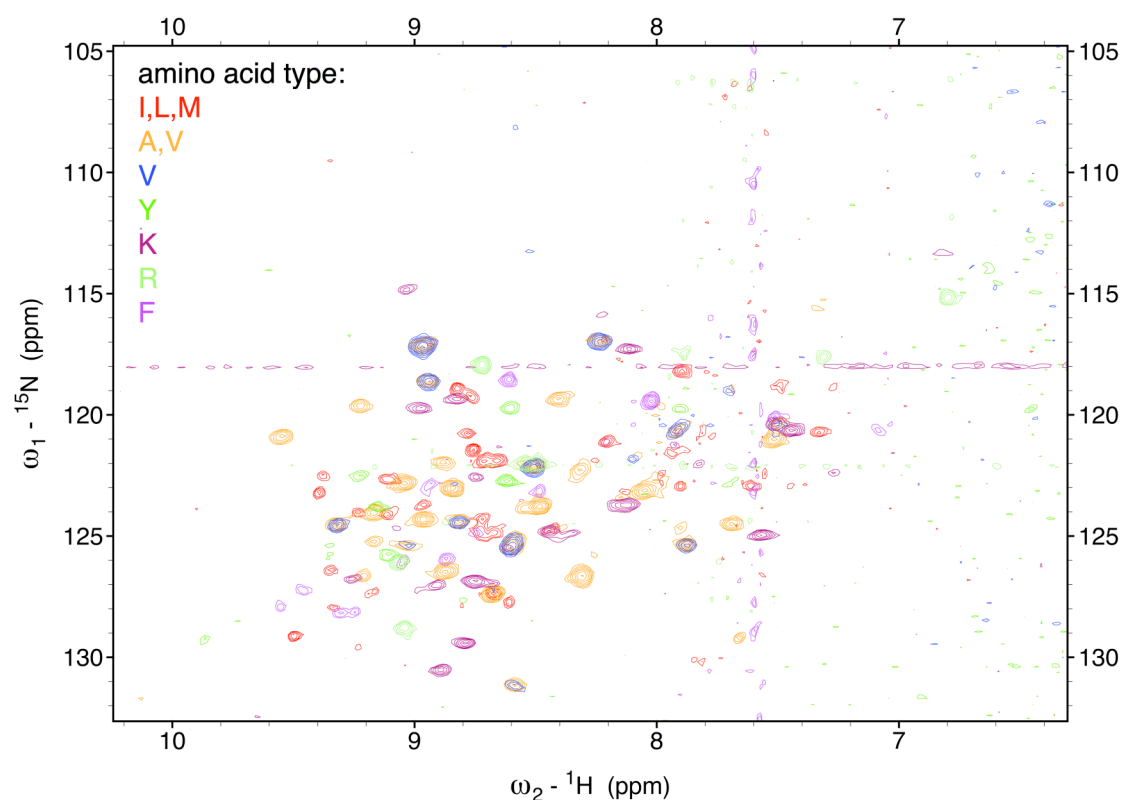


Fig. 4 Overlay of the TROSY-HSQC spectra for the amino acid specific labelled HVDAC samples.

A further problem, which is caused by the low dispersion of the CA chemical shifts, is the strong ambiguity in the sequential information. Every CA frequency appears very often in the spectrum (Fig. 5). Therefore the major effort during assignment was to exclude wrong connectivities. On the one hand this was done based on the selectively labelled samples, on the other hand mutations were helpful, which caused chemical shift perturbations in the NMR-spectra. These perturbations

appear only for residues, which upon mutation experience a different electronic environment, i.e. residues close to the mutation site. Moreover, single cysteine mutants have been modified with the paramagnetic spin label MTSL (2.2.3.8). Due to paramagnetic relaxation enhancement, peak intensities of residues, which are closer than 20-25 Å to the spin label, are reduced^[13]. This helped both for the sequential assignment and for the establishment of the topology model.

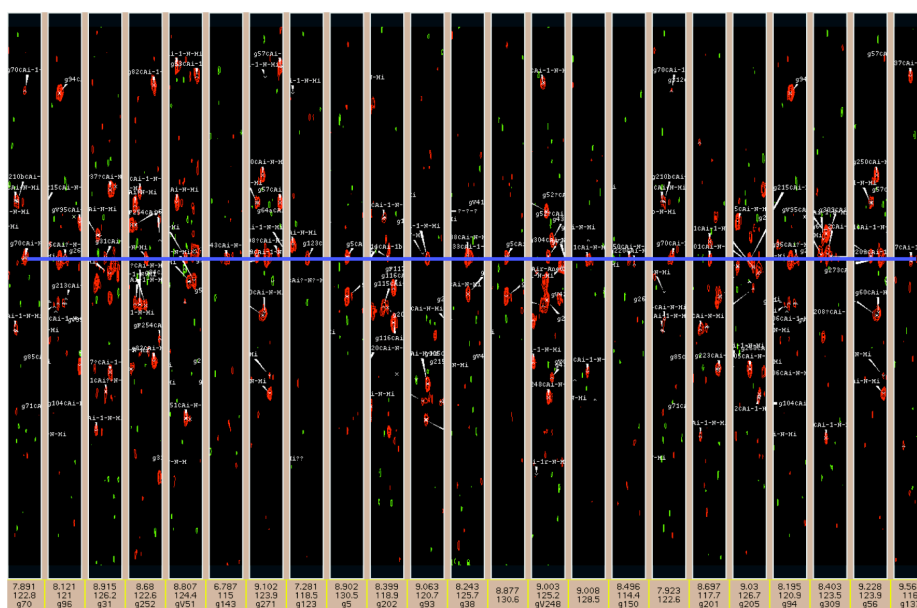


Fig. 5 Strips from the TROSY-HNCA spectrum. The blue bar points out peaks with, in the range of the error, similar CA chemical shifts.

Mainly, the topology model relied on HN-HN interstrand long range NOE's. Additionally the HN-HN NOE's were used to verify the sequential assignment. If inter-strand NOE's could be established, the sequential assignment was considered to be reliable. To maximise the information from NOE's 5 ¹⁵N-edited NOESY spectra were recorded on different samples (see Table 14). The samples were either 50, 75 or 99 % deuterated. The NOESY-TROSY spectrum of the 99% deuterated sample displayed only HN-HN crosspeaks, the 75% had additional crosspeaks to aromatic

and very few to HA protons. Due to strong relaxation, no additional information was gained from the 50% deuterated sample. Initially it was prepared to observe sequential HN-HA crosspeaks. To reduce overlap and determine residues, which are involved in tight hydrogen bonds, one NOESY-TROSY was recorded in 100% D₂O. Because of rapid exchange of the amide protons with the solvent only 19 crosspeaks could still be observed. The NOESY-TROSY spectra were recorded either with low resolution and higher sensitivity or vice versa. In addition to the NOESY-TROSY spectra one HMQC-NOESY^[74] spectrum was recorded on the C235SV20C mutant of HVDAC. In this spectrum the frequency labelling of the NOE-crosspeaks takes place in the direct dimension and therefore the crosspeak-frequency is very well resolved.

Only the combination of all information from the different assignment and NOESY spectra and from various selectively labelled and mutant samples made the assignment process and the establishment of the topology model possible.

3.3.2 Resonance Assignment and Secondary Structure

The molecular weight of the HVDAC/LDAO complex was estimated by T1ρ measurements (see 2.2.5.5) to be approx. 100 kDa. For a complex of that size, the ¹⁵N TROSY-HSQC of HVADC displayed excellent chemical shift dispersion indicative of a well folded protein composed mainly of β-strands (Fig. 6). Out of the 288 expected signals of the fully ¹⁵N labelled sample 247 (86 %) could be observed.

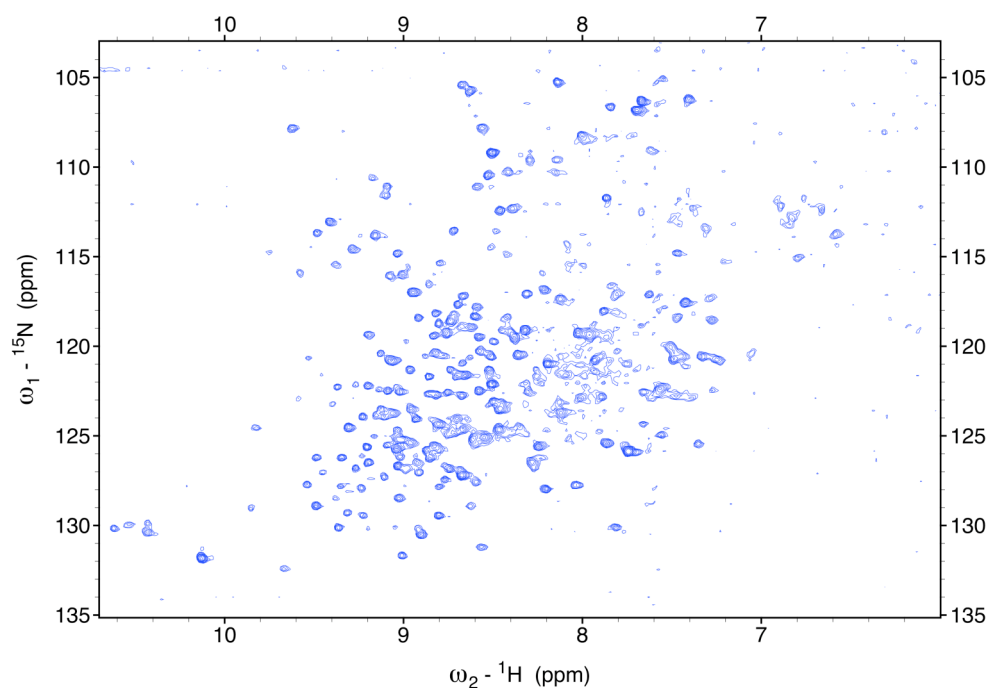


Fig. 6 ^{15}N TROSY-HSQC spectrum of 0.6 mM HVDAC in approx. 250 mM LDAO micelles in 25 mM BisTris buffer, pH 6.8. The spectrum was recorded on a 900 MHz spectrometer equipped with cryogenic probehead at 310 K.

In total 56 % of the backbone resonances were assigned (see Appendix A). Since only 86 % of the peaks were observed in the TROSY-HSQC this corresponds to 65 % of all possible assignments. In general the majority of assigned residues are in the C-terminal two thirds of the HVDAC, therefore the N-terminal third is less well defined. The assignment process was aided by site-directed mutations. The chemical shift perturbations of assigned residues upon mutations are exemplarily shown for the mutants C130S and C235S in Figure 7. Strong perturbations are observed for the mutated residue and its direct neighbours. Further away from the mutation site the perturbations decrease but appear again periodically. A linear anti-parallel β -strands fold can explain this behaviour. In such a case residues in adjacent β -strands cause the periodic reappearance of perturbations.

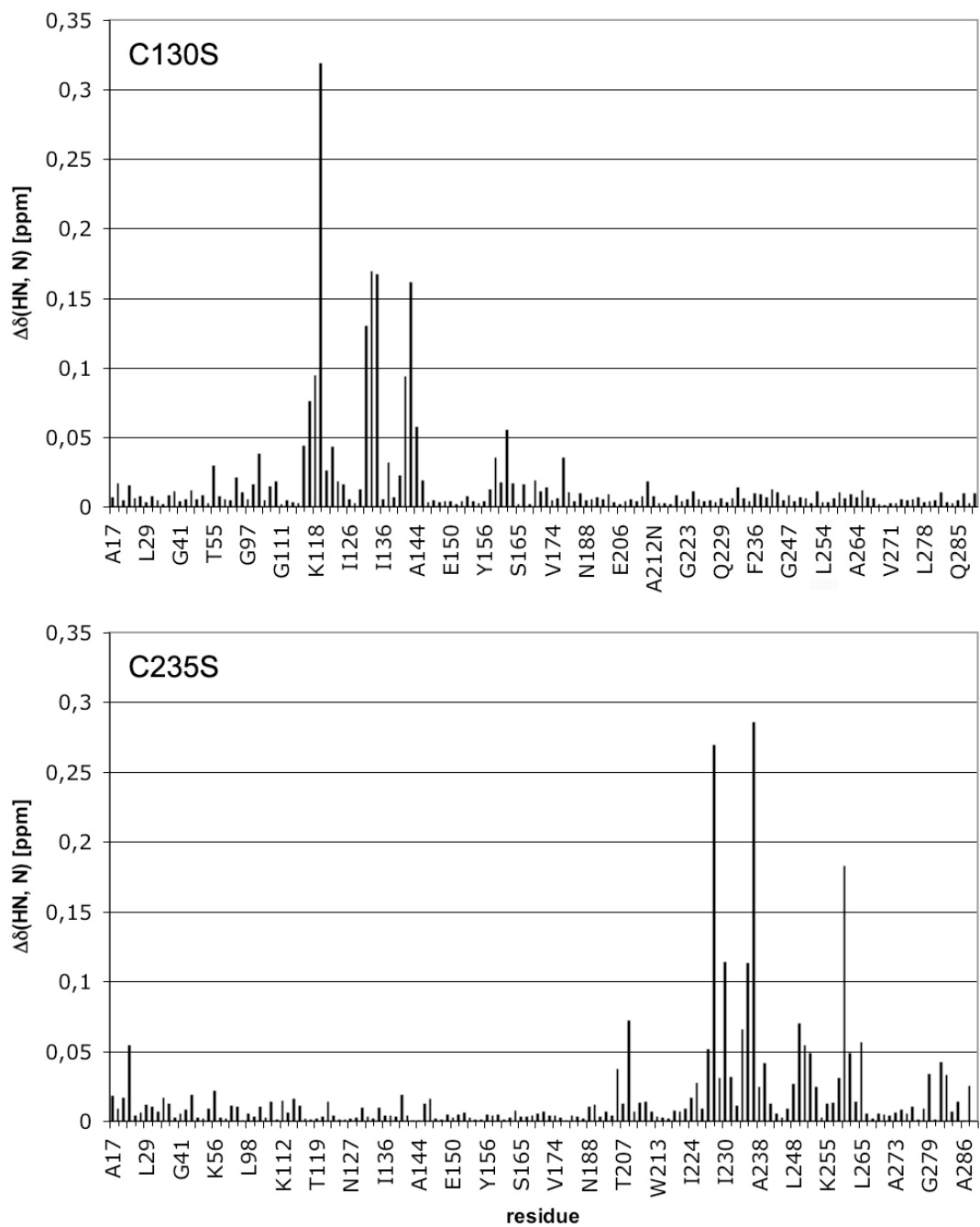


Fig. 7 Chemical shift changes of HN and N upon mutation to either C130S or C235S. Only assigned residues are plotted.

Secondary structure elements were identified by the difference of the observed CA and C' chemical shifts to random coil values^[30] (see 2.2.5.1) (Fig. 8).

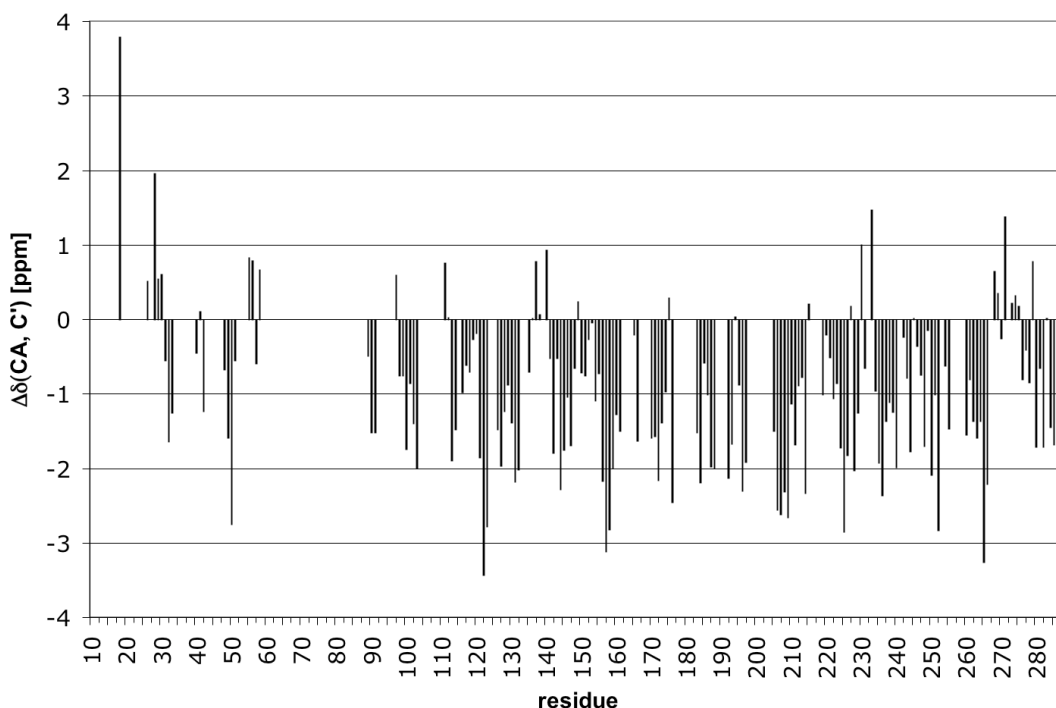


Fig. 8 Secondary chemical shifts of CA and C' for HVDAC plotted against the residue number.

The majority of secondary chemical shifts are negative. These negative shifts cumulate in most cases. Consequently HVDAC consists mainly of β -strands. Small positive values found between the β -strands indicate loop regions. The biggest positive values are located in the N-terminus, which agrees with the predicted N-terminal α -helix.

3.3.3 Solvent Accessibility And Dynamics

In order to probe the solvent accessibility of single residues in HVDAC, a D_2O exchange experiment was performed (see 2.2.5.3). The first TROSY-HSQC spectrum was recorded 1 h after dissolving the sample in D_2O . It displayed 91 peaks, which is 32 % of all resonances (Fig. 9). Out of these 91 resonances 90 have been assigned.

Only three of them correspond to residues, which are located in the N-terminal third of HVDAC. These are L29, I30 and K31. This indicates, that hydrogen bonds in the

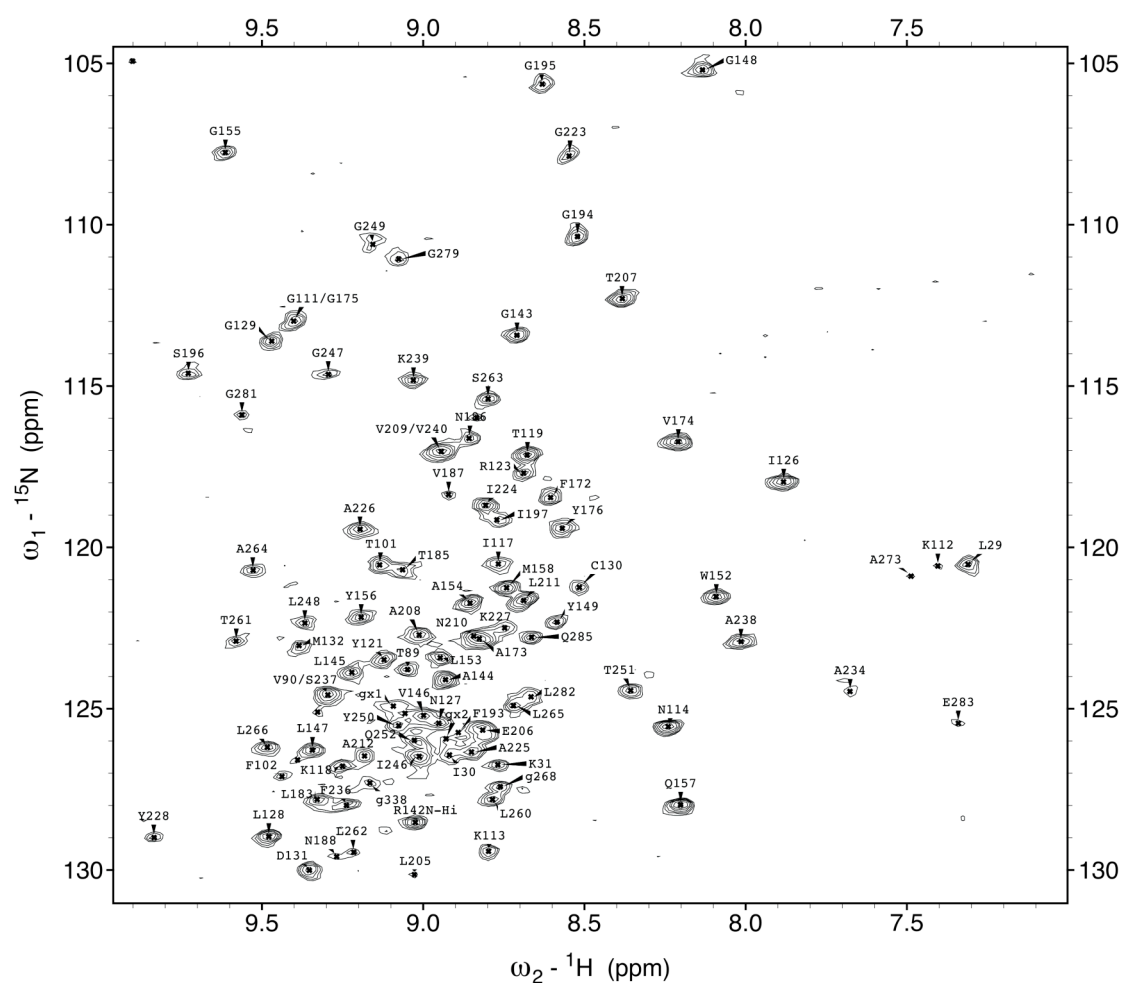


Fig. 9 TROSY-HSQC of HVDAC in 100 % D₂O, recorded 1 h after solvation in D₂O. Assigned residues are labelled with the one letter amino acid code.

N-terminal third of HVDAC are weaker than in the rest of the protein. This implies, that the secondary structure is less pronounced, or that enhanced flexibility can be observed for the N-terminal third of HVDAC. The D₂O-exchange data correlate very well with secondary structure determined by secondary chemical shift analysis (Fig. 10a). In most cases residues with strong negative secondary chemical shift do not exchange with D₂O after 1 h. This indicates a β -strand. In all cases where assignment is available, β -strands are flanked by residues, which exchange with water after 1 h.

This corresponds to loops or turns, which connect the β -strands. From this analysis 13 β -strands can unambiguously be established. These are between residue 286 – 281, 266 – 260, 252 – 246, 240 – 236, 228 – 223, 212 – 205, 197 – 193, 188 – 183, 176 – 172, 158 – 152, 148 – 142 and 132 – 126. An additional β -strand can be identified between residue 103 and 98. In this strand only two residues, T101 and F102, don't exchange with D₂O after 1 h. This points out that already this strand is more flexible than the others. Furthermore, three fragments of β -strands can be identified in the N-terminus. These are between residue 91 – 89, 51 – 48 and 33 – 31. In these fragments only three residues don't exchange with D₂O after 1 h. These are V90, T89 and K32. This again points out the enhanced flexibility of the N-terminus.

Additional proof for enhanced N-terminal flexibility stems from the measurement of heteronuclear NOEs (2.2.5.6) (Fig. 10b). Overall 62.5 % of the steady state heteronuclear ¹⁵N{¹H}-NOEs are above 0.7, indicating a well-ordered protein in solution. Residues with ¹⁵N{¹H}-NOEs above 1 are peaks with low signal to noise ratio. A more detailed analysis reveals, that for 61 % of the residues in the N-terminal third (from 1-96) and for 65 % of the unassigned residues the ¹⁵N{¹H}-NOEs are below 0.7 (see Table 15). Since the majority of the assignments is in the C-terminus, this demonstrates that the N-terminal third of HVDAC is more mobile, than the rest of the protein. A closer inspection of the C-terminal part of HVDAC reveals, that 62 % of the residues with higher flexibility are located in loop regions. Most pronounced is the loop between residues G268 and L278.

Table 15 ¹⁵N{¹H}-NOE values for HVDAC parts

	¹⁵ N{ ¹ H}-NOEs below 0.7
N-terminus (1 – 96)	61 %
C-terminus (97 – 288)	33 % (of these are 62 % located in loops)
unassigned residues	65 %

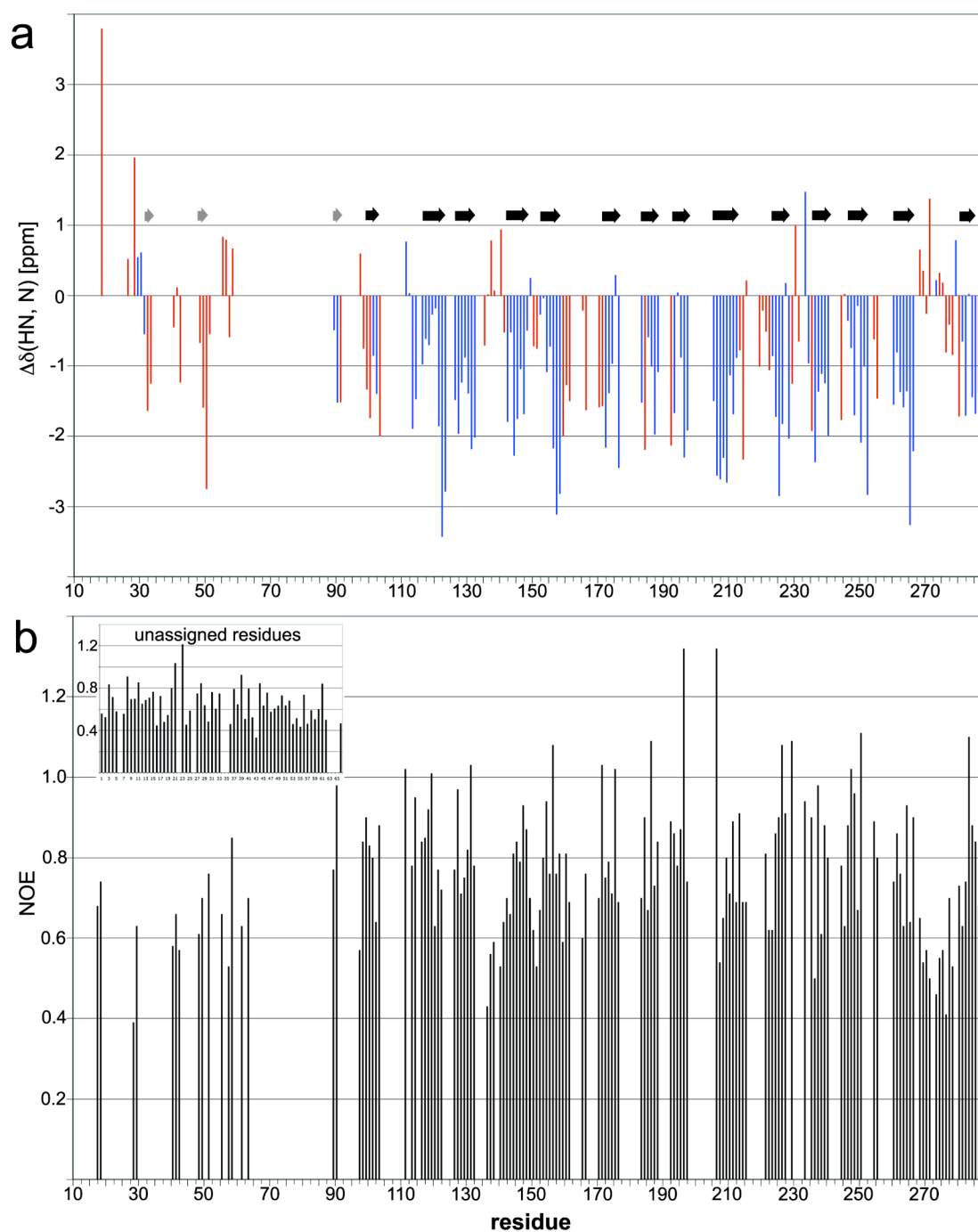


Fig. 10 a) Secondary chemical shifts of CA and C' for HVDAC plotted against the residue number. Red bars indicate residues, which exchange with D_2O after 1 h, blue bars, which don't exchange with D_2O after 1 h. Black arrows indicate β -strands, grey arrows potential β -strand fragments. **b)** The $^{15}\text{N}\{^1\text{H}\}$ -NOEs plotted against the residue number. The inlet shows the values for unassigned residues.

3.3.4 Topology model

The topology model of the β -strands given in Figure 11 is based on HN-HN NOE connectivities, secondary chemical shift analysis and the amide proton exchanging behaviour with D_2O . The topology could unambiguously be determined

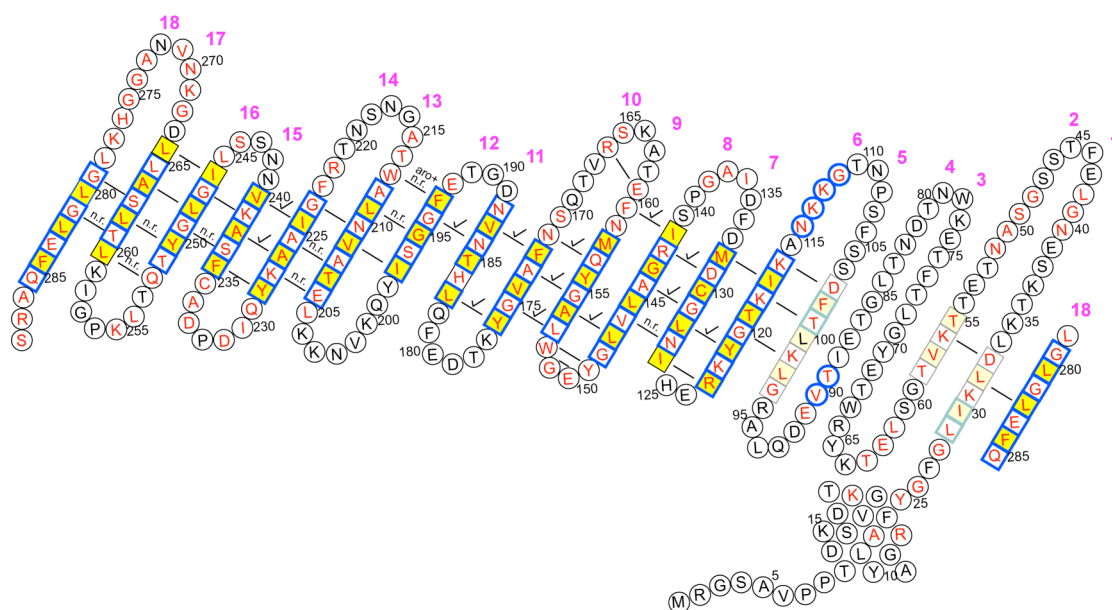


Fig. 11 Topology model of HVDAC. Amino acids are given in the one letter code. Red letters denote assigned, black letters unassigned residues. Black lines indicate HN-HN NOE connectivities. A check on top of the line refers to NOE-peaks, which are also present in 100 % D_2O . The abbreviation “n.r.” on top of the line stands for not resolved NOEs, “aro” indicates NOEs of aromatic protons. Residues bordered blue, or light blue do not exchange with D_2O after 1 h. Residues in squares are part of a β -strand. β -strands are based on HN-HN NOE connectivities, secondary chemical shift analysis and the amide proton exchanging behaviour with D_2O . The β -strands could theoretically extend further because negative secondary chemical shifts are also found for some residues, which exchange rapidly with D_2O . Strands given in light grey and light blue feature increased flexibility. Residues in yellow boxes have side chains pointing towards the hydrophobic membrane, whereas white squares indicate side chains facing the hydrophilic channel pore. The β -strands are numbered from the N- to the C-terminus, numbers are given in magenta. The helix is based on the PSIPRED^[91, 92] prediction and secondary chemical shift analysis.

for the 14 C-terminal β -strands. They are basically similar to the ones given in 5.3.3, including the more flexible β -strand between residue 98 and 103. These 14 β -strands

occupy 2/3 of the sequence. Theoretically the β -strands could extend further because negative secondary chemical shifts are also found for some residues, which exchange rapidly with D₂O. Additionally 2 N-terminal β -strands were localised between residue 55 – 58 and 29 – 33, but the NOE connectivities are not unambiguous (Fig 11). Furthermore the secondary chemical shifts for the strand between 55 and 58 are not negative, except for V57. The helix is based on a prediction by the PSIPRED server^[91, 92] (Fig. 23) and secondary chemical shift analysis.

3.3.4.1 Mutations that probe the position of the N-terminal helix

The position of the N-terminal helix was probed by the mutation V20C and the corresponding chemical shift perturbation in the TROSY-HSQC spectrum. The residue V20 was predicted to be part of the α -Helix. The strongest perturbations upon this mutation are observed for residues close to V20. An additional cluster of strong effects can be located around residue A226. This region is indicated by a blue ellipsoid in Fig. 12. Additional effects can be observed for residues located in loops, opposite to the helix. Residues that show upon mutation chemical shift changes of HN and N bigger than 0.05 ppm are A17, R18, K23, G26, N114, I141, R166, T207, A226, Y228, A238, L262, Q285 (they are bordered in dark green in Fig. 12). Residues with perturbations between 0.035-0.05 ppm are N40, K112, A137, A208, L211, Q229, K255, L265 (they are bordered in light green in Fig. 12).

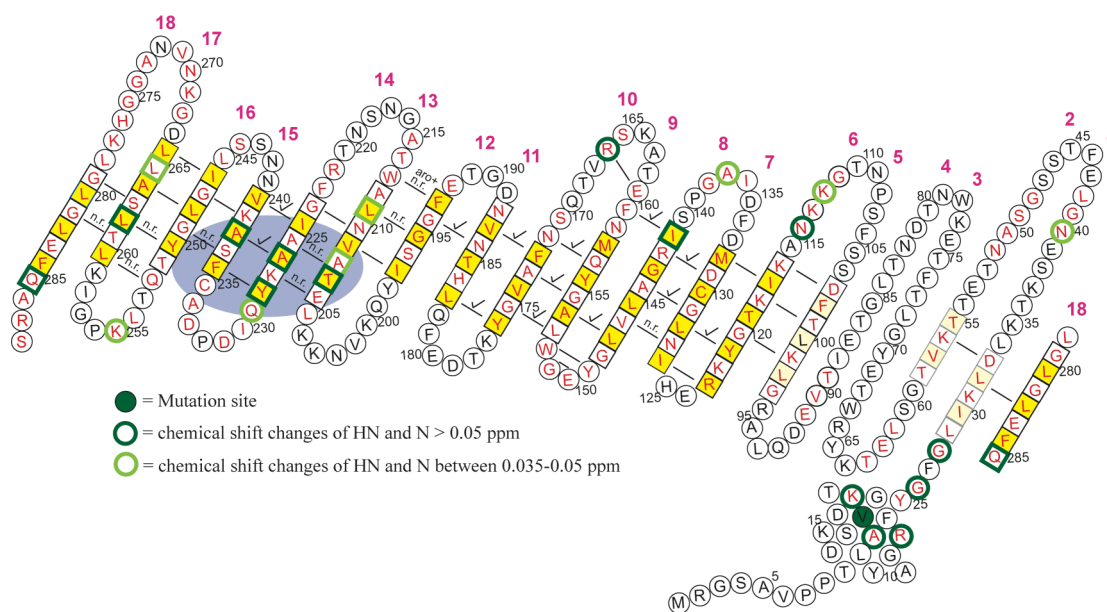


Fig. 12 Effects due to the mutation V20C in the TROSY-HSQC spectrum mapped on the topology model of HVDAC. The green circle denotes the mutation site. Residues bordered dark green show chemical shift changes of HN and N bigger than 0.05 ppm, for residues bordered in light green the perturbations are between 0.035-0.05 ppm. The blue ellipsoid highlights the most clustered effects. The rest of the nomenclature is the same as in Figure 11.

Additionally PRE data of the mutant C130S (Fig. 13) probed the helix position. In this case the MTSL spin label was at the position C235. The signal to noise ratio of the TROSY-HSQC was very low. Therefore only peaks, which were broadened beyond detection, were actually counted as an effect. Residues specifically broadened beyond detection are: A17, R18, I30, G48, K56, K118 - Y121, G129, D131, G143, A144, L205 - A208, A225 - D231, A234 - K239, S244, G249 - T251, L260, L262 - A264, G281, L282, Q285 (bordered dark blue in Fig. 13). Additionally some residues were unspecifically broadened beyond detection. These are residues which are not broadened beyond detection in the case of the wild type HVDAC with MTSL labels at positions C130 and C235. These residues are: Y25, I117, S196, L248, Q252, T261, K277, L278 (bordered light blue in Fig. 13). Therefore most effects are located in the

region around the mutation site. However, additionally the resonances of A17 and R18, which are located in the N-terminal helix, are broadened beyond detection.

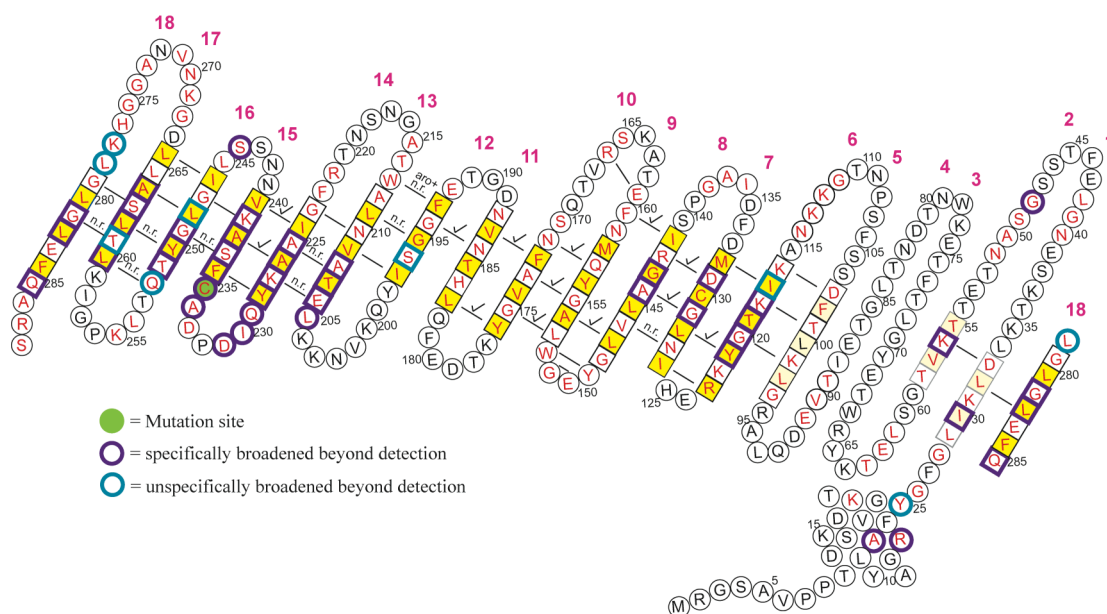


Fig. 13 Effects due to spin labelling of the mutant C130S with MTSL at the position C235 in the TROSY-HSQC spectrum mapped on the topology model of HVDAC. The green circle denotes the position of the MTSL. Peaks of residues bordered dark blue are specifically broadened beyond detection. Peaks of residues bordered in light blue are unspecifically broadened beyond detection. The rest of the nomenclature is the same as in Figure 11.

3.3.5 Structure Determination of human VDAC by NMR and X-ray crystallography

In solution the N-terminus of HVDAC shows an enhanced flexibility, which leads to exchange broadening of the NMR signals. Thus for this part only partial assignment was possible, which was insufficient to build a reliable two-dimensional model. However, HN-HN NOE-crosspeaks could be unambiguously assigned for the 14 C-terminal β -strands. Therefore the β -barrel fold for this part of the protein could be established. Consequently a two-dimensional model with atomic resolution for the backbone was built. This was fitted into the electron density map, based on the

selenomethionine positions M132, M158 and M230. This resulting 3D-model is reliable because starting from any of the selenomethionine positions in the electron density and following the hydrogen bonds according to the NMR-topology model always results in the correct two other selenomethionine positions in the electron density. Additionally all loops determined by NMR fit in the electron density envelope, if density is present at the corresponding position. Due to a resolution of 4 Å building of this 3D-model of HVDAC would not have been possible without the NMR-topology model. Spare electron density, which does not belong to the 14 β -strands defined by NMR, gives rise to 4 additional N-terminal β -strands (Fig. 14).

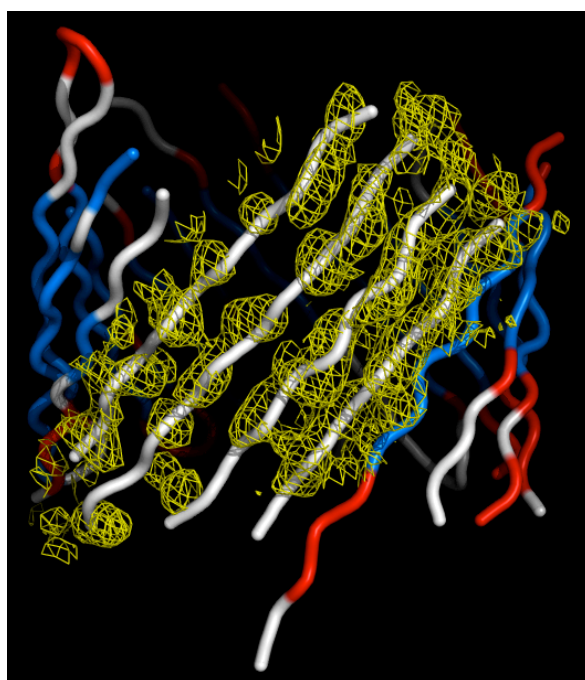


Fig. 14 NMR/X-ray structure of human VDAC. **A)** The backbone is shown as a string. Red indicates residues which exchange with D₂O after 1 h, blue indicates residues which don't exchange with D₂O after 1 h. Electron density, which forms 4 β -strands in addition to the NMR-model, is shown in yellow.

In the present structure these sheets are between residues 27 – 35, 54 – 64, 67 – 76 and 84 – 93. This is consistent with the two ambiguous β -strands between residues

31 – 33 and 55 – 58 and with the β -strand-fragment between residue 31 and 33 determined by NMR. The structure of human VDAC displays a typical β -barrel fold. It consists of 18 anti-parallel β -strands, which construct the β -barrel, and a N-terminal α -helix, which is located inside the barrel, close to the C-terminus (Fig. 15). The position of the helix is based on the electron density map. It is in agreement with the NMR-data, because V20 is located close to A226 in strand number 14 as can be seen from Fig 15.

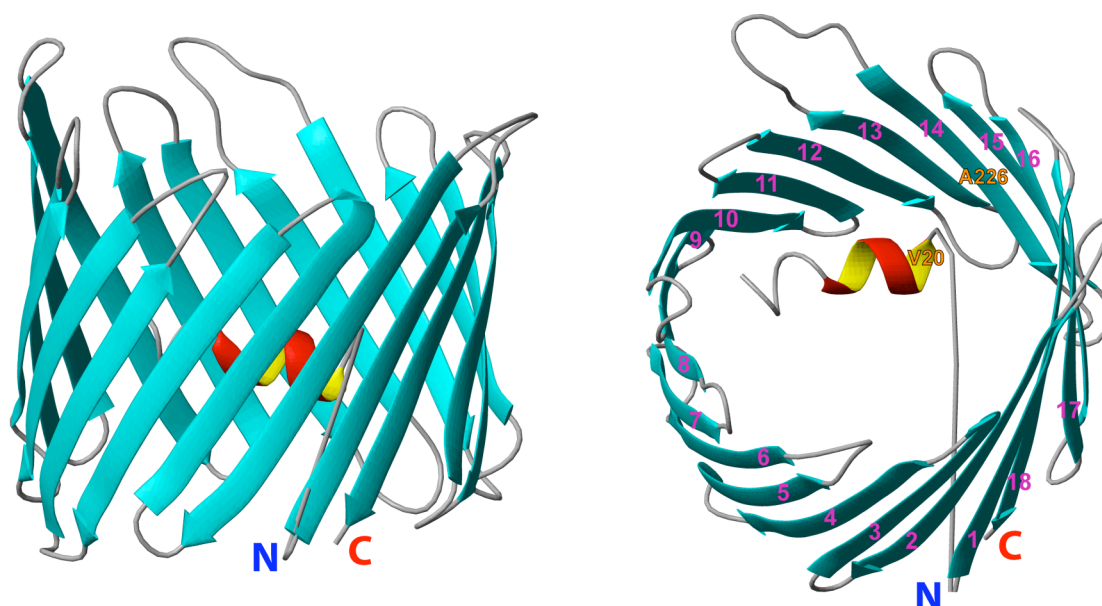


Fig. 15 NMR/X-ray structure of human VDAC. It is a ribbon presentation of the backbone. Helices are marked in red and β -strands in cyan. The β -strands are numbered from the N- to the C-terminus, numbers are given in magenta. The position of V20 and A226 are indicated with the one letter amino acid code. The N-terminus is marked with a blue N, the C-terminus with a red C.

3.3.6 Functional investigation of HVDAC

To investigate the functional behaviour of HVDAC several titrations of effectors to a ^2H , ^{15}N -labelled HVDAC sample were carried out. After each titration point a 2D TROSY-HSQC spectrum was recorded.

3.3.6.1 ADP-Titration

VDAC is primarily responsible for nucleotide transport across the outer mitochondrial membrane (reviewed in [44]). To map potential interaction sites of nucleotides and HVDAC an ADP titration was performed. Chemical shift perturbations based on addition of ADP are mapped on the topology model in Figure 16. ADP was added up to a 16-fold molar excess. Residues with chemical shift changes of HN and N upon ADP addition bigger than 0.02 ppm are: G26, K56, R123, N159, T185, A212, S237, A273, S288 (labelled with a green star in Fig. 16). In general, the effects are equally distributed over the whole channel.

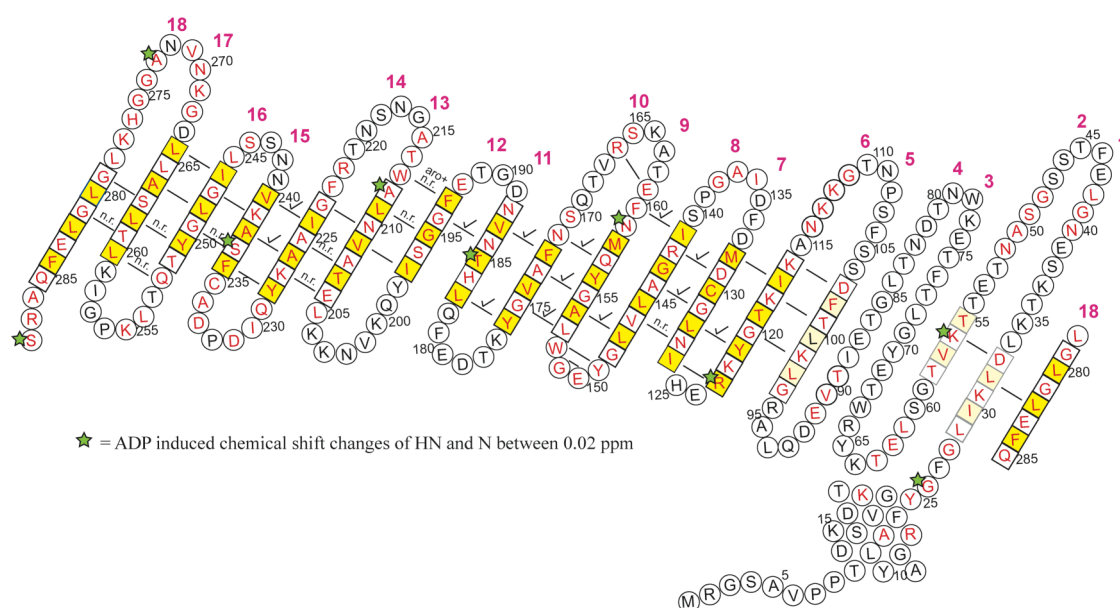


Fig. 16 Effects in the TROSY-HSQC spectrum due to addition of ADP mapped on the topology model of HVDAC. Residues labelled with a green star show perturbations bigger than 0.02 ppm upon addition of a 16-fold molar excess of ADP. The rest of the nomenclature is the same as in Figure 11.

3.3.6.2 Fluoxetine-Titration

Fluoxetine is a clinically used potent antidepressant^[93]. It is known under trade names like Prozac[®] or Fluctin[®]. Thinnes^[94] demonstrated that fluoxetine increases the

voltage dependence of HVDAC. In order to understand the interaction of fluoxetine with VDAC on an atomic level, a fluoxetine titration was performed.

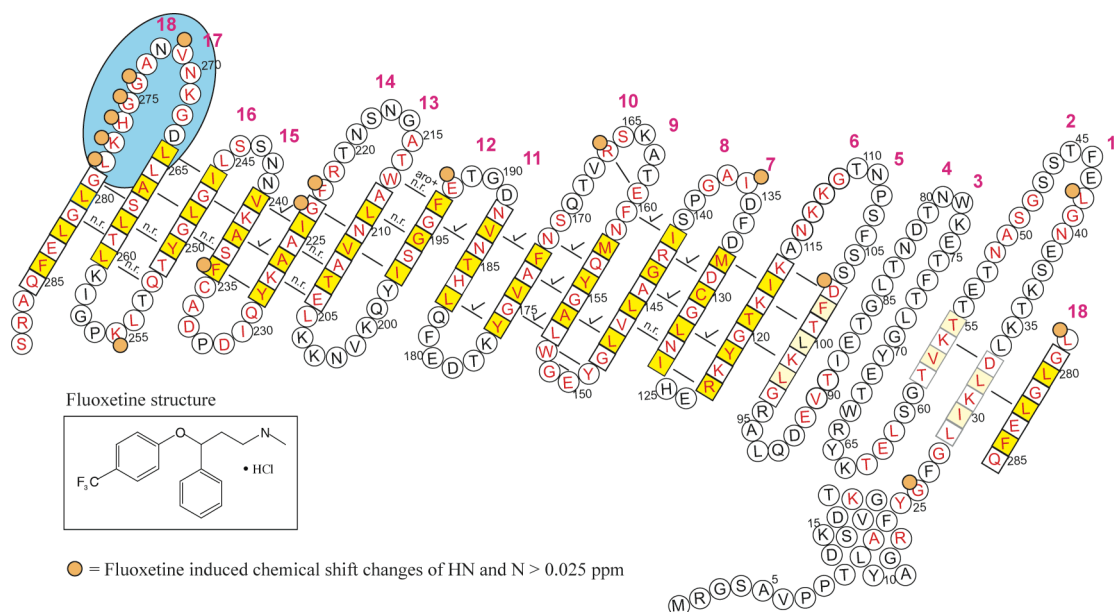


Fig. 17 Effects in the TROSY-HSQC spectrum upon addition of the antidepressant fluoxetine mapped on the topology model of HVDAC. Residues labelled with a yellow circle show chemical shift changes of HN and N bigger than 0.025 ppm upon addition of a 32-fold molar excess of fluoxetine. The blue ellipsoid highlight interaction sites with fluoxetine. The inlet shows the structure of fluoxetine. The rest of the nomenclature is the same as in Figure 11.

Chemical shift perturbations upon titration are mapped on the topology model of HVDAC in Fig. 17. Fluoxetine was added up to a 32-fold molar excess. The most clustered effects with chemical shift changes of HN and N bigger than 0.025 ppm are found in the C-terminal loop from residue V271 and G274-L278. Additional effects can be observed in other loops on the same side. Affected residues are L42, D103, I136, R166, E192, F222, G223. Other affected residues are G26, F234 and K255.

3.3.6.3 Interaction of HVDAC with anti-apoptotic Bcl-x_L^[47]

Malia et al.^[47] described the interaction of the anti-apoptotic protein Bcl-x_L with HVDAC. They presented an unassigned ¹⁵N-TROSY-HSQC spectrum of ²H, ¹⁵N-HVDAC in the presence of 50 % Bcl-x_L (Fig. 18).

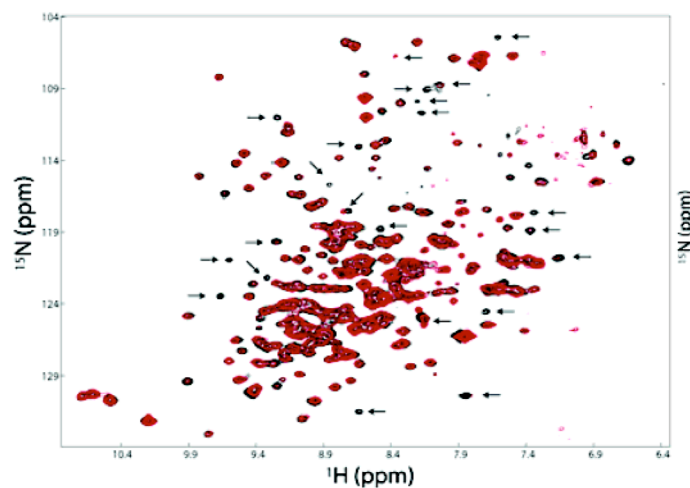


Fig. 18^[47] Chemical shift perturbations of ²H, ¹⁵N-HVDAC in the presence of unlabeled Bcl-x_L. The TROSY-HSQC spectrum of HVDAC in the absence (black) and presence (red) of 50 % Bcl-x_L. Arrows indicate some of the major changes in the HVDAC spectrum.

Since HVDAC was reconstituted in LDAO micelles the TROSY-HSQC spectrum looks similar to the one shown in Fig. 6. Therefore the assignment could be transferred and the interaction site of HVDAC with Bcl-x_L was established. Fig. 19 shows major chemical shift perturbations upon addition of Bcl-x_L as classified by Malia et al. mapped on the topology model of HVDAC.

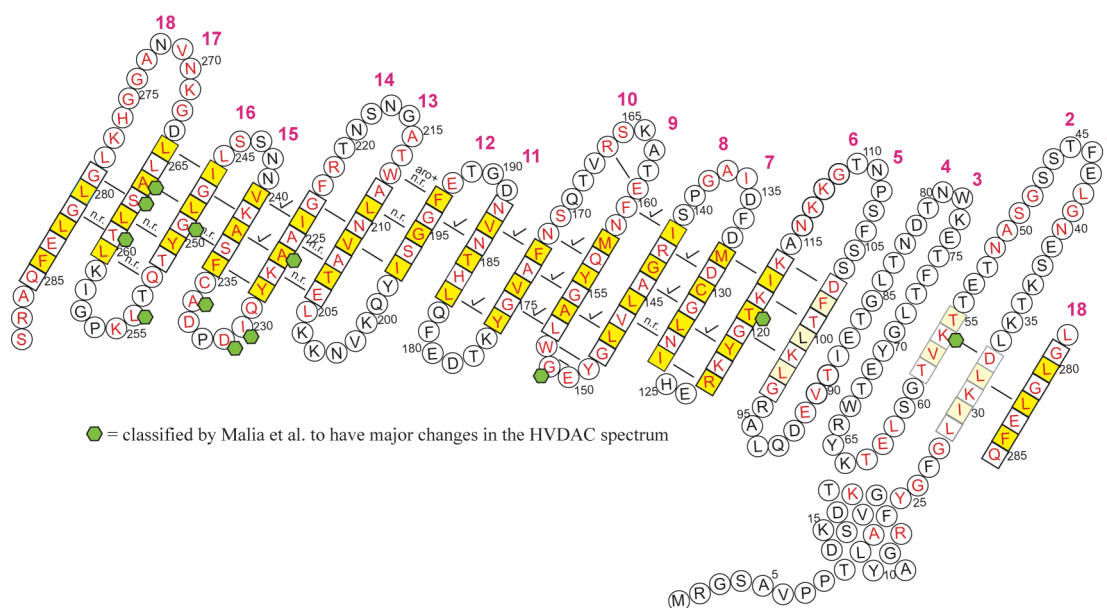


Fig. 19 Chemical shift perturbations in the presence of Bcl-x_L^[47] mapped on the topology model of HVDAC. Residues, which are classified by Malia et al. to have major changes in the HVDAC spectrum, are labelled with a green hexagon. In the original publication these residues are pointed out with a black arrow in the unassigned TROSY-HSQC spectrum. The rest of the nomenclature is the same as in Figure 11.

These are: K56, T119, G151, A226, I230, D231, A234, G249, L254, T261, S263, A264. The majority of residues, which are affected by Bcl-x_L, are located in the C-terminus between A226 and A264.

3.3.6.4 Interaction of HVDAC with pro-apoptotic Bid

Rostovtseva et al.^[45] reported, that pro-apoptotic Bid, which was activated by Caspase 8, induced channel closure of VDAC. To investigate the binding interface of Bid and HVDAC ¹⁵N-TROSY-HSQC spectra of ²H, ¹⁵N-HVDAC in the presence of a 4-fold molar excess of unlabelled mouse Bid were recorded. Human and mouse Bid share 91.5 % sequence identity (based on the sequences in the PDB files 2BID (human) and 1DDB (mouse)). Additionally a sample with MTSL-labelled Bid was prepared. The effects of Bid and Bid-MTSL on the TROSY-HSQC spectrum of

HVDAC are summarised in Fig. 20. On the one hand chemical shift and peak intensity changes upon Bid addition compared to the reference spectrum without Bid are plotted. On the other hand peak intensity changes are indicated, which additionally appear upon MTSL-labelling of Bid. Effects with Bid alone appear

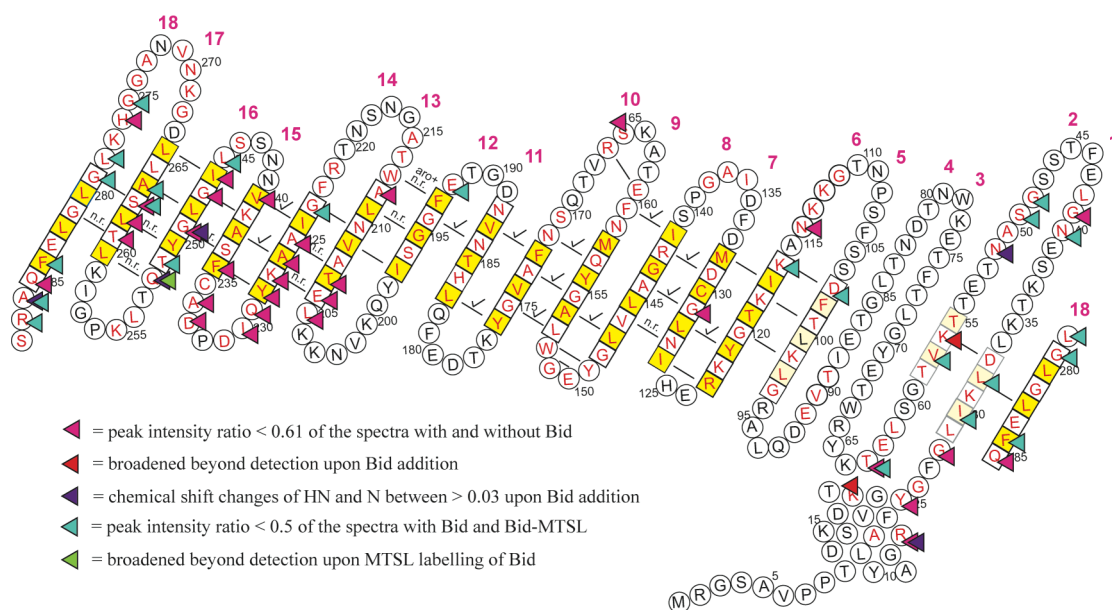


Fig. 20 Chemical shift perturbations in the presence of mouse Bid mapped on the topology model of HVDAC. Residues with a peak intensity ratio < 0.61 of the spectra with and without Bid are labelled with a magenta triangle. Residues, which upon Bid addition are broadened beyond detection, are labelled with a red triangle. Residues, which upon Bid addition show HN and N chemical shift changes > 0.03, are labelled with a purple triangle. Residues with a peak intensity ratio < 0.5 of the spectra with Bid and Bid-MTSL are labelled with a turquoise triangle. Residues, which upon MTSL labelling of Bid, are additionally broadened beyond detection are labelled with a green triangle. The rest of the nomenclature is the same as in Figure 11.

primarily in the C-terminal region starting from L205. Affected residues in this area are L205 – T207, A212, A225 – I230, D233 – A234, F236, V240, I246 – G247, G249, Q252, T261 – S263, H276 and Q285 – A286. Interestingly, again residues in the N-terminal helix are affected together with the residues in the C-terminus. These are R18, K23 and Y25. Additional effects, which show up upon MTSL-labelling of Bid, appear like a semicircle around the region, which is also influenced by Bid alone.

These MTSL induced effects extend up to the N-terminus. Effected residues are I30, L32, N40, G48 – S49, V57, T63, D103, K116, E192, G223, L245, T251, Q252, S263 – A264, G275, L278 – G279, F284 and A286 – R287.

Addition of Bid to the HVDAC sample led to partial unfolding of HVDAC. However, HVDAC slowly refolded again and was completely folded after one month. Fig. 21 shows the first 1 D spectrum of a TROESY-HSQC of HVDAC after addition of Bid and of the same sample one month later.

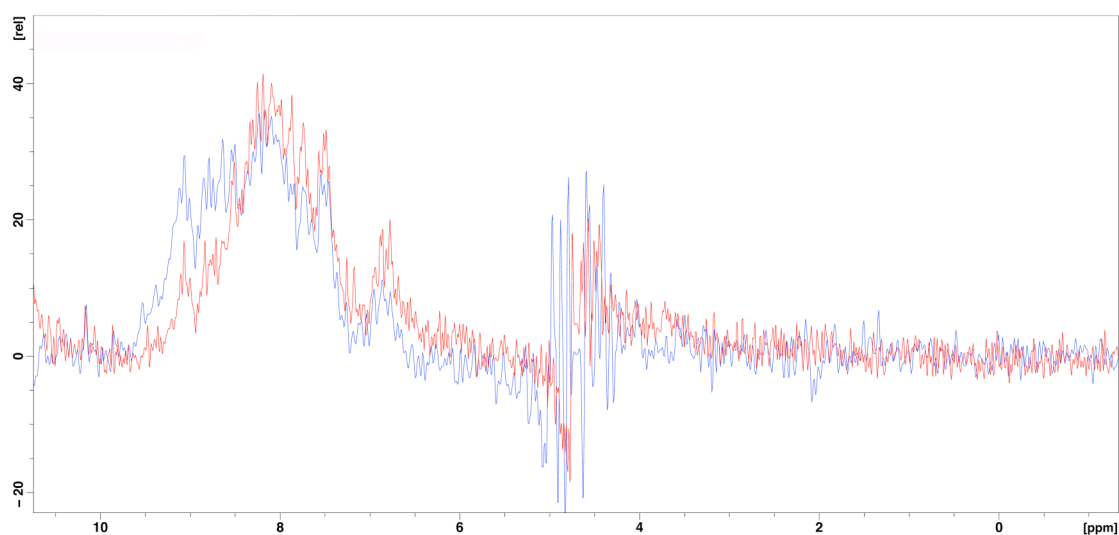


Fig. 21 Overlay of the first 1 D spectra of a TROESY-HSQC of HVDAC directly after addition of Bid (red) and one month later (blue).

3.3.6.5 Calcium (II) chloride and Gadolinium (III) chloride-Titration

Gincel et al^[95]. reported, that VDAC is highly permeable to Ca^{2+} and has Ca^{2+} -binding sites. In contrast, Ruthenium Red and lanthanides close the VDAC. The authors suggest, that the inhibition of mitochondrial Ca^{2+} uptake by Ruthenium Red and lanthanides results from their interaction with the Ca^{2+} -binding site. Israelson et. al^[96] established the Ca^{2+} -binding sites as E72 and E202 (E76 and E206 in the nomenclature used here) by interaction of VDAC with azido ruthenium. In order to

test these results a Ca^{2+} -titration was performed. However no major chemical shift perturbations or peak intensity changes could be observed upon addition of a 32-fold molar excess of Ca^{2+} . Since it was suggested, that lanthanides interact with the Ca^{2+} -binding site of VDAC, an additional titration with GdCl_3 was performed. Gd^{3+} is paramagnetic. Because of paramagnetic relaxation enhancement, the interaction of Gd^{3+} with HVDAC will have much stronger effects on the TROSY-HSQC than the interaction of Ca^{2+} . Thus the interaction site of Gd^{3+} with HVDAC could be established. It is mapped on the topology model in Fig. 22. Residues, which are

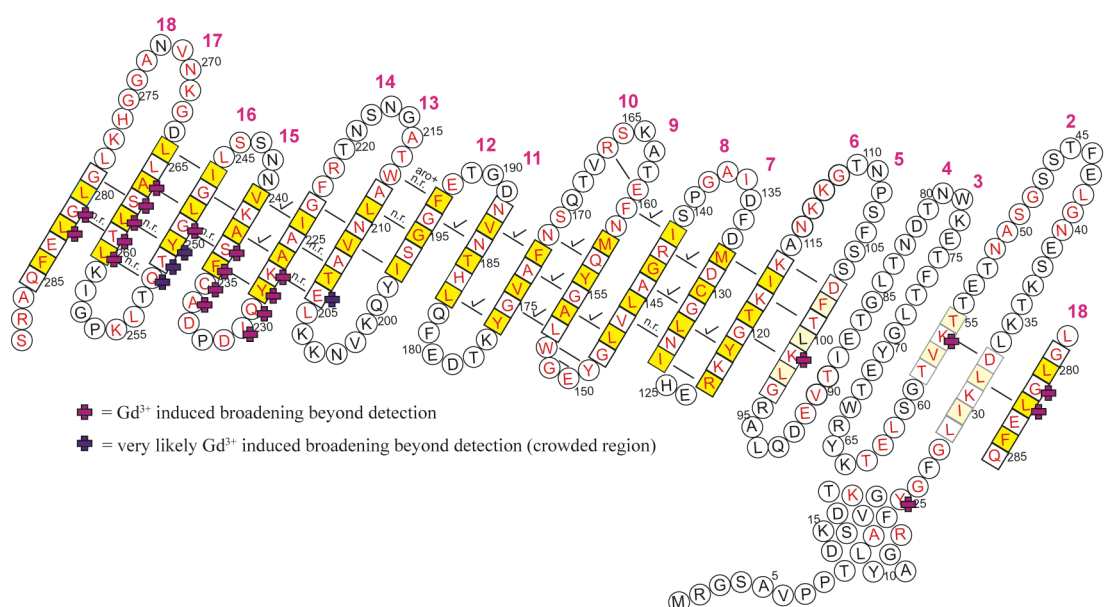


Fig. 22 Effects in the TROSY-HSQC spectrum upon addition of GdCl_3 mapped on the topology model of HVDAC. Residues labelled with a purple cross are broadened beyond detection upon addition of an equimolar amount of GdCl_3 . Purple crosses indicate peaks, which are very likely to be broadened beyond detection. They are in very overlapping regions. The rest of the nomenclature is the same as in Figure 11.

broadened beyond detection upon addition of an equimolar amount of Gd^{3+} , are in the majority observed at the C-terminus in the last 5 β -strands. Affected residues are E204, K227 – I230, A234 – S237, G249 – Q252, L260 – A264 and Q281-L282. Additional effects can be observed for Y25, K56, K99.

3.4 Discussion

In this work, the structure of HVDAC was determined conjointly by NMR-spectroscopy and X-ray crystallography. In addition, binding interfaces of HVDAC and different effectors were established.

3.4.1 The combination of NMR and X-ray crystallography for structure determination of membrane proteins

The structure elucidation of the human VDAC pushes both methods, NMR spectroscopy and X-ray crystallography, to their limits. As mentioned in the introduction, the major problem for solution NMR is the size limit. As molecular masses increase, NMR spectra become increasingly difficult to interpret because of spectral crowding and line broadening due to fast transverse relaxation^[5]. The human VDAC has a molecular weight of 32 kDa and is reconstituted in LDAO detergent micelles. This leads to an overall molecular weight of approx. 80 to 120 kDa, as estimated from T1ρ measurements. Additionally challenging is the fact, that the NMR measurements cannot be performed at a temperature higher than 37 °C. Since VDAC is a human protein it degrades above this temperature. Compared to other structural investigations of membrane proteins by NMR this temperature is still intermediate, e.g. spectra for the β-barrel protein PagP were recorded at 45 °C^[97]. This situation does not only make the resonance assignment difficult but most important, it makes long range distance restraints for structure calculations hard to obtain. Because of the strong relaxation it was not possible to attain accurate isotropic $^1J_{\text{HN}}$ couplings. Therefore the utilization of residual dipolar couplings (RDCs) as long-range restraints was impossible. This restricts long-range distance restraints to NOEs and paramagnetic relaxation enhancement data. Due to the high deuteration level the

NOEs are limited to HN-HN crosspeaks. Nevertheless, in anti-parallel β -strands interstrand HN-HN crosspeaks can be observed. These are sufficient to determine the global fold of a β -barrel. In general, a structure calculation from NMR data would be difficult and time consuming. Yet, to obtain a 2 dimensional model with atomic resolution is from this data, compared to the structure calculation, rather straightforward.

The biggest problem for X-ray crystallography is the fact that the so far obtained crystals of human VDAC I only diffract up to 4 Å. Nevertheless, it was possible to obtain an electron density map corresponding to about 4 Å resolution. So far, the maps enabled the detection of the overall fold as well as several secondary structure elements in some areas of the electron density after b-factor sharpening. Unfortunately, the low resolution of the electron density map did not allow an exact tracing of the protein backbone. Hence, an initial map interpretation was only possible by placing poly-alanine fragments of high-resolution beta barrel protein structures into the more distinct defined portions of the electron density. The remaining somewhat ambiguous sites of the electron density map were further interpreted through the fitting of additional poly-alanine beta sheet fragments under consideration of the established beta barrel geometries. The final electron density map seems to be most consistently explained by an idealized 18 stranded beta barrel. In conclusion, this map only allowed the rough localisation of secondary structure elements, but not the placement of single amino acids.

In order to gain an extended molecular structure of the VDAC protein, the NMR derived topology was applied on the X-ray derived model. This was done by replacing manually the alanines of the X-ray model with the HVDAC sequence according to the NMR topology model. The resulting structure complies with both

restrains, interstrand HN-HN NOEs and the selenium sites of M132, M158 and M230. Although the NMR topology structure covers only about two thirds of the whole barrel accurately, the derived hybrid model enabled a significantly improved interpretation of the electron density map. Until now, the electron density map could not be improved by the NMR-data. Nevertheless the resulting hybrid model is well suited for the ongoing structural refinement process.

In the end the combination of the local information from NMR-spectroscopy and the global information from X-ray crystallography yielded the structure of human VDAC. This clearly points out, that the combination of the two methods can be advantageous for the structure determination of integral membrane proteins.

3.4.2 NMR and X-ray Structure of HVDAC

The structure of human VDAC resembles the typical β -barrel fold (Fig. 23). It consists of 18 anti-parallel β -strands, which construct the β -barrel, and a N-terminal α -helix, which is located inside the barrel, pointing in the direction of the C-terminus. Additional proof, that the N-terminal helix is not part of the barrel wall, as proposed by other studies^[63, 65], is given by NMR spectroscopy.

It was observed that the mutation V20C, which is located in the helix, affects the chemical shift of residues located in the 6 C-terminal β -strands (from strand number 13 to 18) around residue A226. If the helix would close the barrel and would be part of the barrel wall, this effect would very likely be restricted to residues in β -strands next to the helix, for example sheet number one and eighteen. Noteworthy is the fact, that upon this mutation in the C-terminus mainly residues are affected, whose side chains point outside of the barrel wall towards the micelle. Therefore the amide

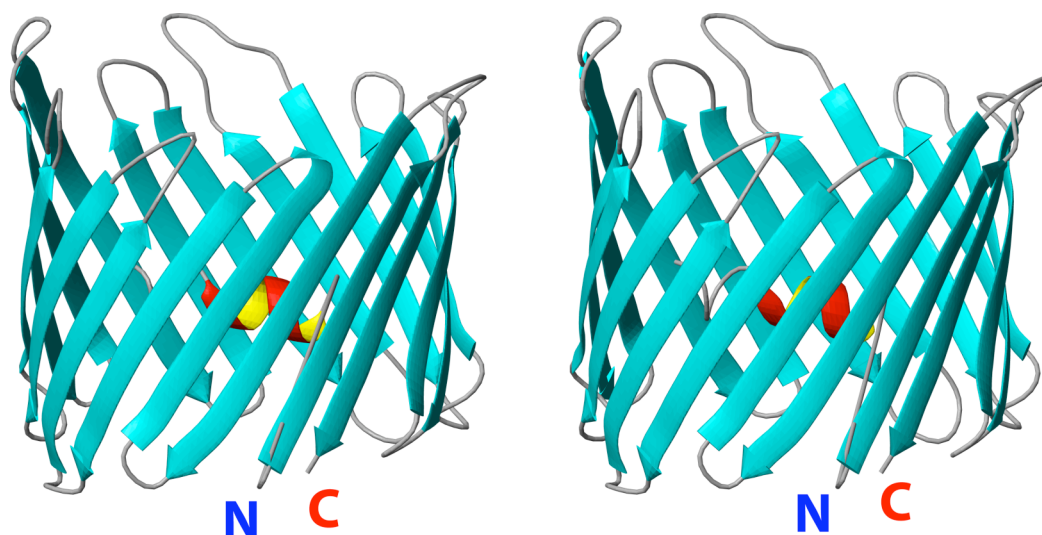


Fig. 23 Stereo view of the NMR/X-ray structure of human VDAC. It is a ribbon presentation of the backbone. Helices are marked in red and β strands in cyan. The N-terminus is marked with a blue N, the C-terminus with a red C.

bond of these residues is inside the barrel less shielded. This implies, that the helix is rather located inside the barrel, because stronger effects are observed for residues that are rather unshielded from the inside. Additional effects can be observed for residues located in loops, that are positioned on the top of the barrel, according to the presentation in Fig. 23. This can be due to another conformation because of the enhanced flexibility of the N-terminus.

Further support, that the helix is located in the neighbourhood of the C-terminal part stems from PRE data of the mutant C130S (Fig. 13). In this case the spin label is attached to C235. Most effects are located in the region around this mutation site. However, additionally the resonances of A17 and R18, which are located in the N-terminal helix, are broadened beyond detection. This indicates, that the helix is located close to residue C230 and therefore at the C-terminal side of HVDAC. Further effects can be observed around residue G129. In the presented topology model this region is located directly opposite to C235. The effects can be explained by the position of the MTSL tag. The side chain of C235 points to the inside of the barrel,

therefore also the MTSL points inward. Broadening effects of the MTSL can be observed up to 20-25 Å^[13]. The distance between the CA of C235 and the nitroxide radical is approx. 11 Å. Therefore the diameter of the barrel from backbone to backbone must be approx. between 31-36 Å. Otherwise no effects would be observed in a region opposite to the spin label. This distance correlates very well with the diameter of 35 Å observed by X-ray crystallography. Another explanation for the effects around G129 can be an impurity of the sample, which would still contain C130. Consequently a spin-label would also be present at position C130 and would cause the line broadening around G129.

In addition to the mutational data, also the functional investigations indicated that the N-terminal helix is close to the C-terminal part. For example the proapoptotic Bid (Fig. 20) interacts most strongly with the C-terminal part of HVDAC but in addition also with residues located in the N-terminal α -helix.

3.4.3 Comparison of the human VDAC structure with existing models

Models, which are based on sequence alignment with bacterial porins^[60-62], suffer from the fact that the flexible N-terminal part differs significantly from the bacterial homologues. This is probably due to a widely observed extensive divergence of the primary sequences of β -barrels^[98]. Therefore these methods are unlikely to give decent results for the human VDAC.

The model proposed by De Pinto et al.^[64] is based on analysis of amphipathic secondary structure elements and enzymatic digestion of hydrophilic, extramembranous segments of human VDAC. The authors suggest 16 transmembrane β -strands and a N-terminal α -helix, which lies on the membrane surface on the

cytosolic side (see Fig. 24A). The reported enzymatic cleavage sites are at P232, Y176, Y121 and K116. In our structure P232 is located in a loop, Y176 is vicinal to a loop, but Y121 and K116 are located in a β -strand (see Fig. 24B). Nevertheless, the β -strand is directly adjacent to the flexible N-terminus and might therefore be accessible to proteases.

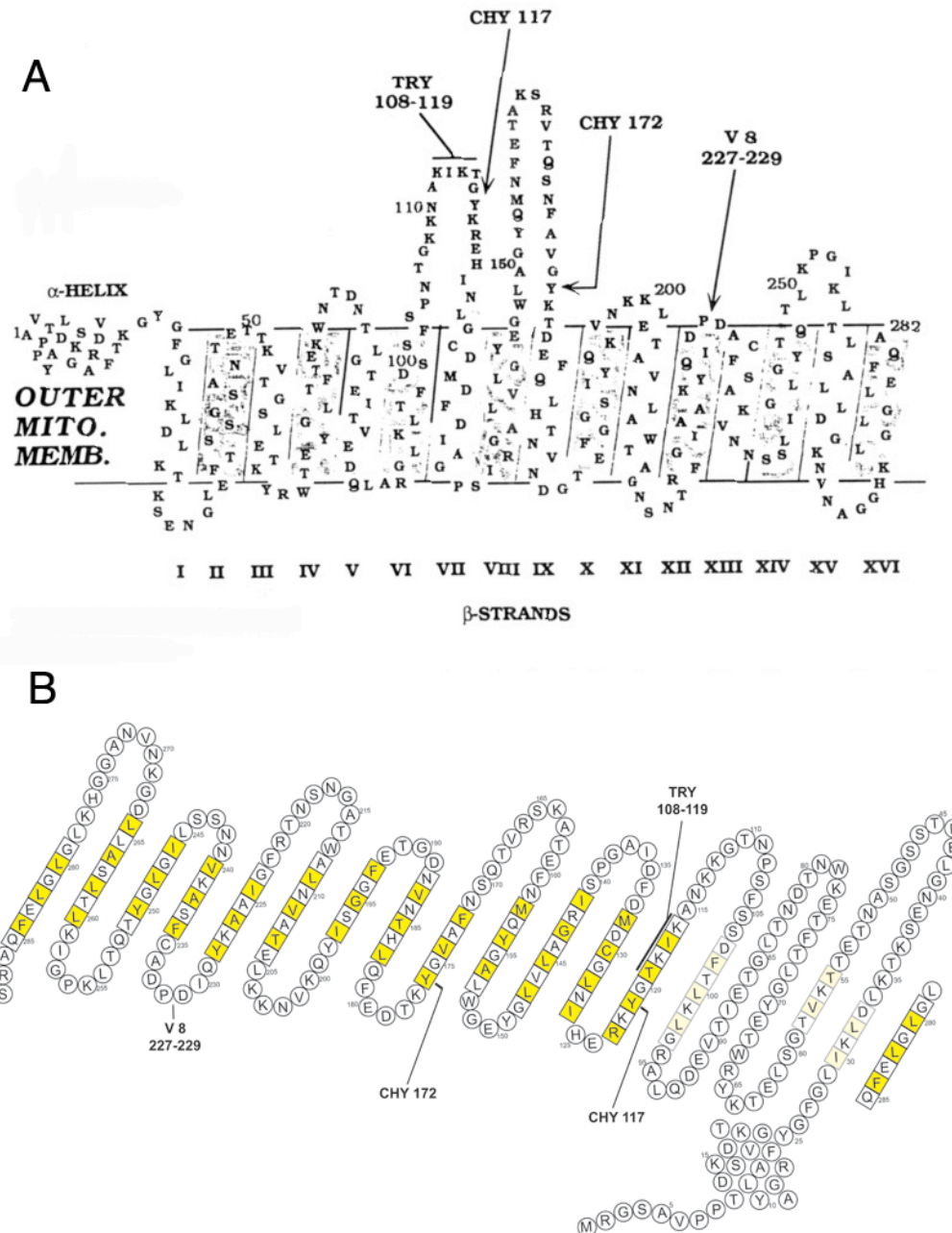


Fig. 24 **A)** Topology model of human VDAC from B-lymphocytes according to De Pinto et al.^[64] The loops contain the cleavage sites of protease V8, trypsin and chemotrypsin. **B)** Enzymatic cleavage sites of De Pinto^[64] mapped on the NMR-derived topology model of human VDAC.

The model proposed by Blachly-Dyson et al.^[63] is based on site directed mutagenesis with subsequent electrophysiological investigation of yeast VDAC. They suggest that replacement of positively charged residues within the channel wall should change the selectivity of VDAC. Contrary a change in charge of residues located outside of the pore might not affect the selectivity. Residues, which upon mutation change the selectivity, are: D15, K19, D30, K46, K61, K65, K84, K95, R124, G179, K234, K248, T256, D282. These correspond to D19, K23, D33, S49, K64, T68, E87, K99, G129, H184, S237, T251, K269, Q285 in our human VDAC construct (see Fig. 25). Residues, which upon mutation don't change the selectivity, are: D51, K108, K132, D156, K174, K205, K211, E220, R252, K267, K274. These correspond to T54, K113, A137, E161, D179, N210, G216, G223, K255, N270, K267 in our human VDAC construct (see Fig. 25). In general, there is a good agreement between Blachly-Dysons data and our structure. Only the residues, for which the backbone is resolved on an atomic level, will be discussed here. The majority of residues for which mutation does not alter the selectivity are in our structure located in loops. The only exceptions are N210 and G223, which are close in space. Additionally G223 is on the border of a β -strand. Likewise all residues, which upon mutation do alter the selectivity, are in our structure located in β -strands or at the border of one. Furthermore residues, which are located in the N-terminal α -Helix, change the selectivity upon mutation. Since in our structure the helix is located inside the barrel this is as well in good agreement with the presented data.

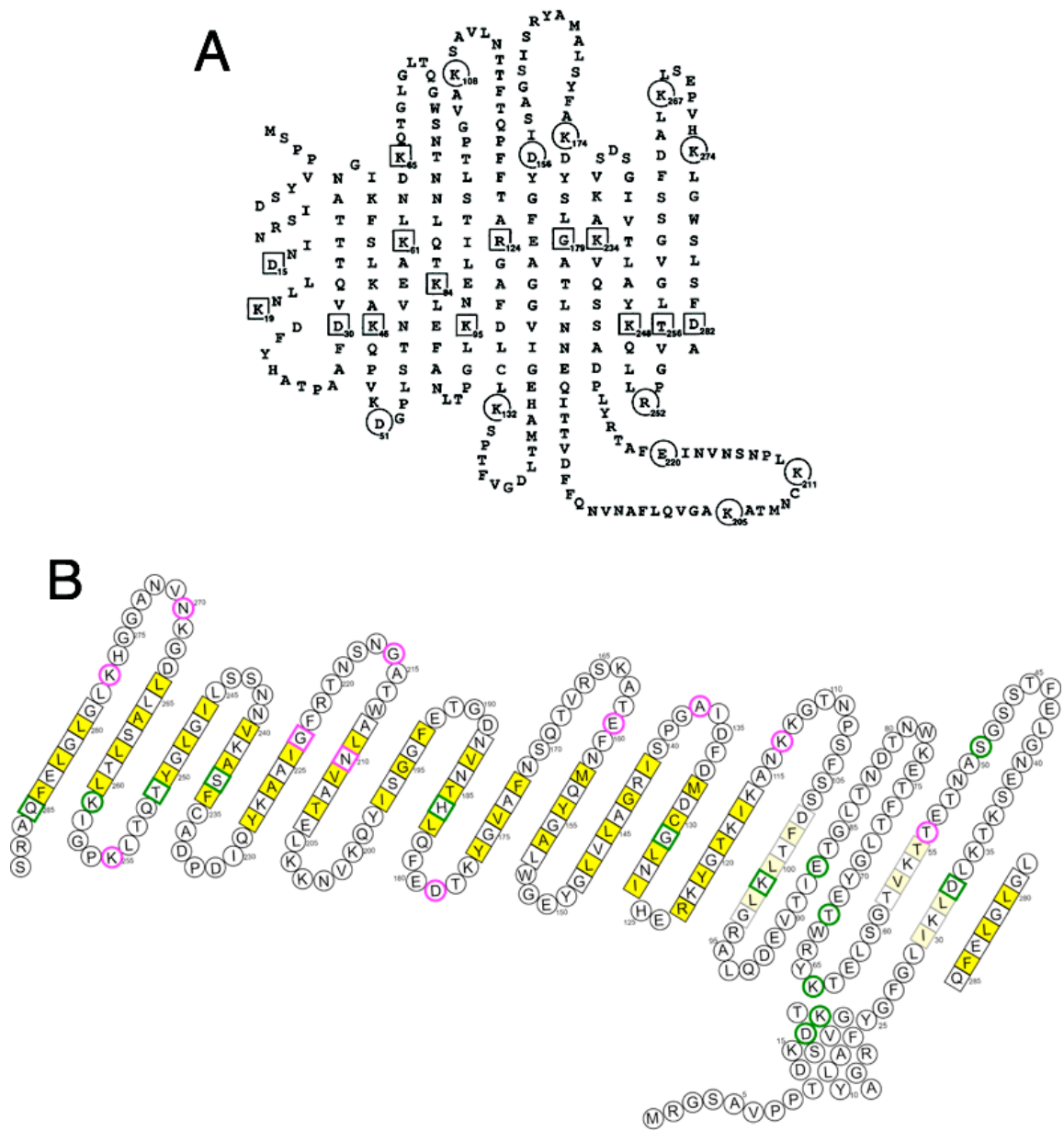


Fig. 25 **A)** Topology model of yeast VDAC according to Blachly-Dyson et al.^[63]. Residues for which mutation altered selectivity are boxed; residues for which the mutation left the selectivity unchanged are circled. **B)** Mutation sites of Blachly-Dyson^[63] mapped on homologous residues in the NMR-derived topology model of human VDAC. Residues for which mutation altered selectivity are encircled green; residues for which the mutation left the selectivity unchanged are encircled magenta.

Columbini^[44] proposes a model for the human VDAC that is based on Biotin modification data from Song et al.^[65] that was obtained for the *Neurospora crassa* VDAC. The model consists of 13 anti parallel β -strands and a N-terminal

transmembrane helix, which closes the barrel (see Fig. 26A). In this study streptavidin was bound to biotinylated sites of the protein followed by electrophysiological investigation. Amino acids were classified in type 1 and type 2. Type 1 amino acids show reduced conductance, type 2 a total block of current upon streptavidin binding to biotinylated sites. Previous studies revealed, that type 1 sites are static and permanently located on the VDAC surface. Type 2 sites are located on mobile domains, which only get accessible upon conformational rearrangement. By double mutations it was then investigated, if the corresponding amino acids are on the same or on opposite sites of the membrane. These mutations are all related to T53, which belongs to type 2. In human VDAC V57 corresponds T53. Since V57 is located in the flexible N-terminus its exact position cannot be determined, but it is most likely located in a β -strand. Our structure only agrees with the data for those residues, which are type 1 sites and are predicted to be located on the same side as T53, these are T135, D156, R240 and D264. In our structure homologous residues (S140, E161, S243, D267) are located in loops at the cytosolic side of the channel (see. Fig 26). Residues, which are said to be on the opposite site of T53, are in our structure mostly located in β -strands. The only exception is S111, which corresponds to A215. It is a type 1 residue and is located in a loop at the cytosolic side. Overall the data presented by Song et al.^[65] do not agree very well with our structure. One explanation could be, that the observed effects are influenced by the flexibility of T53. Another explanation would be, that data obtained from *Neurospora crassa* VDAC are not directly transferable to the human VDAC.

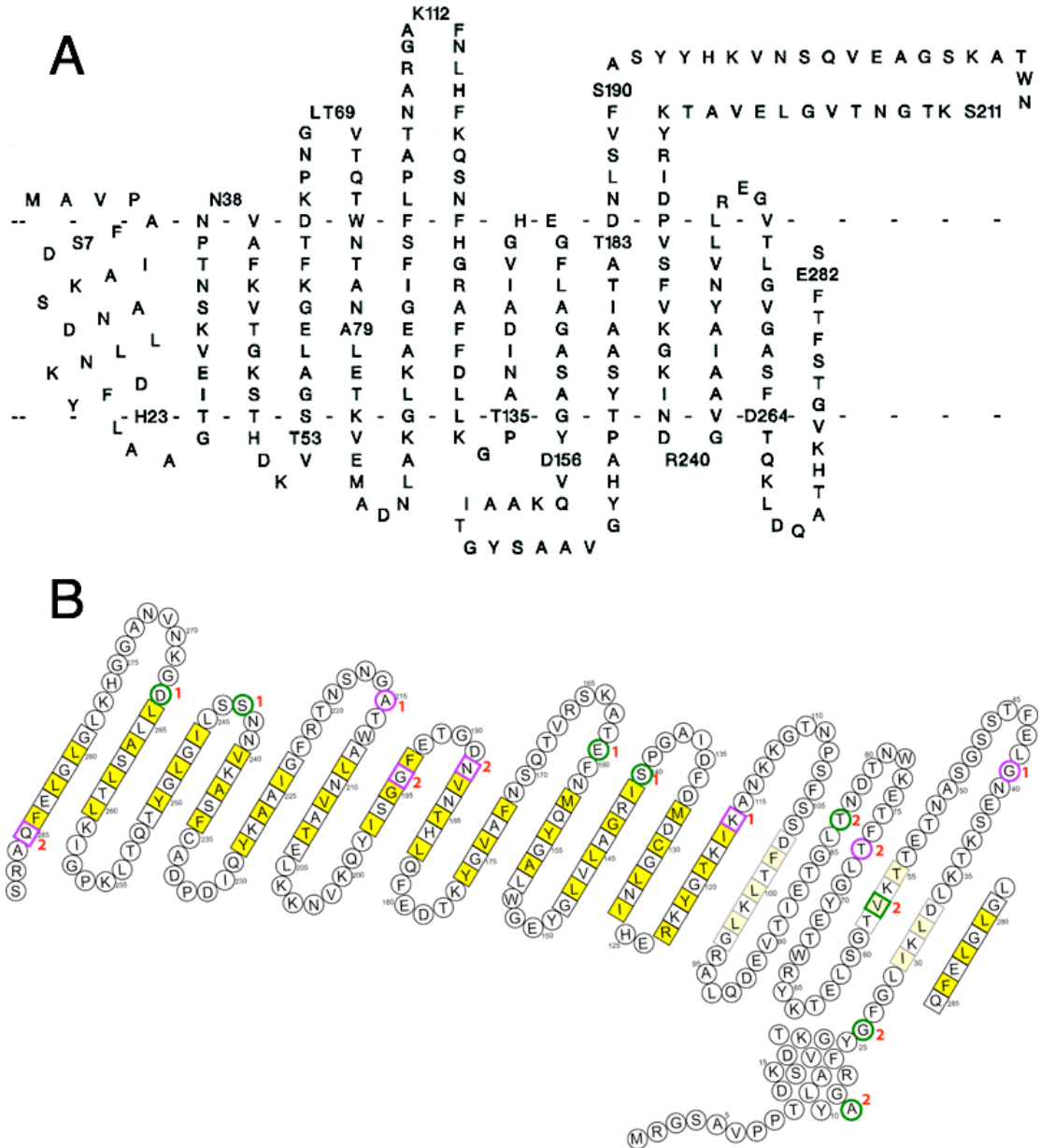


Fig. 26 A) Topology model of *Neurospora Crassa* VDAC according to Song et al.^[65] Residues, which were mutated to cysteins, are numbered. **B)** Mutation sites of Song^[65] mapped on homologous residues in the NMR-derived topology model of human VDAC. Residues, which should be on the same side as V57, are encircled green; residues, which should be on the opposite side as V57, are encircled magenta. Type 1 and type 2 residues are indicated with a red 1 or 2, respectively.

Nevertheless, Columbinis model, which is based on Songs et al.^[65] data, is also used in other studies for the visualisation of results. For example, Israelson et al.^[96] localised the Ca^{2+} binding sites of human VDAC as E72 and E202. They

mapped these residues on Columbinis model, which reveals that they are in loops at the cytosolic side of the barrel. Even though this does make sense, because these residues can come close in space, the authors would have expected the Ca binding site at the intermembrane space. This is because Ca^{2+} induces the opening of the permeability transition pore and therefore should accumulate in the inner membrane space. However in our structure E202 is located in a loop in the intermembrane space. E72 is in the N-terminal part and cannot be localised reliably.

3.4.4 Support for the presented structure from “in silico” analysis

The presented structure is supported by results of several web servers, which predict secondary structure elements or flexible parts in proteins. The secondary structure prediction was done with the PSIPRED server^[91, 92]. It revealed an N-terminal helix and 19 β -strands separated by coil regions. The prediction was run at a very early stage of the structure determination and was considered as very unlikely to be correct. The reason for this was the fact, that a β -barrel, which solely consists of anti parallel β -strands, can only be composed of an even number of β -strands. However, at an advanced stage of the structure determination the located β -strands were aligned to the PSIPRED prediction. Surprisingly the position of the 14 C-terminal β -strands determined by NMR spectroscopy were in very good agreement with the PSIPRED prediction (Fig. 27).

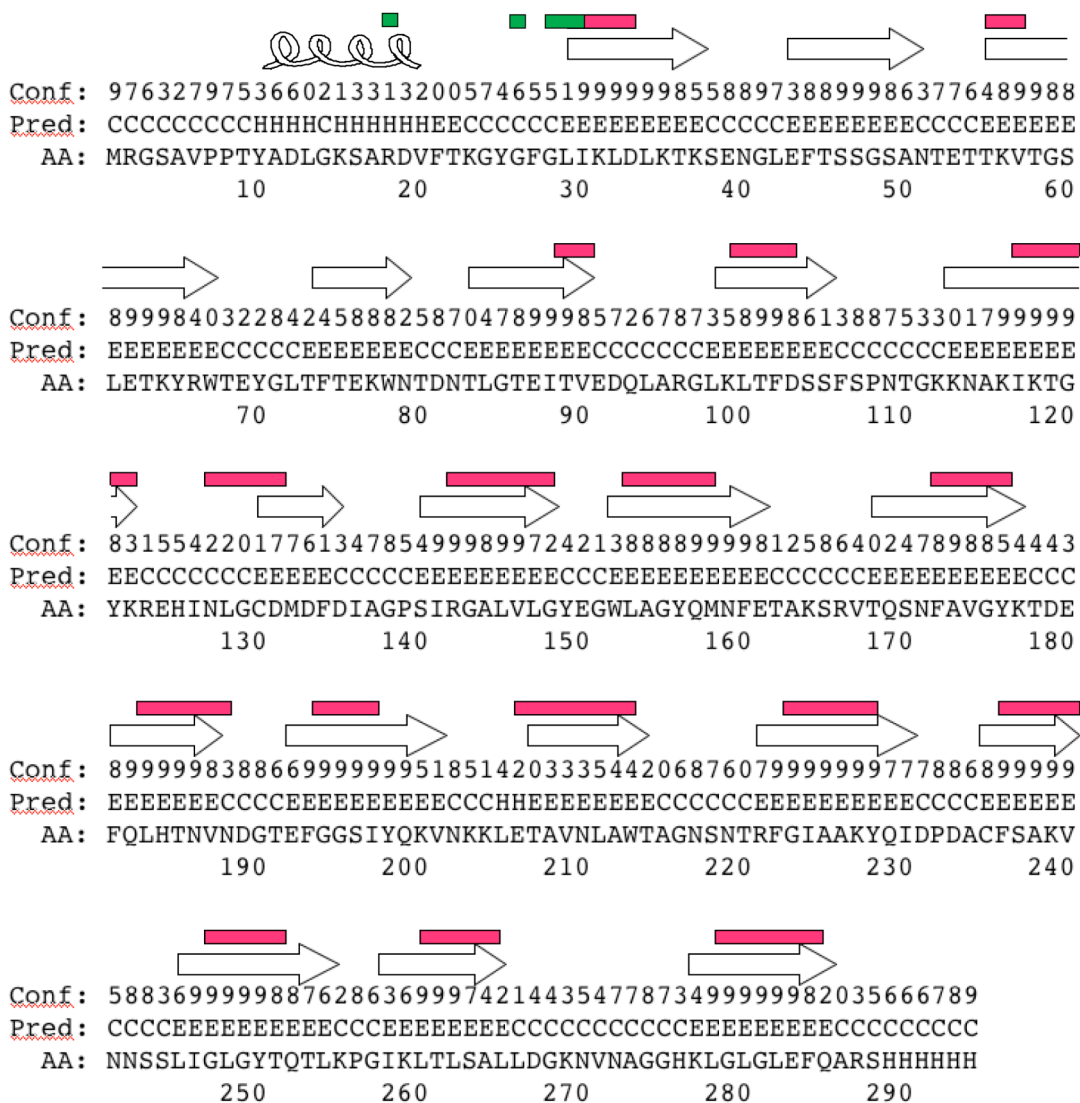


Fig. 27 Comparison of secondary structure elements determined either with the Psipred^[91, 92] server or experimentally. Red boxes indicate experimentally established β -strands; white arrows β -strands predicted by Psipred. Green boxes indicate negative secondary chemical shifts in the N-terminus, which gives rise to a loop or a helix, the white helix indicates a helix predicted by Psipred. The numbers in the row marked with “Conf” specify the confidence of the prediction, with 0 = low and 9 = high. The line marked with “Pred” shows the prediction, where H stands for Helix, E for strand and C for coil. The line marked with “AA” gives the one letter amino acid code for our construct of human VDAC.

The prediction of flexible parts was done with the DisProt^[99] (Fig. 28a) and with the DisEMBLTM 1.5^[100] (Fig. 28b) server. Even though these servers are optimized for natively unfolded proteins, the results fitted very well to the presented structure. DisProt showed significantly higher flexibility for residues between 25 to

125 than for residues between 126 to 255. DisEMBL differentiates between loops/coils and hot-loops. Loops are considered as a necessary but not a sufficient requirement of disorder. Hot-loops are loops with a high degree of mobility. For the human VDAC these hot loops can only be found in region between residue 40 and 120, except of the N- and C-terminus. In conclusion, both programs predicted higher flexibility for the N-terminal third of human VDAC, which is in good agreement with the NMR data.

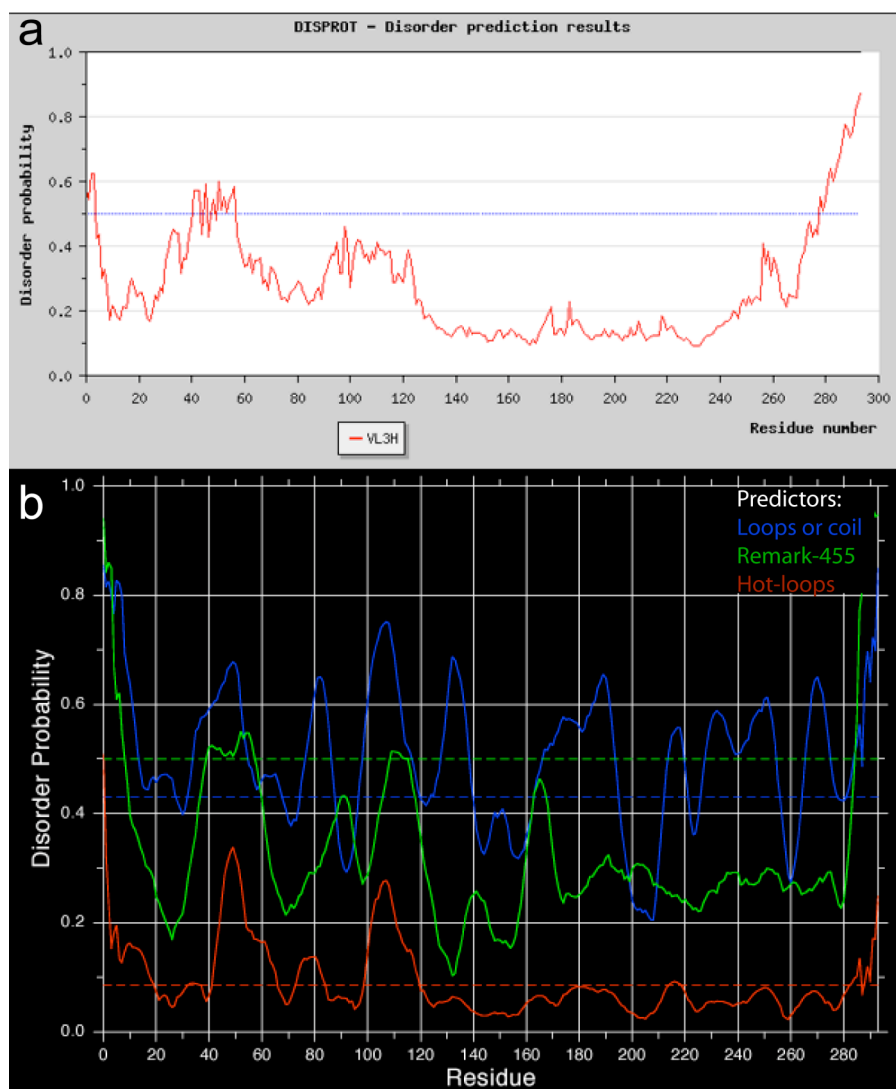


Fig. 28 Output of a) DisProt and b) DisEMBLTM 1.5 protein disorder prediction servers for human VDAC.

3.4.5 Biological relevance of enhanced flexibility in the N-terminus

The enhanced flexibility in the N-terminus, which makes structure determination for this part difficult, results from interesting biological features of the human VDAC. The protein is encoded in the nucleus, synthesised in the cytosol, targeted to mitochondria as a chaperone-bound species, recognized by the translocase of the outer membrane (TOM complex) and then inserted into the outer membrane^[101] by the help of the sorting and assembly machinery (Sam or Tob complex)^[102]. In most cases of pre-protein import into the mitochondria the Tom complex recognizes a N-terminal amphiphilic helix, with one positively charged and one hydrophobic phase^[103]. Since the N-terminal amphiphatic helix is sufficient for TOM recognition, this part interacts first with the TOM complex. Therefore the translocation of the proteins will start with the N-terminus. However for β -barrel proteins it is believed that the targeting information is encoded in a structural element, which involves different regions of the protein, rather than exclusively the N or the C-terminus^[104-107]. Nevertheless the human VDAC has an N-terminal amphiphatic helix from residue P8 to K23. The polar site has a net charge of +1. It is therefore very likely, that this helix is, besides other targeting sites, involved into TOM recognition, even though a $\Delta(1-19)$ HVDAC deletion mutant can still be incorporated into the mitochondrial membrane^[108]. Thus the direction of the translocation of human VDAC is expected to be from the N- to the C-terminus. It is known, that the driving force for protein translocation through the TOM complex does neither come from ATP nor from the membrane potential across the inner membrane. It rather stems from interactions with different binding sites with increasing affinity. Therefore the cis-binding site at the cytosol has a lower affinity to the pre-protein than the trans-binding site at the inter membrane space. This trans-binding site is thought to hold the pre-proteins until

further sorting to the mitochondrial sub-compartments takes place^[98, 102, 109, 110]. Thus, once the protein is trapped at the inter membrane space it can be easily incorporated into the mitochondria. An enhanced flexibility at the recognition site of the pre-protein would be extremely beneficial for this process, because it facilitates the sliding of the pre-protein through the TOM complex to the high affinity binding site. Therefore the observed flexibility in the N-terminus of human VDAC can be readily explained by its translocation behaviour through the TOM complex.

An additional explanation for the observed N-terminal flexibility is given by the study of Thomas et al.^[111]. They investigated the voltage-sensing domain of VDAC and found that a large portion of the protein, particularly the N-terminal third, contains residues that upon mutation affect the voltage gating properties of yeast VDAC. Therefore these residues identify regions of the protein that are translocated through the field in response to voltage changes. Additionally Thomas et al.^[111] refer to a previous study by Peng et al.^[112] where residues were located, which only affect the voltage gating properties of the open state but not, or only slightly, of the closed state of VDAC. Therefore the authors conclude, that the residues with impact on the voltage gating move out of the channel wall during channel closure. This behaviour is only possible, if this moving part has conformational freedom, which leads to increased flexibility. Thus, these results agree very well with the flexibility of the N-terminal third of VDAC observed by NMR.

Additionally, this helps to understand the difference between eukaryotic VDAC and bacterial porins. In contrast to the VDAC, bacterial porins are in vivo not voltage-gated^[113, 114]. This could be an explanation for the bad correlation between structural models for VDAC based on sequence alignment with bacterial porins and the actual structure.

3.4.6 Functional investigation of HVDAC

3.4.6.1 ADP-Titration

The residues, which are affected by the addition ADP, are equally distributed over the sequence (see 3.3.6.1). This corresponds well to the fact, that HVDAC is permeable to nucleotides. Since the nucleotides pass the channel, they can come close to the majority of residues. Additionally interactions can only be observed, if the nucleotide is present in large excess. This indicates a weak binding affinity. Again, this corresponds to VDAC's permeability to nucleotides. They should not bind tightly to the channel, but rather pass through it quickly. Of the 19 residues, which are influenced by ADP, 10 could not be assigned. Thus the existence of an additional binding site cannot be excluded.

3.4.6.2 Fluoxetine-Titration

The anti-depressant fluoxetine interacts primarily with the C-terminal loop. Additional effects can be observed in other loops, which are on the same side of the barrel (see 3.3.6.2). Since fluoxetine stabilises the low conducting state of VDAC^[115], the C-terminal loop might, upon binding to fluoxetine, block the channel pore. This could be initiated by moving this loop like a cap on top of the barrel. This would explain, why also other loops on the same side of the barrel are affected. This model is demonstrated in Fig. 29. Fluoxetine is a small organic compound. Therefore additional effects that are wider distributed over the sequence can be caused by further binding sites. Of the 28 peaks which are influenced by fluoxetine 12 could not be assigned. Since most assignments are missing in the N-terminus and in loops, these parts are also affected.

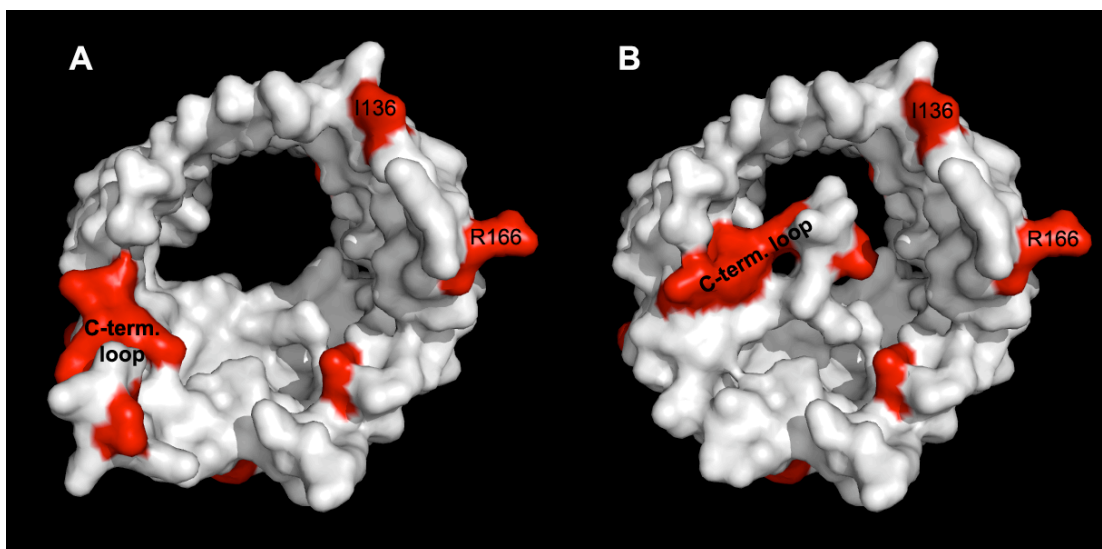


Fig. 29 Interaction sites of fluoxetine with HVDAC mapped on the NMR/x-ray structure of HVDAC. The position of the C-terminal loop is modelled in A and B because no electron density is present at this position. Residues with chemical shift changes of HN and N bigger than 0.025 ppm upon addition of a 32-fold molar excess of fluoxetine are shown in red (these residues are labelled with a yellow circle in Fig. 17). The position of the C-terminal loop is indicated. Residues Ile136 and Arg166 are labelled with the one letter amino acid code. A) Model without fluoxetine. B) Model upon fluoxetine binding.

Nahon et al^[115]. reported that fluoxetine inhibited the opening of the PTP, the release of cytochrome c and protected against staurosporine-induced apoptosis. It is suggested, that the apoptosis-related effects are mediated by the interaction of fluoxetine with the VDAC. Therefore the interaction of fluoxetine with the C-terminal loop of HVDAC might prevent apoptosis and might thus lead to an increased cancer risk upon fluoxetine treatment. However there are conflicting reports about this cancer risk. In vitro studies with tumor cells exposed to fluoxetine have shown inhibition^[116] or stimulation^[117, 118] of cell growth or DNA synthesis.

3.4.6.3 Interactions with pro- and anti-apoptotic proteins

Apoptosis is an essential cellular process strictly regulated by proteins of the Bcl-2 family^[47]. Members of this family are the anti-apoptotic Bcl-x_L and the BH3-only pro-apoptotic Bid. Both proteins interact with HVDAC. Most interestingly, they bind to the same site of HVDAC (see 3.3.6.3 and 3.3.6.4), even though their function is contrary. This implies, that pro- and anti-apoptotic proteins compete for the binding site in HVDAC. This site is located at the C-terminus (see Fig. 30).

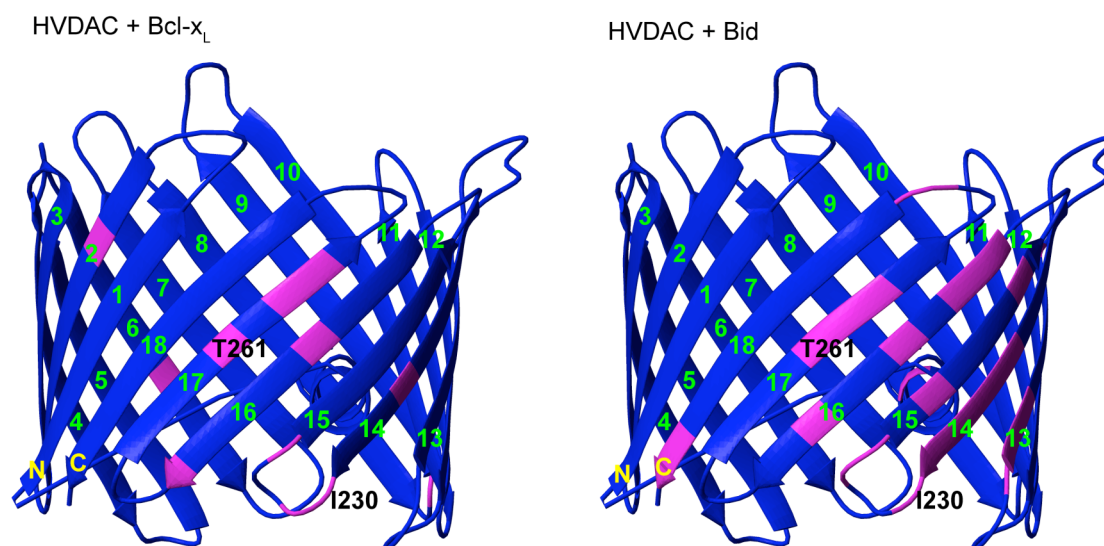


Fig. 30 Comparison of the interaction sites of Bcl-x_L and Bid with HVDAC mapped on the NMR/X-ray structure of HVDAC. In the case of Bcl-x_L residues, which are classified by Malia et al.^[47] to have major changes in the HVDAC spectrum, are coloured magenta. In the case of Bid residues with a peak intensity ratio < 0.61 of the spectra with and without Bid or which, upon Bid addition are broadened beyond detection, are coloured magenta. The N- and the C-terminus are labelled with a yellow N or C, respectively. The β -strand numbers are given in green. Residues Thr261 and Ile230 are labelled with the one letter amino acid code.

Bid interacts primarily with residues between L205 and A284, Bcl-x_L with residues between A224 and A284. Of the 48 residues, which are influenced by Bid or Bid-MTSL 15 could not be assigned. These missing assignments are most probably located in the N-terminus, since many assigned residues in the N-terminus are

affected and many assignments are missing in this region. The binding interface of Bcl-x_L was established by transferring the assignment of HVDAC on a published^[47], unassigned ¹⁵N-TROSY-HSQC spectrum of HVDAC in the presence of Bcl-x_L. Malia et al. pointed out some residues with major changes in the HVDAC spectrum. Of these 17 residues 5 could not be assigned. As for the case of Bid, these residues are most probably located in the N-terminus. Because of the low quality of the figure only these residues are considered to be in the binding interface of Bcl-x_L and HVDAC. The fact, that the binding site of Bid seems to be more extended than the one of Bcl-x_L, is most probably due to a more sophisticated evaluation of the Bid/HVDAC spectra. Most interestingly, the pro- and anti-apoptotic factors bind to a different site than fluoxetine, indicating a different binding mechanism.

Malia et al^[47] proposed, that helices 5 and 6 of Bcl-x_L move out of the protein core, insert into the mitochondrial membrane and that way bind to HVDAC. These helices are shown in green in Figure 31A. Bid is homologous to Bcl-x_L and both proteins interact with the same site of HVDAC. Therefore it is possible, that also the binding site of Bid is homologous to the one in Bcl-x_L. The helices homologous to helix 5 and 6 in Bcl-x_L are in mouse bid between M142 – H162 and L167 – Q180. They are also coloured green in Figure 31B. An indirect hint, that these helices can indeed be involved in HVDAC binding is provided by PRE-data of MTSL-labelled Bid. Mouse Bid contains two cysteines, C30 and C126, that can react with the MTSL. They are shown in red in Figure 31B. Both cysteines are not located in the helices hypothetically binding to HVDAC. Therefore no additional line broadening upon MTSL labelling of Bid are expected for residues in the binding core. Rather residues in the neighbourhood should be affected. This is exactly the observed situation (see 5.3.5.4). Therefore the helices from M142 – H162 and L167 – Q180 in mouse Bid

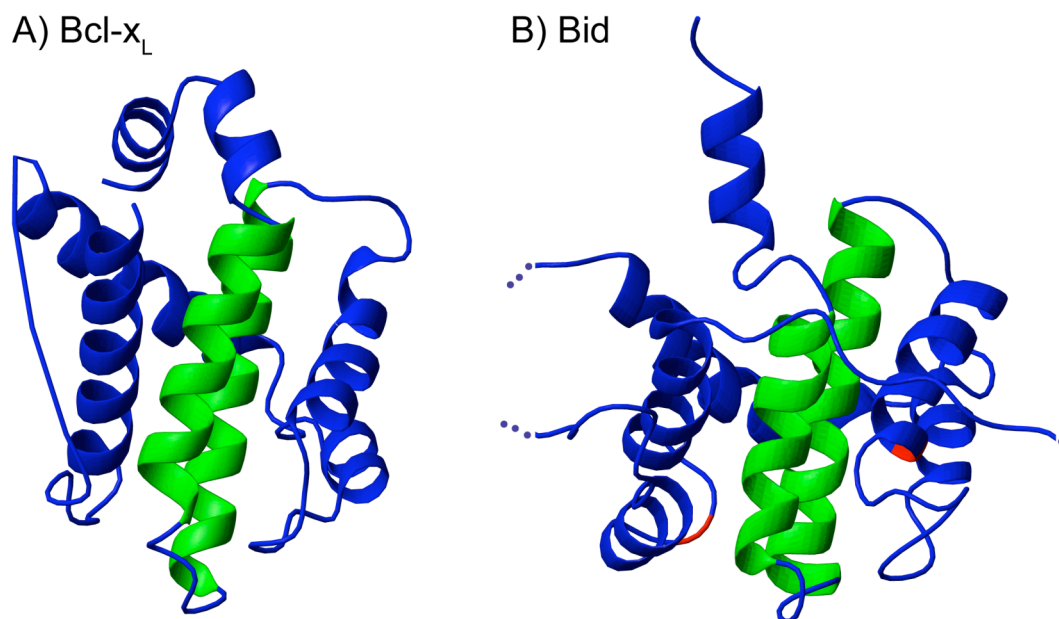


Fig. 31 **A)** Crystal structure of human Bcl-x_L^[119] (PDB code: 1R2D). Helices, which are proposed to insert into the membrane^[47], are coloured green **B)** NMR-structure of mouse Bid^[120] (PDB code: 1DDB). Helices, which are homologous to the membrane inserting ones of Bcl-x_L, are coloured green. Cysteine residues are shown in red.

should bind to the C-terminal part of HVDAC, namely to residues L205-T207, A225-I230 and D233-F236. These are the most clustered residues in HVDAC affected by Bid addition, but unaffected by further MTSL labelling of Bid. MTSL-labelling of Bid induces line broadening in the upper C-terminal part and in the N-terminus of HVDAC. Therefore the rest of the Bid molecule must bend towards the N-terminus of HVDAC.

VDAC is known to appear in oligomeric states^[121]. Malia et al^[47]. reported, that micelle-bound HVDAC is in intermediate exchange between monomer and trimer. If Bcl-x_L is present, a heterotrimer (HVDAC : Bcl-x_L 2:1) or a heterodimer is favoured. Therefore Bcl-x_L can break down the oligomeric state of HVDAC. A similar result was observed for the interaction of Bid with HVDAC^[29]. Chemical crosslinking experiments with glutaraldehyde and Ruthenium Red were performed. In the absence of Bid HVDAC monomers, dimers and trimers were observed. The

presence of Bid led to a decrease of the oligomeric HVDAC population and the appearance of HVDAC/Bid heterodimers. The fact, that in the presence of Bid HVDAC dimers are not favoured can be rationalised with the HVDAC/Bid binding interface. This interface overlaps on the HVDAC site with the region, where crystal contacts of HVDAC dimers are observed (Fig. 32). This points out, that upon HVDAC/Bid complex formation, the dimerisation site of VDAC is blocked.

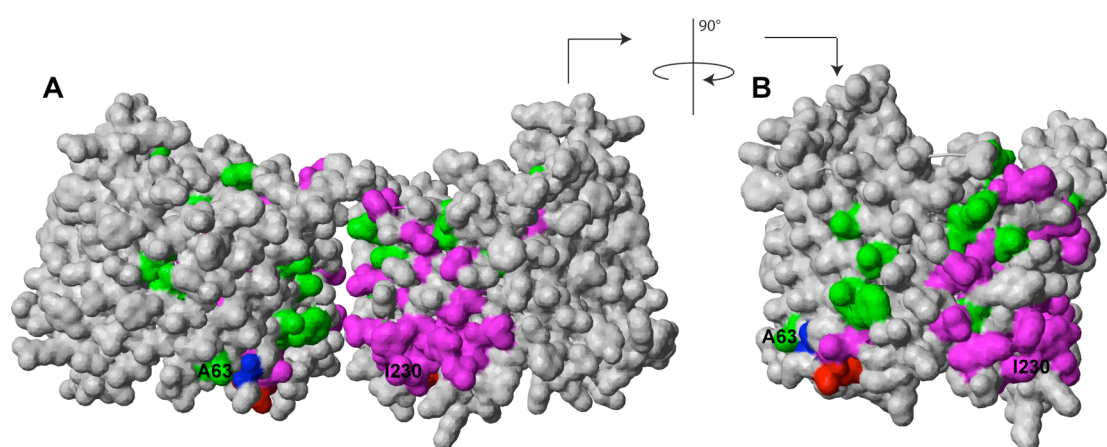


Fig. 32 Bid interaction sites are visualised on the Van-der-Waals surface plot of HVDAC. Residues with a peak intensity ratio < 0.61 of the spectra with and without Bid or which upon Bid addition are broadened beyond detection are coloured in magenta. Residues with a peak intensity ratio < 0.5 of the spectra with Bid and Bid-MTSL or which upon MTSL labelling of Bid, are additionally broadened beyond detection are coloured in green. The N-terminus is shown in blue, the C-terminus in red. Grey residues are unaffected by Bid. The residues Ala63 and Ile230 are labelled with the one letter amino acid code. **A)** HVDAC dimer. Crystal contacts are observed at the dimeric interface. **B)** HVDAC monomer. The direct view on the dimeric interface is given. For this purpose the dimer in **A** was rotated by 90° and one molecule was removed.

Addition of Bid leads to partial unfolding with successive refolding of HVDAC. This behaviour was never observed for any other partially unfolded HVDAC sample. Usually once HVDAC is partially unfolded it stays like this. Therefore Bid influences the folding of HVDAC. Bid binds to the region in HVDAC

where the N- and the C-terminus close the barrel (Fig. 32). Therefore the influence on the HVDAC folding might be due to an opening of the HVDAC pore. This could be a hint for HVDAC's possible involvement in the permeability transition pore. If HVDAC was involved in the PTP it would experience a structural rearrangement. This might therefore be induced by the pro-apoptotic Bid.

3.4.6.4 Calcium (II) chloride and Gadolinium (III) chloride- Titration

The binding interface of HVDAC and Ca^{2+} could not be established. No chemical shift perturbations or peak intensity changes were observed in the ^{15}N -TROSY-HSQC of HVDAC upon addition of a 32-fold molar excess of Ca^{2+} . Gincel et al.^[95] suggested that Ca^{2+} and lanthanides bind to the same site in VDAC. The paramagnetic relaxation enhancement of lanthanide ions causes severe line broadening in the NMR spectra of their interaction partners. Therefore it was possible to establish the binding site Gd^{3+} in HVDAC (see Fig. 33). It is located in the C-terminal part of HVDAC. Primarily affected by the addition of Gd^{3+} are the 5 C-terminal β -strands. Of the 29 residues, which are influenced by Gd^{3+} , six could not be assigned. The Ca^{2+} binding sites established by Israelson et al.^[96] are at E76 and E206. These Ca^{2+} binding sites were indirectly identified by the interaction with azido ruthenium. The region around E76 could not be identified as a Gd^{3+} binding site, because this region was not assigned. However, 6 peaks that interact with Gd^{3+} were not assigned. Thus these peaks could possibly correspond to residues, which are located around E76. E206 also interacts with Gd^{3+} but it is rather located at the border of the Gd^{3+} -binding cluster. If Gd^{3+} would primarily interact with E206 the paramagnetic broadening would extend around E206. Yet, the Ca^{2+} and Gd^{3+} binding

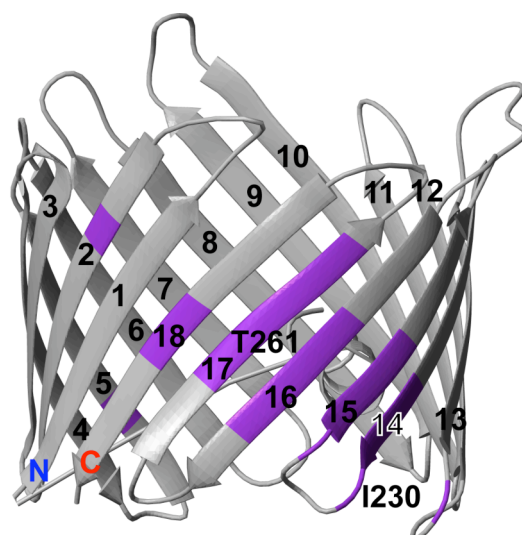


Fig. 33 Interaction site of Gd^{3+} with HVDAC mapped on the NMR/X-ray structure of HVDAC. Residues labelled in purple are broadened beyond detection upon addition of an equimolar amount of $GdCl_3$. Additionally residues, which are very likely to be broadened beyond detection because they are in very overlapping regions, are labelled purple. The N- and the C-terminus are indicated with a blue N or red C, respectively. The β -strand numbers are given in black. Residues Thr261 and Ile230 are labelled with the one letter amino acid code.

sites are definitely very close in space. Additionally this region in the 5 C-terminal β -strands also interacts with the pro-apoptotic protein Bid and the anti-apoptotic protein Bcl-x_L. Ca^{2+} influences apoptosis^[122, 123] and lanthanides inhibit mitochondrial Ca^{2+} uptake^[124, 125]. This points out that apoptosis related factors compete for the same binding site in HVDAC. Most interestingly the N-terminal helix is located close to this area. Thus the helix might perhaps be involved in the regulation of interactions between HVDAC and apoptotic factors.

3.5 Conclusions

In conclusion, the structure of HVDAC was determined conjointly by NMR-spectroscopy and X-ray crystallography. This is the first time that these methods were united to solve a de novo membrane protein structure. It is the first structure of a

human, mitochondrial ion channel. HVDAC adopts a β -barrel fold composed of 18 β -strands and one α -Helix that is not part of the barrel wall. The N-terminal part, which contains the voltage-sensing domain^[111], shows in solution an increased flexibility. The C-terminal part is mainly responsible for binding of interaction partners. The pro-apoptotic protein Bid and the anti-apoptotic protein Bcl-x_L are interacting with the same site in the C-terminal part of HVDAC. Bid and Bcl-x_L both belong to the Bcl-2 family and are structurally homologous. Due to their contrary function related to apoptosis their similar binding behaviour with HVDAC is surprising. The lanthanide Gadolinium binds to the same site as Bid and Bcl-x_L, close to the Ca²⁺ binding site known from literature. This points out that apoptosis related factors compete for the same binding site in HVDAC. The antidepressant fluoxetine interacts mainly with the C-terminal loop that is not affected by apoptotic factors. Fluoxetine, like Bid, stabilises the low conducting state of HVDAC. Since the interaction sites of both molecules are not the same this indicates a different mechanism of channel closure. ADP interacts with low affinity with HVDAC and the binding sites distributed over the whole sequence. This is in line with nucleotide conductivity of HVDAC. The nucleotides should not bind tightly to the channel, but rather pass through it quickly.

4

Structural and functional investigation of Conk-S1

4.1 Introduction

Kunitz domain proteins, like the bovine pancreatic trypsin inhibitor (BPTI)^[126] or the dendrotoxins^[127], are small, basic proteins that contain three highly conserved disulfide bonds. The three disulfide crosslinks make these extracellular proteins extremely stable. Two different general functions are known for the different Kunitz proteins. One group, including BPTI consists of potent protease inhibitors. The complex of BPTI and trypsin is exceptionally stable, with an association constant of $>10^{13} \text{ M}^{-1}$ ^[128]. The dendrotoxins belong to another group of Kunitz peptides found in the venom of the black mamba, that block different potassium channels with high specificity and selectivity^[129]. In snake and scorpion venoms a diverse set of different potassium channel blockers has been identified^[127].

Despite the great variety of toxins from the venoms of the predatory cone snails, relatively few have been identified so far that interact with K^+ channels^[20]. Most conotoxins are small, peptidic toxins, that typically contain 10-30 amino acids and bind with high affinity and specificity to various ligand gated or voltage gated ion channels. One striking feature of these peptides is that they usually contain a diverse complement of posttranslational modifications, like C-terminal amidation, hydroxyprolines or glycosylation of serine or threonine^[130]. Conotoxins can be broadly divided into two groups, the non-disulfide-rich peptides and the disulfide-rich

conotoxins. The latter conotoxins are further separated into several families based on cysteine bridge pattern and biological activities ^[20].

The K⁺ channel-targeted toxin Conkunitzin-S1 (Conk-S1) from the venom of *Conus striatus* is the first member of a new family of polypeptides. Recently it has been shown that Conk-S1 blocks *Shaker* K⁺ channels with an IC₅₀ of less than 100 nM (Imperial et al., unpublished results). Compared to most toxins from *Conus* venoms, Conk-S1 is unusually long (60 amino acids). The only post-translational modification of this peptide is the amidation of the C-terminal carboxylic acid. Conk-S1 shares 33% sequence identity with BPTI and 35% with Dendrotoxin I, indicating that it belongs to the Kunitz domain family of proteins (see Table 16). Therefore we do not use the term “conotoxin” for Conk-S1, which is restricted to smaller disulfide-rich peptide toxins from cone snails.

Table 16 Amino acid sequence of Conk-S1 and alignment with selected Kunitz domain proteins

	1	10	20	30	40	50	60
Conk-S1	KDRPSL	CDLPADSGSGT	KAEKRIYYNSARKQ	CLRFDYTGQGGNENNFRR	TYDCQRT	CLYT	
BPTI	RPDF	CLEPPYTGP	CKARIIRYFYNAKAGL	CQTFVYGG	CRAKRNNFKSAED	CMRT	CGGA
DTI	QPLRKL	CILHRNPGR	CYQKIPAFYYNQKKKQ	CEGFTWSG	CGGNSNRFKTIEE	CRRT	CIRK
DTK	AAKY	CKLPLRIGP	CKRKIPSFYYKWKAKQ	CLPFDYSG	CGGNANRFKTIIEE	CRRT	CVG

BPTI is the bovine pancreatic trypsin inhibitor ^[131], DTI and DTK are dendrotoxin I and K from *Dendroaspis polylepsis polylepsis* ^[131].

One striking difference between Conk-S1 and other native Kunitz-type proteins is that it contains only four cysteine residues, resulting in only two disulfide-bridges instead of the three found in all other native proteins that have been biochemically characterized in this group. The homologous cysteine residues of BPTI and Dendrotoxin I are replaced by Gly16 and Gln40 of Conk-S1. Therefore, Conk-S1 is a Kunitz domain protein, in which one of the highly conserved disulfide bridges is missing.

4.2 Materials and methods

4.2.1 Expression, refolding and purification of Conk-S1

The expression construct was prepared and the expression conditions were optimized by Roland Graf under supervision of Stefan Becker at the Max-Planck-Institute for Biophysical Chemistry in Göttingen. Full-length Konkunitzin-S1 cDNA sequence was obtained by 5' and 3' RACE procedures, as previously described^[132, 133] Degenerate oligonucleotide PCR primers were based on portions of amino acid sequence of the isolated peptide^[134] and mRNA was isolated from *C. striatus* venom ducts. Details of the isolation of the konkunitzin gene family are being prepared in a separate manuscript (J. Garrett et al., in preparation). The cDNA clone coding for the Conk-S1 precursor protein (Fig. 34) was used as a template to amplify by PCR the coding sequence of mature Conk-S1.

```
ATG GAG GGA CGT CGT TTT GCT GCT GTT CTG ATC CTG ACC ATC
M E G R R F A A V L I L T I
TGT ATG CTT GCA CCT GGG ACT GGT ACT TTG CTA CCT AAG GAT
C M L A P G T G T L L P K D
CGA CCG AGT CTA TGC GAT CTA CCA GCG GAC AGT GGG TCG GGC
R P S L C D L P A D S G S G
ACA AAG GCT GAG AAG AGA ATT TAC TAC AAT AGC GCT AGA AAA
T K A E K R I Y Y N S A R K
CAG TGT TTA AGG TTC GAT TAC ACA GGA CAA GGA GGC AAC GAA
Q C L R F D Y T G Q G G N E
AAC AAT TTT CGC CGT ACT TAC GAT TGC CAA CGA ACG TGT CTG
N N F R R T Y D C Q R T C L
TAT ACA TGA
Y T STOP
```

Fig. 34 Sequence of the Conk-S1 precursor protein cDNA. The arrowhead indicates the signal sequence cleavage site.

The forward primer 5'-GGT GGT TGC TCT TCC AAC AAG GAT CGA CCG AGT CTA TGC G-3' contained an engineered *SapI* restriction site (underlined). The reverse primer 5'-GCT GAA TTC CTG CAG TCA TGT ATA CAG ACA CGT TCG TTG GC-3' contained an engineered *PstI* restriction site (underlined). The PCR product was purified with the MinElute PCR purification kit (Qiagen). The *SapI*- and *PstI*-digested fragment was purified and cloned into the corresponding sites of the pTWIN1 vector (New England Biolabs) downstream of the coding sequence of a modified form of the *Synechocystis* sp. *dnaB* gene (Ssp DnaB) intein^[23, 135]. The selected clone was verified by DNA sequencing.

Conk-S1 and its mutants were expressed in *E. coli* BL21 (DE3). A one liter culture was grown at 37° C in Luria Bertani medium. Six hours after induction with 1 mM IPTG the culture was harvested and resuspended in a buffer containing 20 mM Tris, pH 8.5, 500 mM NaCl, 1 mM EDTA and 0.5 mM PMSF. The cells were lysed by ultrasonication and the inclusion bodies were pelleted by centrifugation.

The inclusion body pellet was dissolved in 20 ml of 6 M guanidinium hydrochloride and 50 mM β-mercaptoethanol. Insoluble debris was removed by centrifugation. The supernatant was dialysed for 16 h at 4 °C against 1 liter of a buffer containing 3 M guanidinium hydrochloride, 2 mM reduced glutathione, 0.2 mM oxidized glutathione, 2 mM EDTA and 50 mM Tris at pH 8. Afterwards the sample was dialysed for 16 h at 4 °C against 1 l of the same buffer without guanidinium hydrochloride. Precipitant was removed by centrifugation at 75000 x g for 20 min. For cleaving the CBD-Ssp DnaB intein tag from the peptide, the supernatant was dialysed against a buffer containing 0.5 M NaCl, 1 mM EDTA, 0.5 mM PMSF and 20 mM Tris, pH 6.5 for 5h at 4 °C, followed by 16 h of dialysis at room temperature. Afterwards the buffer was exchanged via dialysis to 50 mM HEPES, pH 7.0. The

solution was loaded on a 1 ml HiTrapTM SP XL cation exchange column and the peptide was eluted with a 30 ml linear gradient to 1 M NaCl in the same buffer. Fractions containing the toxin were pooled, dialyzed against water and lyophilized. The toxin was further purified by high performance liquid chromatography (HPLC) on a preparative VYDAC C18 reversed phase column. It was eluted with a 30 ml linear gradient from 0 to 60% acetonitrile in water and 0.1% trifluoroacetic acid.

4.2.2 NMR Sample Preparation

NMR spectra were recorded from two samples, which contained either 0.5 mM ¹⁵N-labeled, or 1 mM ¹⁵N/¹³C-labeled Conk-S1 in 0.1 M sodium acetate buffer, pH 5.2, with 10% ²H₂O. Dipolar couplings were measured from an anisotropic sample, in which the peptide was partially aligned. It contained 0.5 mM ¹⁵N/¹³C-labeled Conk-S1 in 85.5% 0.1 M sodium acetate buffer, pH 5.2, 9.5% ²H₂O, 4.3% pentaethylene glycol monododecyl ether (C₁₂E₅) and 0.7% n-hexanol. The nematic phase was formed after vigorous mixing^[35].

4.2.3 NMR Resonance Assignment and Structure Calculation

All spectra were recorded at 27°C on Bruker 600, 700, 800 or 900 MHz spectrometers equipped with shielded gradient triple resonance probes. For the backbone and side chain assignment the standard heteronuclear (¹H, ¹³C, ¹⁵N) strategy based on 3D HNCACB, CBCA(CO)NH, HNC(O), HN(CA)CO, HCCNH-TOCSY, CCONH-TOCSY, and HCCH-TOCSY experiments was used^[89]. The backbone resonance assignment was achieved automatically with the assignment program MARS^[136]. ³J_{HN-HA} coupling constants were obtained using two-dimensional CT-HMQC-J spectra and were converted to Φ torsion angles with the empirical Karplus

equation ^[137]. χ_1 torsion angles were gained from two-dimensional HNCG spectra ^[138]. The program TALOS was used to obtain the backbone dihedral angles (Φ and Ψ) on the basis of chemical shift information ^[139]. Interproton distance restraints were derived from 3D ¹⁵N-edited NOESY (120 ms mixing time) and ¹³C-edited NOESY spectra (128 ms mixing time). The NMR data were processed and analyzed using NMRPipe, NMRDraw ^[76] and SPARKY (T. D. Goddard and D. G. Kneller, SPARKY 3, University of California, San Francisco, CA).

The NOE spectra were automatically peak picked and integrated with SPARKY. NOE cross peaks were assigned both manually and automatically by the programs ARIA2alpha ^[140]. Unambiguous cross peak assignments with a range of 1.7 to 5 Å set by ARIA2alpha were used for the final structure calculations.

Residual ¹D_{N-H}, ¹D_{CA-HA}, ¹D_{N-C} and ¹D_{C-CA} dipolar couplings were gained from the difference between the *J* couplings measured in the aligned and isotropic media. ¹J_{N-H} and ¹J_{N-C} couplings were measured simultaneously from interleaved 3D TROSY-HNCO ^[141] spectra and ¹J_{CA-HA} and ¹J_{CA-C} were obtained simultaneously from interleaved 3D CBCA(CO)NH spectra ^[142]. The magnitude (normalized to ¹D_{N-H}) and rhombicity of the alignment tensor were 13.0 Hz and 0.38, respectively, as determined from the histogram of dipolar couplings by the program PALES ^[37].

Initially, a medium resolution structure was calculated with the program Rosetta NMR ^[143] based on dipolar couplings and chemical shift information, and applying the ITAS approach ^[144]. This structure was used as a starting point for calculation of a high-resolution structure using CNS Solve 1.1 ^[145], interfaced with ARIA 2alpha. A simulated annealing protocol with 14 iterations was performed. In the last iteration step a total of 500 structures were calculated. The 20 structures with lowest total energy were further refined in explicit water ^[146] and were used for the

statistics. A total of 659 NOE's, 493 of them short range ($|i - j| \leq 1$), 78 medium range ($1 < |i - j| < 5$) and 88 long range ($|i - j| \geq 5$) NOE's, 201 dipolar couplings, 126 dihedral angles and two disulfide bridge constraints were used in structure calculations.

4.2.4 Electrophysiological Measurements

To study the effects of the wild type and mutants of Conk-S1 with the *Shaker* K channel the *Xenopus* oocyte expression system was used. Oocyte preparation and *Shaker* RNA injection were basically performed as described by Jacobson et al. ^[147] (see 2.2.4).

4.3 Results

4.3.1 Refolding and Purification of Conk-S1

Conk-S1 could be expressed as a fusion protein with a modified Ssp DnaB intein^[23, 135] in large amounts, but mainly in insoluble form. Active Conk-S1 contains two disulfide bridges. Therefore oxidants for the disulfide bridge formation were added during refolding trials. Initially refolding was done at pH 7.7 in the presence of 1 mM β -mercaptoethanol as a reducing agent. The C-terminal cleavage reaction of the Ssp DnaB intein was found to be pH-dependent, with an optimum between pH 6.0 and 7.5^[23]. Therefore after refolding the fusion protein was cleaved by shifting the pH from 7.7 to 6.5. Since the Ssp DnaB intein tag also contained a chitin-binding domain (CBD) the cleavage reaction was at first carried out on chitin resin. However only approx. 50 % of the fusion protein could be cleaved this way. Executing the cleavage reaction in solution during a dialysis step resulted in an almost complete cleavage. In an SDS-PAGE analysis (Fig. 35, lanes 1-2) only a minor band of the fusion protein

was left after cleavage while a new band with the expected molecular weight of Conk-S1 became clearly visible. Subsequent purification by HPLC resulted in an average yield of 0.5 mg. By introducing a cation exchange chromatography step before HPLC the yield was increased more than 1.5 fold. Hereby the very basic Conk-S1 (pI 9.12) was successfully separated by cation exchange chromatography from the acidic fusion partner Ssp DnaB (pI 6.15) as well as from most *E. coli* proteins (Fig. 35, lane 3). Furthermore, replacing β -mercaptoethanol as oxido shuffling agent by 2 mM reduced glutathione and 0.2 mM oxidized glutathione resulted in doubling of the yield. The combination of reduced/oxidized glutathione in the refolding buffer at pH 8.0 with the two step purification by cation exchange chromatography and

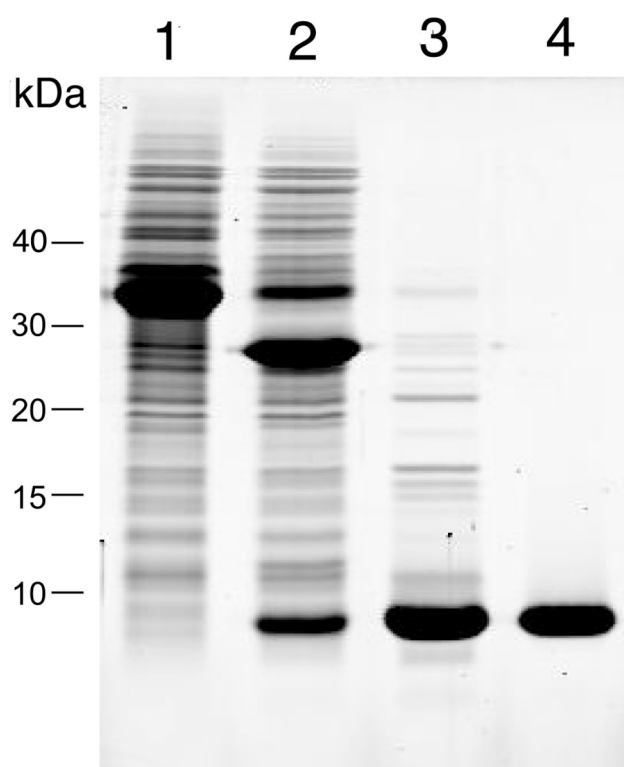


Fig. 35 Analysis by Coomassie-stained SDS-PAGE. Lane 1: supernatant of refolding from 6 M Gdn-HCl; lane 2: after cleavage of the SspDnaB/Conk-S1 fusion protein by pH shift; lane 3: combined fractions below peak 2 from SP Sepharose column; lane 4: final product after HPLC purification.

HPLC proved to be most successful. In the end from 1 L of LB expression culture 1.9 mg of highly pure, refolded Conk-S1 (Fig. 35, lane 4) were reproducibly obtained.

4.3.2 Resonance Assignment and Tertiary Structure

The ^{15}N HSQC of Conk-S1 displayed an excellent chemical shift dispersion indicative of a well-folded, rigid protein (Fig. 36)

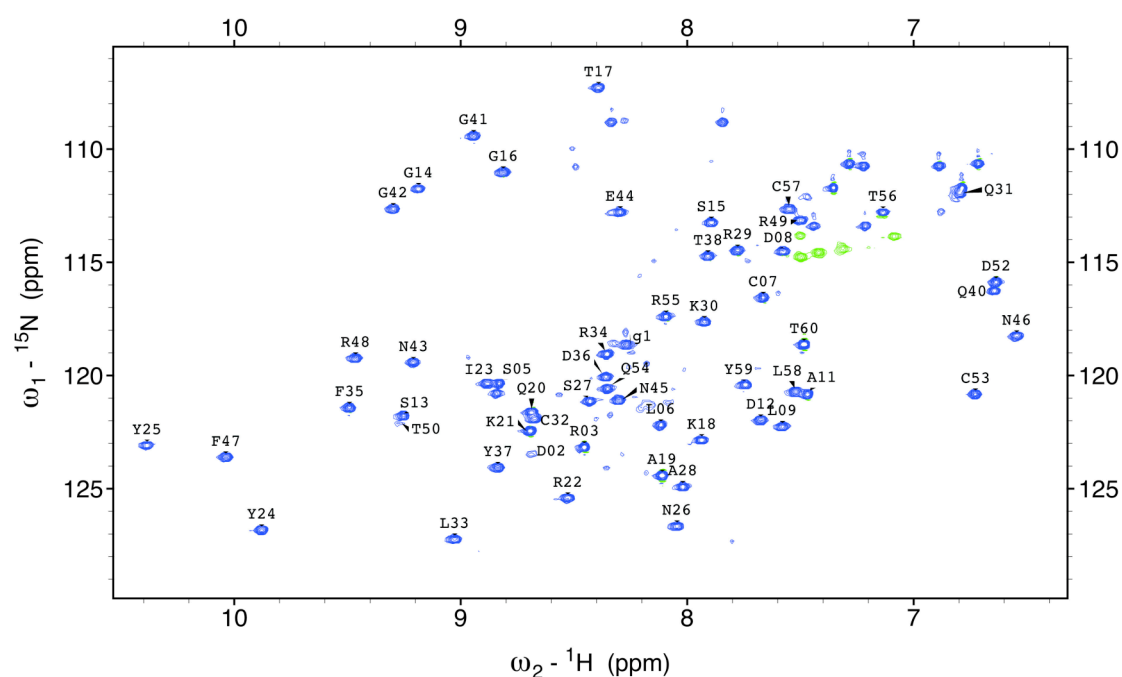


Fig. 36: ^{15}N -HSQC spectrum of 1 mM Conk-S1 in 0.1 M sodium acetate buffer, pH 5.2. The spectrum was recorded at 27°C on a 600 MHz spectrometer. Assigned residues are labelled with the one letter amino acid code.

Backbone resonances for all residues except Gly39 and Tyr51 could be identified in the ^{15}N HSQC spectrum. In total 96.97% of the backbone resonances and 91.63% of the side chain chemical shifts have been assigned. The superposition of the 20 structures with the lowest total energy is shown in Figure 37b.

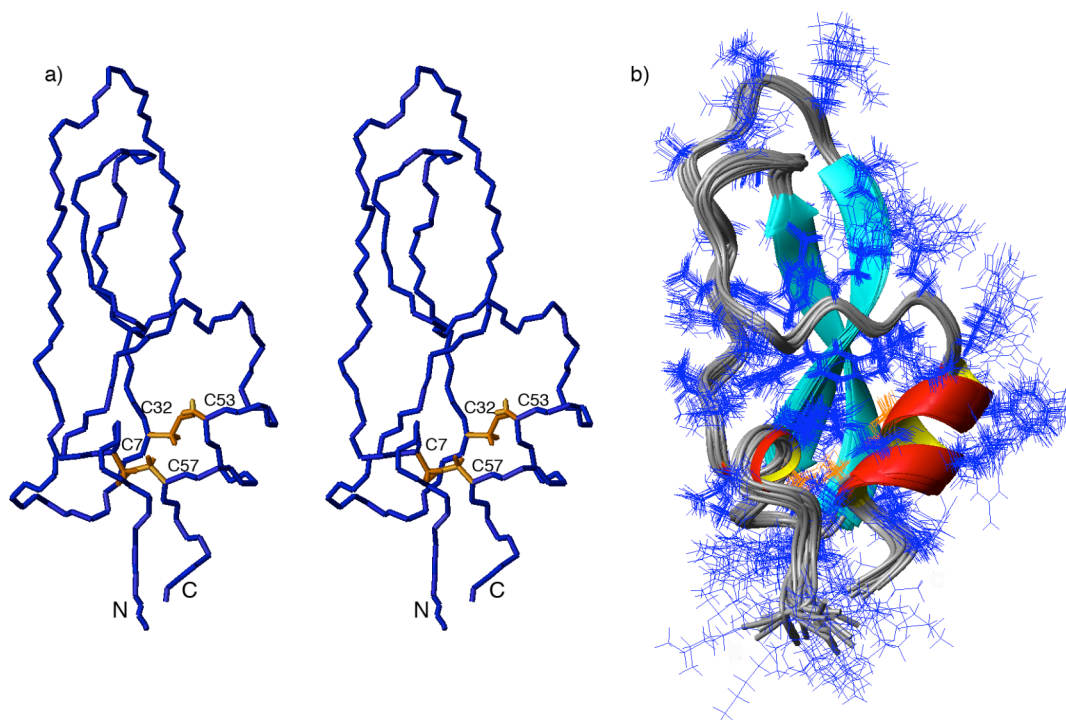


Fig. 37: NMR solution structures of Conk-S1. (a) Stereo view of the backbone atoms (N, C α , C, O). Represented is the mean structure of the 20 structures with lowest total energy. Cysteine bridges are marked in orange. (b) Superposition of the 20 structures with lowest total energy. Ribbon presentation of the backbone including side chains, represented as lines. Helices are marked in red and β strands in cyan. All figures were created with the program MOLMOL ^[148]

The quality of the solution structures is summarised in Table 17. In the Ramachandran plot 82.5% of the dihedral angles appear in the most favourable region and 16.5% in the additionally allowed region. For all heavy atoms the root mean square deviation from the mean structure is 1.4 Å and for the backbone atoms it is 0.5 Å. Side chains are well defined, as can be seen from Fig. 37b.

Table 17 Structural statistics

Parameter	
R.m.s.d.s from experimental restraints	
NOEs (659) [Å]	0.085 ± 0.023
Dihedral angles (126) [°]	2.75 ± 0.15
Correlation coefficients of experimental RDCs	
¹ D _{NH}	0.988
¹ D _{C'N}	0.983
¹ D _{CAC'}	0.984
¹ D _{CAHA}	0.986
R.m.s.d.s to the averaged coordinates [Å]	
Backbone heavy atoms	0.5
All heavy atoms	1.4
Distance restraint violations	
Number > 0.5 Å	0.6 ± 0.9
Maximum [Å]	1.60 ± 0.65
Energies [kcal/mol]	
E _{all}	-560 ± 108
E _{angle}	322 ± 12
E _{NOE}	187 ± 24
Ramachandran statistics	
Most favourable region (%)	82.5
Additional allowed region (%)	16.5
Generally allowed region (%)	0.3
Disallowed region (%)	0.7

Steady state heteronuclear ¹⁵N{¹H}-NOEs for most of the Conk-S1 backbone amides are above 0.6 indicating that the backbone of Conk-S1 is well ordered in solution (Fig. 38). Only Thr 60 and Ala19 are flexible with ¹⁵N{¹H}-NOE values of 0.22 and 0.15, respectively, and the three N-terminal residues are affected by motion. Ala19 is located in the region homologous to the antiprotease loop of BPTI and is close to the “missing” third disulfide bond, which would link the positions of Gly16 and Gln40.

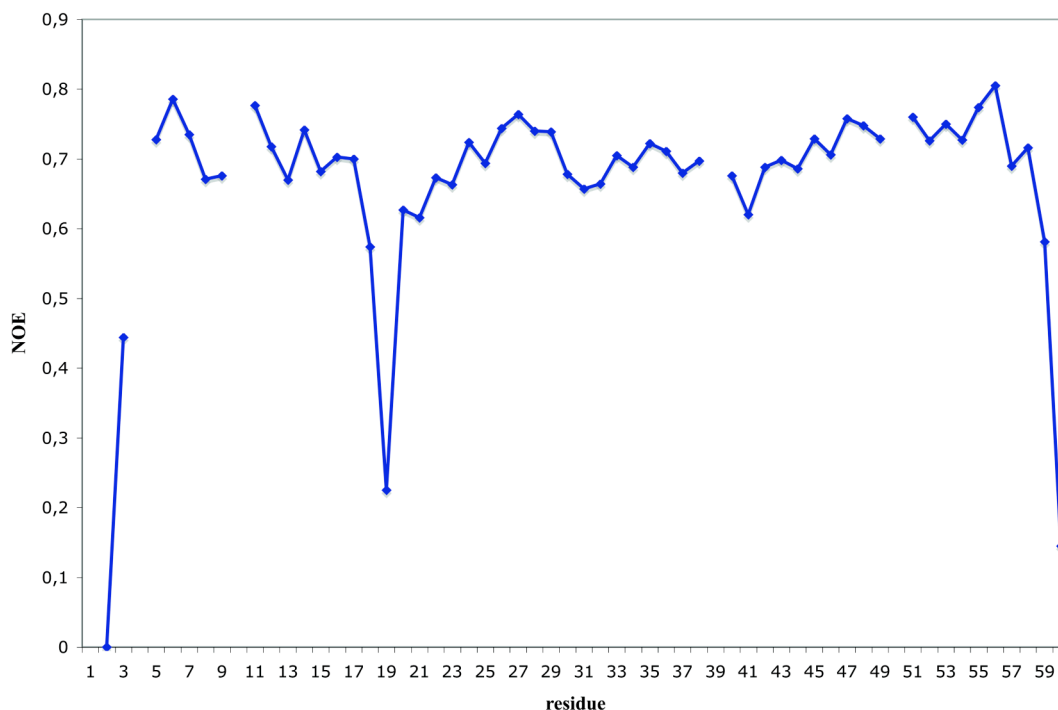


Fig. 38 The ^{15}N - ^1H -NOE of Conk-S1 plotted against the residue number

The solution structure of Conk-S1 resembles the typical Kunitz type fold. It consists of a 3_{10} -helix of residues 6 to 8, a twisted β -hairpin of residues 20 to 36 and an α -helix of residues 50 to 56. The two helices are connected by the disulfide bridge between Cys7 and Cys57. The C-terminal helix is also connected to the β sheet by the disulfide bridge between Cys32 and Cys53. The disulfide bridge 7-57 was confirmed by 4 direct NOE contacts between these residues. For the other S-S pairing no direct contact could be observed. In this case NOEs between Cys32 and Gln54 and other long-range NOEs between residues close to the cysteines were used to confirm the cysteine bridge.

To verify, that the disulfide bonds were actually formed, electrospray quadrupole mass spectra were recorded. The theoretical mass of Conk-S1 without disulfide bridge formation would be 6933,6 Da. The experimentally derived mass was $6929,3 \pm 0.8$ Da, consistent with the formation of two disulfide bonds. The same

analysis was carried out for the G16CQ40C mutant Conk-S1^{CC}. Theoretical mass of the reduced state and experimental mass are 6954,7 Da and $6948,2 \pm 0.9$ Da, respectively, consistent with the formation of three disulfide bonds.

4.3.3 Functional characterization with voltage clamp experiments

Since the recombinant Conk-S1 does not contain the amidated C-terminus observed in the native peptide, the affinity of the recombinant peptide on *Shaker* K⁺ channels expressed in *Xenopus* oocytes was measured. The functionality of the recombinant Conk-S1 with the free acid at the C-terminus was assayed by two-electrode voltage clamp measurements. For these experiments the *Shaker* K⁺ channel with removed N-terminal inactivation domain (*Shaker-Δ6-46*)^[149] was used because it was reported that the current mediated by this mutant is more strongly modified by the presence of toxins^[150, 151]. Fig. 39 shows that this channel was blocked by Conk-S1 with an IC₅₀ value of 502 ± 140 nM (n = 3).

Since it has been reported that κM-conotoxin RIIK^[152], which is also blocking *Shaker* K⁺ channels, showed an increase in affinity when tested on a pore mutant of this channel (K427D), the functional effect of Conk-S1 on this mutated *Shaker* channel was also investigated. Most interestingly the affinity of Conk-S1 for this mutant was 0.22 ± 0.08 nM (n = 4), which is more than 2000-fold higher than for the wild type channel (see Fig. 39).

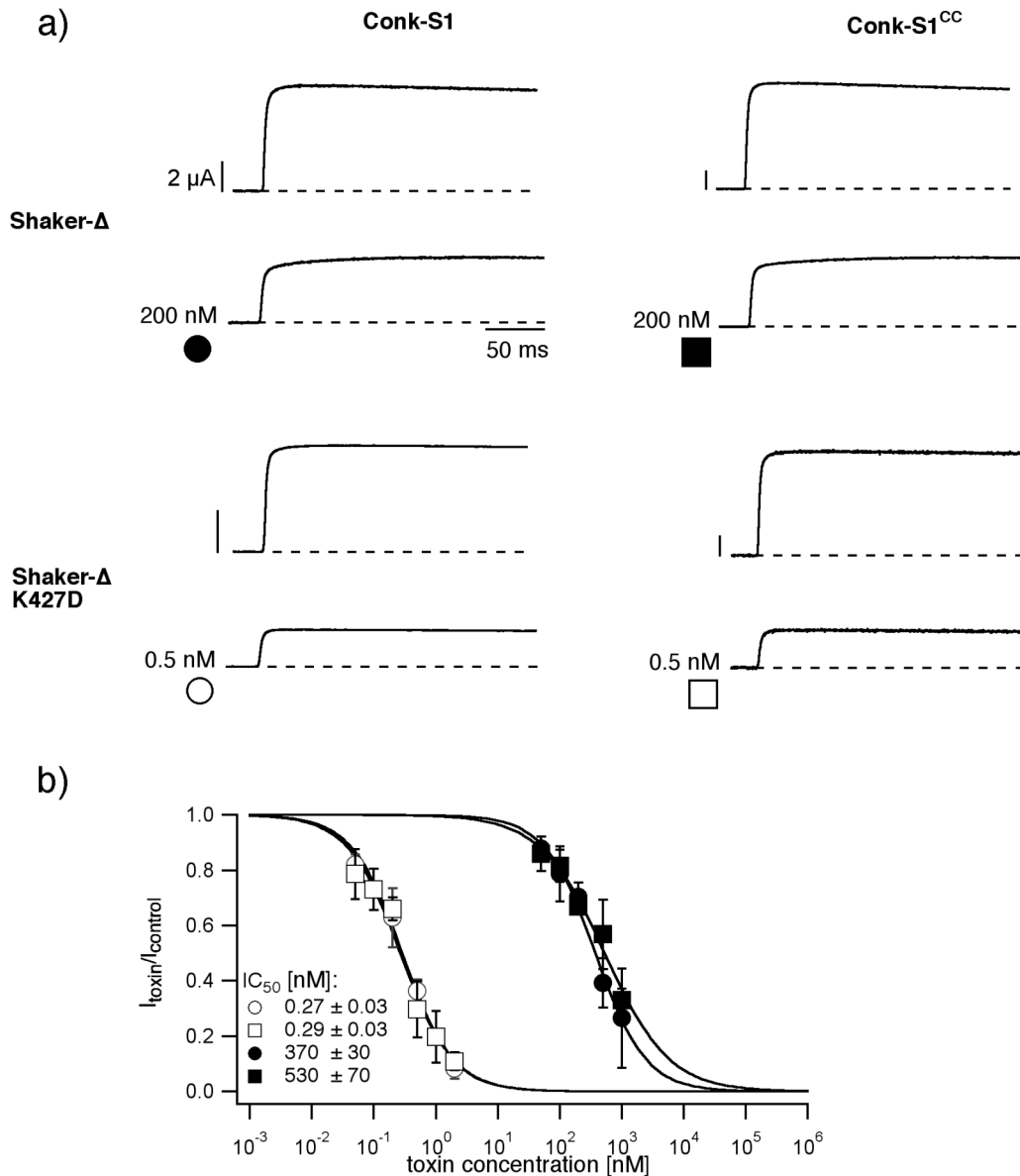


Fig. 39 a) Whole cell currents upon depolarizing from -100 to 0 mV are shown before and after toxin application. Currents were recorded from oocytes expressing either wild type or K427D *Shaker-Δ6-46* channel. The corresponding channel is indicated beside, the corresponding toxin above the curves, respectively. The toxin concentration is shown next to the curve, which was recorded after toxin application. The vertical bars represent $2 \mu\text{A}$. The filled and open circles and squares are related to section b. b) Dose-response curves of wild type (filled symbols) and K427D (open symbols) *Shaker-Δ6-46* channels. Currents were blocked by Conk-S1 (circles) and Conk-S1^{CC} (squares). The symbols are also shown in section a) at the corresponding toxin/channel combination. The test potential was 0 mV and n was between 2 and 5 for the different toxin concentrations.

All Kunitz domain proteins functionally analysed so far contain three disulfide bridges. To evaluate the importance of the "missing" disulfide bridge in Conk-S1 a

double cysteine mutant (Conk-S1^{CC}) carrying an additional cysteine bridge between the positions 16 and 40 was constructed and the activity of this peptide on K⁺ channels was measured. Most interestingly the affinity of Conk-S1^{CC} to *Shaker-Δ6-46* was 385 ± 58 nM (n= 3) showing that within the accuracy of measurements wild type and mutant Conk-S1 displayed the same inhibitory potential for *Shaker* channels. In addition, the affinity of Conk-S1^{CC} to *Shaker-Δ6-46* K427D channels is 0.22 ± 0.05 nM (n= 3), which is also identical to the binding affinity of Conk-S1 to this channel mutant. Therefore, for both the wild type sequence and Conk-S1^{CC} an increase in affinity by a factor of approximately 2000 is observed. For Conk-S1 and Conk-S1^{CC} dose response measurements with the wild type and K427D K⁺ channels were performed as well, resulting in almost identical IC₅₀ values (see Fig. 39). The Hill coefficients for the block of both channels by both peptides were all about 1, indicating no cooperativity for the binding of both peptides to the channels.

The kinetic analysis of the block of *Shaker-Δ6-46* K427D channels by Conk-S1 and Conk-S1^{CC} resulted in k_{on} values (for the forth reaction) of 17 ± 5 s⁻¹μM⁻¹ for Conk-S1 and 7 ± 3 s⁻¹μM⁻¹ for Conk-S1^{CC}. The k_{off} values (for the back reaction) were 0.0041 ± 0.0006 s⁻¹ for Conk-S1 and 0.0029 ± 0.0023 s⁻¹ for Conk-S1^{CC}. This analysis revealed that although the steady state affinity of Conk-S1 and Conk-S1^{CC} is virtually identical there are some differences in the kinetics of binding of both peptides to the ion channel.

Like Conk-S1, dendrotoxins are also Kunitz domain proteins, which interact with potassium channels. From literature^[129, 153-158] it is known, that mainly positively charged and aromatic residues of the dendrotoxins are involved in receptor binding. Based on this knowledge, alanine-scanning mutagenesis of positively charged and aromatic residues in Conk-S1 was carried out, in order to characterise the binding

surface. The affinity of the toxin mutants was functionally investigated by voltage clamp experiments using *Xenopus* oocytes expressing either Shaker- Δ 6-46 or Shaker- Δ 6-46 K427D channel. The results of this assay are summarised in Table 18.

Table 18 IC₅₀ values for Shaker- Δ 6-46 and Shaker- Δ 6-46 K427D block by Conk-S1 and its mutants. The ratio of mutant and wild type IC₅₀ value is given in brackets.

IC ₅₀ [nM]	Shaker- Δ 6-46	Shaker- Δ 6-46 K427D
Conk-S1 wt	502 ± 140	0.22 ± 0.8
Conk-S1 ^{CC}	385 ± 58 (0.8)	0.22 ± 0.05 (1)
K18A	1047 ± 619 (2)	0.42 ± 0.06 (2)
R29A	3678 ± 1500 (7.3)	3.36 ± 1.9 (16)
K30A	4127 ± 2397 (8.2)	3.77 ± 1.1 (18)
R29KK30A	1016 ± 89 (2)	0.56 ± 2.7 (2.5)
R3A	5124 ± 1289 (10.2)	2.98 ± 0.75 (12.9)
Y37A	did not refold	
R48A	3186 ± 1672 (6.4)	0.9 ± 0.5 (4.3)
Y24A	4273 ± 2342 (8.4)	0.92 ± 0.2 (4.4)
R22A	2177 ± 747 (4.3)	1.2 ± 0.7 (5.7)
R55A	7076 ± 2719 (14)	3.16 ± 1.2 (15)
K21A	273 ± 143 (0.5)	7.1 ± 3.8 (33.8)
R49A	5111 ± 2253 (10)	7.6 ± 3.9 (36.2)
R34A	924 ± 102 (1.8)	8.3 ± 2.7 (39.5)
F35A	no block	9.33 ± 3.2 (44.4)
Y51A	no block	9.55 ± 1 (45.5)

The mutants can be divided into 4 groups, based on their affinity to the receptors. The first group (coloured in white in Fig. 40) contains residues for which the alanine substitution resulted in an IC₅₀ value, which was up to 5 fold bigger than the one of the wild type blocking Shaker- Δ 6-46 K427D. These are K18, R48 and Y22. G16 and Q40 were replaced by cysteine, which had no effect, and therefore join this group. The second group (coloured in yellow in Fig. 40) contains the residues, which gave rise to a 5 to 10 fold increase of the IC₅₀ value. This is R22. The third group (coloured in orange in Fig. 40) contains the residues, which gave rise to a 10 to 30 fold increase of the IC₅₀ value. These are R3, R29, K30 and R55. The fourth group (coloured in red

in Fig. 40) includes the residues with the strongest effect, resulting in IC_{50} values, which are more than 30 times bigger than that of the wild type Conk-S1. These are K21, R34, F35, R49 and Y51. These results are visualized on the Van-der-Waals surface plot of Conk-S1 in Fig. 40.

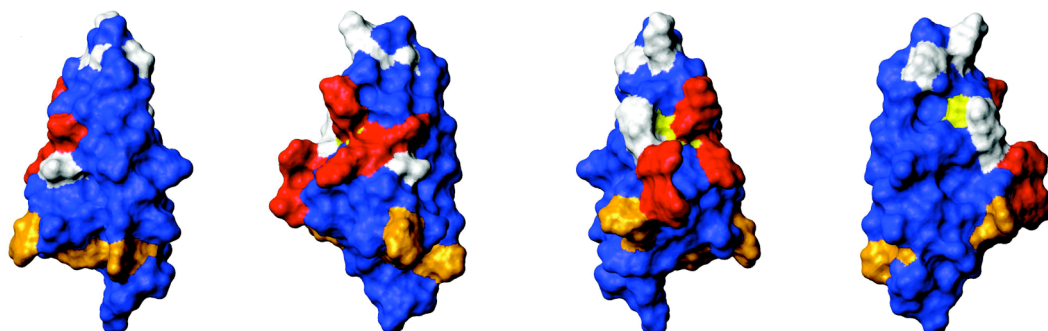


Fig. 40 Van-der-Waals surface plots of Conk-S1 stepwise rotated by 90° . Residues in Conk-S1 coloured in blue are not mutated, coloured in red are mutated to alanine and have a more than 30 times (group 4), coloured in orange a 30-10 times (group 3), in yellow a 10-5 (group 2) times and in white less than 5 times (group 1) lower affinity to K427D Shaker- $\Delta 6-46$ channel.

4.4 Discussion

In this work, the structure of a Kunitz domain polypeptide toxin from the venom of the fish-hunting cone snail *Conus striatus* was solved. Proteins with Kunitz domains can be divided into two general classes: the “heterogeneous Kunitz-domain-containing proteins”, with one or more Kunitz domains, but in combination with other structural motifs, and the “homogeneous Kunitz-domain polypeptides” (which was referred to above simply as “Kunitz domain proteins”) that are exclusively composed of Kunitz domains. Such polypeptides may contain one or more Kunitz domains, but have no other domain motifs. Conkunitzin-S1 clearly belongs to the latter class.

Conkunitzin-S1 is the first natural Kunitz-domain protein with only two disulfide bonds (all other natural Kunitz-domain proteins such as BPTI or the dendrotoxins have three disulfide crosslinks). Only among the heterogeneous Kunitz-domain-containing proteins Kunitz domains with only two disulfides have been reported (the trophoblast Kunitz-domain proteins (TKDPs) ^[159]). These appear to function as protease inhibitors, and their structure has not been solved yet.

It has been demonstrated that, despite containing only two cysteine bridges, the structure of Conk-S1 is very similar to that of other Kunitz domain peptides like BPTI (backbone C^α r.m.s.d. = 1.3 Å) and the dendrotoxins (backbone C^α r.m.s.d. to Dendrotoxin I = 2.2 Å).

4.4.1 Comparison of Conk-S1 with the structures of BPTI and dendrotoxins

Native BPTI with three disulphide bonds is extremely stable. It has been demonstrated that removing any one of these cysteine bridges still results in the native conformation, which is stable under normal conditions ^[160]. The most productive BPTI folding pathway includes a cysteine bridge rearrangement of non-native disulfide intermediates. This rearrangement facilitates the folding process under most experimental conditions. The most important of these intermediates of BPTI are (Cys30-Cys51, Cys5-Cys14) and (Cys30-Cys51, Cys5-Cys38)^[161]. This folding pathway is not possible for Conk-S1 because the cysteines 14 and 38 (corresponding to 16 and 40 in Conk-S1) are replaced by glycine and glutamine, respectively. The folding of Dendrotoxin I and Dendrotoxin K uses similar folding pathways as BPTI, but with important energetic and kinetic differences. In particular, a direct pathway, without disulfide rearrangements, is significantly more populated than in BPTI

folding^[160]. The existence of a native Kunitz domain with two replaced cysteines, as determined in this study, confirms that non-native disulfide intermediates are not necessary for the folding of Kunitz domains. This is also consistent with other studies, where mutants of BPTI, which lack Cys14 and Cys38, still folded properly^[162]. Another mutant of BPTI with only two disulfide bridges (Cys30-Cys51, Cys14-Cys38) also shows a native fold while the corresponding mutant in Dendrotoxin K is only partly folded. This is due to the generally lower stability of dendrotoxins compared to BPTI^[160]. Conk-S1 is structurally and functionally similar to the dendrotoxins. Considering the compromised folding of cysteine mutants in dendrotoxins, it is surprising that Conk-S1 still attains the typical Kunitz fold.

4.4.2 Comparison of the NMR and crystal structure of Conk-S1

Dy et al^[163]. solved the crystal structure of Conk-S1 by X-ray crystallography. The fold determined by NMR agrees very well with the crystal structure^[163]. The backbone RMSD of the NMR-structure with lowest total energy compared to one representative of the crystal structure (PDB code 1Y62) is 0.98 Å. This value is similar to others reported for NMR and X-ray structure comparisons at similar experimental resolution^[163, 164]. To test, if differences in the atomic coordinates are due to real structural differences, protons were added to the crystal structure by Dy and co-workers and the NOE energies were calculated. These energies were similar to or lower as the NOE distant restraint energies of the NMR ensemble. Therefore greater perturbation of Conk-S1 by crystallisation can be excluded. The difference in the atomic coordinates can rather be explained by different mathematical treatment of the X-ray and NMR data^[163]. The correlation of the experimentally observed RDCs

compared to the ones calculated based on the NMR structure with lowest total energy is 0.983 (see Fig.41a).

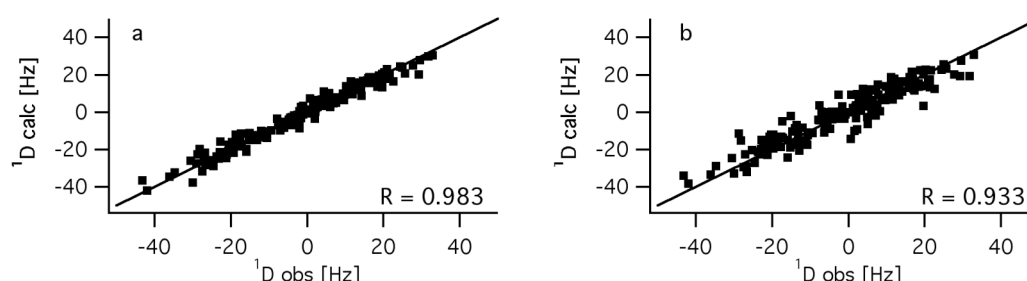


Fig. 41 Correlation between experimentally observed and calculated HN, C'N, C'C $_{\alpha}$ and C $_{\alpha}$ H $_{\alpha}$ RDCs of Conk-S1. The C'N, C'C $_{\alpha}$ and C $_{\alpha}$ H $_{\alpha}$ RDCs are normalized to the values of HN by the factor $\gamma_H\gamma_Nr_{HN}^{-3}/\gamma_A\gamma_Br_{AB}^{-3}$, where γ_x is the gyromagnetic ratio of x and r_{AB} is the distance between A and B. In a) the RDCs are calculated based on the NMR structure with the lowest total energy, in b) they are calculated based on one of the crystal structures deposited in 1Y62 in the PDB, which has the lowest RMSD to the observed RDCs.

RDCs calculated based on one member of the crystal structure ensemble have a correlation of 0.933 (see Fig. 41b) to experimentally observed ones. This also supports the view, that Conk-S1 is not much perturbed by crystallisation.

4.4.3 Functional investigation of Conk-S1

Recently it has been shown that the native, C-terminally amidated Conk-S1 blocks *Shaker* K $^{+}$ channels with an IC $_{50}$ of about 60 nM (Imperial et al., unpublished results). In our study a recombinant Conk-S1 has been used, which is lacking the C-terminal amidation. The functional consequence of this difference was studied by measuring the affinity of the recombinant Conk-S1 on *Shaker*- Δ 6-46 channels expressed in *Xenopus* oocytes. The IC $_{50}$ value of the recombinant Conk-S1 used in this study is 6 to 7 times higher than that of the native Conk-S1, indicating a reduced

inhibitory potential of the recombinant toxin. Despite this contribution of C-terminal amidation of Conk-S1 for K⁺ channel inhibition, our results demonstrate that recombinant Conk-S1 is functional. This provided the opportunity to use this recombinant neurotoxin for investigating structure, dynamics, electrophysiological properties and the effects of mutations.

Most interestingly the electrophysiological measurements revealed that there is no difference in the affinity between Conk-S1 with two disulfide bonds and the three-disulfide bonded mutant Conk-S1^{CC}. Furthermore, both peptides exhibit an approximately 2000 fold higher affinity to the K427D mutant of the *Shaker* K⁺ channel than to the wild type channel. This result indicates that Conk-S1 blocks K⁺ channels by interacting with the ion channel pore. Furthermore it underscores the importance of residue 427, located in the outer vestibule of the ion permeation pathway, for the binding of different conotoxins to K⁺ channels. In addition, it suggests that the "missing" cysteine bridge is not of critical functional importance for the block of the K⁺ channel by Conk-S1.

Despite the identical steady state values, the kinetic analysis revealed some differences in the binding of both toxin analogues. The k_{on} and the k_{off} values for Conk-S1 were approximately two times higher than for Conk-S1^{CC}. Thus, Conk-S1 binds twice as fast to the channel as Conk-S1^{CC}, but it is also released twice as fast from its binding site. Therefore, the two effects compensate, resulting in identical IC₅₀ values of Conk-S1 and Conk-S1^{CC}. From the kinetic point of view, this indicates that for Conk-S1^{CC} the formation of the complex with the channel as well as the dissociation of this complex might have a higher energy barrier. This is likely related to the number of disulfide bonds: the additional cysteine bridge makes Conk-S1^{CC} more rigid, especially because Conk-S1 shows decreased ¹⁵N{¹H}-NOE values in the

region of the “missing” disulfide bond (Fig. 38). These residues are K18, A19 and G41 with $^{15}\text{N}\{^1\text{H}\}$ -NOE values of 0.57, 0.22 and 0.62, respectively. Due to a low expression level of Conk-S1^{CC} no NMR-sample of Conk-S1^{CC} was prepared. Therefore $^{15}\text{N}\{^1\text{H}\}$ -NOE values could not be obtained. However it is very likely that the $^{15}\text{N}\{^1\text{H}\}$ -NOE values in the region of the “missing” disulfide bond will be increased compared to the wild type. For binding of the toxin to the channel, flexibility within Conk-S1 may enhance the rate of binding to the channel by allowing the toxin to adjust more easily into the binding pocket within the ion channel pore. This agrees very well with the observation that KcsA-Kv1.3, a K^+ channel homologous to Shaker, undergoes particular conformational changes upon Kaliotoxin binding^[165]. The authors suggest that these intrinsic dynamics are prerequisite for high-affinity receptor binding. These results imply, that toxins and their receptors act like ligand/enzyme complexes, because all enzymes require dynamic processes during substrate binding events (reviewed in ^[166]). It was described, that pre-existing equilibria of conformational substates are important for conformational changes (reviewed in ^[167]). The presented data suggest that this is also the case for the interaction of Conk-S1 with Shaker K^+ .

Interestingly, experiments with non-native disulfide bond patterns in dendrotoxins resulted in the reverse situation ^[168] as for Conk-S1. When the disulfide bond homologous to the missing third disulfide bond of Conk-S1^{CC} was selectively removed from Dendrotoxins I and K with iodoacetamide, derivatized dendrotoxins showed a 5 to 10 times lower affinity than the unmodified toxins. One possible explanation for this effect could be steric hindrance by the acetamide group. On the other hand, the different results obtained for dendrotoxins and Conk-S1 may indicate a different binding mode of Conk-S1 and dendrotoxins, even though these peptides

both target voltage gated K^+ channels. In another report it was shown, that by selectively reducing the cysteine bridge in BPTI, which is homologous to the one introduced into Conk-S1^{CC}, with borohydride, no change in activity was observed [169]. Therefore, Conk-S1 more closely resembles BPTI than the dendrotoxins with respect to the importance of this disulfide bond for the functional activity of the peptide.

Further mutational analysis of Conk-S1 support the hypothesis of a different binding mode compared to dendrotoxins. Several studies present the functionally important side chains of dendrotoxins that are involved in receptor interactions. The residues in the N-terminus, especially in the 3_{10} -helix, are known to be important in dendrotoxins for the interaction with the K^+ channel [129] [153] [154] [155] [156]. Particularly the point mutation K3A in Dendrotoxin K [155] [153] or K5A and L9A in α Dendrotoxin [154] show more than 1000 times lower binding affinities to the receptor. The β hairpin region, where a lysine triplet is located, is known to be involved into the channel recognition only in Dendrotoxin K [153], δ Dendrotoxin [129] and Dendrotoxin I [157] but not in α Dendrotoxin [158]. Another binding site in Dendrotoxin I which is proposed by Katho et al. [156] is the triad Lys19/Thyr17/Trp37, which is located in the anti-protease loop (Fig. 42a-d).

Based on these data, the following mutations were introduced into Conk-S1: R3A, which is located in the N-terminus of Conk-S1, R29A and K30A, which are located in the hairpin region, and K18A and Y37A, which are located in the anti-protease loop. Electrophysiological measurements revealed that, against any expectation, only moderate changes in affinity to the receptor were observed for the mutants compared to wild type Conk-S1. Therefore one can assume, that the mutated residues are not or very weakly involved in the binding to the channel. To map

functionally important residues, also positively charged and aromatic residues were investigated by alanine scanning mutagenesis. The mutants K21A, R34A, R49A, F35A and Y51A showed the strongest decrease of affinity to the Shaker channels. Therefore they most likely belong to the binding interface of Conk-S1. The binding sites of Conk-S1 and, in comparison to that, of the dendrotoxins are visualized on the Van-der-Waals surface plots in Figure 42.

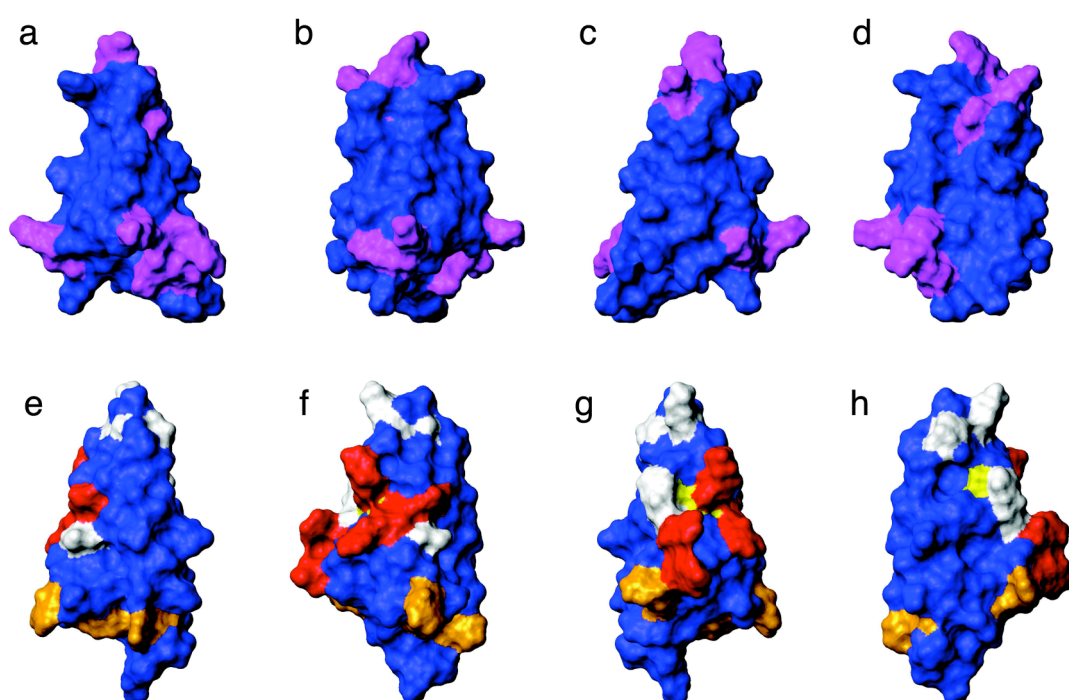


Fig. 42 Equivalent views of Van-der-Waals surface plots of DTX-I (a-d) and Conk-S1 (e-h), stepwise rotated by 90° from a to d and e to h, respectively. a-d) Residues in Dendrotoxins known from literature^[129, 153-158] to be involved into receptor binding are coloured in magenta. e-h) Residues in Conk-S1 coloured in blue are not mutated, coloured in red are mutated to alanine and have a more than 30 times (group 4), coloured in orange a 30-10 times (group 3), in yellow a 10-5 (group 2) times and in white less than 5 times (group 1) lower affinity to K427D Shaker- Δ 6-46 channel.

Most interestingly the binding sites of the dendrotoxins are located on the bottom and on the top of the molecule, while for Conk-S1 the residues, which are most likely

involved in receptor binding are located in the middle of the toxin (Fig. 42). This demonstrates a different mode of binding of Conk-S1 compared to the dendrotoxins.

4.5 Conclusions

In conclusion, the structure of Conk-S1 was determined by solution NMR. It is an unusual K channel-targeting toxin that has a consensus Kunitz-domain amino acid sequence, but lacks one of the three disulfide bonds that are conserved in all natural Kunitz domain peptides characterized to date. The structure does not strongly diverge from those of standard Kunitz domains with three disulfide bonds. A Conk-S1 double mutant with the third Kunitz domain disulfide bond had similar K channel blocking activity, indistinguishable from that of the native peptide. Both the two- and three-disulfide crosslinked toxins had much higher affinity for the K427D Shaker K-channel mutant, suggesting that they interacted equally avidly with the vestibule of the ion channel pore. Interestingly, Conk-S1 adopts a different mode of receptor binding than the dendrotoxins.

REFERENCES

- [1] J. Liu, B. Rost, *Protein Sci* **2001**, *10*, 1970.
- [2] S. White, **2007**.
- [3] C. G. Tate, *FEBS Lett* **2001**, *504*, 94.
- [4] T. P. Roosild, J. Greenwald, M. Vega, S. Castronovo, R. Riek, S. Choe, *Science* **2005**, *307*, 1317.
- [5] M. Kainosho, T. Torizawa, Y. Iwashita, T. Terauchi, A. Mei Ono, P. Guntert, *Nature* **2006**, *440*, 52.
- [6] C. R. Sanders, F. Sonnichsen, *Magn Reson Chem* **2006**, *44 Spec No*, S24.
- [7] A. Arora, F. Abildgaard, J. H. Bushweller, L. K. Tamm, *Nat Struct Biol* **2001**, *8*, 334.
- [8] K. Pervushin, R. Riek, G. Wider, K. Wuthrich, *Proc Natl Acad Sci U S A* **1997**, *94*, 12366.
- [9] L. E. Kay, K. H. Gardner, *Curr Opin Struct Biol* **1997**, *7*, 722.
- [10] N. K. Goto, L. E. Kay, *Curr Opin Struct Biol* **2000**, *10*, 585.
- [11] M. J. Parker, M. Aulton-Jones, A. M. Hounslow, C. J. Craven, *J Am Chem Soc* **2004**, *126*, 5020.
- [12] N. Tjandra, A. Bax, *Science* **1997**, *278*, 1111.
- [13] J. L. Battiste, G. Wagner, *Biochemistry* **2000**, *39*, 5355.
- [14] J. P. Overington, B. Al-Lazikani, A. L. Hopkins, *Nat Rev Drug Discov* **2006**, *5*, 993.
- [15] D. S. Wishart, C. Knox, A. C. Guo, S. Shrivastava, M. Hassanali, P. Stothard, Z. Chang, J. Woolsey, *Nucleic Acids Research* **2006**, *34*, D668.
- [16] D. Röckel, W. Korn, A. J. Kohn, *Manual of the Living Conidae*, Verlag Christa Hemmen, Wiesbaden, Germany, **1995**.
- [17] B. M. Olivera, *Annual Review of Ecology and Systematics* **2002**, *33*, 25.
- [18] H. Terlau, K. J. Shon, M. Grilley, M. Stocker, W. Stuhmer, B. M. Olivera, *Nature* **1996**, *381*, 148.
- [19] R. S. Norton, B. M. Olivera, *Toxicon* **2006**, *48*, 780.
- [20] H. Terlau, B. M. Olivera, *Physiol Rev* **2004**, *84*, 41.
- [21] J. Grodberg, J. J. Dunn, *J Bacteriol* **1988**, *170*, 1245.
- [22] J. Sambrook, F. F. Fritsch, M. Maniatis, *Molecular Cloning: A laboratory manual*, Cold Spring Harbor laboratory Press, Cold Spring Harbor, **1989**.
- [23] S. Mathys, T. C. Evans, I. C. Chute, H. Wu, S. Chong, J. Benner, X. Q. Liu, M. Q. Xu, *Gene* **1999**, *231*, 1.
- [24] U. K. Laemmli, *Nature* **1970**, *227*, 680.
- [25] T. Okajima, T. Tanabe, T. Yasuda, *Analytical Biochemistry* **1993**, *211*, 293.
- [26] W. L. Hubbell, A. Gross, R. Langen, M. A. Lietzow, *Curr Opin Struct Biol* **1998**, *8*, 649.
- [27] <http://lapecoranera.splinder.com/archive/2005-12>, p. xenopus laevi.
- [28] <http://www.mpg.de/bilderBerichteDokumente/dokumentation/pressemitteilungen/2002/pri0267.htm>, p. oocytes.
- [29] T. Meins, Max-Planck-Institute for Biochemistry (Munich), **2007**.
- [30] W. J. Metzler, K. L. Constantine, M. S. Friedrichs, A. J. Bell, E. G. Ernst, T. B. Lavoie, L. Mueller, *Biochemistry* **1993**, *32*, 13818.
- [31] D. J. Craik, J. A. Wilce, *Methods Mol Biol* **1997**, *60*, 195.

- [32] A. Bax, A. Grishaev, *Curr Opin Struct Biol* **2005**, *15*, 563.
- [33] G. M. Clore, M. R. Starich, A. M. Gronenborn, *Journal of the American Chemical Society* **1998**, *120*, 10571.
- [34] R. Tycko, F. J. Blanco, Y. Ishii, *Journal of the American Chemical Society* **2000**, *122*, 9340.
- [35] M. Ruckert, G. Otting, *Journal of the American Chemical Society* **2000**, *122*, 7793.
- [36] T. Cierpicki, J. H. Bushweller, *J Am Chem Soc* **2004**, *126*, 16259.
- [37] M. Zweckstetter, A. Bax, *Journal of the American Chemical Society* **2000**, *122*, 3791.
- [38] J. Cavanagh, W. J. Fairbrother, A. G. Palmer III, N. J. Skelton, *Protein NMR Spectroscopy Principles And Practice*, Academic Press, Inc., **1996**.
- [39] L. Banci, I. Bertini, C. Luchinat, *Nuclear and electron relaxation: the magnetic nucleus-unpaired electron coupling in solution*, VCH, Weinheim, **1991**.
- [40] G. Pintacuda, A. Kaikkonen, G. Otting, *J Magn Reson* **2004**, *171*, 233.
- [41] J. R. Gillespie, D. Shortle, *Journal of Molecular Biology* **1997**, *268*, 170.
- [42] P. A. Kosen, *Methods Enzymol* **1989**, *177*, 86.
- [43] M. Colombini, *Curr. Top. Membr.* **1994**, *42*, 73.
- [44] M. Colombini, *Mol Cell Biochem* **2004**, *256-257*, 107.
- [45] T. K. Rostovtseva, B. Antonsson, M. Suzuki, R. J. Youle, M. Colombini, S. M. Bezrukov, *J Biol Chem* **2004**, *279*, 13575.
- [46] M. G. Vander Heiden, X. X. Li, E. Gottlieb, R. B. Hill, C. B. Thompson, M. Colombini, *J Biol Chem* **2001**, *276*, 19414.
- [47] T. J. Malia, G. Wagner, *Biochemistry* **2007**, *46*, 514.
- [48] S. Shimizu, M. Narita, Y. Tsujimoto, *Nature* **1999**, *399*, 483.
- [49] M. Crompton, *Biochem J* **1999**, *341 (Pt 2)*, 233.
- [50] L. S. Zalman, H. Nikaido, Y. Kagawa, *J Biol Chem* **1980**, *255*, 1771.
- [51] S. Shimizu, Y. Matsuoka, Y. Shinohara, Y. Yoneda, Y. Tsujimoto, *J Cell Biol* **2001**, *152*, 237.
- [52] M. Zoratti, I. Szabo, *Biochim Biophys Acta* **1995**, *1241*, 139.
- [53] M. Narita, S. Shimizu, T. Ito, T. Chittenden, R. J. Lutz, H. Matsuda, Y. Tsujimoto, *Proc Natl Acad Sci U S A* **1998**, *95*, 14681.
- [54] Y. Tsujimoto, S. Shimizu, *Apoptosis* **2006**.
- [55] V. Shoshan-Barmatz, A. Israelson, D. Brdiczka, S. S. Sheu, *Curr Pharm Des* **2006**, *12*, 2249.
- [56] M. G. Vander Heiden, N. S. Chandel, X. X. Li, P. T. Schumacker, M. Colombini, C. B. Thompson, *Proc Natl Acad Sci U S A* **2000**, *97*, 4666.
- [57] B. Antonsson, F. Conti, A. Ciavatta, S. Montessuit, S. Lewis, I. Martinou, L. Bernasconi, A. Bernard, J. J. Mermod, G. Mazzei, K. Maundrell, F. Gambale, R. Sadoul, J. C. Martinou, *Science* **1997**, *277*, 370.
- [58] C. P. Baines, R. A. Kaiser, T. Sheiko, W. J. Craigen, J. D. Molkentin, *Nat Cell Biol* **2007**, *9*, 550.
- [59] X. W. Guo, P. R. Smith, B. Cognon, D. D'Arcangelis, E. Dolginova, C. A. Mannella, *J Struct Biol* **1995**, *114*, 41.
- [60] R. Casadio, I. Jacoboni, A. Messina, V. De Pinto, *FEBS Lett* **2002**, *520*, 1.
- [61] C. A. Mannella, A. F. Neuwald, C. E. Lawrence, *J Bioenerg Biomembr* **1996**, *28*, 163.
- [62] G. Rauch, O. Moran, *Biochem Biophys Res Commun* **1994**, *200*, 908.
- [63] E. Blachly-Dyson, S. Peng, M. Colombini, M. Forte, *Science* **1990**, *247*, 1233.

- [64] V. De Pinto, G. Prezioso, F. Thinner, T. A. Link, F. Palmieri, *Biochemistry* **1991**, *30*, 10191.
- [65] J. Song, C. Midson, E. Blachly-Dyson, M. Forte, M. Colombini, *J Biol Chem* **1998**, *273*, 24406.
- [66] S. Stanley, J. A. Dias, D. D'Arcangelis, C. A. Mannella, *J Biol Chem* **1995**, *270*, 16694.
- [67] R. Kleene, N. Pfanner, R. Pfaller, T. A. Link, W. Sebald, W. Neupert, M. Tropschug, *Embo J* **1987**, *6*, 2627.
- [68] M. Dolder, K. Zeth, P. Tittmann, H. Gross, W. Welte, T. Wallimann, *J Struct Biol* **1999**, *127*, 64.
- [69] C. A. Mannella, M. Radermacher, J. Frank, in *42nd Annual Meeting of the Electron Microscopy Society of America* (Ed.: G. W. Three-Bailey), San Francisco Press, San Francisco, **1984**, pp. 644.
- [70] H. Engelhardt, T. Meins, M. Poynor, V. Adams, S. Nussberger, W. Welte, K. Zeth, *J Membr Biol* **2007**, *in press*.
- [71] J. Fiaux, E. B. Bertelsen, A. L. Horwich, K. Wuthrich, *J Biomol NMR* **2004**, *29*, 289.
- [72] H. Patzelt, A. S. Ulrich, H. Egbrinchoff, P. Dux, J. Ashurst, B. Simon, H. Oschkinat, D. Oesterhelt, *J Biomol NMR* **1997**, *10*, 96.
- [73] G. Zhu, X. M. Kong, K. H. Sze, *Journal of Biomolecular Nmr* **1999**, *13*, 77.
- [74] J. Ying, J. H. Chill, J. M. Louis, A. Bax, *J Biomol NMR* **2007**, *37*, 195.
- [75] G. Zhu, Y. Xia, L. K. Nicholson, K. H. Sze, *J Magn Reson* **2000**, *143*, 423.
- [76] F. Delaglio, S. Grzesiek, G. W. Vuister, G. Zhu, J. Pfeifer, A. Bax, *Journal of Biomolecular Nmr* **1995**, *6*, 277.
- [77] A. G. W. Leslie, *Joint CCP4 and ESF-EACBM Newsletter on Protein Crystallography* **1992**, *26*.
- [78] W. Kabsch, *Journal of Applied Crystallography* **1993**, *26*, 795.
- [79] J. W. Pflugrath, *Acta Crystallogr D Biol Crystallogr* **1999**, *55*, 1718.
- [80] P. R. Evans, *Joint CCP4 and ESF-EACBM Newsletter on Protein Crystallography* **1997**, *33*, 22.
- [81] T. R. Schneider, G. M. Sheldrick, *Acta Crystallogr D Biol Crystallogr* **2002**, *58*, 1772.
- [82] G. Bricogne, C. Vonrhein, C. Flensburg, M. Schiltz, W. Paciorek, *Acta Crystallogr D Biol Crystallogr* **2003**, *59*, 2023.
- [83] J. P. Abrahams, A. G. Leslie, *Acta Crystallogr D Biol Crystallogr* **1996**, *52*, 30.
- [84] K. Cowtan, *Joint CCP4 and ESF-EACBM Newsletter on Protein Crystallography* **1994**, *31*, 34.
- [85] B. DeLaBarre, A. T. Brunger, *Acta Crystallogr D Biol Crystallogr* **2006**, *62*, 923.
- [86] A. Vagin, A. Teplyakov, *Journal of Applied Crystallography* **1997**, *30*, 1022.
- [87] T. A. Jones, J. Y. Zou, S. W. Cowan, M. Kjeldgaard, *Acta Crystallogr A* **1991**, *47 (Pt 2)*, 110.
- [88] P. Emsley, K. Cowtan, *Acta Crystallogr D Biol Crystallogr* **2004**, *60*, 2126.
- [89] A. Bax, S. Grzesiek, *Accounts Chem Res* **1993**, *26*, 542.
- [90] J. Shi, J. G. Pelton, H. S. Cho, D. E. Wemmer, *J Biomol NMR* **2004**, *28*, 235.
- [91] K. Bryson, L. J. McGuffin, R. L. Marsden, J. J. Ward, J. S. Sodhi, D. T. Jones, *Nucleic Acids Res* **2005**, *33*, W36.
- [92] L. J. McGuffin, K. Bryson, D. T. Jones, *Bioinformatics* **2000**, *16*, 404.
- [93] D. T. Wong, F. P. Bymaster, E. A. Engleman, *Life Sci* **1995**, *57*, 411.

- [94] F. P. Thinnies, *Mol Genet Metab* **2005**, *84*, 378.
- [95] D. Gincel, H. Zaid, V. Shoshan-Barmatz, *Biochem J* **2001**, *358*, 147.
- [96] A. Israelson, S. Abu-Hamad, H. Zaid, E. Nahon, V. Shoshan-Barmatz, *Cell Calcium* **2007**, *41*, 235.
- [97] P. M. Hwang, W. Y. Choy, E. I. Lo, L. Chen, J. D. Forman-Kay, C. R. Raetz, G. G. Prive, R. E. Bishop, L. E. Kay, *Proc Natl Acad Sci U S A* **2002**, *99*, 13560.
- [98] S. A. Paschen, W. Neupert, D. Rapaport, *Trends Biochem Sci* **2005**, *30*, 575.
- [99] K. Peng, S. Vucetic, P. Radivojac, C. J. Brown, A. K. Dunker, Z. Obradovic, *J Bioinform Comput Biol* **2005**, *3*, 35.
- [100] R. Linding, L. J. Jensen, F. Diella, P. Bork, T. J. Gibson, R. B. Russell, *Structure* **2003**, *11*, 1453.
- [101] S. A. Paschen, T. Waizenegger, T. Stan, M. Preuss, M. Cyrklaff, K. Hell, D. Rapaport, W. Neupert, *Nature* **2003**, *426*, 862.
- [102] N. Pfanner, N. Wiedemann, C. Meisinger, T. Lithgow, *Nat Struct Mol Biol* **2004**, *11*, 1044.
- [103] S. Meier, W. Neupert, J. M. Herrmann, *J Biol Chem* **2005**, *280*, 7777.
- [104] D. Rapaport, *EMBO Rep* **2003**, *4*, 948.
- [105] D. Rapaport, W. Neupert, *J Cell Biol* **1999**, *146*, 321.
- [106] S. Hamajima, M. Sakaguchi, K. Mihara, S. Ono, R. Sato, *J Biochem (Tokyo)* **1988**, *104*, 362.
- [107] D. A. Court, R. Kleene, W. Neupert, R. Lill, *FEBS Lett* **1996**, *390*, 73.
- [108] V. De Pinto, F. Tomasello, A. Messina, F. Guarino, R. Benz, D. La Mendola, A. Magri, D. Milardi, G. Pappalardo, *Chembiochem* **2007**, *8*, 744.
- [109] S. A. Paschen, W. Neupert, *IUBMB Life* **2001**, *52*, 101.
- [110] T. Endo, D. Kohda, *Biochim Biophys Acta* **2002**, *1592*, 3.
- [111] L. Thomas, E. Blachly-Dyson, M. Colombini, M. Forte, *Proc Natl Acad Sci U S A* **1993**, *90*, 5446.
- [112] S. Peng, E. Blachly-Dyson, M. Forte, M. Colombini, *Biophys J* **1992**, *62*, 123.
- [113] C. A. Mannella, *J Bioenerg Biomembr* **1997**, *29*, 525.
- [114] B. K. Jap, P. J. Walian, *Physiol Rev* **1996**, *76*, 1073.
- [115] E. Nahon, A. Israelson, S. Abu-Hamad, S. B. Varda, *FEBS Lett* **2005**, *579*, 5105.
- [116] A. Serafeim, M. J. Holder, G. Grafton, A. Chamba, M. T. Drayson, Q. T. Luong, C. M. Bunce, C. D. Gregory, N. M. Barnes, J. Gordon, *Blood* **2003**, *101*, 3212.
- [117] L. J. Brandes, R. J. Arron, R. P. Bogdanovic, J. Tong, C. L. Zaborniak, G. R. Hogg, R. C. Warrington, W. Fang, F. S. LaBella, *Cancer Res* **1992**, *52*, 3796.
- [118] S. C. Wright, J. Zhong, J. W. Larrick, *Faseb J* **1994**, *8*, 654.
- [119] M. K. Manion, J. W. O'Neill, C. D. Giedt, K. M. Kim, K. Y. Zhang, D. M. Hockenbery, *J Biol Chem* **2004**, *279*, 2159.
- [120] J. M. McDonnell, D. Fushman, C. L. Milliman, S. J. Korsmeyer, D. Cowburn, *Cell* **1999**, *96*, 625.
- [121] R. Zalk, A. Israelson, E. S. Garty, H. Azoulay-Zohar, V. Shoshan-Barmatz, *Biochem J* **2005**, *386*, 73.
- [122] M. J. Berridge, M. D. Bootman, P. Lipp, *Nature* **1998**, *395*, 645.
- [123] A. P. Halestrap, J. P. Gillespie, A. O'Toole, E. Doran, *Symp Soc Exp Biol* **2000**, *52*, 65.
- [124] K. C. Reed, F. L. Bygrave, *Biochem J* **1974**, *140*, 143.

- [125] G. C. Sparagna, K. K. Gunter, S. S. Sheu, T. E. Gunter, *J Biol Chem* **1995**, *270*, 27510.
- [126] A. Pardi, G. Wagner, K. Wuthrich, *Eur J Biochem* **1983**, *137*, 445.
- [127] F. Dreyer, *Rev Physiol Biochem Pharmacol* **1990**, *115*, 93.
- [128] J. P. Vincent, M. Lazdunski, *Biochemistry* **1972**, *11*, 2967.
- [129] J. P. Imredy, R. MacKinnon, *J Mol Biol* **2000**, *296*, 1283.
- [130] A. G. Craig, P. Bandyopadhyay, B. M. Olivera, *Eur J Biochem* **1999**, *264*, 271.
- [131] K. D. Berndt, P. Guntert, K. Wuthrich, *J Mol Biol* **1993**, *234*, 735.
- [132] P. K. Bandyopadhyay, J. E. Garrett, R. P. Shetty, T. Keate, C. S. Walker, B. M. Olivera, *Proc Natl Acad Sci U S A* **2002**, *99*, 1264.
- [133] G. Bulaj, O. Buczek, I. Goodsell, E. C. Jimenez, J. Kranski, J. S. Nielsen, J. E. Garrett, B. M. Olivera, *Proc Natl Acad Sci U S A* **2003**, *100 Suppl 2*, 14562.
- [134] M. Bayrhuber, V. Vijayan, M. Ferber, R. Graf, J. Korukottu, J. Imperial, J. E. Garrett, B. M. Olivera, H. Terlau, M. Zweckstetter, S. Becker, *Journal of Biological Chemistry* **2005**, *280*, 23766.
- [135] H. Wu, M. Q. Xu, X. Q. Liu, *Biochim Biophys Acta* **1998**, *1387*, 422.
- [136] Y. S. Jung, M. Zweckstetter, *J Biomol NMR* **2004**, *30*, 11.
- [137] A. Pardi, M. Billeter, K. Wuthrich, *Journal of Molecular Biology* **1984**, *180*, 741.
- [138] J. S. Hu, A. Bax, *J Biomol NMR* **1997**, *9*, 323.
- [139] G. Cornilescu, F. Delaglio, A. Bax, *Journal of Biomolecular Nmr* **1999**, *13*, 289.
- [140] J. P. Linge, S. I. O'Donoghue, M. Nilges, *Methods Enzymol* **2001**, *339*, 71.
- [141] J. J. Chou, F. Delaglio, A. Bax, *J Biomol NMR* **2000**, *18*, 101.
- [142] V. Vijayan, M. Zweckstetter, *Journal of Magnetic Resonance* **2005**, *174*, 245.
- [143] K. T. Simons, C. Kooperberg, E. Huang, D. Baker, *Journal of Molecular Biology* **1997**, *268*, 209.
- [144] Y. S. Jung, M. Sharma, M. Zweckstetter, *Angew Chem Int Ed Engl* **2004**, *43*, 3479.
- [145] A. T. Brunger, P. D. Adams, G. M. Clore, W. L. DeLano, P. Gros, R. W. Grosse-Kunstleve, J. S. Jiang, J. Kuszewski, M. Nilges, N. S. Pannu, R. J. Read, L. M. Rice, T. Simonson, G. L. Warren, *Acta Crystallographica Section D-Biological Crystallography* **1998**, *54*, 905.
- [146] J. P. Linge, M. A. Williams, C. A. Spronk, A. M. Bonvin, M. Nilges, *Proteins* **2003**, *50*, 496.
- [147] R. B. Jacobsen, E. D. Koch, B. Lange-Malecki, M. Stocker, J. Verhey, R. M. Van Wagoner, A. Vyazovkina, B. M. Olivera, H. Terlau, *Journal of Biological Chemistry* **2000**, *275*, 24639.
- [148] R. Koradi, M. Billeter, K. Wuthrich, *J Mol Graph* **1996**, *14*, 51.
- [149] T. Hoshi, W. N. Zagotta, R. W. Aldrich, *Science* **1990**, *250*, 533.
- [150] H. Terlau, A. Boccaccio, B. M. Olivera, F. Conti, *J Gen Physiol* **1999**, *114*, 125.
- [151] M. J. Scanlon, D. Naranjo, L. Thomas, P. F. Alewood, R. J. Lewis, D. J. Craik, *Structure* **1997**, *5*, 1585.
- [152] M. Ferber, A. Sporning, G. Jeserich, R. DeLaCruz, M. Watkins, B. M. Olivera, H. Terlau, *J Biol Chem* **2003**, *278*, 2177.
- [153] L. A. Smith, P. F. Reid, F. C. Wang, D. N. Parcej, J. J. Schmidt, M. A. Olson, J. O. Dolly, *Biochemistry* **1997**, *36*, 7690.

- [154] S. Gasparini, J. M. Danse, A. Lecoq, S. Pinkasfeld, S. Zinn-Justin, L. C. Young, C. C. de Medeiros, E. G. Rowan, A. L. Harvey, A. Menez, *J Biol Chem* **1998**, *273*, 25393.
- [155] F. C. Wang, N. Bell, P. Reid, L. A. Smith, P. McIntosh, B. Robertson, J. O. Dolly, *Eur J Biochem* **1999**, *263*, 222.
- [156] E. Katoh, H. Nishio, T. Inui, Y. Nishiuchi, T. Kimura, S. Sakakibara, T. Yamazaki, *Biopolymers* **2000**, *54*, 44.
- [157] A. L. Harvey, E. G. Rowan, H. Vatanpour, A. Engstrom, B. Westerlund, E. Karlsson, *Toxicon* **1997**, *35*, 1263.
- [158] J. M. Danse, E. G. Rowan, S. Gasparini, F. Ducancel, H. Vatanpour, L. C. Young, G. Poorheidari, E. Lajeunesse, P. Drevet, R. Menez, *FEBS Lett* **1994**, *356*, 153.
- [159] J. A. MacLean, 2nd, R. M. Roberts, J. A. Green, *Biol Reprod* **2004**, *71*, 455.
- [160] T. Kortemme, M. Hollecker, J. Kemmink, T. E. Creighton, *J Mol Biol* **1996**, *257*, 188.
- [161] C. P. van Mierlo, J. Kemmink, D. Neuhaus, N. J. Darby, T. E. Creighton, *J Mol Biol* **1994**, *235*, 1044.
- [162] C. B. Marks, H. Naderi, P. A. Kosen, I. D. Kuntz, S. Anderson, *Science* **1987**, *235*, 1370.
- [163] C. Y. Dy, P. Buczek, J. S. Imperial, G. Bulaj, M. P. Horvath, *Acta Crystallogr D Biol Crystallogr* **2006**, *62*, 980.
- [164] S. O. Garbuzynskiy, B. S. Melnik, M. Y. Lobanov, A. V. Finkelstein, O. V. Galzitskaya, *Proteins* **2005**, *60*, 139.
- [165] A. Lange, K. Giller, S. Hornig, M. F. Martin-Eauclaire, O. Pongs, S. Becker, M. Baldus, *Nature* **2006**, *440*, 959.
- [166] J. R. Schnell, H. J. Dyson, P. E. Wright, *Annu Rev Biophys Biomol Struct* **2004**, *33*, 119.
- [167] D. Kern, E. R. Zuiderweg, *Curr Opin Struct Biol* **2003**, *13*, 748.
- [168] M. Hollecker, D. L. Marshall, A. L. Harvey, *Br J Pharmacol* **1993**, *110*, 790.
- [169] L. F. Kress, M. Laskowski, Sr., *J Biol Chem* **1967**, *242*, 4925.

Appendix

A Chemical shift assignment of HVDAC

	CAi	CAi-1	C'i-1	H _N	N		CAi	CAi-1	C'i-1	H _N	N
A17	-	-	-	8.317	122.1	S140	57.55	64.69	-	8.492	119.8
R18	59.86	-	-	7.285	117.3	I141	59.55	57.33	172.7	9.083	122.5
K23	-	-	-	7.816	122.0	R142	53.82	59.62	173.3	9.027	128.5
Y25	55.82	44.24	171.6	6.585	113.7	G143	43.79	53.88	176.1	8.720	113.4
G26	46.02	55.96	175.9	8.672	105.3	A144	50.83	43.76	170.7	8.928	124.0
G28	46.54	-	178.2	7.550	105.0	L145	53.60	50.83	174.9	9.229	123.9
L29	53.86	46.74	175.8	7.331	120.5	V146	60.92	53.62	174.4	9.009	125.2
I30	60.62	53.67	-	8.916	126.3	L147	51.98	60.88	174.7	9.344	126.2
K31	54.81	60.75	175.0	8.746	126.8	G148	44.66	51.93	176.2	8.136	105.2
L32	53.32	54.87	174.0	8.699	124.1	Y149	59.06	44.71	172.9	8.577	122.4
D33	53.73	-	173.9	9.104	123.9	E150	56.91	59.10	173.6	9.203	125.6
N40	52.65	54.84	175.2	8.572	120.3	G151	45.09	57.04	175.3	8.006	108.1
G41	45.16	52.63	-	7.849	106.5	W152	57.23	45.09	173.3	8.100	121.5
L42	53.03	45.19	172.9	7.466	118.4	L153	53.47	57.21	177.4	8.954	123.5
G48	44.92	53.58	173.2	9.111	111.5	A154	50.68	53.47	175.4	8.860	121.7
S49	56.66	44.88	172.0	9.076	116.0	G155	45.25	50.70	175.4	9.625	107.7
A50	49.40	56.67	172.2	9.149	123.9	Y156	55.91	45.26	171.2	9.200	122.2
N51	52.64	49.40	-	8.303	122.5	Q157	53.08	55.97	171.9	8.204	128.0
T55	62.03	60.26	176.2	7.652	122.5	M158	52.87	52.75	172.2	8.736	121.3
K56	56.32	62.10	-	9.273	122.2	N159	52.27	52.60	174.3	7.961	119.4
V57	59.74	56.25	176.8	8.606	125.1	F160	56.11	52.30	175.4	9.539	127.7
T58	60.17	59.67	177.1	7.863	111.7	E161	54.87	56.17	173.5	8.035	127.7
E62	54.88	54.71	175.0	8.685	127.0	S165	58.34	54.53	175.3	7.469	114.7
T63	60.06	55.02	-	9.008	116.0	R166	53.72	58.65	173.1	6.795	115.0
T89	60.73	59.82	174.5	9.064	123.7	S170	57.05	55.27	174.6	8.320	119.0
V90	59.92	60.83	173.0	9.300	124.4	N171	51.47	57.03	172.6	9.110	127.3
E91	54.88	-	-	8.765	124.5	F172	56.04	51.47	171.9	8.602	118.3
G97	45.08	57.74	177.2	9.382	115.5	A173	50.97	56.05	173.4	8.818	122.7
L98	53.69	45.00	173.7	7.896	122.8	V174	60.09	50.98	176.2	8.211	116.8
K99	55.13	53.81	175.3	9.674	132.5	G175	45.66	60.13	175.5	9.415	113.0
T101	61.15	53.49	174.5	9.123	120.4	Y176	56.54	45.67	170.0	8.578	119.4
F102	56.05	49.96	172.8	9.448	127.1	L183	53.42	53.54	173.9	9.349	127.8
D103	52.22	56.10	173.0	8.623	129.0	T185	60.22	53.74	174.5	9.064	120.8
G111	45.70	60.02	175.5	9.377	112.8	N186	53.06	60.02	171.8	8.854	116.5
K112	56.33	45.45	173.7	7.445	120.5	V187	60.00	52.97	172.6	8.915	118.4
K113	55.39	56.55	173.8	8.804	129.5	N188	51.27	59.98	175.0	9.315	129.3
N114	53.63	55.58	172.9	8.248	125.6	E192	54.47	60.94	172.7	8.918	126.9
K116	54.53	-	-	8.987	119.7	F193	55.80	54.51	174.3	8.869	125.8
I117	59.34	-	177.8	8.778	120.4	G194	44.50	55.80	175.7	8.533	110.5
K118	54.64	59.25	175.0	9.268	126.8	G195	45.43	44.46	171.6	8.626	105.6
T119	60.15	54.62	175.8	8.671	117.2	S196	56.02	45.49	171.4	9.752	114.7
G120	44.45	60.64	174.5	9.157	113.8	I197	56.49	56.29	174.6	8.752	119.3
Y121	56.54	44.33	171.1	9.126	123.5	L205	53.10	-	-	9.043	130.0
K122	52.80	56.48	172.2	7.572	124.9	E206	54.11	53.30	174.1	8.830	125.6
R123	53.77	52.85	172.9	8.697	117.6	T207	59.45	54.02	174.8	8.383	112.2
I126	59.84	-	173.5	7.886	118.0	A208	50.75	59.43	171.6	9.022	122.5
N127	52.77	59.90	171.9	8.962	125.4	V209	59.45	50.71	-	8.951	116.9
L128	53.25	52.78	174.5	9.487	128.9	N210	51.98	59.45	174.4	8.858	122.6
G129	44.77	53.18	175.8	9.480	113.6	L211	54.12	51.90	172.5	8.705	121.7
C130	58.10	44.78	171.9	8.519	121.3	A212	51.81	54.14	175.2	9.193	126.5
D131	52.41	58.19	172.7	9.366	130.1	W213	57.67	51.78	175.4	8.965	121.3
M132	52.44	-	174.9	9.396	123.2	T214	60.35	57.77	173.2	8.513	120.6
I136	62.70	53.07	174.8	8.375	119.4	A215	53.19	60.35	173.7	8.672	127.2
A137	52.42	63.02	-	8.461	123.4	R221	54.98	62.66	174.5	9.036	125.6
G138	44.52	52.42	178.0	7.670	106.3	F222	55.79	54.92	175.1	8.026	119.2

	CA _i	CA _{i-1}	C ⁱ⁻¹	H _N	N		CA _i	CA _{i-1}	C ⁱ⁻¹	H _N	N
G223	45.01	55.86	173.5	8.561	107.8	L260	52.98	54.71	174.7	8.803	127.8
I224	59.57	45.01	171.0	8.804	118.7	T261	61.28	52.94	174.3	9.585	122.9
A225	50.16	59.60	172.1	8.857	126.3	L262	52.87	61.26	-	9.216	129.6
A226	50.20	49.68	175.3	9.198	119.4	S263	56.80	52.47	174.6	8.797	115.3
K227	56.11	50.27	177.0	8.755	122.6	A264	51.11	56.73	172.8	9.536	120.6
Y228	55.22	56.06	174.2	9.855	129.0	L265	52.41	51.11	173.4	8.709	124.9
Q229	54.39	55.26	173.5	9.010	131.6	L266	52.33	52.28	175.2	9.486	126.2
I230	64.58	54.29	173.7	7.810	130.1	G268	46.03	52.32	176.9	8.457	112.4
D231	52.69	-	175.7	8.422	118.4	K269	56.79	45.99	173.8	8.124	117.3
D233	53.54	-	177.7	7.210	115.2	N270	51.80	56.76	177.1	7.423	117.5
A234	51.62	53.82	-	7.662	124.3	V271	65.06	51.82	175.1	8.508	122.1
C235	56.21	51.62	175.1	8.452	119.1	A273	51.73	54.27	175.8	7.488	120.7
F236	55.63	56.00	171.8	9.232	128.0	G274	44.74	51.71	177.7	7.694	106.7
S237	57.35	55.55	173.0	9.319	124.5	G275	45.46	44.81	174.0	8.509	109.1
A238	50.70	57.38	-	8.016	122.9	H276	54.54	45.45	174.0	7.251	120.7
K239	54.61	50.67	175.7	9.033	114.8	K277	54.64	64.35	176.1	8.831	119.4
V240	59.45	54.62	174.6	8.948	117.0	L278	53.50	54.74	175.2	8.654	121.6
S244	56.50	56.30	-	8.630	120.6	G279	45.03	53.44	178.0	9.096	111.1
L245	54.77	56.37	175.8	8.464	124.7	L280	53.78	45.13	170.9	8.198	121.0
I246	59.45	53.77	176.7	9.037	126.7	G281	44.27	53.82	-	9.574	115.9
G247	44.03	59.49	174.8	9.280	114.5	L282	53.36	44.28	171.6	8.669	124.6
L248	53.21	44.05	171.4	9.370	122.3	E283	55.90	53.30	177.5	7.354	125.4
G249	44.66	53.20	-	9.169	110.5	F284	55.90	-	-	9.313	128.1
Y250	56.15	44.64	170.9	9.088	125.5	Q285	53.72	56.15	174.2	8.675	122.7
T251	60.76	56.06	174.7	8.354	124.5	A286	51.25	53.91	174.4	8.282	126.4
Q252	52.52	-	-	9.019	126.1	R287	55.89	51.27	-	9.030	125.0
L254	53.73	59.44	-	7.279	118.5	S288	57.14	55.74	174.1	7.745	125.8
K255	55.69	53.63	174.5	8.901	130.5						

B Chemical shift assignments of Conk-S1

1	1	LYS	CB	C	33.080	0.042	1	36	5	SER	CB	C	62.776	0.037	1
2	1	LYS	CD	C	29.158	0.03	1	37	5	SER	C	C	177.273	0.03	1
3	1	LYS	CE	C	42.048	0.03	1	38	5	SER	H	H	8.829	0.001	1
4	1	LYS	CG	C	23.873	0.03	1	39	5	SER	HA	H	4.194	0.003	1
5	1	LYS	C	C	172.311	0.03	1	40	5	SER	HB2	H	3.983	0.003	2
6	1	LYS	HA	H	4.009	0.003	1	41	5	SER	N	N	120.366	0.138	1
7	1	LYS	HB2	H	1.901	0.003	2	42	6	LEU	CA	C	57.762	0.03	1
8	1	LYS	HD2	H	1.689	0.003	2	43	6	LEU	CB	C	40.582	0.023	1
9	1	LYS	HE2	H	2.991	0.003	2	44	6	LEU	CD1	C	26.591	0.03	1
10	1	LYS	HG2	H	1.455	0.003	2	45	6	LEU	C	C	176.584	0.03	1
11	2	ASP	CA	C	54.432	0.03	1	46	6	LEU	H	H	8.115	0.001	1
12	2	ASP	CB	C	41.344	0.009	1	47	6	LEU	HA	H	4.102	0.003	1
13	2	ASP	C	C	175.290	0.03	1	48	6	LEU	HB2	H	1.799	0.004	2
14	2	ASP	H	H	8.690	0.001	1	49	6	LEU	HB3	H	1.438	0.001	2
15	2	ASP	HA	H	4.651	0.003	1	50	6	LEU	HD1	H	0.931	0.007	2
16	2	ASP	HB2	H	2.515	0.003	2	51	6	LEU	HD2	H	0.800	0.003	2
17	2	ASP	HB3	H	2.694	0.003	2	52	6	LEU	HG	H	1.558	0.003	2
18	2	ASP	N	N	123.473	0.057	1	53	6	LEU	N	N	122.169	0.012	1
19	3	ARG	CA	C	54.211	0.03	1	54	7	CYS	CA	C	57.260	0.050	1
20	3	ARG	CB	C	30.490	0.03	1	55	7	CYS	CB	C	39.349	0.026	1
21	3	ARG	H	H	8.454	0.001	1	56	7	CYS	C	C	173.714	0.03	1
22	3	ARG	N	N	123.151	0.005	1	57	7	CYS	H	H	7.669	0.002	1
23	4	PRO	CA	C	63.199	0.001	1	58	7	CYS	HA	H	4.292	0.003	1
24	4	PRO	CB	C	32.121	0.018	1	59	7	CYS	HB2	H	2.812	0.003	2
25	4	PRO	CD	C	51.116	0.03	1	60	7	CYS	HB3	H	3.104	0.003	2
26	4	PRO	CG	C	27.753	0.03	1	61	7	CYS	N	N	116.543	0.003	1
27	4	PRO	C	C	178.002	0.03	1	62	8	ASP	CA	C	54.368	0.029	1
28	4	PRO	HA	H	4.509	0.003	1	63	8	ASP	CB	C	41.901	0.013	1
29	4	PRO	HB2	H	2.431	0.001	2	64	8	ASP	C	C	177.020	0.03	1
30	4	PRO	HB3	H	2.069	0.003	2	65	8	ASP	H	H	7.582	0.003	1
31	4	PRO	HD2	H	3.950	0.004	2	66	8	ASP	HA	H	4.931	0.003	1
32	4	PRO	HD3	H	3.847	0.003	2	67	8	ASP	HB2	H	2.590	0.003	2
33	4	PRO	HG2	H	2.166	0.003	2	68	8	ASP	HB3	H	2.964	0.003	2
34	4	PRO	HG3	H	2.062	0.003	2	69	8	ASP	N	N	114.479	0.008	1
35	5	SER	CA	C	61.191	0.031	1	70	9	LEU	CA	C	53.388	0.03	1

71	9	LEU	CB	C	41.062	0.03	1
72	9	LEU	H	H	7.580	0.002	1
73	9	LEU	N	N	122.253	0.003	1
74	10	PRO	CA	C	61.764	0.011	1
75	10	PRO	CB	C	32.087	0.032	1
76	10	PRO	CD	C	49.756	0.03	1
77	10	PRO	CG	C	26.997	0.03	1
78	10	PRO	C	C	175.352	0.03	1
79	10	PRO	HA	H	4.516	0.003	1
80	10	PRO	HB2	H	1.848	0.003	2
81	10	PRO	HB3	H	2.220	0.004	2
82	10	PRO	HD2	H	3.565	0.003	2
83	10	PRO	HD3	H	3.787	0.003	2
84	10	PRO	HG2	H	2.046	0.003	2
85	11	ALA	CA	C	52.088	0.010	1
86	11	ALA	CB	C	15.363	0.046	1
87	11	ALA	C	C	178.573	0.03	1
88	11	ALA	H	H	7.469	0.001	1
89	11	ALA	HA	H	3.555	0.003	1
90	11	ALA	HB	H	-0.401	0.003	1
91	11	ALA	N	N	120.824	0.005	1
92	12	ASP	CA	C	52.375	0.013	1
93	12	ASP	CB	C	43.863	0.005	1
94	12	ASP	C	C	176.480	0.03	1
95	12	ASP	H	H	7.676	0.002	1
96	12	ASP	HA	H	4.904	0.003	1
97	12	ASP	HB2	H	2.302	0.003	2
98	12	ASP	HB3	H	2.616	0.003	2
99	12	ASP	N	N	121.934	0.004	1
100	13	SER	CA	C	61.726	0.03	1
101	13	SER	CB	C	64.029	0.031	1
102	13	SER	C	C	175.398	0.03	1
103	13	SER	H	H	9.252	0.001	1
104	13	SER	HA	H	4.794	0.003	1
105	13	SER	HB2	H	4.186	0.003	2
106	13	SER	N	N	121.765	0.011	1
107	14	GLY	CA	C	45.264	0.009	1
108	14	GLY	C	C	173.969	0.03	1
109	14	GLY	H	H	9.184	0.003	1
110	14	GLY	HA2	H	3.844	0.003	2
111	14	GLY	HA3	H	4.526	0.003	2
112	14	GLY	N	N	111.730	0.008	1
113	15	SER	CA	C	57.360	0.037	1
114	15	SER	CB	C	64.269	0.030	1
115	15	SER	C	C	175.079	0.03	1
116	15	SER	H	H	7.896	0.002	1
117	15	SER	HA	H	4.737	0.003	1
118	15	SER	HB2	H	3.627	0.003	2
119	15	SER	HB3	H	4.111	0.003	2
120	15	SER	N	N	113.228	0.005	1
121	16	GLY	CA	C	44.568	0.021	1
122	16	GLY	C	C	174.472	0.03	1
123	16	GLY	H	H	8.816	0.002	1
124	16	GLY	HA2	H	3.598	0.003	2
125	16	GLY	HA3	H	4.448	0.003	2
126	16	GLY	N	N	111.011	0.006	1
127	17	THR	CA	C	61.119	0.03	1
128	17	THR	CB	C	70.004	0.065	1
129	17	THR	CG2	C	21.482	0.03	1
130	17	THR	C	C	174.870	0.03	1
131	17	THR	H	H	8.390	0.001	1
132	17	THR	HA	H	4.572	0.006	1
133	17	THR	HB	H	4.492	0.005	2
134	17	THR	HG1	H	1.121	0.003	2
135	17	THR	N	N	107.262	0.004	1
136	18	LYS	CA	C	55.081	0.056	1
137	18	LYS	CB	C	33.763	0.009	1
138	18	LYS	CD	C	28.897	0.03	1
139	18	LYS	CE	C	42.288	0.03	1
140	18	LYS	CG	C	24.895	0.03	1
141	18	LYS	C	C	174.331	0.03	1
142	18	LYS	H	H	7.939	0.002	1
143	18	LYS	HA	H	4.493	0.003	1
144	18	LYS	HB2	H	1.438	0.003	2
145	18	LYS	HB3	H	1.789	0.003	2
146	18	LYS	HD2	H	1.621	0.003	2
147	18	LYS	HE2	H	2.953	0.003	2
148	18	LYS	HG2	H	1.314	0.003	2
149	18	LYS	N	N	122.813	0.003	1
150	19	ALA	CA	C	52.286	0.025	1
151	19	ALA	CB	C	19.485	0.050	1
152	19	ALA	C	C	176.224	0.03	1
153	19	ALA	H	H	8.111	0.001	1
154	19	ALA	HA	H	4.497	0.003	1
155	19	ALA	HB	H	1.181	0.003	1
156	19	ALA	N	N	124.378	0.007	1
157	20	GLU	CA	C	54.586	0.037	1
158	20	GLU	CB	C	33.176	0.012	1
159	20	GLU	CG	C	36.159	0.03	1
160	20	GLU	C	C	174.985	0.03	1
161	20	GLU	H	H	8.683	0.002	1
162	20	GLU	HA	H	4.642	0.003	1
163	20	GLU	HB2	H	1.982	0.006	2
164	20	GLU	HB3	H	2.064	0.006	2
165	20	GLU	HG2	H	2.070	0.001	2
166	20	GLU	HG3	H	2.220	0.003	2
167	20	GLU	N	N	121.603	0.022	1
168	21	LYS	CA	C	55.460	0.043	1
169	21	LYS	CB	C	32.763	0.012	1
170	21	LYS	CD	C	28.762	0.03	1
171	21	LYS	CE	C	42.193	0.03	1
172	21	LYS	CG	C	24.578	0.03	1
173	21	LYS	C	C	177.006	0.03	1
174	21	LYS	H	H	8.690	0.001	1
175	21	LYS	HA	H	4.839	0.003	1
176	21	LYS	HB2	H	1.915	0.003	2
177	21	LYS	HB3	H	1.665	0.003	2
178	21	LYS	HD2	H	1.701	0.003	2
179	21	LYS	HD3	H	1.452	0.003	2
180	21	LYS	HE2	H	2.910	0.003	2
181	21	LYS	N	N	122.447	0.015	1
182	22	ARG	CA	C	52.253	0.024	1
183	22	ARG	CB	C	34.978	0.009	1
184	22	ARG	CD	C	42.606	0.03	1
185	22	ARG	CG	C	29.554	0.03	1
186	22	ARG	C	C	173.035	0.03	1
187	22	ARG	H	H	8.527	0.003	1
188	22	ARG	HA	H	4.673	0.003	1
189	22	ARG	HB2	H	0.822	0.003	2
190	22	ARG	HB3	H	1.808	0.003	2
191	22	ARG	HD2	H	2.875	0.003	2
192	22	ARG	HD3	H	3.456	0.003	2
193	22	ARG	HG2	H	1.216	0.003	2
194	22	ARG	N	N	125.387	0.007	1
195	23	ILE	CA	C	58.038	0.018	1
196	23	ILE	CB	C	40.023	0.026	1
197	23	ILE	CG1	C	27.749	0.03	1
198	23	ILE	CG2	C	20.592	0.03	1
199	23	ILE	C	C	174.732	0.03	1
200	23	ILE	H	H	8.881	0.002	1
201	23	ILE	HA	H	5.492	0.003	1
202	23	ILE	HB	H	1.738	0.003	2
203	23	ILE	HD1	H	0.654	0.003	1
204	23	ILE	HG12	H	1.125	0.003	2
205	23	ILE	HG13	H	1.318	0.003	2
206	23	ILE	HG2	H	0.923	0.003	1
207	23	ILE	N	N	120.316	0.008	1
208	24	TYR	CA	C	54.760	0.022	1
209	24	TYR	CB	C	41.202	0.009	1
210	24	TYR	CD1	C	54.990	0.03	1
211	24	TYR	C	C	172.540	0.03	1
212	24	TYR	H	H	9.882	0.002	1
213	24	TYR	HA	H	5.244	0.003	1
214	24	TYR	HB2	H	2.667	0.003	2
215	24	TYR	HB3	H	2.714	0.003	2
216	24	TYR	HD1	H	6.959	0.003	3
217	24	TYR	HE1	H	6.653	0.003	3
218	24	TYR	N	N	126.812	0.006	1
219	25	TYR	CA	C	58.048	0.035	1
220	25	TYR	CB	C	39.656	0.013	1
221	25	TYR	C	C	173.477	0.03	1
222	25	TYR	H	H	10.385	0.002	1
223	25	TYR	HA	H	4.352	0.003	1
224	25	TYR	HB2	H	3.237	0.003	2
225	25	TYR	HB3	H	2.788	0.003	2
226	25	TYR	N	N	123.062	0.005	1
227	26	ASN	CA	C	51.612	0.019	1
228	26	ASN	CB	C	40.014	0.013	1

229	26	ASN	C	C	174.623	0.03	1	308	34	ARG	CA	C	55.951	0.008	1
230	26	ASN	H	H	8.048	0.002	1	309	34	ARG	CB	C	32.149	0.016	1
231	26	ASN	HA	H	4.585	0.003	1	310	34	ARG	CD	C	43.994	0.03	1
232	26	ASN	HB2	H	2.603	0.003	2	311	34	ARG	CG	C	27.868	0.03	1
233	26	ASN	HB3	H	1.967	0.003	2	312	34	ARG	C	C	176.755	0.03	1
234	26	ASN	N	N	126.650	0.007	1	313	34	ARG	H	H	8.351	0.002	1
235	27	SER	CA	C	60.626	0.090	1	314	34	ARG	HA	H	5.436	0.003	1
236	27	SER	CB	C	63.008	0.073	1	315	34	ARG	HB2	H	1.809	0.005	2
237	27	SER	C	C	176.131	0.03	1	316	34	ARG	HB3	H	1.885	0.002	2
238	27	SER	H	H	8.429	0.003	1	317	34	ARG	HD2	H	3.162	0.003	2
239	27	SER	HA	H	3.827	0.004	1	318	34	ARG	HG2	H	1.671	0.003	2
240	27	SER	HB2	H	4.082	0.003	2	319	34	ARG	HG3	H	1.796	0.002	2
241	27	SER	N	N	121.116	0.006	1	320	34	ARG	N	N	119.037	0.005	1
242	28	ALA	CA	C	54.788	0.011	1	321	35	PHE	CA	C	55.927	0.003	1
243	28	ALA	CB	C	18.297	0.047	1	322	35	PHE	CB	C	41.344	0.047	1
244	28	ALA	C	C	179.723	0.03	1	323	35	PHE	C	C	171.916	0.03	1
245	28	ALA	H	H	8.017	0.001	1	324	35	PHE	H	H	9.497	0.002	1
246	28	ALA	HA	H	4.201	0.003	1	325	35	PHE	HA	H	4.947	0.003	1
247	28	ALA	HB	H	1.486	0.003	1	326	35	PHE	HB2	H	3.103	0.003	2
248	28	ALA	N	N	124.917	0.003	1	327	35	PHE	HB3	H	2.992	0.003	2
249	29	ARG	CA	C	55.533	0.029	1	328	35	PHE	HD1	H	7.104	0.003	3
250	29	ARG	CB	C	31.087	0.019	1	329	35	PHE	HE1	H	7.157	0.003	3
251	29	ARG	CD	C	43.232	0.03	1	330	35	PHE	N	N	121.396	0.006	1
252	29	ARG	CG	C	27.181	0.03	1	331	36	ASP	CA	C	54.108	0.045	1
253	29	ARG	C	C	175.418	0.03	1	332	36	ASP	CB	C	41.241	0.008	1
254	29	ARG	H	H	7.779	0.002	1	333	36	ASP	C	C	173.714	0.03	1
255	29	ARG	HA	H	4.112	0.003	1	334	36	ASP	H	H	8.359	0.001	1
256	29	ARG	HB2	H	1.078	0.003	2	335	36	ASP	HA	H	4.843	0.003	1
257	29	ARG	HB3	H	1.923	0.003	2	336	36	ASP	HB2	H	2.580	0.003	2
258	29	ARG	HD2	H	3.033	0.003	2	337	36	ASP	HB3	H	2.410	0.002	2
259	29	ARG	HG2	H	1.539	0.003	2	338	36	ASP	N	N	120.047	0.048	1
260	29	ARG	N	N	114.463	0.002	1	339	37	TYR	CA	C	55.304	0.046	1
261	30	LYS	CA	C	56.794	0.017	1	340	37	TYR	CB	C	41.800	0.013	1
262	30	LYS	CB	C	29.253	0.003	1	341	37	TYR	C	C	175.382	0.03	1
263	30	LYS	CD	C	29.571	0.03	1	342	37	TYR	H	H	8.837	0.002	1
264	30	LYS	CE	C	42.523	0.03	1	343	37	TYR	HA	H	4.976	0.001	1
265	30	LYS	CG	C	24.886	0.03	1	344	37	TYR	HB2	H	2.297	0.003	2
266	30	LYS	C	C	174.803	0.03	1	345	37	TYR	HB3	H	2.401	0.001	2
267	30	LYS	H	H	7.927	0.003	1	346	37	TYR	N	N	124.067	0.004	1
268	30	LYS	HA	H	3.677	0.003	1	347	38	THR	CA	C	58.747	0.03	1
269	30	LYS	HB2	H	2.039	0.003	2	348	38	THR	CB	C	63.914	0.030	1
270	30	LYS	HB3	H	1.814	0.003	2	349	38	THR	C	C	175.226	0.03	1
271	30	LYS	HD2	H	1.667	0.003	2	350	38	THR	H	H	7.911	0.002	1
272	30	LYS	HD3	H	1.701	0.003	2	351	38	THR	HA	H	4.435	0.003	1
273	30	LYS	HE2	H	3.018	0.003	2	352	38	THR	HB	H	3.894	0.003	2
274	30	LYS	HG2	H	1.380	0.003	2	353	38	THR	N	N	114.714	0.005	1
275	30	LYS	HG3	H	1.298	0.003	2	354	39	GLY	CA	C	45.724	0.018	1
276	30	LYS	N	N	117.604	0.006	1	355	39	GLY	C	C	172.504	0.03	1
277	31	GLN	CA	C	54.072	0.026	1	356	39	GLY	HA2	H	4.192	0.003	2
278	31	GLN	CB	C	35.027	0.120	1	357	39	GLY	HA3	H	3.337	0.003	2
279	31	GLN	CG	C	33.758	0.03	1	358	40	GLN	CA	C	54.741	0.014	1
280	31	GLN	C	C	174.118	0.03	1	359	40	GLN	CB	C	32.600	0.212	1
281	31	GLN	H	H	6.800	0.003	1	360	40	GLN	CG	C	33.735	0.03	1
282	31	GLN	HA	H	4.546	0.006	1	361	40	GLN	C	C	175.264	0.03	1
283	31	GLN	HB2	H	1.378	0.001	2	362	40	GLN	H	H	6.647	0.003	1
284	31	GLN	HB3	H	1.753	0.001	2	363	40	GLN	HA	H	4.577	0.003	1
285	31	GLN	HG2	H	2.246	0.001	2	364	40	GLN	HB2	H	1.696	0.002	2
286	31	GLN	N	N	111.927	0.009	1	365	40	GLN	HB3	H	1.845	0.003	2
287	32	CYS	CA	C	57.264	0.095	1	366	40	GLN	HG2	H	2.187	0.003	2
288	32	CYS	CB	C	44.627	0.005	1	367	40	GLN	N	N	116.234	0.018	1
289	32	CYS	C	C	173.556	0.03	1	368	41	GLY	CA	C	45.085	0.019	1
290	32	CYS	H	H	8.674	0.001	1	369	41	GLY	C	C	175.797	0.03	1
291	32	CYS	HA	H	5.157	0.003	1	370	41	GLY	H	H	8.943	0.001	1
292	32	CYS	HB2	H	3.096	0.003	2	371	41	GLY	HA2	H	4.182	0.003	2
293	32	CYS	HB3	H	2.620	0.003	2	372	41	GLY	HA3	H	3.906	0.003	2
294	32	CYS	N	N	121.910	0.014	1	373	41	GLY	N	N	109.417	0.006	1
295	33	LEU	CA	C	53.319	0.034	1	374	42	GLY	CA	C	43.803	0.002	1
296	33	LEU	CB	C	46.394	0.010	1	375	42	GLY	C	C	172.996	0.03	1
297	33	LEU	CD1	C	22.887	0.03	1	376	42	GLY	H	H	9.292	0.001	1
298	33	LEU	CG	C	26.234	0.03	1	377	42	GLY	HA2	H	4.516	0.003	2
299	33	LEU	C	C	174.921	0.03	1	378	42	GLY	HA3	H	3.711	0.003	2
300	33	LEU	H	H	9.026	0.002	1	379	42	GLY	N	N	112.607	0.008	1
301	33	LEU	HA	H	4.768	0.003	1	380	43	ASN	CA	C	51.708	0.030	1
302	33	LEU	HB2	H	1.385	0.003	2	381	43	ASN	CB	C	40.620	0.014	1
303	33	LEU	HB3	H	1.667	0.003	2	382	43	ASN	C	C	175.253	0.03	1
304	33	LEU	HD1	H	0.778	0.003	2	383	43	ASN	H	H	9.210	0.001	1
305	33	LEU	HD2	H	0.821	0.003	2	384	43	ASN	HA	H	4.927	0.003	1
306	33	LEU	HG	H	1.167	0.003	2	385	43	ASN	HB2	H	3.185	0.003	2
307	33	LEU	N	N	127.175	0.034	1	386	43	ASN	HB3	H	2.910	0.003	2

387	43	ASN	N	N	119.403	0.004	1	466	53	CYS	CA	C	58.631	0.041	1
388	44	GLU	CA	C	58.274	0.028	1	467	53	CYS	CB	C	44.619	0.004	1
389	44	GLU	CB	C	30.696	0.003	1	468	53	CYS	C	C	175.009	0.03	1
390	44	GLU	CG	C	37.380	0.03	1	469	53	CYS	H	H	6.730	0.003	1
391	44	GLU	C	C	176.940	0.03	1	470	53	CYS	HA	H	1.885	0.001	1
392	44	GLU	H	H	8.289	0.003	1	471	53	CYS	HB2	H	2.535	0.003	2
393	44	GLU	HA	H	4.039	0.003	1	472	53	CYS	HB3	H	2.962	0.003	2
394	44	GLU	HB2	H	1.750	0.003	2	473	53	CYS	N	N	120.799	0.002	1
395	44	GLU	HB3	H	2.188	0.003	2	474	54	GLN	CA	C	58.508	0.005	1
396	44	GLU	HG2	H	2.339	0.001	2	475	54	GLN	CB	C	27.764	0.035	1
397	44	GLU	N	N	112.749	0.010	1	476	54	GLN	CG	C	34.735	0.03	1
398	45	ASN	CA	C	50.762	0.027	1	477	54	GLN	C	C	178.023	0.03	1
399	45	ASN	CB	C	34.877	0.008	1	478	54	GLN	H	H	8.355	0.002	1
400	45	ASN	C	C	173.938	0.03	1	479	54	GLN	HA	H	3.565	0.003	1
401	45	ASN	H	H	8.303	0.002	1	480	54	GLN	HB2	H	2.126	0.002	2
402	45	ASN	HA	H	4.652	0.003	1	481	54	GLN	HB3	H	1.765	0.001	2
403	45	ASN	HB2	H	3.159	0.003	2	482	54	GLN	HG2	H	2.042	0.003	2
404	45	ASN	HB3	H	2.902	0.003	2	483	54	GLN	HG3	H	2.501	0.002	2
405	45	ASN	N	N	121.075	0.006	1	484	54	GLN	N	N	120.571	0.004	1
406	46	ASN	CA	C	53.459	0.024	1	485	55	ARG	CA	C	58.106	0.017	1
407	46	ASN	CB	C	38.976	0.023	1	486	55	ARG	CB	C	29.495	0.026	1
408	46	ASN	C	C	173.714	0.03	1	487	55	ARG	CD	C	43.064	0.03	1
409	46	ASN	H	H	6.547	0.003	1	488	55	ARG	CG	C	26.660	0.03	1
410	46	ASN	HA	H	4.740	0.003	1	489	55	ARG	C	C	176.856	0.03	1
411	46	ASN	HB2	H	2.453	0.003	2	490	55	ARG	H	H	8.098	0.002	1
412	46	ASN	HB3	H	2.578	0.004	2	491	55	ARG	HA	H	3.898	0.003	1
413	46	ASN	N	N	118.242	0.008	1	492	55	ARG	HB2	H	1.578	0.003	2
414	47	PHE	CA	C	55.726	0.021	1	493	55	ARG	HD2	H	3.019	0.003	2
415	47	PHE	CB	C	42.353	0.006	1	494	55	ARG	HD3	H	2.901	0.003	2
416	47	PHE	C	C	175.525	0.03	1	495	55	ARG	HG2	H	1.432	0.003	2
417	47	PHE	H	H	10.039	0.002	1	496	55	ARG	N	N	117.371	0.005	1
418	47	PHE	HA	H	4.947	0.003	1	497	56	THR	CA	C	66.062	0.057	1
419	47	PHE	HB2	H	3.265	0.003	2	498	56	THR	CB	C	69.047	0.055	1
420	47	PHE	HB3	H	2.593	0.003	2	499	56	THR	CG2	C	22.118	0.03	1
421	47	PHE	HD1	H	7.265	0.003	3	500	56	THR	C	C	175.235	0.03	1
422	47	PHE	HE1	H	7.563	0.003	3	501	56	THR	H	H	7.140	0.003	1
423	47	PHE	N	N	123.588	0.004	1	502	56	THR	HA	H	3.992	0.003	1
424	48	ARG	CA	C	57.622	0.052	1	503	56	THR	HB	H	3.893	0.003	2
425	48	ARG	CB	C	31.162	0.019	1	504	56	THR	HG1	H	1.377	0.001	2
426	48	ARG	CD	C	43.185	0.03	1	505	56	THR	N	N	112.797	0.015	1
427	48	ARG	CG	C	28.627	0.03	1	506	57	CYS	CA	C	54.328	0.047	1
428	48	ARG	C	C	176.771	0.03	1	507	57	CYS	CB	C	42.393	0.012	1
429	48	ARG	H	H	9.466	0.002	1	508	57	CYS	C	C	173.311	0.03	1
430	48	ARG	HA	H	4.396	0.003	1	509	57	CYS	H	H	7.553	0.002	1
431	48	ARG	HB2	H	2.042	0.003	2	510	57	CYS	HA	H	4.633	0.003	1
432	48	ARG	HB3	H	1.819	0.009	2	511	57	CYS	HB2	H	1.672	0.003	2
433	48	ARG	HD2	H	3.224	0.003	2	512	57	CYS	HB3	H	1.363	0.003	2
434	48	ARG	HG2	H	1.813	0.005	2	513	57	CYS	N	N	112.636	0.006	1
435	48	ARG	HG3	H	1.590	0.004	2	514	58	LEU	CA	C	56.270	0.03	1
436	48	ARG	N	N	119.221	0.004	1	515	58	LEU	CB	C	44.237	0.006	1
437	49	ARG	CA	C	53.942	0.024	1	516	58	LEU	CD1	C	25.252	0.03	1
438	49	ARG	CB	C	33.507	0.021	1	517	58	LEU	CG	C	27.320	0.03	1
439	49	ARG	CG	C	26.809	0.03	1	518	58	LEU	C	C	176.548	0.03	1
440	49	ARG	H	H	7.498	0.002	1	519	58	LEU	H	H	7.522	0.002	1
441	49	ARG	HA	H	4.886	0.003	1	520	58	LEU	HA	H	4.257	0.003	1
442	49	ARG	HB2	H	2.076	0.003	2	521	58	LEU	HB2	H	1.206	0.003	2
443	49	ARG	HB3	H	1.910	0.003	2	522	58	LEU	HB3	H	1.525	0.002	2
444	49	ARG	HD2	H	3.307	0.003	2	523	58	LEU	HD1	H	0.867	0.003	2
445	49	ARG	HG2	H	1.786	0.003	2	524	58	LEU	HD2	H	0.739	0.003	2
446	49	ARG	HG3	H	1.600	0.003	2	525	58	LEU	HG	H	1.176	0.003	2
447	49	ARG	N	N	113.085	0.005	1	526	58	LEU	N	N	120.701	0.003	1
448	50	THR	H	H	9.263	0.002	1	527	59	TYR	CA	C	56.469	0.040	1
449	50	THR	N	N	122.046	0.007	1	528	59	TYR	CB	C	37.679	0.025	1
450	51	TYR	CA	C	60.984	0.230	1	529	59	TYR	C	C	175.127	0.03	1
451	51	TYR	CB	C	38.922	0.025	1	530	59	TYR	H	H	7.745	0.002	1
452	51	TYR	C	C	176.579	0.03	1	531	59	TYR	HA	H	4.744	0.003	1
453	51	TYR	HA	H	4.280	0.004	1	532	59	TYR	HB2	H	3.167	0.003	2
454	51	TYR	HB2	H	2.562	0.001	2	533	59	TYR	HB3	H	2.822	0.003	2
455	51	TYR	HB3	H	3.272	0.003	2	534	59	TYR	HD1	H	6.982	0.003	3
456	51	TYR	HD1	H	7.134	0.003	3	535	59	TYR	HE1	H	6.745	0.003	3
457	51	TYR	HE1	H	6.831	0.003	3	536	59	TYR	N	N	120.378	0.006	1
458	52	ASP	CA	C	57.161	0.039	1	537	60	THR	CA	C	62.782	0.03	1
459	52	ASP	CB	C	41.122	0.004	1	538	60	THR	CB	C	70.624	0.03	1
460	52	ASP	C	C	177.257	0.03	1	539	60	THR	H	H	7.486	0.001	1
461	52	ASP	H	H	6.640	0.004	1	540	60	THR	N	N	118.585	0.006	1
462	52	ASP	HA	H	4.249	0.003	1								
463	52	ASP	HB2	H	3.106	0.003	2								
464	52	ASP	HB3	H	2.839	0.003	2								
465	52	ASP	N	N	115.867	0.010	1								

C NMR restraints of Conk-S1

C.1 Residual dipolar couplings

Table 3 H_N N-RDCs of Conk-S1

Residue 1	Atom 1	Residue 2	Atom 2	D [Hz]
3	N	3	HN	4.382
5	N	5	HN	-3.092
6	N	6	HN	12.505
7	N	7	HN	-20.229
11	N	11	HN	4.851
12	N	12	HN	16.789
13	N	13	HN	21.371
15	N	15	HN	10.715
16	N	16	HN	-5.478
17	N	17	HN	5.788
18	N	18	HN	-20.673
19	N	19	HN	-7.587
20	N	20	HN	7.302
21	N	21	HN	6.391
22	N	22	HN	21.147
23	N	23	HN	5.649
25	N	25	HN	2.689
27	N	27	HN	-2.612
28	N	28	HN	-21.061
29	N	29	HN	-6.266
30	N	30	HN	19.603
31	N	31	HN	29.311
32	N	32	HN	21.366
34	N	34	HN	8.869
35	N	35	HN	14.104
36	N	36	HN	16.081
37	N	37	HN	17.244
38	N	38	HN	5.068
39	N	39	HN	0.627
40	N	40	HN	9.685
41	N	41	HN	7.842
43	N	43	HN	11.588
44	N	44	HN	1.986
45	N	45	HN	18.790
46	N	46	HN	-4.266
48	N	48	HN	-3.909
49	N	49	HN	-11.954
53	N	53	HN	-17.750
54	N	54	HN	-28.635
55	N	55	HN	-25.261
56	N	56	HN	-30.443
57	N	57	HN	-13.133
58	N	58	HN	-1.008
59	N	59	HN	-11.870
60	N	60	HN	3.270

Table 4 C' N-RDCs of Conk-S1

Residue 1	Atom 1	Residue 2	Atom 2	D [Hz]
2	C	3	N	-0.158
4	C	5	N	2.014
5	C	6	N	0.538
6	C	7	N	-1.098
7	C	8	N	0.880
8	C	9	N	-1.013
10	C	11	N	-0.485
11	C	12	N	0.160
12	C	13	N	-1.197
13	C	14	N	1.339
14	C	15	N	-0.245
15	C	16	N	2.589
16	C	17	N	-0.826
17	C	18	N	-0.159
18	C	19	N	1.916
19	C	20	N	-3.296
20	C	21	N	2.182
21	C	22	N	-1.004
22	C	23	N	-2.734
23	C	24	N	0.160
24	C	25	N	-2.109
25	C	26	N	0.415
26	C	27	N	1.545
27	C	28	N	0.388
28	C	29	N	-1.466
29	C	30	N	0.453
30	C	31	N	-3.401
31	C	32	N	1.453
32	C	33	N	0.062
33	C	34	N	-2.095
34	C	35	N	0.262
35	C	36	N	0.388
36	C	37	N	0.925
37	C	38	N	1.596
38	C	39	N	0.129
39	C	40	N	2.500
40	C	41	N	-1.435
41	C	42	N	0.372
42	C	43	N	-0.158
43	C	44	N	-2.353
44	C	45	N	0.606
45	C	46	N	1.779
47	C	48	N	1.645
48	C	49	N	-2.844
51	C	52	N	-1.191
52	C	53	N	0.150
53	C	54	N	1.958
54	C	55	N	0.930
55	C	56	N	0.566
56	C	57	N	0.475
57	C	58	N	2.329
58	C	59	N	1.123
59	C	60	N	-0.122

Table 5 CAHA-RDCs of Conk-S1

Residue 1	Atom 1	Residue 2	Atom 2	D [Hz]
1	CA	1	HA	0.252
2	CA	2	HA	12.392
4	CA	4	HA	-12.394
5	CA	5	HA	-4.727
6	CA	6	HA	32.221
7	CA	7	HA	-32.452
8	CA	8	HA	10.480
10	CA	10	HA	9.266
11	CA	11	HA	27.490
12	CA	12	HA	24.486
13	CA	13	HA	40.151
15	CA	15	HA	20.952
17	CA	17	HA	20.754
18	CA	18	HA	-32.378
19	CA	19	HA	-9.803
20	CA	20	HA	2.458
21	CA	21	HA	23.361
22	CA	22	HA	33.248
25	CA	25	HA	34.016
26	CA	26	HA	27.866
27	CA	27	HA	29.870
28	CA	28	HA	-39.994
29	CA	29	HA	-1.480
31	CA	31	HA	26.955
32	CA	32	HA	24.484
33	CA	33	HA	22.897
34	CA	34	HA	11.525
35	CA	35	HA	5.522
36	CA	36	HA	38.599
37	CA	37	HA	24.048
38	CA	38	HA	4.611
40	CA	40	HA	15.438
43	CA	43	HA	11.700
44	CA	44	HA	-9.919
45	CA	45	HA	9.769
47	CA	47	HA	8.926
48	CA	48	HA	-7.004
49	CA	49	HA	-26.711
51	CA	51	HA	-12.324
52	CA	52	HA	-12.583
53	CA	53	HA	24.849
54	CA	54	HA	19.993
55	CA	55	HA	-19.145
56	CA	56	HA	-12.933
57	CA	57	HA	-8.267
58	CA	58	HA	26.260
59	CA	59	HA	-2.156

Table 6 CaC²-RDCs of Conk-S1

Residue 1	Atom 1	Residue 2	Atom 2	D [Hz]
1	CA	1	C	1.597
2	CA	2	C	-4.968
4	CA	4	C	2.9125
5	CA	5	C	-4.209
6	CA	6	C	0.527
7	CA	7	C	2.895
8	CA	8	C	-1.292
10	CA	10	C	-1.8185
11	CA	11	C	0.38
12	CA	12	C	-3.8165
14	CA	14	C	-2.327
15	CA	15	C	-2.948
16	CA	16	C	-3.291
17	CA	17	C	2.839
18	CA	18	C	-1.199
19	CA	19	C	2.0015
20	CA	20	C	-3.877
21	CA	21	C	-3.51
22	CA	22	C	-4.806
26	CA	26	C	-4.6885
27	CA	27	C	-0.278
28	CA	28	C	2.748
29	CA	29	C	0.6455
31	CA	31	C	-3.3695
32	CA	32	C	-4.058
33	CA	33	C	-1.8915
34	CA	34	C	2.8385
35	CA	35	C	-2.6045
36	CA	36	C	0.7975
37	CA	37	C	-4.624
38	CA	38	C	0.386
40	CA	40	C	-0.7465
41	CA	41	C	-2.520
42	CA	42	C	-3.959
43	CA	43	C	3.689
44	CA	44	C	2.176
45	CA	45	C	-3.636
47	CA	47	C	-3.479
48	CA	48	C	3.147
49	CA	49	C	-3.0025
51	CA	51	C	1.4185
52	CA	52	C	1.827
53	CA	53	C	-3.923
54	CA	54	C	-2.5265
55	CA	55	C	3.372
56	CA	56	C	1.0275
57	CA	57	C	-1.341
58	CA	58	C	-1.849
59	CA	59	C	-0.78

C.2 Dihedral angles

Table 7 Phi angles of Conk-S1 from Talos

Residue 1	Atom 1	Residue 2	Atom 2	Residue 3	Atom 3	Residue 4	Atom 4	Phi angle [°]
3	C	4	N	4	CA	4	C	-70.0
4	C	5	N	5	CA	5	C	-76.3
5	C	6	N	6	CA	6	C	-81.2
7	C	8	N	8	CA	8	C	-97.0
8	C	9	N	9	CA	9	C	-77.0
9	C	10	N	10	CA	10	C	-72.0
10	C	11	N	11	CA	11	C	-78.0
11	C	12	N	12	CA	12	C	-100.0
12	C	13	N	13	CA	13	C	-74.0
14	C	15	N	15	CA	15	C	-96.0
15	C	16	N	16	CA	16	C	-84.0
16	C	17	N	17	CA	17	C	-90.0
17	C	18	N	18	CA	18	C	-100.0
18	C	19	N	19	CA	19	C	-97.0
19	C	20	N	20	CA	20	C	-114.0
20	C	21	N	21	CA	21	C	-90.0
21	C	22	N	22	CA	22	C	-138.0
22	C	23	N	23	CA	23	C	-112.0
23	C	24	N	24	CA	24	C	-127.0
24	C	25	N	25	CA	25	C	-100.0
25	C	26	N	26	CA	26	C	-106.0
26	C	27	N	27	CA	27	C	-66.0
27	C	28	N	28	CA	28	C	-71.0
28	C	29	N	29	CA	29	C	-96.0
29	C	30	N	30	CA	30	C	57.0
30	C	31	N	31	CA	31	C	-126.0
31	C	32	N	32	CA	32	C	-117.0
32	C	33	N	33	CA	33	C	-116.0
33	C	34	N	34	CA	34	C	-103.0
34	C	35	N	35	CA	35	C	-130.0
35	C	36	N	36	CA	36	C	-99.0
36	C	37	N	37	CA	37	C	-114.0
37	C	38	N	38	CA	38	C	-112.0
38	C	39	N	39	CA	39	C	88.0
39	C	40	N	40	CA	40	C	-121.0
40	C	41	N	41	CA	41	C	75.0
41	C	42	N	42	CA	42	C	-85.0
42	C	43	N	43	CA	43	C	-110.0
43	C	44	N	44	CA	44	C	-81.0
44	C	45	N	45	CA	45	C	-79.0
45	C	46	N	46	CA	46	C	-83.0
46	C	47	N	47	CA	47	C	-111.0
47	C	48	N	48	CA	48	C	-80.0
48	C	49	N	49	CA	49	C	-129.0
50	C	51	N	51	CA	51	C	-67.0
51	C	52	N	52	CA	52	C	-83.0
52	C	53	N	53	CA	53	C	-68.0
53	C	54	N	54	CA	54	C	-65.0
54	C	55	N	55	CA	55	C	-66.0
55	C	56	N	56	CA	56	C	-80.0
56	C	57	N	57	CA	57	C	-85.0
57	C	58	N	58	CA	58	C	-90.0
58	C	59	N	59	CA	59	C	-100.0

Table 8 Psi angles of Conk-S1 from Talos

Residue 1	Atom 1	Residue 2	Atom 2	Residue 3	Atom 3	Residue 4	Atom 4	Psi angle [°]
4	N	4	CA	4	C	5	N	138.0
5	N	5	CA	5	C	6	N	-20.7
6	N	6	CA	6	C	7	N	-3.2
8	N	8	CA	8	C	9	N	-1.0
9	N	9	CA	9	C	10	N	147.1
10	N	10	CA	10	C	11	N	146.0
11	N	11	CA	11	C	12	N	134.0
12	N	12	CA	12	C	13	N	141.0
13	N	13	CA	13	C	14	N	-38.0
15	N	15	CA	15	C	16	N	4.0
16	N	16	CA	16	C	17	N	167.0
17	N	17	CA	17	C	18	N	-15.0
18	N	18	CA	18	C	19	N	146.0
19	N	19	CA	19	C	20	N	126.0
20	N	20	CA	20	C	21	N	135.0
21	N	21	CA	21	C	22	N	133.0
22	N	22	CA	22	C	23	N	153.0
23	N	23	CA	23	C	24	N	132.0
24	N	24	CA	24	C	25	N	155.0
25	N	25	CA	25	C	26	N	117.0
26	N	26	CA	26	C	27	N	126.0
27	N	27	CA	27	C	28	N	-27.0
28	N	28	CA	28	C	29	N	-32.0
29	N	29	CA	29	C	30	N	0.0
30	N	30	CA	30	C	31	N	35.0
31	N	31	CA	31	C	32	N	154.0
32	N	32	CA	32	C	33	N	149.0
33	N	33	CA	33	C	34	N	151.0
34	N	34	CA	34	C	35	N	139.0
35	N	35	CA	35	C	36	N	146.0
36	N	36	CA	36	C	37	N	116.0
37	N	37	CA	37	C	38	N	140.0
38	N	38	CA	38	C	39	N	2.0
39	N	39	CA	39	C	40	N	-2.0
40	N	40	CA	40	C	41	N	146.0
41	N	41	CA	41	C	42	N	25.0
42	N	42	CA	42	C	43	N	137.0
43	N	43	CA	43	C	44	N	163.0
44	N	44	CA	44	C	45	N	-28.0
45	N	45	CA	45	C	46	N	124.0
46	N	46	CA	46	C	47	N	118.0
47	N	47	CA	47	C	48	N	150.0
48	N	48	CA	48	C	49	N	-20.0
49	N	49	CA	49	C	50	N	151.0
51	N	51	CA	51	C	52	N	-36.0
52	N	52	CA	52	C	53	N	-17.0
53	N	53	CA	53	C	54	N	-38.0
54	N	54	CA	54	C	55	N	-29.0
55	N	55	CA	55	C	56	N	-37.0
56	N	56	CA	56	C	57	N	-14.0
57	N	57	CA	57	C	58	N	-8.0
58	N	58	CA	58	C	59	N	-15.0
59	N	59	CA	59	C	60	N	117.0

Table 9 Chi1 angles (C' CA CB CG) of Conk-S1

Residue	Chi1 angle [°]	Residue	Chi1 angle [°]
11	180.0	46	180.0
18	180.0	47	-60.0
20	180.0	48	180.0
21	180.0	49	180.0
23	180.0	51	180.0
24	60.0	54	180.0
25	180.0	55	180.0
30	180.0	56	180.0
34	180.0	58	180.0
35	60.0	59	-60.0
37	180.0	60	180.0
40	180.0		
45	180.0		

C.3 Coupling constants

Table 10 ${}^3J_{\text{HnHa}}$ coupling constants

Residue 1	Atom 1	Residue 2	Atom 2	${}^3J_{\text{HnHa}}$ [Hz]
5	H	5	HA	4.0
7	H	7	HA	5.4
8	H	8	HA	9.9
9	H	9	HA	7.5
11	H	11	HA	6.2
12	H	12	HA	12.6
13	H	13	HA	6.4
15	H	15	HA	11.6
16	H	16	HA	10.1
17	H	17	HA	10.1
18	H	18	HA	11.0
19	H	19	HA	9.5
20	H	20	HA	11.2
21	H	21	HA	9.4
22	H	22	HA	10.9
23	H	23	HA	12.4
24	H	24	HA	10.2
26	H	26	HA	10.1
27	H	27	HA	5.4
28	H	28	HA	7.2
29	H	29	HA	9.9
30	H	30	HA	9.7
31	H	31	HA	10.1
32	H	32	HA	10.3
33	H	33	HA	11.2
34	H	34	HA	7.7
35	H	35	HA	9.7
36	H	36	HA	9.6
37	H	37	HA	10.1
38	H	38	HA	9.6
40	H	40	HA	10.2
43	H	43	HA	9.7
44	H	44	HA	5.5
45	H	45	HA	10.1
46	H	46	HA	9.9
47	H	47	HA	10.2
48	H	48	HA	9.5
49	H	49	HA	10.8
52	H	52	HA	7.3
53	H	53	HA	6.1
54	H	54	HA	4.6
55	H	55	HA	5.5
56	H	56	HA	9.5
57	H	57	HA	11.3
58	H	58	HA	9.8
59	H	59	HA	9.7
60	H	60	HA	10.2

C.4 Distance constraints

Table 11 NOE distance restraints for Conk-S1

Residue 1	Atom 1	Residue 2	Atom 2	Distance [Å]	Residue 1	Atom 1	Residue 2	Atom 2	Distance [Å]
4	HG2	4	HA	2.547	58	HB1	54	HG2	3.573
20	HG2	22	HG2	3.550	34	HA	33	HA	4.025
10	HG2	44	HN	3.927	14	HA1	15	HN	3.539
30	HB1	30	HN	3.465	47	HA	49	HN	2.591
48	HG1	22	HD2	2.192	47	HA	46	HA	3.348
34	HB2	24	HB2	3.535	32	HA	58	HG	3.174
18	HB1	17	HG1	3.579	16	HA1	15	HA	3.200
48	HG1	48	HN	3.105	48	HA	49	HA	3.538
48	HB2	52	HB2	3.827	7	HA	8	HA	3.619
49	HG1	49	HN	3.145	35	HA	24	HA	4.020
49	HG1	23	HG11	4.387	35	HA	34	HA	4.812
54	HB2	54	HN	2.618	8	HA	27	HB2	4.234
29	HB1	29	HB2	2.064	31	HA	31	HB1	1.939
21	HB1	21	HN	2.050	31	HA	58	HA	4.086
21	HB1	22	HG2	3.907	39	HA1	15	HB2	4.644
49	HB2	52	HB1	3.325	11	HA	45	HB2	3.859
49	HB2	52	HA	3.881	11	HA	45	HN	3.435
21	HB1	21	HE2	3.441	54	HA	32	HB1	3.874
24	HB1	11	HB2	3.564	11	HA	35	HB1	4.071
24	HB1	11	HB1		48	HD2	20	HA	4.587
24	HB1	11	HB3		47	HB1	53	HN	3.274
24	HB2	11	HA	3.746	47	HB1	47	HB2	2.114
24	HB1	33	HB1	3.972	51	HB1	55	HD1	3.561
7	HB2	57	HB2	2.245	10	HD1	44	HN	3.761
7	HB2	57	HA	3.278	10	HD1	10	HD2	2.121
47	HB2	47	HD1	2.392	15	HB2	16	HA1	3.870
24	HB2	11	HB2	3.291	30	HE2	57	HA	5.379
24	HB2	11	HB1		55	HD1	52	HA	4.570
24	HB2	11	HB3		55	HD1	55	HA	3.713
32	HB2	54	HB2	3.402	34	HD2	34	HN	4.030
8	HB1	4	HA	4.303	45	HB1	45	HA	2.670
1	HE2	1	HA	3.844	59	HB1	59	HB2	1.960
8	HB1	5	HA	3.846	45	HB2	45	HB1	1.932
22	HD2	22	HB2	3.467	45	HB1	47	HE1	3.382
52	HB2	53	HA	3.343	27	HB2	32	HA	4.578
22	HD2	37	HB1	4.900	6	HA	6	HB2	2.550
55	HD2	55	HA	3.841	52	HA	56	HN	2.766
45	HB2	45	HN	2.579	28	HA	30	HE2	3.759
45	HB2	45	HA	2.870	44	HA	43	HB1	4.058
51	HB2	55	HD1	3.334	2	HB2	2	HA	3.017
40	HG2	15	HB2	3.307	2	HB1	2	HA	2.562
20	HG1	22	HG2	3.736	4	HB2	6	HD22	3.048
4	HB2	7	HN	3.673	4	HB2	6	HD21	
4	HB1	6	HG	2.774	4	HB2	6	HD23	
52	HB2	51	HB2	3.397	4	HA	4	HB2	2.590
51	HB2	51	HB1	2.028	4	HB2	6	HN	3.651
44	HG2	43	HB1	3.575	4	HA	4	HB1	1.864
12	HB2	13	HN	3.621	4	HD2	4	HB2	3.255
58	HB2	58	HB1	2.141	4	HD1	4	HB2	3.102
58	HG	58	HA	3.348	6	HB2	6	HD11	2.491
57	HB2	58	HA	3.682	6	HB1	6	HA	2.593
31	HB2	31	HG2	3.519	6	HB1	6	HD11	1.729
58	HB2	54	HG2	3.750	7	HB2	7	HN	2.387
49	HG2	52	HN	3.125	7	HB2	57	HB1	1.981
18	HD2	18	HA	1.955	7	HB1	7	HN	2.836
48	HG2	48	HN	2.752	7	HB1	7	HA	2.628
49	HG2	49	HN	2.090	8	HA	8	HB2	2.411
55	HB2	55	HD1	1.920	8	HB1	8	HN	2.804
21	HB2	21	HN	2.913	8	HA	8	HB1	2.032
48	HG2	52	HB2	3.962	10	HA	10	HB2	2.461
40	HB2	40	HG2	3.413	10	HB1	10	HD2	2.008
21	HD1	21	HE2	2.716	10	HA	10	HB1	2.566
31	HB1	31	HG2	2.901	10	HB1	10	HD1	2.808
40	HB2	40	HA	2.634	6	HA	10	HD1	3.672
33	HB1	33	HB2	1.885	10	HD1	10	HG2	2.469
29	HG2	29	HA	2.425	10	HG2	10	HD2	2.541
29	HG2	29	HN	2.422	11	HA	11	HB1	2.419

Residue 1	Atom 1	Residue 2	Atom 2	Distance [Å]	Residue 1	Atom 1	Residue 2	Atom 2	Distance [Å]
12	HA	12	HB2	2.721	24	HB2	25	HN	3.286
12	HB2	12	HB1	2.095	24	HB1	24	HN	3.274
12	HB1	14	HA1	3.797	24	HB1	24	HA	2.167
12	HB1	12	HA	2.978	24	HB1	24	HD1	1.968
12	HB1	42	HA2	2.836	24	HB1	24	HE1	3.055
14	HA2	14	HN	1.815	24	HB1	25	HN	3.387
15	HB2	15	HA	2.669	24	HD1	23	HA	3.650
15	HB2	15	HB1	2.108	24	HD1	35	HB1	2.825
16	HA2	40	HG2	3.467	24	HD1	24	HN	2.893
16	HA2	18	HN	3.251	24	HB2	24	HD1	2.546
17	HG1	17	HB	2.325	24	HD1	25	HN	4.467
17	HG1	15	HB2	4.077	24	HD1	34	HN	3.046
18	HB2	18	HN	2.779	25	HA	33	HN	3.321
18	HB2	18	HA	2.921	25	HB2	57	HB1	3.316
18	HA	18	HB1	2.663	25	HA	25	HB2	1.808
19	HA	19	HN	3.441	25	HA	25	HB1	2.449
19	HA	19	HB2	2.425	25	HB1	26	HN	3.251
20	HB2	20	HA	2.915	26	HB2	33	HB1	3.946
20	HB1	20	HA	2.575	26	HB2	33	HB2	3.070
20	HG2	20	HN	3.247	26	HB2	26	HA	3.627
20	HG2	20	HA	3.286	26	HB2	29	HB2	2.808
20	HG1	20	HA	3.424	26	HB2	33	HD11	2.839
21	HA	21	HB2	2.417	26	HB1	33	HB1	3.876
21	HA	21	HB1	3.046	26	HB1	26	HN	2.648
21	HD2	21	HA	3.111	26	HB1	26	HA	2.780
22	HB2	22	HA	2.974	26	HB2	26	HB1	1.933
22	HB2	22	HG2	2.474	26	HB1	29	HB2	1.779
22	HB2	23	HN	2.854	26	HB1	33	HD11	2.740
22	HB2	37	HB1	2.832	27	HA	30	HN	3.108
22	HB1	22	HA	1.985	27	HB2	28	HN	3.161
22	HB2	22	HB1	2.133	27	HB2	30	HE2	3.521
22	HB1	23	HN	2.555	28	HA	28	HB1	2.223
22	HB1	47	HN	3.665	29	HA	29	HN	2.709
22	HD2	23	HN	3.542	29	HA	29	HB1	2.548
22	HD2	22	HA	2.763	29	HB2	33	HD12	3.334
22	HB1	22	HD2	1.702	29	HB2	31	HG2	3.462
22	HD2	48	HA	3.011	29	HA	29	HB2	2.436
22	HD1	48	HB1	3.592	29	HB2	29	HD2	2.873
22	HD1	23	HN	3.883	29	HB1	33	HD12	3.943
22	HD1	22	HA	2.579	29	HB1	29	HN	2.847
22	HB1	22	HD1	2.867	29	HB1	29	HD2	2.767
22	HD1	22	HG2	2.633	30	CA	30	HN	2.375
22	HD1	48	HA	2.844	30	HA	30	HB2	2.361
22	HG2	22	HA	2.832	30	HB1	30	HA	2.336
22	HG2	22	HB1	2.291	30	HA	30	HG2	2.589
22	HD2	22	HG2	2.545	30	HB2	30	HG2	2.585
22	HG2	23	HN	3.207	31	HA	31	HB2	3.377
22	HG2	37	HB1	2.425	31	HB2	33	HD11	2.851
23	HA	23	HN	3.134	31	HG2	33	HD12	3.372
23	HA	23	HB	2.555	31	HA	31	HG2	2.308
23	HA	23	HD11	2.464	32	HA	26	HN	2.796
23	HA	23	HG11	2.711	32	HA	32	HN	2.991
23	HA	23	HG21	2.354	32	HA	32	HB2	2.905
23	HA	35	HN	3.043	32	HA	32	HB1	2.663
23	HB	23	HD11	3.024	32	HA	33	HN	2.242
23	HB	23	HG12	2.501	32	HB2	58	HG	2.985
23	HB	23	HG21	2.497	32	HB1	32	HN	2.812
23	HG12	23	HN	3.429	32	HB1	33	HN	3.362
23	HA	23	HG12	2.933	33	HB2	24	HE1	3.020
23	HG11	23	HD11	2.585	33	HB2	33	HG	2.147
23	HG21	32	HA	3.113	33	HB2	33	HA	2.903
23	HG21	53	HN	3.735	33	HB2	33	HD11	2.478
23	HG21	47	HD1	2.958	33	HB1	33	HG	2.827
23	HG21	24	HD1	3.878	33	HB1	24	HE1	3.020
24	HA	25	HB1	3.278	33	HB1	33	HN	2.976
24	HA	47	HE1	3.413	33	HB1	33	HA	2.722
24	HA	23	HG21	3.362	33	HB1	33	HD11	2.433
24	HA	24	HN	2.863	33	HD11	34	HN	3.270
24	HA	24	HD1	3.357	33	HD11	31	HA	3.751
24	HA	34	HN	3.862	33	HD11	33	HA	2.554
24	HB2	24	HN	4.121	33	HD11	29	HD2	4.282
24	HA	24	HB2	2.183	33	HD11	34	HD2	4.289
24	HB2	24	HE1	3.582	34	HA	33	HB2	3.134

Residue 1	Atom 1	Residue 2	Atom 2	Distance [Å]	Residue 1	Atom 1	Residue 2	Atom 2	Distance [Å]
34	HA	23	HG22	3.981	51	HB2	49	HG1	3.904
34	HA	23	HG21		51	HB2	51	HD1	2.374
34	HA	23	HG23		51	HB2	51	CA	2.883
34	HA	35	HB1	3.783	51	HB1	51	HD1	2.760
34	HA	23	HD11	2.708	51	HB1	49	HB1	3.499
34	HA	24	HN	3.321	51	HA	51	HB1	2.228
34	HA	34	HB2	2.112	52	HA	52	HB2	2.147
34	HB1	34	HN	2.092	52	HA	55	HB2	2.173
34	HB1	34	HD2	1.922	52	HB1	49	HN	2.798
34	HG2	34	HN	3.382	52	HA	52	HB1	2.893
34	HG2	23	HD11	3.446	52	HB1	53	HN	2.567
34	HG2	34	HA	2.945	53	HA	57	HN	3.078
34	HG1	34	HA	3.081	53	HA	53	HN	2.943
34	HD2	34	HG1	2.212	53	HA	53	HB2	2.538
35	HB2	35	HD1	2.354	53	HA	53	HB1	2.747
35	HB2	11	HB1	3.408	53	HA	54	HN	3.889
35	HB2	24	HE1	2.769	53	HA	56	HB	3.180
35	HB2	35	HA	1.831	53	HB2	47	HD1	2.711
35	HB1	35	HD1	2.535	53	HB2	53	HN	2.701
35	HB1	11	HB1	3.517	53	HB2	54	HN	3.122
36	HB2	36	HN	2.160	53	HB1	23	HG21	2.652
36	HB2	36	HA	1.868	53	HB1	54	HN	2.770
36	HA	36	HB1	2.356	54	HA	58	HA	3.955
37	HA	37	HN	2.725	54	HA	58	HD22	2.857
37	HB2	22	HB2	3.022	54	HA	58	HD21	
37	HB2	37	HN	2.899	54	HA	58	HD23	
37	HB2	37	HA	2.819	54	HA	58	HN	2.822
37	HB1	37	HA	2.369	53	HB2	54	HA	2.862
39	HA2	40	HN	2.618	54	HA	54	HB2	2.533
42	HA2	42	HN	2.533	54	HA	54	HB1	2.362
43	HA	43	HB2	2.804	54	HA	58	HB2	2.644
43	HA	43	HB1	2.577	54	HA	58	HB1	2.412
43	HB2	44	HN	2.311	58	HG	54	HG2	3.078
43	HB1	44	HN	2.336	54	HG2	54	HA	2.789
44	HA	44	HN	2.759	54	HG2	58	HD21	2.981
44	HB2	44	HN	2.231	54	HG1	58	HG	2.873
44	HA	44	HB2	2.301	54	HG1	54	HA	2.875
44	HB1	44	HA	2.555	54	HG1	54	HB1	2.850
44	HG2	44	HA	2.636	55	HA	55	HB2	2.485
44	HG2	44	HB2	2.367	55	HA	59	HB1	2.726
46	HB2	46	HN	2.952	55	HG2	56	HN	3.113
46	HB2	46	HA	2.802	55	HG2	52	HA	2.949
46	HB1	46	HA	2.921	56	HG1	52	HA	3.584
47	HA	48	HB2	2.847	56	HG1	59	HB1	4.253
47	HA	47	HB1	1.906	56	HA	56	HG1	2.265
47	HB2	48	HN	2.910	56	HG1	57	HN	2.805
23	HB	47	HB2	2.891	57	HB2	57	HN	2.668
47	HB2	47	HA	2.676	57	HB2	57	HA	2.954
47	HB2	49	HN	2.469	7	HB1	57	HB1	2.836
48	HA	48	HG2	2.666	57	HB1	57	HA	2.691
48	HA	48	HB2	2.233	58	HA	58	HB2	2.490
48	HB2	48	HD2	2.767	58	HA	58	HD11	2.315
48	HB1	48	HN	2.786	58	HB2	58	HN	2.740
48	HA	48	HB1	2.371	58	HB2	58	HD11	2.747
48	HB1	48	HD2	1.817	58	HB1	58	HN	2.579
48	HD2	48	HG1	2.790	58	HB1	58	HA	2.989
48	HG2	48	HD2	2.428	58	HB1	58	HD21	2.690
48	HG1	48	HA	2.348	58	HB1	59	HN	2.499
49	HA	49	HB2	2.438	58	HD11	32	HN	4.032
49	HB2	49	HD2	2.781	58	HD11	60	HN	3.896
49	HB1	52	HN	2.739	58	HD11	31	HA	3.295
49	HB1	49	HN	3.048	59	HB2	59	HD1	3.170
49	HA	49	HB1	2.453	59	HB2	59	HA	2.730
49	HB1	49	HD2	2.815	59	HB2	60	HN	3.597
49	HG2	49	HA	3.372	59	HB1	59	HD1	2.912
49	HG2	49	HB2	2.674	59	HB1	59	HN	2.820
49	HG1	49	HA	3.116	59	HB1	59	HA	2.917
51	HA	51	HD1	2.710	57	HN	59	HN	3.779
51	HA	51	HB2	2.788	57	HN	57	HA	2.876
51	HA	52	HN	2.812	8	HN	7	HN	2.817
51	HA	54	HB2	2.623	57	HN	56	HB	2.689
51	HA	54	HB1	3.105	57	HB1	57	HN	2.687
51	HB2	54	HB1	3.330	54	HA	57	HN	3.678

Residue 1	Atom 1	Residue 2	Atom 2	Distance [Å]	Residue 1	Atom 1	Residue 2	Atom 2	Distance [Å]
57	HN	56	HA	3.522	4	HB1	5	HN	3.194
9	HN	7	HN	3.633	5	HN	4	HB2	2.961
7	HN	6	HA	3.444	37	HN	20	HN	3.028
60	HN	59	HA	2.545	43	HN	44	HN	3.468
60	HN	59	HN	3.305	16	HN	41	HN	3.847
59	HB1	60	HN	3.530	54	HB2	55	HN	3.035
48	HB2	49	HN	2.676	54	HA	55	HN	3.669
49	HN	48	HN	2.528	2	HN	2	HA	2.232
58	HN	58	HG	2.620	5	HN	6	HN	2.898
58	HN	57	HB1	3.396	6	HN	6	HG	2.484
49	HN	49	HA	2.853	5	HB2	6	HN	3.171
49	HN	52	HB2	3.081	6	HN	6	HD22	2.793
48	HA	49	HN	3.214	6	HN	6	HD21	
49	HB2	49	HN	2.845	6	HN	6	HD23	
48	HB1	49	HN	2.874	5	HA	6	HN	3.224
28	HN	30	HN	3.197	4	HB1	6	HN	2.919
55	HA	55	HN	2.692	6	HA	6	HN	2.732
55	HN	52	HA	3.118	6	HB2	6	HN	2.433
54	HB1	55	HN	2.763	6	HB1	6	HN	2.775
55	HG2	55	HN	2.725	7	HN	4	HB1	3.165
55	HB2	55	HN	2.300	6	HN	7	HN	2.822
26	HN	33	HD12	3.587	7	HN	6	HD21	3.046
26	HN	30	HN	3.502	7	HN	6	HG	2.562
18	HN	19	HN	3.707	7	HN	7	HA	3.081
59	HB2	59	HN	2.641	8	HN	6	HA	3.406
58	HB2	59	HN	3.153	8	HN	7	HB2	3.066
59	HN	59	HD1	3.613	8	HA	8	HN	2.931
59	HN	59	HA	2.775	8	HB2	8	HN	2.430
58	HN	59	HN	2.479	9	HN	6	HA	3.362
31	HN	31	HG2	3.381	9	HN	8	HB2	3.339
31	HN	26	HB1	3.021	9	HN	8	HA	3.150
30	HA	31	HN	2.540	10	HB2	11	HN	2.762
31	HN	31	HB1	3.272	10	HB1	11	HN	3.061
31	HN	29	HB2	3.094	10	HA	11	HN	2.260
31	HB2	31	HN	2.810	11	HN	11	HA	2.866
31	HA	31	HN	2.782	11	HA	12	HN	2.300
52	HN	53	HN	2.635	12	HN	12	HA	3.110
52	HN	51	HD1	3.539	12	HB2	12	HN	3.083
52	HN	51	HB2	2.791	12	HB1	12	HN	2.893
52	HN	52	HB1	3.096	12	HA	13	HN	2.229
52	HN	52	HA	2.856	13	HN	13	HA	3.177
49	HB2	52	HN	2.662	13	HB2	13	HN	2.993
52	HN	52	HB2	2.531	14	HN	12	HA	3.257
52	HN	51	HB1	2.993	14	HA2	15	HN	2.397
53	HB1	53	HN	2.497	15	HN	15	HA	2.856
53	HN	52	HA	3.353	15	HB2	15	HN	3.054
53	HN	52	HB2	2.807	15	HB1	15	HN	2.779
53	HN	54	HN	2.590	15	HN	16	HN	2.563
57	HN	56	HN	2.610	16	HN	15	HA	2.860
56	HN	55	HN	2.754	16	HA2	16	HN	2.495
56	HN	56	HA	2.809	16	HA2	17	HN	2.468
56	HN	56	HB	2.472	17	HN	17	HA	2.838
55	HB2	56	HN	2.809	17	HN	18	HN	2.443
32	HN	31	HB2	2.951	18	HN	18	HA	2.468
20	HN	39	HN	4.102	18	HN	18	HB1	2.924
16	HN	20	HN	4.781	18	HN	18	HG2	3.265
22	HN	21	HN	3.678	18	HA	19	HN	2.232
54	HG1	54	HN	2.456	19	HN	18	HB2	2.860
54	HB1	54	HN	2.554	18	HB1	19	HN	2.400
54	HG2	54	HN	3.017	19	HB2	19	HN	2.401
54	HA	54	HN	2.792	19	HN	20	HN	3.914
54	HN	55	HN	2.851	19	HA	20	HN	2.152
51	HA	54	HN	3.231	19	HB2	20	HN	2.782
36	HN	22	HN	3.969	20	HA	20	HN	2.753
42	HN	14	HN	3.539	20	HB1	20	HN	2.877
48	HN	47	HA	2.433	20	HG1	20	HN	2.794
48	HA	48	HN	2.877	20	HB2	20	HN	2.971
48	HB2	48	HN	2.332	21	HN	21	HD2	2.581
47	HB1	48	HN	2.779	20	HB1	21	HN	2.772
23	HN	47	HB2	3.253	20	HA	21	HN	2.229
4	HA	5	HN	2.266	21	HN	21	HA	2.863
5	HA	5	HN	2.884	22	HN	21	HD2	3.372
5	HB2	5	HN	2.540	22	HN	21	HB2	2.872

Residue 1	Atom 1	Residue 2	Atom 2	Distance [Å]	Residue 1	Atom 1	Residue 2	Atom 2	Distance [Å]
21	HA	22	HN	2.144	34	HA	34	HN	2.893
22	HN	22	HA	2.907	34	HB1	35	HN	3.257
22	HB2	22	HN	2.879	34	HB2	35	HN	2.765
22	HN	22	HB1	3.284	35	HN	34	HG2	3.081
22	HG2	22	HN	3.391	34	HA	35	HN	2.224
22	HN	35	HN	2.869	35	HN	35	HA	3.066
23	HN	22	HA	2.669	36	HN	35	HA	2.395
23	HB	23	HN	2.243	35	HB2	36	HN	2.908
23	HG11	23	HN	3.004	36	HN	35	HD1	3.228
23	HN	23	HG21	3.650	36	HN	36	HA	2.981
23	HA	24	HN	2.297	36	HB1	36	HN	2.880
23	HG21	24	HN	2.516	36	HA	37	HN	2.209
24	HN	33	HN	2.903	37	HB1	37	HN	2.579
25	HN	47	HE1	3.593	38	HN	37	HB2	3.765
24	HA	25	HN	2.640	38	HN	13	HA	3.412
25	HA	25	HN	3.522	38	HN	37	HA	2.324
25	HB2	25	HN	2.813	40	HN	38	HN	3.367
25	HB1	25	HN	2.778	40	HN	40	HG2	3.438
25	HA	26	HN	2.388	16	HN	40	HN	2.977
26	HN	26	HA	3.033	16	HA2	40	HN	3.042
26	HB2	26	HN	2.619	40	HN	40	HA	2.809
26	HN	31	HN	3.177	40	HN	40	HB2	2.975
26	HA	27	HN	2.229	40	HB1	40	HN	3.187
27	HA	27	HN	2.888	40	HA	41	HN	2.324
27	HB2	27	HN	2.401	41	HN	40	HB2	3.228
27	HN	28	HN	2.724	41	HN	40	HB1	3.012
28	HN	27	HA	3.348	41	HN	40	HG2	3.091
28	HA	28	HN	2.680	41	HA2	41	HN	2.465
28	HB1	28	HN	2.246	41	HA2	42	HN	2.473
28	HN	29	HN	2.543	12	HB1	43	HN	3.099
28	HA	29	HN	3.242	43	HN	42	HA2	2.417
28	HB1	29	HN	2.304	43	HN	43	HA	2.951
29	HB2	29	HN	2.499	43	HA	44	HN	2.586
30	HN	30	HG1	3.127	44	HB1	44	HN	2.857
30	HN	30	HG2	2.991	44	HG2	44	HN	2.630
30	HN	30	HB2	3.261	45	HN	45	HA	2.769
29	HN	30	HN	2.399	45	HB1	45	HN	2.638
30	HN	29	HA	3.217	46	HN	45	HN	3.555
30	HN	29	HB2	3.121	46	HN	45	HA	2.395
30	HN	30	HA	2.287	46	HN	46	HA	3.214
30	HN	31	HN	2.572	46	HN	46	HB1	2.839
31	HA	32	HN	2.199	23	HB	47	HN	3.091
31	HB1	32	HN	2.797	23	HN	47	HN	2.946
32	HB2	32	HN	2.446	47	HN	46	HA	2.428
33	HN	33	HD12	3.138	47	HA	47	HN	3.422
23	HG21	33	HN	2.865	47	HN	47	HB2	3.433
33	HN	33	HA	2.933	47	HN	47	HB1	2.817
33	HB2	33	HN	2.658	58	HA	58	HN	2.866
34	HN	33	HA	2.269	58	HA	59	HN	2.789
33	HB1	34	HN	2.476					

D Pulse-programs and parameters used for HVDAC

D.1.1 TROSY-HSQC pulse-program

```
;trosetf3gpsi
;avance-version (02/05/31)
;2D H-1/X correlation via TROSY
; using sensitivity improvement
;phase sensitive using Echo/Antiecho gradient selection
;using f3 - channel
;(use parameterset TROSYETF3GPSI)
;
;M. Czisch & R. Boelens, J. Magn. Reson. 134, 158-160 (1998)
;K. Pervushin, G. Wider & K. Wuethrich, J. Biomol. NMR 12,
; 345-348 (1998)
;A. Meissner, T. Schulte-Herbrueggen, J. Briand & O.W. Sorensen, Mol. Phys. 96,
; 1137-1142 (1998)
;J. Weigelt, J. Am. Chem. Soc. 120, 10778-10779 (1998)
;M. Rance, J.P. Loria & A.G. Palmer III, J. Magn. Reson. 136, 91-101 (1999)
;G. Zhu, X.M. Kong & K.H. Sze, J. Biomol. NMR 13, 77-81 (1999)

#include <Avance.incl>
#include <Grad.incl>
#include <Delay.incl>

"p2=p1*2"

"p22=p21*2"

"d0=6u"

"d11=30m"

;"d26=1s/(cnst4*4)"
"d26=1.75m"

"DELTA=d0*2+p21*4/3.1416+10u"
"DELTA1=d26-p16-d16-4u"
"DELTA2=d26-p1-p16-d16-4u"
"DELTA3=p19+d16+8u"

"i0=1"

1 ze
2 d11
3 d1 p11:f1
50u UNBLKGRAD
(p1 ph1)
4u
p16:gp1
d16
DELTA1
(center (p2 ph2) (p22 ph1):f3 )
4u
DELTA1
p16:gp1
d16
(p1 ph3)

p16:gp6

if "i0 %2 == 1"
{
(p21 ph4):f3
}
else
{
(p21 ph5):f3
}
```

```

d0 gron0
d0 gron0*-1
10u groff

p19:gp2*EA
d16
(p22 ph1):f3

DELTA

p19:gp2*-1*EA
d16

(p1 ph6)
4u
p16:gp3
d16
DELTA2 p1:f1
(center (p2 ph1) (p22 ph1):f3 )
4u
DELTA1
p16:gp3
d16
(center (p1 ph1) (p21 ph2):f3 )

4u
p16:gp4
d16
DELTA1
(center (p2 ph1) (p22 ph1):f3 )
DELTA1
p16:gp4
d16
4u
(p21 ph7):f3

DELTA3
(p2 ph1)
4u
p19:gp5
d16
4u BLKGRAD

go=2 ph31
d11 mc #0 to 2
F1EA(igrad EA & ip6*2 & ip7*2 & iu0, id0 & ip4*2 & ip5*2 & ip31*2)
exit

ph1=0
ph2=1
ph3=3
ph4=1 3 2 0
ph5=3 1 2 0
ph6=1
ph7=0
ph31=0 2 3 1

;p11 : f1 channel - power level for pulse (default)
;p13 : f3 channel - power level for pulse (default)
;p1 : f1 channel - 90 degree high power pulse
;p2 : f1 channel - 180 degree high power pulse
;p16: homospoil/gradient pulse [1 msec]
;p19: gradient pulse 2 [500 usec]
;p21: f3 channel - 90 degree high power pulse
;p22: f3 channel - 180 degree high power pulse
;d0 : incremented delay (2D) [6 usec]
;d1 : relaxation delay; 1-5 * T1
;d11: delay for disk I/O [30 msec]
;d16: delay for homospoil/gradient recovery
;d26 : 1/(4J)YH
;cnst4: = J(YH)
;in0: 1/(2 * SW(X)) = DW(X)
;nd0: 2

```



```

##$DPNAME7= <>
##$DPOAL= (0..7)
0.5 0.5 0.5 0.5 0.5 0.5 0.5 0.5
##$DPOFFS= (0..7)
0 0 0 0 0 0 0 0
##$DQDMODE= 0
##$DR= 17
##$DS= 16
##$DSLST= <SSSSSSSSSSSSSS>
##$DSPFIRM= 0
##$DSPFVS= 12
##$DTYPA= 0
##$EXP= <>
##$F1LIST= <1111111111111111>
##$F2LIST= <2222222222222222>
##$F3LIST= <3333333333333333>
##$FCUCHAN= (0..9)
0 1 2 3 0 0 0 0 0 0
##$FL1= 90
##$FL2= 90
##$FL3= 90
##$FL4= 90
##$FOV= 20
##$FQ1LIST= <freqlist>
##$FQ2LIST= <freqlist>
##$FQ3LIST= <freqlist>
##$FQ4LIST= <freqlist>
##$FQ5LIST= <freqlist>
##$FQ6LIST= <freqlist>
##$FQ7LIST= <freqlist>
##$FQ8LIST= <freqlist>
##$FS= (0..7)
83 83 83 83 83 83 83 83
##$FTLPGN= 0
##$FW= 125000
##$FnMODE= 0
##$GP031= 0
##$GPNAM0= <sine.100>
##$GPNAM1= <SINE.100>
##$GPNAM10= <sine.100>
##$GPNAM11= <sine.100>
##$GPNAM12= <sine.100>
##$GPNAM13= <sine.100>
##$GPNAM14= <sine.100>
##$GPNAM15= <sine.100>
##$GPNAM16= <sine.100>
##$GPNAM17= <sine.100>
##$GPNAM18= <sine.100>
##$GPNAM19= <sine.100>
##$GPNAM2= <SINE.50>
##$GPNAM20= <sine.100>
##$GPNAM21= <sine.100>
##$GPNAM22= <sine.100>
##$GPNAM23= <sine.100>
##$GPNAM24= <sine.100>
##$GPNAM25= <sine.100>
##$GPNAM26= <sine.100>
##$GPNAM27= <sine.100>
##$GPNAM28= <sine.100>
##$GPNAM29= <sine.100>
##$GPNAM3= <SINE.100>
##$GPNAM30= <sine.100>
##$GPNAM31= <sine.100>
##$GPNAM4= <SINE.100>
##$GPNAM5= <SINE.50>
##$GPNAM6= <SINE.100>
##$GPNAM7= <sine.100>
##$GPNAM8= <sine.100>
##$GPNAM9= <sine.100>
##$GPX= (0..31)
0 0 0 0 0 0 0 0 0 0 0 0 0 0 0 0 0 0 0 0 0 0 0 0 0 0 0 0 0 0 0 0
0
##$GPY= (0..31)
0 0 0 0 0 0 0 0 0 0 0 0 0 0 0 0 0 0 0 0 0 0 0 0 0 0 0 0 0 0 0 0
0

```

```

##$GPZ= (0.31)
3 30 80 45 50 16.2 15 0 0 0 0 0 0 0 0 0 0 0 0 0 0 0 0 0 0 0 0 0 0 0 0
0 0 0 0 0 0
##$GRDPROG= <grad_out>
##$HDDUTY= 20
##$HDRATE= 20
##$HGAIN= (0..3)
0 0 0 0
##$HL1= 256
##$HL2= 35
##$HL3= 16
##$HL4= 17
##$HOLDER= 0
##$HPMOD= (0..7)
0 0 0 0 0 0 0 0
##$HPPRGN= 0
##$IN= (0..31)
0.0001813625 0.001 0.001 0.001 0.001 0.001 0.001 0.001 0.001 0.001
0.001 0.001 0.001 0.001 0.001 0.001 0.001 0.001 0.001 0.001 0.001
0.001 0.001 0.001 0.001 0.001 0.001 0.001 0.001 0.001 0.001 0.001
##$INP= (0..31)
0 0 0 0 0 0 0 0 0 0 0 0 0 0 0 0 0 0 0 0 0 0 0 0 0 0 0 0 0 0 0 0 0 0
0
##$INSTRUM= <spect>
##$L= (0..31)
1 1 1 1 1 1 1 1 1 1 1 1 1 1 1 1 1 1 1 1 1 1 1 1 1 1 1 1 1 1 1 1 1 1 1 1
1
##$LFILTER= 200
##$LGAIN= -32
##$LOCKED= no
##$LOCKFLD= 2815
##$LOCKGN= 131.100006103516
##$LOCKPOW= -20
##$LOCKPPM= 4.69999980926514
##$LOCNUC= <2H>
##$LOCPHAS= 287.9
##$LOCSHFT= no
##$LTIME= 0.200000002980232
##$MASR= 0
##$MASRLST= <masrlist>
##$NBL= 1
##$NCR= -1
##$NS= 24
##$NUC1= <1H>
##$NUC2= <13C>
##$NUC3= <15N>
##$NUC4= <off>
##$NUC5= <off>
##$NUC6= <off>
##$NUC7= <off>
##$NUC8= <off>
##$NUCLEI= 0
##$NUCLEUS= <off>
##$O1= 3764.70575
##$O2= 10663.4875340035
##$O3= 9628.07128129839
##$O4= 0
##$O5= 0
##$O6= -19999.9999999818
##$O7= -19999.9999999818
##$O8= -19999.9999999818
##$OBSCHAN= (0..9)
0 0 0 0 0 0 0 0 0 0
##$OVERFLW= 0
##$P= (0..31)
11 13.3 26.6 0.1 0 0 0 0 0 0 0 0 0 0 0 0 0 0 0 0 0 0 0 0 0 0 0 0 0 0 0 0
68 0 0 0 0 0 0 11 0 0
##$PAPS= 2
##$PARMODE= 1
##$PCPD= (0..9)
100 100 100 100 100 100 100 100 100 100
##$PHCOR= (0..31)
0 0 0 0 0 0 0 0 0 0 0 0 0 0 0 0 0 0 0 0 0 0 0 0 0 0 0 0 0 0 0 0 0 0
0

```



```
##$ZGOPTNS= <-DLABEL_CN>
##$ZL1= 120
##$ZL2= 120
```

```
##$ZL3= 120
##$ZL4= 120
##END=
```

D.2.1 HetNOE pulse-program

```
;trnoef3gpsi
;avance-version (02/07/15)
;2D H-1/X correlation via TROSY and inept transfer
; using sensitivity improvement
;for measuring H1-N15 NOEs
;phase sensitive using Echo/Antiecho-TPPI gradient selection
;using f3 - channel
;recording NOE and NONOE interleaved
;(use parameterset TRNOEF3GPSI)
;
;G. Zhu, Y. Xia, L.K. Nicholson & K.H. Sze,
; J. Magn. Reson. 143, 423-426 (2000)

prosol relations=<triple>

#include <Avance.incl>
#include <Grad.incl>
#include <Delay.incl>

"p2=p1*2"
"p22=p21*2"
"d0=3u"
"d11=70m"
"d12=50u"
"d26=1s/(cnst4*4)"

"p0=p1*4/3"

"d31=aq"

"DELTA1=d26-p1-p11-p19-d16-4u"
"DELTA3=d26-p11-p19-d16-12u"
"DELTA4=d26-p11-p19-d16-p21-12u"

;# ifdef LABEL_CN
;"DELTA=d0*2+p8-p21*4/3.1416"
;"DELTA2=d26-p11-p19-d16-8u"
;# else
"DELTA2=d26+d0*2-p11-p19-d16-8u"
;# endif /*LABEL_CN*/

"l1=1"
"l0=1"
"l4=d1/(p0+5m)"

1 ze
2 d11
  d12
3 d12*4
4 d12*4
5 d12
6 d12 p116:f3
  d31 cpd3:f3
  4u do:f3

if "l1==2" goto 7

d1

4u p10:f1 ;flip back like in the hsqc version of hetnoe
(p11:sp1 ph2):f1
4u
4u p11:f1

goto 8
7 (p0 ph1)
```

```

5m
lo to 7 times l4
4u
; goto 8
;10 d1
8 50u
100u UNBLKGRAD

p16:gp1 ;instead of gradient flip back pulse
d16

(p1 ph1)
4u
p16:gp2
d16 pl3:f3

if "l0 %2 == 1"
{
(p21 ph4):f3
}
else
{
(p21 ph5):f3
}

;# ifdef LABEL_CN
; DELTA
; (p22 ph1):f3
; d0
; (p8:sp13 ph1):f2
; d0
;# else
d0
d0
;# endif /*LABEL_CN*/

(p1 ph6)
4u pl0:f1
(p11:sp1 ph6):f1
p19:gp3
d16
DELTA1 pl1:f1
(center (p2 ph1) (p22 ph1):f3 )
DELTA2
p19:gp3
d16 pl0:f1
(p11:sp1 ph9):f1
4u
4u pl1:f1

(center (p1 ph1) (p21 ph2):f3 )

4u
p19:gp4
d16
DELTA3 pl0:f1
(p11:sp1 ph3:r):f1
4u
4u pl1:f1
(center (p2 ph1) (p22 ph1):f3 )
4u pl0:f1
(p11:sp1 ph3:r):f1
DELTA4
p19:gp4
d16 pl1:f1
4u
4u BLKGRAD
(p21 ph7):f3

go=2 ph31
d11 wr #0 if #0 zd

;d11 mc #0 to 2
;F1(iu0, 2)
;F1EA(ip6*2 & ip7*2, id0 & ip4*2 & ip5*2 & ip31*2)

```



```

d12 iu1
lo to 3 times 2
d12 ru1
d12 iu0
d12 ip6*2
d12 ip7*2
lo to 4 times 2
d12 id0
d12 ip4*2
d12 ip5*2
d12 ip31*2
lo to 5 times l3
exit

ph1=0
ph2=1
ph3=2
ph9=0
;# ifdef LABEL_CN
;ph4=3 1 2 0
;ph5=1 3 2 0
;# else
ph4=1 3 2 0
ph5=3 1 2 0
;# endif /*LABEL_CN*/
ph6=1
ph8=1
ph7=0
ph31=0 2 3 1

;p10 : 120dB
;p11 : f1 channel - power level for pulse (default)
;p13 : f3 channel - power level for pulse (default)
;p116: f3 channel - power level for CPD/BB decoupling
;sp1 : f1 channel - shaped pulse 90 degree
;sp13: f2 channel - shaped pulse 180 degree (adiabatic)
;p0 : f1 channel - 120 degree high power pulse
;p1 : f1 channel - 90 degree high power pulse
;p2 : f1 channel - 180 degree high power pulse
;p8 : f2 channel - 180 degree shaped pulse for inversion (adiabatic)
;p11 : f1 channel - 90 degree shaped pulse
;p16: homospoil/gradient pulse [1 msec]
;p19: gradient pulse 2 [500 usec]
;p21: f3 channel - 90 degree high power pulse
;p22: f3 channel - 180 degree high power pulse
;d0 : incremented delay (2D) [3 usec]
;d1 : relaxation delay; 1-5 * T1
;d11: delay for disk I/O [30 msec]
;d12: delay for power switching [20 usec]
;d16: delay for homospoil/gradient recovery
;d26: 1/(4J(YH))
;d31: = aq
;cnst4: = J(YH)
;l0: flag to switch between NOE and NONOE
;in0: 1/(2 * SW(X)) = DW(X)
;nd0: 2
;NS: 4 * n
;DS: >= 32
;td1: total number of experiments
; = number of experiments for each 2D * 2
;FnMODE: echo-antiecho
;cpd3: decoupling according to sequence defined by cpdprg3
;pcpd3: f3 channel - 90 degree pulse for decoupling sequence

;use gradient ratio: gp 1 : gp 2 : gp 3 : gp 4
; 11 : 7 : 10 : 25

;for z-only gradients:
;gpz1: 11%
;gpz2: 7%
;gpz3: 10%
;gpz4: 25%

```



```

##$F2LIST= <2222222222222222>
##$F3LIST= <3333333333333333>
##$FCUCHAN= (0..9)
0 2 1 3 0 0 0 0 0 0
##$FL1= 90
##$FL2= 90
##$FL3= 90
##$FL4= 90
##$FOV= 20
##$FQ1LIST= <freqlist>
##$FQ2LIST= <freqlist>
##$FQ3LIST= <freqlist>
##$FQ4LIST= <caco.vivi>
##$FQ5LIST= <freqlist>
##$FQ6LIST= <freqlist>
##$FQ7LIST= <freqlist>
##$FQ8LIST= <freqlist>
##$FS= (0..7)
83 83 83 83 83 83 83 83
##$FTLPGN= 0
##$FW= 125000
##$FnMODE= 0
##$GP031= 0
##$GPNAM0= <sine.100>
##$GPNAM1= <SINE.100>
##$GPNAM10= <sine.100>
##$GPNAM11= <sine.100>
##$GPNAM12= <sine.100>
##$GPNAM13= <sine.100>
##$GPNAM14= <sine.100>
##$GPNAM15= <sine.100>
##$GPNAM16= <sine.100>
##$GPNAM17= <sine.100>
##$GPNAM18= <sine.100>
##$GPNAM19= <sine.100>
##$GPNAM2= <SINE.100>
##$GPNAM20= <sine.100>
##$GPNAM21= <sine.100>
##$GPNAM22= <sine.100>
##$GPNAM23= <sine.100>
##$GPNAM24= <sine.100>
##$GPNAM25= <sine.100>
##$GPNAM26= <sine.100>
##$GPNAM27= <sine.100>
##$GPNAM28= <sine.100>
##$GPNAM29= <sine.100>
##$GPNAM3= <SINE.50>
##$GPNAM30= <sine.100>
##$GPNAM31= <sine.100>
##$GPNAM4= <SINE.50>
##$GPNAM5= <SINE.50>
##$GPNAM6= <sine.100>
##$GPNAM7= <sine.100>
##$GPNAM8= <sine.100>
##$GPNAM9= <sine.100>
##$GPX= (0..31)
0 0 0 0 0 0 0 0 0 0 0 0 0 0 0 0 0 0 0 0 0 0 0 0 0 0 0 0 0 0 0 0
0
##$GPY= (0..31)
0 0 0 0 0 0 0 0 0 0 0 0 0 0 0 0 0 0 0 0 0 0 0 0 0 0 0 0 0 0 0 0
0
##$GPZ= (0..31)
3 5 0 7 10 25 16.2 0 0 0 0 0 0 0 0 0 0 0 0 0 0 0 0 0 0 0 0 0 0 0 0
0 0 0 0
##$GRDPROG= <grad_out>
##$HDDUTY= 20
##$HDRATE= 20
##$HGAIN= (0..3)
0 0 0 0
##$HL1= 200
##$HL2= 35
##$HL3= 16
##$HL4= 17
##$HOLDER= 0
##$SHPMOD= (0..7)
0 1 1 0 0 0 0 0
##$SHPPRGN= 0
##$SIN= (0..31)
0.0001523 0.001 0.001 0.001 0.001 0.001 0.001 0.001 0.001
0.001 0.001 0.001 0.001 0.001 0.001 0.001 0.001 0.001
0.001 0.001 0.001 0.001 0.001 0.001 0.001 0.001 0.001
0.001 0.001 0.001 0.001 0.001 0.001
##$SNP= (0..31)
0 0 0 0 0 0 0 0 0 0 0 0 0 0 0 0 0 0 0 0 0 0 0 0 0 0 0 0 0 0 0 0
0
##$SINSTRUM= <spect>
##$SL= (0..31)
1 1 1 101 996 1 1 1 1 1 1 1 1 1 1 1 1 1 1 1 1 1 1 1 1 1 1 1 1 1 1 1
1 1 1
##$SLFILTER= 100
##$SLGAIN= -15
##$SLOCKED= yes
##$SLOCKFLD= 7620
##$SLOCKGN= 135.5
##$SLOCKPOW= -11.1000003814697
##$SLOCKPPM= 4.69999980926514
##$SLOCNUC= <2H>
##$SLOCPHAS= 274.8
##$SLOCSHFT= no
##$SLTIME= 0.200000002980232
##$SMASR= 0
##$SMASRLST= <masrlist>
##$SNBL= 1
##$SNC= -2
##$SNS= 120
##$SNUC1= <1H>
##$SNUC2= <13C>
##$SNUC3= <15N>
##$SNUC4= <off>
##$SNUC5= <off>
##$SNUC6= <off>
##$SNUC7= <off>
##$SNUC8= <off>
##$SNUCLEI= 0
##$SNUCLEUS= <off>
##$SO1= 4245.1074
##$SO2= 11996.1735940137
##$SO3= 10808.5517295109
##$SO4= 0
##$SO5= 0
##$SO6= 0
##$SO7= -100010000
##$SO8= -100010000
##$SOBSCHAN= (0..9)
0 0 0 0 0 0 0 0 0 0
##$SOVERFLW= 0
##$SP= (0..31)
15.46667 11.6 23.2 0.1 15.6 0 0 0 0 0 0 1000 0 0 0 0 1000
0 0 500 26 37 74 0 0 0 0 0 0 11 0 0
##$SPAPS= 2
##$SPARMODE= 1
##$SPCPD= (0..9)
100 100 100 160 100 100 100 100 100 100
##$SPHCOR= (0..31)
0 0 0 0 0 0 0 0 0 0 0 0 0 0 0 0 0 0 0 0 0 0 0 0 0 0 0 0 0 0 0 0
0
##$SPHP= 1
##$SPH_ref= 0
##$SPL= (0..31)
120 -1 120 -3 -0.5 120 120 120 120 56 120 120 120 120
120 120 9.6 120 -3 120 120 120 120 120 120 120 120 120
120 120 120 120
##$SPOWMOD= 0
##$SPR= 1
##$SPRECHAN= (0..15)
-1 2 -1 -1 0 1 -1 -1 -1 -1 4 -1 -1 -1 -1 -1
##$SPRGAIN= 0
##$SPROBHD= <5 mm CPTCI 1H-13C/15N Z-GRD
Z44910/0009>
##$SPROSOL= no

```


D.3.1 T1rho pulse-program

```
#include "bits.mz"
#include <Avance.incl>
#include <Grad.incl>

;1 hn, 15n edited n15 t2 measurement according to linda
;history
;written by sg 2/23/93
;put in water flip_back 6/1/93
;change to watermh 7/29/93
;change to t2n15.sg 10/18/93

#define ONE_D
#define TWO_D
#define CARB

;p1      proton 90 at p11, 9u
;p2      1ms proton 90 at p12 ;sklenar

;"p9=2m"
;p17=p1"

;p7      high power n15 90 on N p17:N
;p31     low power n15 90 (160ms) on N at p131:N
;p8      SL 15N for 8ms at p18:N

;Carbon pulses
;C1=Ca   C2=C'

;"p5=23.7u"      ;selective 180
;p5=15.6u"
;d28=p5"

;nitrogen evolution:
;d9=4u"
;d10=2.7m"
;d0=d9+d10+p7*0.637"

;in0=d0/(13+1)
;in9=in10-in0
;in10=1/(2sw)

"d4=2.25m"              ;hsq h to n15
"d7=p7*0.637"

"d11=50m"
"d12=10m"
"d17=p1*2.0"
"d26=p7-p1"
"d25=p7-p1*2.11-2u"

;Gradient pulses
;"p11=4.25m"           ;gp1 = +50%
;"p12=1.75m"           ;gp1 = +50%
;"p13=0.70m"           ;gp1 = +50%
;"p14=2.35m"           ;gp0 = -50%
;"p15=0.40m"           ;gp0 = -50%

#define ON
#undef OFF

1      ze
2      d11 BLKGRAD
        d12 do:N
3      d12
21     d12*3.0
4      d12*6.0
25     d12*4.0
26     10u do:C1
        10u
```

```

10u p17:N
#ifdef ON
d1
1m UNBLKGRAD
10u fq1:H
10u p11:f1
;***** start 90-degree on h-n *****
(p1 ph0)
2u
d4
(p7*2 ph6):N (d26 p1*2 ph4)
d4
2u
;***** hsqc to nitrogen *****
(p1 ph16)
2u
p11:gp2
2.5m
(p7 ph3):N
2u
p12:gp0
928u
(p7*2 ph0):N (d25 p1 ph4 2u p1*2.22 ph0 2u p1 ph4)
2u
p12:gp0
928u p18:N ; SL power 2.5KHz
d7
100u
;***** n15 relaxation delay *****
;70 (p18 ph8):N
; (p17*1.5 ph8):N (p1*1.5 ph4)
; (p18 ph8):N
; lo to 70 times 2
; (p9 ph8):N
;***** n15 evolution delay *****
d0 p15:C1
#endif CARB
2u
d28*2.0
4u
2u fq2:C1
d28*2.0 p17:N
#else
d17 p17:N
#endif
(p7*2 ph20):N
d9
#ifdef CARB
2u p15:C1
(p5*2 ph10):C1 (p1*2 ph0)
4u
2u fq2:C1
(p5*2 ph10):C1
#else
(p1*2 ph0)
#endif
d10
;***** end n15 evolution delay *****
(p7 ph7):N
2u
p14:gp1
10u fq1:H
2m
(p1 ph0)
2u
p15:gp1
950u p12:f1
(p2 ph14)
2u
5u p11:f1
(p1*2 ph15)
2u
5u p12:f1
(p7*2 ph10):N (p2 ph14)
2u

```

```

        p15:gp1
        (2u ph0)
        950u pl31:N
#endif
#ifdef ONE_D
go=2 ph31 cpd2:N
1m do:N
1m BLKGRAD
d11 wr #0
#endif
#ifdef TWO_D
        go=2 ph31 cpd2:N
        1m BLKGRAD
        d11 do:N wr #0 if #0 zd
#endif
#ifdef TWO_D
d12 ivp
lo to 3 times 1
d12 ip7
lo to 21 times 2
d12*0.25 dd0
d12*0.25 id9
d12*0.25 id10
d12*0.25
d12 ip31
d12 ip31
lo to 4 times 13
d12*0.25 rd0
d12*0.25 rd9
d12*0.25 rd10
d12*0.25
d12 rf #0
d12 ip16
d12 ip16
d12 ip31
d12 ip31
lo to 25 times 2
d12*0.25 rd0
d12*0.25 rd9
d12*0.25 rd10
d12*0.25
d12 rf #0
d12 ip8
d12 ip8
lo to 26 times 16 ; loop of 2 is a total of 8 scans
#endif
d11 do:N
d11 do:C1
exit

ph0=0
ph1=0
ph3=0 0 2 2
ph4=1
ph6=1
ph7=0
ph8=2
ph10=0
ph14=(360) 180
ph15=0
ph16=1 3
ph20=0 0 0 0 1 1 1 1 2 2 2 2 3 3 3 3
ph31=0 2 2 0 2 0 2

```

D.3.2 T1rho parameters

```

##TITLE= Parameter file, XWIN-NMR
        Version 3.5
##JCAMPDX= 5.0
##DATATYPE= Parameter Values
##ORIGIN= Bruker Analytik GmbH

```

```

##OWNER= guest
$$ Mon Mar 5 10:45:45 2007 CET (UT+1h)
guest@nmr900
$$
/opt/xwinnmr/data/momo/nmr/hvdac1_mar0507/10/acqus

```



```

##$SPNAM3= <Crp60,0.5,20.1>
##$SPNAM30= <gauss>
##$SPNAM31= <gauss>
##$SPNAM4= <gauss>
##$SPNAM5= <gauss>
##$SPNAM6= <gauss>
##$SPNAM7= <gauss>
##$SPNAM8= <gauss>
##$SPNAM9= <gauss>
##$SPOAL= (0..31)
0.5 0.5 0.5 0.5 0.5 0.5 0.5 0.5 0.5 0.5 0.5 0.5 0.5 0.5 0.5
0.5 0.5 0.5 0.5 0.5 0.5 0.5 0.5 0.5 0.5 0.5 0.5 0.5 0.5
0.5 0.5
##$SPOFFS= (0..31)
0 0 0 0 0 0 0 0 0 0 0 0 0 0 0 0 0 0 0 0 0 0 0 0 0 0 0 0 0 0
0
##$SUBNAM0= <"">
##$SUBNAM1= <"">
##$SUBNAM2= <"">
##$SUBNAM3= <"">
##$SUBNAM4= <"">
##$SUBNAM5= <"">
##$SUBNAM6= <"">
##$SUBNAM7= <"">
##$SUBNAM8= <"">
##$SUBNAM9= <"">
##$SW= 12.9780458581692
##$SWIBOX= (0..15)
0 1 4 4 0 5 6 7 0 0 10 0 0 0 0
##$SW_h= 11682.2429906542
##$STD= 1024
##$STD0= 1
##$STE= 310
##$TE2= 300
##$TE3= 300
##$TEG= 300
##$TL= (0..7)
120 120 120 120 120 120 120 120
##$TP= (0..7)
150 150 150 150 150 150 150 150
##$TP07= 0
##$STPNAME0= <>

##$STPNAME1= <>
##$STPNAME2= <>
##$STPNAME3= <>
##$STPNAME4= <>
##$STPNAME5= <>
##$STPNAME6= <>
##$STPNAME7= <>
##$STPOAL= (0..7)
0.5 0.5 0.5 0.5 0.5 0.5 0.5 0.5
##$STPOFFS= (0..7)
0 0 0 0 0 0 0 0
##$STUNHIN= 0
##$STUNHOUT= 0
##$STUNXOUT= 0
##$USERA1= <user>
##$USERA2= <user>
##$USERA3= <user>
##$USERA4= <user>
##$USERA5= <user>
##$V9= 5
##$VALIST= <valist>
##$VCLIST= <CCCCCCCCCCCCCCC>
##$VD= 0
##$VDLIST= <DDDDDDDDDDDDDDDD>
##$VPLIST= <PPPPPPPPPPPPPPPP>
##$VTLIST= <TTTTTTTTTTTTTTTT>
##$WBST= 1024
##$WBSW= 6
##$XGAIN= (0..3)
0 0 0 0
##$XL= 0
##$YL= 0
##$YMAX_a= 87083
##$YMIN_a= -72388
##$ZGOPTS= <>
##$ZL1= 120
##$ZL2= 120
##$ZL3= 120
##$ZL4= 120
##$END=

```

D.4.1 NOESY-TROSY-HSQC pulse-program

```

;noesytrtf3gp3d
;avance-version (02/07/15)
;NOESY-TROSY
;3D sequence with
; homonuclear correlation via dipolar coupling
; dipolar coupling may be due to noe or chemical exchange
; H-1/X correlation via TROSY
; using sensitivity improvement
;phase sensitive (t1)
;phase sensitive using Echo/Antiecho-TPPI gradient selection (t2)
;using f3 - channel
;(use parameterset NOESYTRETF3GP3D)
;
;G. Zhu, X.M. Kong & K.H. Sze, J. Biomol. NMR 13, 77-81 (1999)
;M. Czisch & R. Boelens, J. Magn. Reson. 134, 158-160 (1998)
;K. Pervushin, G. Wider & K. Wuethrich, J. Biomol. NMR 12,
; 345-348 (1998)
;A. Meissner, T. Schulte-Herbrueggen, J. Briand & O.W. Sorensen, Mol. Phys. 96,
; 1137-1142 (1998)
;J. Weigelt, J. Am. Chem. Soc. 120, 10778-10779 (1998)
;M. Rance, J.P. Loria & A.G. Palmer III, J. Magn. Reson. 136, 91-101 (1999)

#include <Avance.incl>
#include <Grad.incl>
#include <Delay.incl>

"p2=p1*2"

```

```

"p22=p21*2"

"d0=6u"

"d10=6u"

"d11=30m"

"d26=1s/(cnst4*4)"

"DELTA1=d26-p16-d16-4u"
"DELTA2=d26-p1-p16-d16-4u"
"DELTA3=p19+d16+8u"

# ifdef LABEL_CN
"DELTA=d10*2+p4*4+8u+p21*4/3.1416+12u"
"DELTA4=d0*2+p4*4+p22+8u+4u"
# else
"DELTA=d10*2+p21*4/3.1416+12u"
"DELTA4=d0*2+p22+4u"
# endif /*LABEL_CN*/

"TAU=d8-p16-d16"

"l0=1"

aqseq 321

1 ze
2 d11
3 d1 p1:f1
50u UNBLKGRAD
(p1 ph3)
DELTA4
(p2 ph9)
d0 gron0
2u groff

# ifdef LABEL_CN
;(center (p14:sp3 ph1):f2 (p22 ph1):f3 )

(p22 ph1):f3
2u p14:f2
2u fq4:f2
(p4*2 ph1):f2
2u p14:f2
2u fq4:f2
(p4*2 ph1):f2

# else
(p22 ph1):f3
# endif /*LABEL_CN*/

d0 gron0*-1
2u groff

(p1 ph1)
TAU
p16:gp6
d16
(p1 ph1)
4u
p16:gp1
d16
DELTA1
(center (p2 ph2) (p22 ph1):f3 )
4u
DELTA1
p16:gp1
d16
(p1 ph4)

;p16:gp7

if "l0 %2 == 1"

```

```

    {
    (p21 ph5):f3
    }
else
    {
    (p21 ph6):f3
    }

d10 gron0
6u groff

# ifdef LABEL_CN
:(p14:sp3 ph1):f2

    2u p14:f2
    2u fq4:f2
    (p4*2 ph1):f2
    2u p14:f2
    2u fq4:f2
    (p4*2 ph1):f2

# else
# endif /*LABEL_CN*/

d10 gron0*-1
6u groff

p19:gp2*EA
d16
(p22 ph1):f3

DELTA

p19:gp2*-1*EA
d16

(p1 ph7)
4u
p16:gp3
d16
DELTA2 p1:f1
(center (p2 ph1) (p22 ph1):f3 )
4u
DELTA1
p16:gp3
d16
(center (p1 ph1) (p21 ph2):f3 )

4u
p16:gp4
d16
DELTA1
(center (p2 ph1) (p22 ph1):f3 )
DELTA1
p16:gp4
d16
4u
(p21 ph8):f3

DELTA3
(p2 ph1)
4u
p19:gp5
d16
4u BLKGRAD

go=2 ph31
d11 mc #0 to 2
    F1PH(rd10 & ip3 & ip9, id0)
    F2EA(igrad EA & ip7*2 & ip8*2 & iu0, id10 & ip5*2 & ip6*2 & ip31*2)
exit

ph1=0
ph2=1

```

```

ph3=0 0 0 0 2 2 2 2
ph4=3
ph5=1 3 2 0
ph6=3 1 2 0
ph7=1
ph8=0
ph9=1
ph31=0 2 3 1 2 0 1 3

;p11 : f1 channel - power level for pulse (default)
;p13 : f3 channel - power level for pulse (default)
;sp3 : f2 channel - shaped pulse 180 degree
;p1 : f1 channel - 90 degree high power pulse
;p2 : f1 channel - 180 degree high power pulse
;p14: f2 channel - 180 degree shaped pulse for inversion
;p16: homospoil/gradient pulse          [1 msec]
;p19: gradient pulse 2                  [500 usec]
;p21: f3 channel - 90 degree high power pulse
;p22: f3 channel - 180 degree high power pulse
;d0 : incremented delay (F1 in 3D)      [6 usec]
;d1 : relaxation delay; 1-5 * T1
;d8 : mixing time
;d10: incremented delay (F2 in 3D)      [6 usec]
;d11: delay for disk I/O                [30 msec]
;d16: delay for homospoil/gradient recovery
;d26 : 1/(4J)YH
;cnst4 = J(YH)
;in0: 1/(2 * SW(H)) = DW(H)
;nd0: 2
;in10: 1/(2 * SW(X)) = DW(X)
;nd10: 2
;NS: 8 * n
;DS: 16
;td1: number of experiments
;td2: number of experiments in F2
;FnMODE: States-TPPI (or TPPI) in F1
;FnMODE: echo-antiecho in F2

;use gradient ratio:  gp 0 : gp 1 : gp 2 : gp 3 : gp 4 : gp 5 : gp 6
;                    3 : 30 : 80 : 45 : 50 : 16.2 : 19

;for z-only gradients:
;gpz0: 3%
;gpz1: 30%
;gpz2: 80%
;gpz3: 45%
;gpz4: 50%
;gpz5: 16.2%
;gpz6: 19%

;use gradient files:
;gpnam1: SINE.100
;gpnam2: SINE.50
;gpnam3: SINE.100
;gpnam4: SINE.100
;gpnam5: SINE.50
;gpnam6: SINE.100

;preprocessor-flags-start
;LABEL_CN: for C-13 and N-15 labeled samples start experiment with
;          option -DLABEL_CN (eda: ZGOPTNS)
;preprocessor-flags-end

;$Id: noesytrtf3gp3d,v 1.8.2.2 2002/09/24 09:43:30 ber Exp $

```

D.4.2 NOESY-TROSY-HSQC parameters

```

##TITLE= Parameter file, XWIN-NMR
Version 3.5
##JCAMPDX= 5.0
##DATATYPE= Parameter Values
##ORIGIN= Bruker Analytik GmbH
##OWNER= guest

$$ Mon Mar 13 10:39:23 2006 MEZ (UT+1h)
spektrum@nmr800.nmr.mpibpc.mpg.de
$$ /u/data/momo/nmr/hvdac090306/7/acqus
##$AMP= (0..31)

```



```

##$SPNAM30= <gauss>
##$SPNAM31= <gauss>
##$SPNAM4= <gauss>
##$SPNAM5= <g3.256>
##$SPNAM6= <Gaus1.1000>
##$SPNAM7= <Crp60comp.4>
##$SPNAM8= <g4tr.256>
##$SPNAM9= <g3.256>
##$SPOAL= (0..31)
0.5 0.5 0.5 0.5 0.5 0.5 0.5 0.5 0.5 0.5 0.5 0.5 0.5 0.5
0.5 0.5 0.5
0.5 0.5 0.5 0.5 0.5 0.5 0.5 0.5 0.5 0.5 0.5 0.5 0.5
##$SPOFFS= (0..31)
0 0 0 0 0 32005.68 0 -32005.68 0 0 0 0 0 0 -20000 0 0 0
0 0 0 0 0 0
0 0 0 0 0 0
##$SUBNAM0= <"">
##$SUBNAM1= <"">
##$SUBNAM2= <"">
##$SUBNAM3= <"">
##$SUBNAM4= <"">
##$SUBNAM5= <"">
##$SUBNAM6= <"">
##$SUBNAM7= <"">
##$SUBNAM8= <"">
##$SUBNAM9= <"">
##$SW= 13.9447264564791
##$SWIBOX= (0..15)
0 1 2 0 0 5 6 0 0 0 0 0 0 0 0 0
##$SW_h= 11160.7142857143
##$STD= 1024
##$TD0= 1
##$TE= 310.0063
##$TE2= 300
##$TE3= 300
##$TEG= 300
##$TL= (0..7)
120 120 120 120 120 120 120 120
##$TP= (0..7)
150 150 150 150 150 150 150 150
##$TP07= 0
##$STPNAME0= <>
##$STPNAME1= <>
##$STPNAME2= <>
##$STPNAME3= <>
##$STPNAME4= <>
##$STPNAME5= <>
##$STPNAME6= <>
##$STPNAME7= <>
##$STPOAL= (0..7)
0.5 0.5 0.5 0.5 0.5 0.5 0.5 0.5
##$STPOFFS= (0..7)
0 0 0 0 0 0 0 0
##$STUNHIN= 0
##$STUNHOUT= 0
##$STUNXOUT= 0
##$USERA1= <user>
##$USERA2= <user>
##$USERA3= <user>
##$USERA4= <user>
##$USERA5= <user>
##$V9= 5
##$VALIST= <valist>
##$VCLIST= <CCCCCCCCCCCCCCCC>
##$VD= 0
##$VDLIST= <DDDDDDDDDDDDDDDD>
##$VPLIST= <PPPPPPPPPPPPPPPP>
##$VTLIST= <TTTTTTTTTTTTTTTT>
##$WBST= 1024
##$WBSW= 10
##$XGAIN= (0..3)
0 0 0 0
##$XL= 0
##$YL= 0
##$YMAX_a= 20727
##$YMIN_a= -21459
##$ZGOPTNS= <-DLABEL_CN>
##$ZL1= 120
##$ZL2= 120
##$ZL3= 120
##$ZL4= 120
##$END=

```

D.5.1 HMQC-NOESY pulse-program^[74]

```

#include "bits.nt"

;Written by Jinfu Ying, 5/11/06
;H-N Parallel evolution MQ
;NOESY transfer to the neighboring HN's
;1H detection

;modified from pareMQ_NOE_gsMQ2B.jfy

;p1 = 90 deg (10us) 1H pulse @p1
;p7 = 90 deg (50us) 15N pulse @p7
;p4 = selective 180 deg (23.7*2us) 13CA
; pulse @p14 (f4) and @p16 (f5)

#define CARBON_LABEL
#define PROTON
#define NITROGEN

"d11=50m"
"d12=1m"

"d25=p7*2.22-p1*2.11"

"d2=2.1m"
"d0=70u" ;needed to place 180N pulse, compensated in d3
"d10=2u"
"d28=3u"
"d29=d2*2-d28-p7*4.44-4u"

```



```

;--- p1*4.22+4u+d0==d6+p7*2+d9 for identical N/H durations
;--- d10*2+d6==d9 for zero 15N evolution to get 0/0 phase correction
"d9=p1*2.11+2u+d0*0.5+d10-p7" ;initial d0 set to 70u to keep d6 & d9 >0
"d6=p1*2.11+2u+d0*0.5-d10-p7"

"d3=d2*2-d0-p7*4.44-d28*2-4u" ;compensate the cs evolution for 1H 0/0 phase correction

"d7=d8-p27-310u" ;d8=noe mixing time
;"d7=d8-p27-p2-318u" ;d8=noe mixing time

"in28=in0"
"in29=in28"

"in9=in10"
"in6=in9"

1 ze
1m RESET
2 d11 do:f3 do:f2
d12 LOCK_ON
3 d12 DEUT_OFF
4 d12 LOCK_ON
5 d12 do:f2 do:f3
6 d12 do:f3
d12 do:f2
7 d12 do:f2 do:f3
8 d12 do:f2 do:f3
1m DEUT_OFF
d1 LOCK_ON
1m LOCK_OFF
10u p11:f1
10u p17:f3

(p7 ph0):f3 ;kill Boltzman
50m

;goto 999

;WURST 13C dec on if 13C labeled
#ifdef CARBON_LABEL
10u p130:f2
10u cpds4:f2
#endif
;---start 90-degree on hn -----
(p1 ph5):f1
d28
(d25 p1 ph0 2u p1*2.22 ph1 2u p1 ph0 d25):f1 (p7 ph0 2u p7*2.44 ph1 2u p7 ph0):f3
d29
(p7 ph6):f3

;---MQ and Parallel Evolution start
(d10 p1 ph0 2u p1*2.22 ph1 2u p1 ph0 d10 d0):f1 (d10 d10 d6 p7*2 d9):f3
(p7 ph0):f3

;---refocusing 1J(N-H)
d3
(p1 ph2):f1

;-----HN-HN NOE mixing-----
10u do:f2 ;turn off the WURST 13C (ie CA and CO) decoupling
d7
p27:gp0
300u p111:f1
;-----HN readout-----
(p11:sp11 ph0):f1 ;eburp2
5u
p20:gp3
100u p12:f1
(p12:sp12 ph0):f1 ;reburp
5u
p20:gp3
100u p131:f3
go=2 ph31 cpd2:f3
d12*0.25 do:f3 do:f2

```

```

d12*0.25 LOCK_ON
d11 wr #0 if #0 zd

#ifdef NITROGEN
d12*0.5 ip6
lo to 3 times 2
d12*0.5 ip31*2
if "d9 > in9"
{
d12*0.25 dd9
d12*0.25 id6
}
else
{
d12*0.5 id10
}

lo to 4 times l3
d12*0.5 rd10 ;must appear before d6 & d9 are re-evaluated
"d9=p1*2.11+2u+d0*0.5+d10-p7"
"d6=p1*2.11+2u+d0*0.5-d10-p7"
#endif

#ifdef PROTON
d12*0.5 ip5
lo to 5 times 2
d12*0.5 ip31*2
if "d29 > in29"
{
d12*0.25 dd29
d12*0.25 id28
}
else
{
d12*0.25 id0
d12*0.25 id0 ;id0 twice to make nd0=2
}
"d9=p1*2.11+2u+d0*0.5+d10-p7" ;d6 & d9 must appear after id0
"d6=p1*2.11+2u+d0*0.5-d10-p7"

lo to 6 times l4
;d12*0.25 rd28
;d12*0.25 rd29
;d12*0.5 rd0 ;must appear before d6 & d9 are re-calculated
;"d9=p1*2.11+2u+d0*0.5+d10-p7"
;"d6=p1*2.11+2u+d0*0.5-d10-p7"
#endif

1m do:f2
1m do:f3
1m RESET
1m
exit

ph0=0
ph1=1
ph2=2
ph5=0
ph6=0 2
ph31=0 2

```

D.5.2 HMQC-NOESY parameters

```

##TITLE= Parameter file, XWIN-NMR
Version 3.5
##JCAMPDX= 5.0
##DATATYPE= Parameter Values
##ORIGIN= Bruker Analytik GmbH
##OWNER= guest
$$ Fri Oct 27 04:07:32 2006 MESZ (UT+2h)
spektrum@nmr800.nmr.mpibpc.mpg.de
$$ /u/data/momo/nmr/hvdac231006/4/acqus
##$AMP= (0..31)
100 100 100 100 100 100 100 100 100 100 100 100 100 100 100
100 100 100 100 100 100 100 100 100 100 100 100 100 100
100 100 100 100 100 100
##$AQSEQ= 1
##$AQ_mod= 3
##$AUNM= <au_zgonly>
##$AUTOPOS= <>
##$BF1= 800.15
##$BF2= 201.197878
##$BF3= 81.078495

```

```

##$BF4= 800.15
##$BF5= 800.15
##$BF6= 800.15
##$BF7= 800.15
##$BF8= 800.15
##$BYTORDA= 1
##$CFDGTYP= 2
##$CFRGTYTYP= 5
##$SCHEMSTR= <none>
##$CNST= (0.31)
1 1 140 1 90 1 1 1 1 1 1 1 1 1 1 1 1 1 1 4.755 8.5 3.5 176 54
39 120 47.63 70 15 6.5 1 1 1
##$CPDPRG= <>
##$CPDPRG1= <dipsi2>
##$CPDPRG2= <garp>
##$CPDPRG3= <garp>
##$CPDPRG4= <mlev>
##$CPDPRG5= <mlev>
##$CPDPRG6= <mlev>
##$CPDPRG7= <mlev>
##$CPDPRG8= <mlev>
##$CPDPRGB= <>
##$CPDPRGT= <>
##$D= (0..31)
7e-05 1 0.0021 0.00396904 0.0018 0 2.26275e-05 0.11869
0.12 2.66275e-05 2e-06 0.05 0.001 4e-06 0 0 0.0005 0 0 0
1e-05 1e-05 0 0 0.00275 5.38525e-05
0.00275 0 3e-06 0.00404204 0 0
##$DATE= 1161607586
##$DBL= (0..7)
120 120 120 120 120 120 120 120
##$DBP= (0..7)
150 150 150 150 150 150 150 150
##$DBP07= 0
##$DBPNAM0= <>
##$DBPNAM1= <>
##$DBPNAM2= <>
##$DBPNAM3= <>
##$DBPNAM4= <>
##$DBPNAM5= <>
##$DBPNAM6= <>
##$DBPNAM7= <>
##$DBPOAL= (0..7)
0.5 0.5 0.5 0.5 0.5 0.5 0.5 0.5
##$DBPOFFS= (0..7)
0 0 0 0 0 0 0 0
##$DE= 6
##$DECBNUC= <off>
##$DECIM= 16
##$DECNUC= <off>
##$DECSTAT= 7
##$DIGMOD= 1
##$DIGTYP= 8
##$DL= (0..7)
120 120 120 120 120 120 120 120
##$DP= (0..7)
150 150 150 150 150 150 150 150
##$DP07= 0
##$DPNAME0= <>
##$DPNAME1= <>
##$DPNAME2= <>
##$DPNAME3= <>
##$DPNAME4= <>
##$DPNAME5= <>
##$DPNAME6= <>
##$DPNAME7= <>
##$DPOAL= (0..7)
0.5 0.5 0.5 0.5 0.5 0.5 0.5 0.5
##$DPOFFS= (0..7)
0 0 0 0 0 0 0 0
##$DQDMODE= 0
##$DR= 18
##$DS= 8
##$DSLST= <SSSSSSSSSSSSSS>
##$DSPFIRM= 0

```

```

##$DSPFVS= 12
##$DTYPA= 0
##$EXP= <PS done>
##$F1LIST= <1111111111111111>
##$F2LIST= <2222222222222222>
##$F3LIST= <3333333333333333>
##$FCUCHAN= (0..9)
0 1 2 3 0 0 0 0 0 0
##$FL1= 90
##$FL2= 90
##$FL3= 90
##$FL4= 90
##$FOV= 20
##$FQ1LIST= <halih2o>
##$FQ2LIST= <cbcaconh>
##$FQ3LIST= <freqlist>
##$FQ4LIST= <caco.vivi>
##$FQ5LIST= <freqlist>
##$FQ6LIST= <freqlist>
##$FQ7LIST= <freqlist>
##$FQ8LIST= <freqlist>
##$SFS= (0..7)
83 83 83 83 83 83 83 83
##$FTLPGN= 0
##$FW= 125000
##$FnMODE= 0
##$GPO31= 0
##$GPNAM0= <SINE.100>
##$GPNAM1= <SINE.100>
##$GPNAM10= <SINE.100>
##$GPNAM11= <SINE.100>
##$GPNAM12= <SINE.100>
##$GPNAM13= <SINE.100>
##$GPNAM14= <SINE.100>
##$GPNAM15= <SINE.100>
##$GPNAM16= <SINE.100>
##$GPNAM17= <SINE.100>
##$GPNAM18= <SINE.100>
##$GPNAM19= <SINE.100>
##$GPNAM2= <SINE.50>
##$GPNAM20= <SINE.100>
##$GPNAM21= <SINE.100>
##$GPNAM22= <SINE.100>
##$GPNAM23= <SINE.100>
##$GPNAM24= <SINE.100>
##$GPNAM25= <SINE.100>
##$GPNAM26= <SINE.100>
##$GPNAM27= <SINE.100>
##$GPNAM28= <SINE.100>
##$GPNAM29= <SINE.100>
##$GPNAM3= <SINE.100>
##$GPNAM30= <SINE.100>
##$GPNAM31= <SINE.100>
##$GPNAM4= <SINE.100>
##$GPNAM5= <SINE.50>
##$GPNAM6= <SINE.100>
##$GPNAM7= <SINE.100>
##$GPNAM8= <SINE.100>
##$GPNAM9= <SINE.100>
##$GPX= (0..31)
0 0 0 0 0 0 0 0 0 0 0 0 0 0 0 0 0 0 0 0 0 0 0 0 0 0 0 0 0 0 0 0
0
##$GPY= (0..31)
0 0 0 0 0 0 0 0 0 0 0 0 0 0 0 0 0 0 0 0 0 0 0 0 0 0 0 0 0 0 0 0
0
##$GPZ= (0..31)
60 30 80 55 50 16.2 19 15 0 0 0 0 0 0 0 0 0 0 0 0 0 0 0 0 0 0 0 0 0 0
0 0 0 0 0
0 0
##$GRDPROG= <grad_out>
##$HDDUTY= 20
##$HDRATE= 20
##$HGAIN= (0..3)
0 0 0 0
##$SHL1= 200

```



```

0.5 0.5 0.5 0.5 0.5 0.5 0.5 0.5 0.5 0.5 0.5 0.5 0.5 0.5 0.5 0.5 0.5 0.5 0.5 0.5
0.5 0.5 0.5 0.5 0.5 0.5 0.5 0.5 0.5 0.5 0.5 0.5 0.5 0.5 0.5 0.5 0.5 0.5
0.5 0.5
##$SPOFFS= (0..31)
0 0 0 0 0 32005.68 0 -32005.68 0 0 0 2360 2360 0 0 -
20000 0 0 0 0 0 0 0 0 0 0 0 0 0 0 0 0 0
##$SUBNAM0= <"">
##$SUBNAM1= <"">
##$SUBNAM2= <"">
##$SUBNAM3= <"">
##$SUBNAM4= <"">
##$SUBNAM5= <"">
##$SUBNAM6= <"">
##$SUBNAM7= <"">
##$SUBNAM8= <"">
##$SUBNAM9= <"">
##$SW= 13.9482119566605
##$SWIBOX= (0..15)
0 1 2 0 0 5 6 0 0 0 0 0 0 0 0 0
##$SW_h= 11160.7142857143
##$TD= 1024
##$TD0= 1
##$TE= 310
##$TE2= 300
##$TE3= 300
##$TEG= 300
##$TL= (0..7)
120 120 120 120 120 120 120 120
##$TP= (0..7)
150 150 150 150 150 150 150 150
##$TP07= 0
##$TPNAME0= <>
##$TPNAME1= <>
##$TPNAME2= <>
##$TPNAME3= <>
##$TPNAME4= <>
##$TPNAME5= <>
##$TPNAME6= <>
##$TPNAME7= <>
##$TPOAL= (0..7)
0.5 0.5 0.5 0.5 0.5 0.5 0.5 0.5
##$TPOFFS= (0..7)
0 0 0 0 0 0 0
##$TUNHIN= 0
##$TUNHOUT= 0
##$TUNXOUT= 0
##$USERA1= <user>
##$USERA2= <user>
##$USERA3= <user>
##$USERA4= <user>
##$USERA5= <user>
##$V9= 5
##$VALIST= <valist>
##$VCLIST= <CCCCCCCCCCCCCCCC>
##$VD= 0
##$VDLIST= <DDDDDDDDDDDDDDDDDD>
##$VPLIST= <PPPPPPPPPPPPPPPP>
##$VTLIST= <TTTTTTTTTTTTTTTT>
##$WBST= 1024
##$WBSW= 10
##$XGAIN= (0..3)
0 0 0 0
##$XL= 0
##$YL= 0
##$YMAX_a= 17353
##$YMIN_a= -11035
##$ZGOPTNS= <>
##$ZL1= 120
##$ZL2= 120
##$ZL3= 120
##$ZL4= 120
##$END=

```

D.6.1 TROSY-HNCA pulse-program

```

;avance-version (04/01/07)
;TROSY-HNCACB
;3D sequence with
; inverse correlation for triple resonance
; via TROSY and inept transfer steps
;
; F1(H) -> F3(N) -> F2(Caliph.,t1) -> F3(N,t2) -> F1(H,t3)
;
;on/off resonance Ca and C=O pulses using shaped pulse
;phase sensitive (t1)
;phase sensitive using Echo/Antiecho gradient selection (t2)
;using constant time in t2
;with H-1 180degree pulses in t1
;uncompensated version d25=d26
;(use parameterset TRHNCACBETGP3D)
;
;T. Schulte-Herbrueggen & O.W. Sorensen, J. Magn. Reson. 144,
; 123 - 128 (2000)
;A. Eletsky, A. Kienhoefer & K. Pervushin,
; J. Biomol. NMR 20, 188-180 (2001)
;(M. Salzmann, G. Wider, K. Pervushin, H. Senn & K. Wuethrich,
; J. Am. Chem. Soc. 121, 844-848 (1999))

prosol relations=<triple>

#include <Avance.incl>
#include <Grad.incl>
#include <Delay.incl>

define list<gradient> EA5 = { 0.8750 1.0000}
define list<gradient> EA7 = { 1.0000 0.6667}
define list<gradient> EA9 = { 0.6595 1.0000}

```

```

"d0=3u"

"d10=3u"

"d11=30m"

"d23=11m"
"d25=2.3m"
;"d26=2.1m"
"d26=2.3m"
"d28=3.6m"

"in30=in10"

"d30=d23/2-d25/2-p14/2-p16/2-d16/2-2u"

"DELTA=d0*4+p2*2+larger(p14,p22)-p14-4u"
"DELTA1=d26-p16-d16"
"DELTA2=d23-d16"
"DELTA3=d28-d16"
"DELTA4=d23/2-d25/2-p14/2-d10+p21*2/3.1416"
"DELTA5=d23/2-d25/2-p14/2-d10-p16-d16-p11+p21*2/3.1416-8u"
"DELTA6=d25-p16-d16"
"DELTA7=d26-p11-p16-d16-8u"

"spoff2=0"
"spoff3=0"
"spoff5=bf2*(cnst21/1000000)-o2"
"spoff8=0"

aqseq 321

1 d11 ze
  d11 LOCKDEC_ON
2 d11
3 d11 H2_LOCK
  6m LOCKH_OFF
  d1 p11:fl
  50u LOCKH_ON
  d12 H2_PULSE
  50u UNBLKGRAMP

4u p10:fl
(p11:sp1 ph2:r):fl
4u
4u p11:fl

(p1 ph3):fl
p16:gp1
d16
DELTA1
(center (p2 ph2) (p22 ph1):f3 )
DELTA1
p16:gp1
d16
(p1 ph2):fl

(p21 ph1):f3
d16
DELTA2
(center (p14:sp3 ph1):f2 (p22 ph1):f3 )
DELTA2
d16
(p21 ph2):f3
4u
4u p14:f4
20u cpd4:f4

(p13:sp2 ph6):f2
d0
(p2 ph1):fl
d0
(center (p14:sp5 ph1):f2 (p22 ph1):f3 )
d0

```

```

(p2 ph1):f1
d0
(p14:sp3 ph1):f2
DELTA
(p14:sp5 ph1):f2
4u
(p13:sp8 ph9):f2

4u do:f4

20u
(p21 ph5):f3
d30
(p14:sp5 ph1):f2
d30
(center (p14:sp3 ph1):f2 (p22 ph1):f3 )
DELTA4
d10
(p14:sp5 ph1):f2
d10
DELTA5
p16:gp5*EA5
d16 pl0:f1
(p11:sp1 ph3:r):f1
4u
4u pl1:f1

(p1 ph7)
p16:gp6
d16
DELTA6
(center (p2 ph2) (p22 ph2):f3 )
DELTA6
p16:gp6
d16
(p1 ph1)

p16:gp7*EA7
d16
4u

(p21 ph1):f3
p16:gp8
d16
DELTA7 pl0:f1
(p11:sp1 ph4:r):f1
4u
4u pl1:f1
(center (p2 ph2) (p22 ph2):f3 )
4u pl0:f1
(p11:sp1 ph4:r):f1
4u
DELTA7
p16:gp8
d16 pl1:f1
(p21 ph8:r):f3

p16:gp9*EA9
d16
4u BLKGRAMP

go=2 ph31
d11 mc #0 to 2
; F1PH(rd10 & rd30 & ip9 & ip10, id0)
; F1PH(rd10 & rd30 & ip9, id0)
; F2EA(igrad EA5 & igrad EA7 & igrad EA9 & ip7*2 & ip8*2, id10 & dd30 & ip5*2 & ip31*2)
; F1EA(igrad EA5 & igrad EA7 & igrad EA9 & ip7*2 & ip8*2, id10 & dd30 & ip5*2 & ip31*2)
d11 H2_LOCK
d11 LOCKH_OFF
d11 LOCKDEC_OFF

exit

ph1=0

```

```

ph2=1
ph3=2
ph4=3
ph5=0 2
ph6=0 0 2 2
ph7=3
ph8=3
ph9=0
ph10=1
ph31=0 2 2 0

;p10 : 120dB
;p11 : f1 channel - power level for pulse (default)
;p13 : f3 channel - power level for pulse (default)
;sp1: f1 channel - shaped pulse 90 degree (H2O on resonance)
;sp2: f2 channel - shaped pulse 90 degree (Cali on resonance)
;sp3: f2 channel - shaped pulse 180 degree (Cali on resonance)
;sp5: f2 channel - shaped pulse 180 degree (C=O off resonance)
;sp8: f2 channel - shaped pulse 90 degree (Cali on resonance)
;
;      for time reversed pulse
;p1 : f1 channel - 90 degree high power pulse
;p2 : f1 channel - 180 degree high power pulse
;p11: f1 channel - 90 degree shaped pulse      [1 msec]
;p13: f2 channel - 90 degree shaped pulse
;p14: f2 channel - 180 degree shaped pulse
;p16: homospoil/gradient pulse      [1 msec]
;p21: f3 channel - 90 degree high power pulse
;p22: f3 channel - 180 degree high power pulse
;d0 : incremented delay (F1 in 3D)      [3 usec]
;d1 : relaxation delay; 1-5 * T1
;d10: incremented delay (F2 in 3D)      [3 usec]
;d11: delay for disk I/O      [30 msec]
;d16: delay for homospoil/gradient recovery
;d23: 1/(4J(NCa))      [11 msec]
;d25: 1/(4J(NH))      [2.3 msec]
;d26: 1/(4J(NH))      [2.3 msec]
;d28: 1/(8J(CaCb))      [3.6 msec]
;d30: decremented delay (F2 in 3D) = d23/2-d25/2-p14/2-p16/2-d16/2-2u
;cnst21: CO chemical shift (offset, in ppm)
;cnst23: Caliphatic chemical shift (offset, in ppm)
;o2p: Caliphatic chemical shift (cnst23)
;in0: 1/(4 * SW(Cali)) = (1/2) DW(Cali)
;nd0: 4
;in10: 1/(4 * SW(N)) = (1/2) DW(N)
;nd10: 4
;in30: = in10
;NS: 8 * n
;DS: >= 16
;td1: number of experiments in F1
;td2: number of experiments in F2      td2 max = 2 * d30 / in30
;FnMODE: States-TPPI (or TPPI) in F1
;FnMODE: echo-antiecho in F2

;use gradient ratio: gp 1:gp 2:gp 3:gp 4:gp 5:gp 6:gp 7:gp 8: gp 9
;      2: 2: 2: 2: -80: 2: 30: 45:30.13

;for z-only gradients:
;gpz1: 2%
;gpz2: 2%
;gpz3: 2%
;gpz4: 2%
;gpz5: -80%
;gpz6: 2%
;gpz7: 30%
;gpz8: 45%
;gpz9: 30.13%

;use gradient files:
;gpnam1: SINE.100
;gpnam2: SINE.100
;gpnam3: SINE.100
;gpnam4: SINE.100
;gpnam5: SINE.100
;gpnam6: SINE.100
;gpnam7: SINE.100

```



```

83 83 83 83 83 83 83 83
##$FTLPGN= 0
##$FW= 125000
##$FnMODE= 0
##$GP031= 0
##$GPNAM0= <sine.100>
##$GPNAM1= <SINE.100>
##$GPNAM10= <sine.100>
##$GPNAM11= <sine.100>
##$GPNAM12= <sine.100>
##$GPNAM13= <sine.100>
##$GPNAM14= <sine.100>
##$GPNAM15= <sine.100>
##$GPNAM16= <sine.100>
##$GPNAM17= <sine.100>
##$GPNAM18= <sine.100>
##$GPNAM19= <sine.100>
##$GPNAM2= <SINE.100>
##$GPNAM20= <sine.100>
##$GPNAM21= <sine.100>
##$GPNAM22= <sine.100>
##$GPNAM23= <sine.100>
##$GPNAM24= <sine.100>
##$GPNAM25= <sine.100>
##$GPNAM26= <sine.100>
##$GPNAM27= <sine.100>
##$GPNAM28= <sine.100>
##$GPNAM29= <sine.100>
##$GPNAM3= <SINE.100>
##$GPNAM30= <sine.100>
##$GPNAM31= <sine.100>
##$GPNAM4= <SINE.100>
##$GPNAM5= <SINE.50>
##$GPNAM6= <SINE.100>
##$GPNAM7= <SINE.100>
##$GPNAM8= <SINE.100>
##$GPNAM9= <SINE.100>
##$GPX= (0..31)
0 0 0 0 0 0 0 0 0 0 0 0 0 0 0 0 0 0 0 0 0 0 0 0 0 0 0 0 0 0 0 0
0
##$GPY= (0..31)
0 0 0 0 0 0 0 0 0 0 0 0 0 0 0 0 0 0 0 0 0 0 0 0 0 0 0 0 0 0 0 0
0
##$GPZ= (0..31)
3 2 18 44 50 -80 2 30 45 30.13 0 0 0 0 0 0 0 0 0 0 0 0 0 0 0 0 0 0
0 0 0 0 0 0 0
##$GRDPROG= <grad_out>
##$SHDDUTY= 20
##$SHDRATE= 20
##$SHGAIN= (0..3)
0 0 0 0
##$SHL1= 128
##$SHL2= 50
##$SHL3= 16
##$SHL4= 17
##$HOLDER= 0
##$SHPMOD= (0..7)
0 0 0 0 0 0 0 0
##$HPPRGN= 0
##$IN= (0..31)
3.945e-05 0.001 0.001 0.001 0.001 0.001 0.001 0.001 0.001
0.001 0.001 9.5175e-05 0.001 0.001 0.001 0.001 0.001 0.001
0.001 0.001 0.001 0.001 9.7e-05 0.001 0.001 0.001 0.001 0.001
0.001 0.001 0.001 9.7e-05 0.001 9.5175e-05 0.001
##$INP= (0..31)
0 0 0 0 0 0 0 0 0 0 0 0 0 0 0 0 0 0 0 0 0 0 0 0 0 0 0 0 0 0 0 0
0
##$INSTRUM= <spect>
##$SL= (0..31)
1 1 1 1 1 1 1 1 1 1 1 1 1 1 1 1 1 1 1 1 1 1 1 1 1 1 1 1 1 1 1 1
1
##$LFILTER= 150
##$LGAIN= -5
##$LOCKED= yes
##$LOCKFLD= -4486

```

```

##$LOCKGN= 132.699996948242
##$LOCKPOW= -16
##$LOCKPPM= 4.69999980926514
##$LOCNUC= <2H>
##$LOCPHAS= 124.2
##$LOCSHFT= no
##$SLTIME= 0.150000005960464
##$MASR= 0
##$MASRLST= <masrlst>
##$NBL= 1
##$SNC= -2
##$SNS= 60
##$NUC1= <1H>
##$NUC2= <13C>
##$NUC3= <15N>
##$NUC4= <2H>
##$NUC5= <off>
##$NUC6= <off>
##$NUC7= <off>
##$NUC8= <off>
##$NUCLEI= 0
##$NUCLEUS= <off>
##$O1= 4233.6
##$O2= 11994.17454
##$O3= 10829.5497
##$O4= 1004.11275474244
##$O5= 0
##$O6= 0
##$O7= 200000000
##$O8= 200000000
##$OBSCHAN= (0..9)
0 0 0 0 0 0 0 0 0 0
##$OVERFLW= 0
##$P= (0..31)
10.5 10.75 21.5 11.8 23.6 23.1 35 70 2000 35 70 1000
2000 400 256 200000 1000 0 0 500 26 34.2 68.4 500 500
0 55 10.5 0 0 0 0
##$PAPS= 2
##$PARMODE= 2
##$PCPD= (0..9)
100 100 100 100 260 100 100 100 100 100
##$PHCOR= (0..31)
0 0 0 0 0 0 0 0 0 0 0 0 0 0 0 0 0 0 0 0 0 0 0 0 0 0 0 0 0 0 0 0
0
##$PHP= 1
##$PH_ref= 0
##$SPL= (0..31)
120 -1 -2 -4 -6 120 120 120 120 59.06 15.96 120 13.46
120 120 7.36 17.8 -6 5.5 19.88 120 120 120 120 120 120
120 120 120 120 120 120
##$POWMOD= 0
##$SPR= 1
##$SPRECHAN= (0..15)
-1 -1 -1 -1 0 -1 1 -1 -1 -1 4 -1 -1 -1 -1 -1
##$SPRGAIN= 0
##$SPROBHD= <5 mm CPTXI 1H-13C/15N/2H Z-GRD
Z44919/0005
>
##$PROSOL= no
##$SPULPROG= <trhnca_tr_d.rtf>
##$SPW= 0
##$QNP= 1
##$QS= (0..7)83 83 83 83 83 83 83 22
##$QSB= (0..7)83 83 83 83 83 83 83 83
##$SRD= 0
##$SRECCHAN= (0..15)
-1 -1 -1 -1 -1 -1 -1 -1 -1 -1 -1 -1 -1 -1 -1 -1
##$RECPH= 0
##$SRG= 1024
##$SRO= 0
##$SROUTWD1= (0..23)
0 0 0 0 0 0 0 0 0 0 0 0 0 0 0 0 0 0 0 0 0 0 0 0 0 0 0 0 0 0 0 0
##$SROUTWD2= (0..23)
0 0 0 0 0 1 0 0 0 0 0 0 0 0 0 0 0 0 0 0 0 0 0 0 0 0 0 0 0 0 0 0
##$SRPUSED= (0..8)

```

```

0 0 0 0 0 0 0 0
##$RSEL= (0..9)
0 1 2 5 0 10 0 0 0
##$S= (0..7)
83 4 83 83 83 83 83 83
##$SEOUT= 0
##$SFO1= 900.0042336
##$SFO2= 226.31717417454
##$SFO3= 91.2070375497
##$SFO4= 138.156484112755
##$SFO5= 600.13
##$SFO6= 600.13
##$SFO7= 800.13
##$SFO8= 800.13
##$SOLVENT= <H2O>
##$SP= (0..31)
120 35 2.6 1.6 3.8 1.6 120 2.8 2.6 8.6 6 120 6 4 120 12.4
150 150 150 150 150 150 150 150 150 150 150 150 150
150 150 150
##$SP07= 0
##$SPECTR= 0
##$SPNAM0= <Gaus1.1000>
##$SPNAM1= <Sinc1.1000>
##$SPNAM10= <Q5.1000>
##$SPNAM11= <Gaus1.1000>
##$SPNAM12= <Q5tr.1000>
##$SPNAM13= <Crf60comp.4>
##$SPNAM14= <Gaus1.1000>
##$SPNAM15= <Q3.1000>
##$SPNAM16= <gauss>
##$SPNAM17= <gauss>
##$SPNAM18= <gauss>
##$SPNAM19= <gauss>
##$SPNAM2= <Q5.1000>
##$SPNAM20= <gauss>
##$SPNAM21= <gauss>
##$SPNAM22= <gauss>
##$SPNAM23= <gauss>
##$SPNAM24= <gauss>
##$SPNAM25= <gauss>
##$SPNAM26= <gauss>
##$SPNAM27= <gauss>
##$SPNAM28= <gauss>
##$SPNAM29= <gauss>
##$SPNAM3= <Q3.1000>
##$SPNAM30= <gauss>
##$SPNAM31= <gauss>
##$SPNAM4= <Q5.1000>
##$SPNAM5= <Q3.1000>
##$SPNAM6= <Gaus1.1000>
##$SPNAM7= <Q3.1000>
##$SPNAM8= <Q5tr.1000>
##$SPNAM9= <Q3.1000>
##$SPOAL= (0..31)
0.5 0.5 0.5 0.5 0.5 0.5 0.5 0.5 0.5 0.5 0.5 0.5 0.5 0.5 0.5
0.5 0.5 0.5 0.5 0.5 0.5 0.5 0.5 0.5 0.5 0.5 0.5 0.5 0.5 0.5
0.5 0.5
##$SPOFFS= (0..31)
0 0 0 0 0 27835.54 0 0 0 0 0 0 0 0 0 0 0 0 0 0 0 0 0 0 0 0 0 0 0 0 0 0 0 0
0 0 0 0 0
##$SUBNAM0= <"">
##$SUBNAM1= <"">
##$SUBNAM2= <"">
##$SUBNAM3= <"">

##$SUBNAM4= <"">
##$SUBNAM5= <"">
##$SUBNAM6= <"">
##$SUBNAM7= <"">
##$SUBNAM8= <"">
##$SUBNAM9= <"">
##$SW= 11.9731237550542
##$SWIBOX= (0..15)
0 1 4 4 0 5 6 0 0 0 10 0 0 0 0 0
##$SW_h= 10775.8620689655
##$STD= 1024
##$STD0= 1
##$STE= 310
##$STE2= 300
##$STE3= 300
##$STEG= 300
##$STL= (0..7)
10 120 120 120 120 120 120 120
##$STP= (0..7)
150 150 150 150 150 150 150 150
##$STP07= 0
##$STPNAME0= <>
##$STPNAME1= <>
##$STPNAME2= <>
##$STPNAME3= <>
##$STPNAME4= <>
##$STPNAME5= <>
##$STPNAME6= <>
##$STPNAME7= <>
##$STPOAL= (0..7)
0.5 0.5 0.5 0.5 0.5 0.5 0.5 0.5
##$STPOFFS= (0..7)
0 0 0 0 0 0 0 0
##$STUNHIN= 0
##$STUNHOUT= 0
##$STUNXOUT= 0
##$USERA1= <user>
##$USERA2= <user>
##$USERA3= <user>
##$USERA4= <user>
##$USERA5= <user>
##$V9= 5
##$VALIST= <valist>
##$VCLIST= <CCCCCCCCCCCCCCCC>
##$VD= 0
##$VDLIST= <DDDDDDDDDDDDDDDD>
##$VPLIST= <PPPPPPPPPPPPPP>
##$VTLIST= <TTTTTTTTTTTTTTTT>
##$WBST= 1024
##$WBSW= 4
##$WS= (0..7)83 83 83 83 83 83 83 83
##$XGAIN= (0..3)
0 0 0 0
##$XL= 3
##$YL= 3
##$YMAX_a= 16987
##$YMIN_a= -18691
##$ZGPTNS= <-DLABEL_CN>
##$ZL1= 120
##$ZL2= 120
##$ZL3= 120
##$ZL4= 120
##$END=

```

D.7.1 TROSY-MQ-HNCOCA pulse-program

This pulse-program was modified from the standard Bruker trhncoactgp3d pulse-program with a multiple quantum carbon evolution time kindly provided by Roland Riek, Salk Institute, San Diego

```

;trhncoactgp3d
;avance-version (04/01/07)
;TROSY-HNCOCA
;3D sequence with
; inverse correlation for triple resonance
; via TROSY and inept transfer steps
;
; F1(H) -> F3(N) -> F2(Ca) -> F2(C=O,t1)
;     -> F2(Ca) -> F3(N,t2) -> F1(H,t3)
;
;on/off resonance Ca and C=O pulses using shaped pulse
;phase sensitive (t1)
;phase sensitive using Echo/Antiecho gradient selection (t2)
;using constant time in t2
;with H-1 180degree pulses in t1
;uncompensated version d25=d26
;(use parameterset TRHNCOCAETGP3D)
;
;T. Schulte-Herbrueggen & O.W. Sorensen, J. Magn. Reson. 144,
; 123 - 128 (2000)
;A. Eletsky, A. Kienhoefer & K. Pervushin,
; J. Biomol. NMR 20, 188-180 (2001)
;(M. Salzmann, G. Wider, K. Pervushin, H. Senn & K. Wuethrich,
; J. Am. Chem. Soc. 121, 844-848 (1999))

prosol relations=<triple>

#include <Avance.incl>
#include <Grad.incl>
#include <Delay.incl>

define list<gradient> EA3 = { 0.8750 1.0000}
define list<gradient> EA5 = { 1.0000 0.6667}
define list<gradient> EA7 = { 0.6595 1.0000}

#define GRADIENT3 10u p23:gp8 190u p12:f2

;p23 = 700u
;gp8=45%

;:"d0=3u"
;:"d10=3u"
;:"d11=30m"

;"d6=10u+d0"!!
;"d7=10u-d0"!!

"d6=10u+6u"
"d7=10u-6u"
"d9=p22"

;"d0=in0*3/2-5u"
"d0=in0*6/2-p15/2-p13*0.6366"

;"d22=4m"
"d22=4.5m"
"d23=12m"
"d25=2.3m"
"d26=2.3m"

"d14=5m-p21-200u"
;:"d15=d14+p13-p14/2" ;maybe use different shaped pulses (like Riek)
;"d15=d14+p13-p15/2"

"in30=in10"

"d30=d23/2-d25/2-p14/2-p16/2-d16/2-2u"

;"d8=DELTA3-p13-54u"
"d8=d22-p14-p16-d16-4u-p13-54u+p14"
;"DELTA=d0*4+p2*2+larger(p14,p22)-p14-4u"
"DELTA1=d26-p16-d16"
"DELTA2=d23-p16-d16"
"DELTA3=d22-p14-p16-d16-4u"

```

"DELTA4=d23/2-d25/2-p14/2-d10+p21*2/3.1416"
 "DELTA5=d23/2-d25/2-p14/2-d10-p16-d16-p11+p21*2/3.1416-8u"
 "DELTA6=d25-p16-d16"
 "DELTA7=d26-p11-p16-d16-8u"

;"spoff2=0"
 ;"spoff3=0"
 ;;"spoff5=bf2*((cnst22-cnst21)/1000000)"
 ;"spoff5=0"
 ;"spoff7=bf2*((cnst21-cnst22)/1000000)"
 ;"spoff8=0"
 ;"spoff9=bf2*((cnst21-cnst22)/1000000)"
 ;"spoff10=bf2*((cnst21-cnst22)/1000000)"

aqseq 321

1 d11 ze
 d11 LOCKDEC_ON
 d11 pl17:f4
 2 d11
 3 d11 H2_LOCK
 9m LOCKH_OFF
 d1 pl1:f1 ;fq=cnst21(bf ppm):f2
 50u UNBLKGRAD
 d12 H2_PULSE

4u pl0:f1
 (p11:sp1 ph2:r):f1
 4u
 4u pl1:f1

(p1 ph3):f1
 p16:gp1
 d16
 DELTA1
 (center (p2 ph2) (p22 ph1):f3)
 DELTA1
 p16:gp1
 d16
 (p1 ph2):f1

(p21 ph1):f3
 p16:gp2
 d16
 DELTA2
 (center (p14:sp6 ph1):f2 (p22 ph1):f3) ;sp3 to sp6, CO 180 with offset
 DELTA2
 p16:gp2
 d16 pl2:f2
 (p21 ph2):f3

;;(p13:sp9 ph6):f2 ;sp2 to sp9, CO
 ;;4u
 ;;(p14:sp7 ph1):f2 ;sp5 to sp7, CA to CO !!!
 ;;p16:gp1
 ;;d16
 ;;DELTA3
 ;;(p14:sp5 ph1):f2 ;sp3 to sp5, Co to Ca !!!
 ;;4u
 ;;(p14:sp7 ph1):f2 ;sp5 to sp7, Ca to Co !!!
 ;;DELTA3
 ;;d8
 ;;p16:gp1
 ;;d16
 ;;(p13:sp8 ph2):f2

4u
 30u fq=cnst22(bf ppm):f2
 10u cpd4:f4

(p5 ph6):f2 ;co hard power
 GRADIENT3
 (d14 p13:sp2 ph7 d0 p15:sp5 d0 p13:sp8 ph1 d14):f2 ;(d15 d0 5u p15:sp5):f2 ;ca co
 GRADIENT3

```

(p5 ph1):f2 ;co hard power

;(p5 ph6):f2 ;co hard power
;GRADIENT3
;(d14 p13:sp2 ph7 d0 d0 10u p13:sp8 ph1 d14):f2 (d15 d0 5u p15:sp5):f2 ;ca co
;GRADIENT3
;(p5 ph1):f2 ;co hard power

;(p5 ph6):f2 ;co hard power
;(p13:sp10 ph6):f2 ;co shaped pulse
;GRADIENT3
;(d14 p5 ph7 d0 d0 10u p5 ph1 d14):f2 (d15 d0 5u p14:sp7 pl2):f2 ;ca co
;GRADIENT3
;(p13:sp11 ph1):f2 ;co shaped pulse
;(p5 ph1):f2 ;co hard power

;;10u ;pl2:f2

;;(p13:sp2 ph7):f2 ;ca
;;;(p15 ph7):f2 ;ca hard power
;;d6
;;d9
;;(p14:sp3 ph1):f2 ;ca
;;d7
;;d0
;;(center (p2 ph1):f1 (p22 ph1):f3 )
;;;(p22 ph1):f3
;;d0
;;;(center (p2 ph1):f1 (p14:sp7 ph1):f2 ) ;co
;;(p14:sp7 ph1):f2 ;co
;;d0
;;(center (p2 ph1):f1 (p22 ph1):f3 )
;;;(p22 ph1):f3
;;d0
;;4u
;;d7
;;(p14:sp3 ph1):f2 ;ca
;;d6
;;d9
;;;DELTA
;;(p14:sp7 ph1):f2 ;co
;;2u
;;2u ;pl2:f2
;;;(p15 ph1):f2 ;ca hard power
;;(p13:sp8 ph1):f2 ;ca

4u do:f4
30u fq=cnst21(bf ppm):f2
20u

;;(p13:sp2 ph2):f2
;4u
;(p14:sp7 ph1):f2 ;sp5 to sp7, Ca to Co !!!
;p16:gp1
;d16
;;d8
;DELTA3
;(p14:sp5 ph1):f2 ;sp3 to sp5, Co to Ca !!!
;4u
;(p14:sp7 ph1):f2 ;sp5 to sp7, Ca to Co !!!
;;DELTA3
;d8
;p16:gp1
;d16
;(p13:sp10 ph1):f2 ;sp8 to sp10, CO

(p21 ph5):f3
d30
(p14:sp7 ph1):f2 ;ca without offset
d30
(center (p14:sp6 ph1):f2 (p22 ph1):f3 ) ;co 180
DELTA4
d10
(p14:sp7 ph1):f2
d10

```

```

DELTA5
p16:gp3*EA3
d16 pl0:f1
(p11:sp1 ph3:r):f1
;(p11:sp1 ph1:r):f1
4u
4u pl1:f1

(p1 ph8)
p16:gp4
d16
DELTA6
(center (p2 ph2) (p22 ph2):f3 )
DELTA6
p16:gp4
d16
(p1 ph1)

p16:gp5*EA5
d16
4u

(p21 ph1):f3
p16:gp6
d16
DELTA7 pl0:f1
(p11:sp1 ph4:r):f1
4u
4u pl1:f1
(center (p2 ph2) (p22 ph2):f3 )
4u pl0:f1
(p11:sp1 ph4:r):f1
4u
DELTA7
p16:gp6
d16 pl1:f1
(p21 ph9:r):f3

p16:gp7*EA7
d16
4u BLKGRAMP

go=2 ph31
d11 mc #0 to 2
  F1PH(rd10 & rd30 & ip7, id0)
  F2EA(igrad EA3 & igrad EA5 & igrad EA7 & ip8*2 & ip9*2, id10 & dd30 & ip5*2 & ip31*2)

d11 H2_LOCK
d11 LOCKH_OFF
d11 LOCKDEC_OFF

exit

ph1=0
ph2=1
ph3=2
ph4=3
ph5=0 2
;ph5=2 0
ph6=0
;ph6=0 0 0 0 2 2 2 2
;ph7=0
ph7=0 0 2 2
ph8=3
ph9=3
ph31=0 2 2 0 ;2 0 0 2
;ph31=2 0 0 2 0 2 2 0

;pl0 : 120dB
;pl1 : f1 channel - power level for pulse (default)
;pl3 : f3 channel - power level for pulse (default)
;sp1: f1 channel - shaped pulse 90 degree (H2O on resonance)
;sp2: f2 channel - shaped pulse 90 degree (on resonance)

```

```

;sp3: f2 channel - shaped pulse 180 degree (on resonance)
;sp5: f2 channel - shaped pulse 180 degree (Ca off resonance)
;sp7: f2 channel - shaped pulse 180 degree (C=O off resonance)
;sp8: f2 channel - shaped pulse 90 degree (on resonance)
;
; for time reversed pulse
;p1 : f1 channel - 90 degree high power pulse
;p2 : f1 channel - 180 degree high power pulse
;p11: f1 channel - 90 degree shaped pulse [1 msec]
;p13: f2 channel - 90 degree shaped pulse
;p14: f2 channel - 180 degree shaped pulse
;p16: homospoil/gradient pulse [1 msec]
;p21: f3 channel - 90 degree high power pulse
;p22: f3 channel - 180 degree high power pulse
;d0 : incremented delay (F1 in 3D) [3 usec]
;d1 : relaxation delay; 1-5 * T1
;d10: incremented delay (F2 in 3D) [3 usec]
;d11: delay for disk I/O [30 msec]
;d16: delay for homospoil/gradient recovery
;d22: 1/(4J(COca)) [4 msec]
;d23: 1/(4J(NCO)) [12 msec]
;d25: 1/(4J(NH)) [2.3 msec]
;d26: 1/(4J(NH)) [2.3 msec]
;d30: decremented delay (F2 in 3D) = d23/2-d25/2-p14/2-p16/2-d16/2-2u
;cnst21: CO chemical shift (offset, in ppm)
;cnst22: Calpha chemical shift (offset, in ppm)
;o2p: Calpha chemical shift (cnst22)
;in0: 1/(4 * SW(Ca)) = (1/2) DW(Ca) ;now in0=1/(2 * SW(Ca))
;nd0: 4 ;now 2
;in10: 1/(4 * SW(N)) = (1/2) DW(N)
;nd10: 4
;in30: = in10
;NS: 8 * n
;DS: >= 16
;td1: number of experiments in F1
;td2: number of experiments in F2 td2 max = 2 * d30 / in30
;FnMODE: States-TPPI (or TPPI) in F1
;FnMODE: echo-antiecho in F2

;use gradient ratio: gp 1 : gp 2 : gp 3 : gp 4 : gp 5 : gp 6 : gp 7
; 2 : 2 : -80 : 2 : 30 : 45 : 30.13

;for z-only gradients:
;gpz1: 2%
;gpz2: 2%
;gpz3: -80%
;gpz4: 2%
;gpz5: 30%
;gpz6: 45%
;gpz7: 30.13%

;use gradient files:
;gpnam1: SINE.100
;gpnam2: SINE.100
;gpnam3: SINE.100
;gpnam4: SINE.100
;gpnam5: SINE.100
;gpnam6: SINE.100
;gpnam7: SINE.100

;Processing

;PHC0(F2): 22.5

;$Id: trhncoactgp3d,v 1.2 2004/01/22 14:59:05 ber Exp $

```

D.7.2 TROSY-MQ-HNCOCA parameters

```

##TITLE= Parameter file, TOPSPIN
          Version 1.3
##JCAMPDX= 5.0
##DATATYPE= Parameter Values

```

```

##ORIGIN= UXNMR, Bruker Analytische Messtechnik
          GmbH
##OWNER= demo
          $$ 2006-01-23 09:11:42.219 +0100 nmrsu@nmr600av
          $$ /opt/topspin/data/momo/nmr/hvdac_160106/53/acqus

```



```

##$SPNAM15=<Q3.1000>
##$SPNAM16=<gauss>
##$SPNAM17=<gauss>
##$SPNAM18=<gauss>
##$SPNAM19=<gauss>
##$SPNAM2=<Q5.1000>
##$SPNAM20=<gauss>
##$SPNAM21=<gauss>
##$SPNAM22=<gauss>
##$SPNAM23=<gauss>
##$SPNAM24=<gauss>
##$SPNAM25=<gauss>
##$SPNAM26=<gauss>
##$SPNAM27=<gauss>
##$SPNAM28=<gauss>
##$SPNAM29=<gauss>
##$SPNAM3=<Q3.1000>
##$SPNAM30=<gauss>
##$SPNAM31=<gauss>
##$SPNAM4=<Q5.1000>
##$SPNAM5=<Q3.1000>
##$SPNAM6=<Q3.1000>
##$SPNAM7=<Q3.1000>
##$SPNAM8=<Q5tr.1000>
##$SPNAM9=<Q3.1000>
##$SPOAL=(0..31)
0.5 0.5 0.5 0.5 0.5 0.5 0.5 0.5 0.5 0.5 0.5 0.5 0.5 0.5 0.5
0.5 0.5 0.5 0.5 0.5 0.5 0.5 0.5 0.5 0.5 0.5 0.5 0.5 0.5 0.5
0.5 0.5
##$SPOFFS=(0..31)
0 0 -17850 0 0 0 17850 0 -17850 0 17850 17850 0 0 0 0 0
0 0 0 0 0 0 0 0 0 0 0 0 0 0 0
##$SUBNAM0=<"">
##$SUBNAM1=<"">
##$SUBNAM2=<"">
##$SUBNAM3=<"">
##$SUBNAM4=<"">
##$SUBNAM5=<"">
##$SUBNAM6=<"">
##$SUBNAM7=<"">
##$SUBNAM8=<"">
##$SUBNAM9=<"">
##$SW= 14.9904376434794
##$SWIBOX=(0..15)
0 1 4 4 0 5 6 0 0 0 0 0 0 0 0
##$SW_h= 8992.80575539568
##$STD= 1024
##$STD0= 1
##$STE= 313
##$STE2= 300
##$STE3= 300
##$STEG= 300
##$STL=(0..7)
10 120 120 120 120 120 120 120
##$STP=(0..7)
150 150 150 150 150 150 150 150
##$STP07= 0
##$STPNAME0=<>
##$STPNAME1=<>
##$STPNAME2=<>
##$STPNAME3=<>
##$STPNAME4=<>
##$STPNAME5=<>
##$STPNAME6=<>
##$STPNAME7=<>
##$STPOAL=(0..7)
0.5 0.5 0.5 0.5 0.5 0.5 0.5 0.5
##$STPOFFS=(0..7)
0 0 0 0 0 0 0 0
##$TUNHIN= 0
##$TUNHOUT= 0
##$TUNXOUT= 0
##$USERA1=<user>
##$USERA2=<user>
##$USERA3=<user>
##$USERA4=<user>
##$USERA5=<user>
##$V9= 5
##$VALIST=<valist>
##$VCLIST=<CCCCCCCCCCCCCCCC>
##$VD= 0
##$VDLIST=<DDDDDDDDDDDDDDDD>
##$VPLIST=<PPPPPPPPPPPPPPPP>
##$VTLIST=<TTTTTTTTTTTTTTTT>
##$WBST= 1024
##$WBWS= 4
##$WWS=(0..7)83 83 83 83 83 83 83 83
##$XGAIN=(0..3)
0 0 0 0
##$XL= 3
##$YL= 3
##$YMAX_a= 94649
##$YMIN_a= -82515
##$ZGPTNS=<-DLABEL_CN>
##$ZL1= 120
##$ZL2= 120
##$ZL3= 120
##$ZL4= 120
##$END=

```

Curriculum Vitae

Personal data

Name	Monika Bayrhuber
Date of birth	07.10.1978
Place of birth	Kiel
Citizenship	German

Education

1985-1989	Primary school Gettorf
1989-1998	Gymnasium Kronshagen
07/1998	General qualification for university entrance
1998-2003	Chemistry studies at the Christian-Albrechts-university of Kiel
10/2000	Intermediate diploma in chemistry
10-12/2001	Internship at the University of Edinburgh in the group of Prof. Dr. Sabine Flitsch
10/2002	Final examinations in chemistry
11/2002-6/2003	Diploma thesis with the title "Synthesis and functional investigation of photo switchable Norbornadien- and Quadricyclan-systems as complex ligands an carrier for alkaline earth ions" in the group of Prof. Dr. Rainer Herges at the Christian-Albrechts-University of Kiel
10/2003-7/2007	Ph.D. thesis with the title "Structural and functional characterisation of a membrane protein and a membrane protein-targeting toxin by solution NMR" in the departement of NMR-based structural biology of Prof. Dr. Christian Griesinger at the Max Planck Institute for Biophysical Chemistry in Göttingen

Lebenslauf

Persönliche Daten

Name	Monika Bayrhuber
Geburtstag	07.10.1978
Geburtsort	Kiel
Staatsangehörigkeit	deutsch

Ausbildung

1985-1989	Grundschule Gettorf
1989-1998	Gymnasium Kronshagen
07/1998	Allgemeine Hochschulreife
1998-2003	Chemiestudium an der Christian-Albrechts-Universität zu Kiel
10/2000	Vordiplom
10-12/2001	Praktikum an der Universität von Edinburgh in der Gruppe von Prof. Dr. Sabine Flitsch
10/2002	Diplomsprüfungen
11/2002-6/2003	Diplomarbeit mit dem Titel "Synthese und Untersuchung der Eigenschaften photoschaltbarer Norbornadien- und Quadricyclan-Systeme als Komplexligenanden für Erdalkali-Ionen" in der Gruppe von Prof. Dr. Rainer Herges an der Christian-Albrechts-Universität zu Kiel
10/2003-7/2007	Doktorarbeit mit dem Titel "Strukturelle und funktionelle Charakterisierung von einem Membranprotein und einem Membranprotein bindendem Toxin mittels Lösungs-NMR" in der Abteilung NMR-basierte Strukturbiologie von Prof. Dr. Christian Griesinger am Max Planck Institute für Biophysikalische Chemie in Göttingen